A T T I

DELLA «FONDAZIONE GIORGIO RONCHI»

Numero Speciale 4 – Serie di Elettromagnetismo
su

MEMS a radiofrequenza
Perugia, 5 Dicembre 2003

Microwave radiometry
and remote sensing applications
Rome, February 24-27, 2004

Schiere riflettenti stampate
Rende (Cosenza), 27 Febbraio 2004

Interazione tra campi elettromagnetici
e soggetti esposti
Roma, 1-2 Aprile 2004

Materiali speciali e metamateriali
per l'elettromagnetismo e le TLC
Roma, 5 Aprile 2004

La figura di Giorgio Barzilai nella ricerca italiana
in elettromagnetismo e in elettronica
Roma, 15-16 Aprile 2004

Il metodo degli elementi finiti nelle applicazioni dell'ingegneria elettrica e dell'informazione

Genova, 3-4 Giugno 2004

"L'avventura della radio"
Un viaggio nella storia, scienza e arte
delle Telecomunicazioni -"Collezione Patanè"

Firenze, 4-28 Giugno 2004

A cura di:

P. Bernardi (Università di Roma "La Sapienza")

C. Capsoni (Politecnico di Milano)

S. Caorsi (Università di Pavia)

E. Del Re (Università di Firenze)

G. Di Massa (Università della Calabria)

F. Frezza (Università di Roma "La Sapienza")

P. Lampariello (Università di Roma "La Sapienza")

F.S. Marzano (Università de L'Aquila)

N. Pierdicca (Università di Roma "La Sapienza")

G. Pelosi (Università di Firenze)

G. Schettini (Università di "Roma Tre")

R. Sorrentino (Università di Perugia)

L. Vegni (Università di "Roma Tre")

Università degli Studi di Firenze

INDICE

Presentazione del Numero Speciale 4
Serie di Elettromagnetismo

Questo Numero Speciale degli *Atti della Fondazione Ronchi*, il quarto della Serie, è introdotto da una breve presentazione di R. Sorrentino (Università di Perugia) e di C. Capsoni (Politecnico di Milano) dei "Quaderni della Società Italiana di Elettromagnetismo" che inizieranno le pubblicazioni all'inzio del prossimo anno.

Il Numero Speciale è dedicato poi, come i precedenti, ad iniziative organizzate recentemente da ricercatori che fanno riferimento alla Società Italiana di Elettromagnetismo (SIEm).

Della prima [*MEMS a radiofrenza*, Perugia, 5 Dicembre 2003, *Chairman*: R. Sorrentino (Università di Perugia)] e dellla terza [*Schiere di antenne stampate*, Rende (Cosenza), 27 Febbraio 2004; *Chairman*: G. Di Massa (Università della Calabria)] iniziativa, si riporta solo una breve presentazione. Queste sono state organizzate nell'ambito di un Programma di ricerca scientifica di Rilevante Interesse Nazionale (PRIN), co-finanziato dal Ministero dell'Istruzione, dell'Università e della Ricerca (MIUR).

Invece la seconda iniziativa, di carattere internazionale, presentata nel volume è *Microwave radiometry and remote sensing applications* [Rome, February 24-27, 2004]. Di questa iniziativa sono stati riportati solo una selezione dei sommari dei lavori presentati.

La quarta iniziativa presentata nel Numero Speciale è il Convegno Nazionale *Interazione tra campi elettromagnetici e soggetti esposti* [Roma, 1-4 Aprile 2004], organizzato nell'ambito del Programma Nazionale di Ricerca MIUR/CNR-ENEA "Salvaguardia dell'uomo e dell'ambiente dalle emissioni elettromagnetiche". Di questo Convegno è riportata solo una breve presentazione del Comitato Scientifico del Progettto Nazionale (Università di Roma "La Sapienza") e il programma.

Della quinta iniziativa *Materiali speciali e metamateriali per l'elettromagnetismo e le TLC* [Roma, 5 Aprile 2004; *Chairmen*: L. Vegni e G. Schettini], organizzata dall'Università di Roma "Tre" in collaborazione con il Centro Interuniversitario MECSA, vengono riportate le memorie estese dei lavori.

Nel Numero Speciale uno spazio significativo è dato poi al Convegno, organizzato dall'Università di Roma "La Sapienza", su *Giorgio Barzilai e la*

ricerca italiana nell'elettromagnetismo e nell'elettronica [Roma, 15-16 Aprile 2004, *Chairmen*: P. Bernardi e P. Lampariello].

La penultima sezione del volume è dedicata alla 2ª Giornata di Studio su *Il metodo degli elementi finiti nelle applicazioni dell'ingegneria elettrica e dell'informazione* [Genova, 3-4 Giugno 2004; *Chairman*: S. Caorsi (Università di Pavia)]. Della manifestazione vengono riportate le versioni estese dei lavori presentati.

Infine il Numero Speciale dedica l'ultima sua sezione alla mostra organizzata dall'Università di Firenze e dal CNIT su *L'avventura della radio. Un viaggio nella storia, scienza ed arte delle telecomunicazioni – "Collezione Patanè"* [Firenze, 4-28 Giugno 2004].

<div align="right">

Giuseppe Pelosi
Università di Firenze
Laura Ronchi Abbozzo
Fondazione G. Ronchi

</div>

I "Quaderni della Società Italiana di Elettromagnetismo"

Nel maggio 2002 si è costituita la SIEm Società Italiana di Elettromagnetismo, associazione a carattere scientifico senza fini di lucro, che "ha per scopo di promuovere, favorire e tutelare lo studio e il progresso dell'Elettromagnetismo in Italia con specifico riguardo alle sue applicazioni all'ingegneria".

La SIEm raccoglie ed amplia l'eredità del Gruppo di Coordinamento Nazionale di Elettromagnetismo, che, per oltre un trentennio ha operato, informalmente ma efficacemente, attraverso le sue unità di ricerca, dando vita, in particolare, fin dal 1976, alla RiNEm, Riunione Nazionale di Elettromagnetismo, convegno biennale dove si fa il punto sulla ricerca italiana nel settore dell'elettromagnetismo e relative applicazioni. Al fine di stimolare e potenziare il raccordo, in Italia purtroppo carente, tra ricerca pubblica e applicazioni industriali, in aggiunta alle tradizionali unità di ricerca universitarie e a quelle riferibili a enti pubblici di ricerca, come gli istituti CNR, la SIEm comprende anche unità di ricerca private, riconducibili a industrie operanti nel settore.

Per raggiungere il suo scopo sociale, la SIEm si propone, tra l'altro:
- di promuovere, coordinare e diffondere la ricerca nell'elettromagnetismo;
- di collaborare con istituzioni nazionali e internazionali attive in elettromagnetismo;
- di promuovere e gestire scuole e corsi di formazione, di organizzare riunioni scientifiche anche in collaborazione con altre associazioni o istituzioni;
- di favorire la costituzione di gruppi di studio e di cooperazione su problemi scientifici, teorici o applicativi, anche ai fini di consulenza verso altri enti;
- di curare la pubblicazione di bollettini, riviste, atti scientifici e la realizzazione e gestione di un sito della rete Internet.

È con grande soddisfazione che, a due anni dalla sua costituzione, coerentemente con l'ultimo dei punti sopra menzionati, diamo ora vita ai *Quaderni della Società Italiana di Elettromagnetismo*. Con ciò, la SIEm non ha certo la pretesa di far concorrenza ad altre pubblicazioni scientifiche largamente affermate anche a livello internazionale. Come scrive il suo direttore

nella presentazione, i *Quaderni* vogliono essere lo strumento per acquisire una migliore coesione interna alla comunità tecnica e scientifica, e, insieme, un *biglietto da visita* per presentarsi all'esterno e proporsi come interlocutori scientifici autorevoli nei confronti degli enti pubblici e privati deputati o interessati alla promozione della ricerca e allo sviluppo delle conoscenze nel settore dell'elettromagnetismo e delle sue applicazioni all'ingegneria.

È una sfida che lanciamo a noi stessi, convinti che l'impegno della nostra comunità scientifica sarà in grado di vincerla, nello stesso modo con cui abbiamo avviato e saputo consolidare la RiNEm, portandola, quest'anno, alla sua quindicesima edizione.

È doveroso, da parte mia, esprimere a nome di tutti i soci SIEm un sentito ringraziamento a Carlo Capsoni che ha accettato, come primo direttore della rivista, di caricarsi un fardello certo non lieve, mettendo fattivamente in essere, con il suo stile sommesso e privo di baldanza, questa iniziativa, non senza la collaborazione valida degli altri colleghi del comitato di redazione, che lascio a lui di ringraziare. Come diceva il Poeta: cosa fatta capo ha. Fatto questo primo numero, sono convinto che, tra qualche anno, guarderemo alla data odierna con il medesimo compiacimento con cui ricordiamo l'Aquila 1976 come l'inizio della Riunione Nazionale di Elettromagnetismo.

<div style="text-align: right">

Roberto Sorrentino
Università di Perugia
(Presidente della SIEm)

</div>

<div style="text-align: center">

*****

</div>

A due anni dalla sua costituzione, la Società Italiana di Elettromagnetismo, SIEm per gli amici, ha sentito l'esigenza di dotarsi di una rivista che faccia da specchio al suo essere il punto di riferimento per tutti coloro che operano nell'area dell'elettromagnetismo.

In questa fase iniziale, la rivista vuole essere, in primo luogo, uno strumento per migliorare la coesione tra i ricercatori che fanno parte della SIEm e per aiutare la crescita culturale delle persone più giovani che domani avranno il compito di continuare la lunga e gloriosa tradizione dell'elettromagnetismo in Italia a suo tempo iniziata da Barzilai, Boella, Latmiral e Toraldo di Francia.

Nel seguito, se sapremo dimostrare di essere capaci di sostenere questa iniziativa con regolari pubblicazioni di elevato livello, questa rivista potrà diventare anche un potente mezzo di dialogo con il mondo esterno, un *"biglietto da visita"* della SIEm, per promuovere e migliorare sia a livello

quantitativo che qualitativo i rapporti con le industrie, grandi e piccole, che possono fare buon uso della conoscenze teoriche e sperimentali che noi possediamo.

La rivista sarà organizzata in sezioni affidate a responsabili che si occuperanno di impostarne la strategia, promuovere la raccolta dei contributi e armonizzare il materiale ricevuto. Ad essa si affiancherà il sito web della SIEm su cui verranno riportate regolarmente tutte quelle notizie come gli avvisi di convegni, seminari, borse di studio, richieste di collaborazione di giovani ricercatori su specifici contratti di ricerca e così via, che possiamo definire "volatili" sia per la tempestività con cui devono essere annunciate sia per il tempo di vita limitato, caratteristiche che mal si conciliano con una pubblicazione quadrimestrale quale quella ipotizzata.

In una di queste sezioni (*Notizie dalle unità di ricerca/laboratori*) ci preoccuperemo di pubblicizzare la struttura delle unità e le attività sperimentali condotte nei grandi laboratori con lo scopo di incrementare, se possibile, l'utilizzo di costose apparecchiature, attivare sinergie tra gruppi di ricerca, mettere in comune esperienze. Inoltre si pubblicheranno sintesi approfondite su attività di particolare rilievo svolte nell'ambito di progetti nazionali e internazionali da gruppi di ricerca interuniversitari.

Ampio spazio verrà dedicato agli aspetti culturali, che ci accomunano in quanto base dell'elettromagnetismo. A questo scopo verranno pubblicati contributi (*tutorial*) su svariati argomenti sia relativi a tematiche "classiche" come le antenne o la propagazione troposferica, sia rivolti alle nuove applicazioni come, ad esempio, i metamateriali o i MEMS, sia di carattere storico. Questo permetterà a tutti noi di essere aggiornati anche su argomenti non specifici della nostra attività di ricerca e, per i più giovani, sarà una fonte di riferimento, di approfondimento e di crescita culturale.

Un'altra sezione rilevante riguarda l'argomento generale dei *finanziamenti*, che non vuole solo essere una vetrina delle attività che le unità di ricerca sviluppano a fronte di specifici contratti con soggetti pubblici, quali le regioni, il CNR, l'ASI, il MIUR, e con soggetti privati, quali le industrie del settore, ma anche un momento di riflessione propositiva sulle problematiche connesse alle fonti di finanziamento, che sono di vitale importanza in questo momento storico in cui i canali istituzionali sono particolarmente "avari". Ognuno di noi sa bene, infatti, come gli introiti dei contratti siano in molti casi indispensabili per la sopravvivenza dei gruppi di ricerca.

Ovviamente non poteva mancare la sezione dedicata alla *didattica*, che vuole porsi come punto di raccolta e successiva disseminazione delle idee e delle attività che si sviluppano presso le nostre università alle prese con il nuovo ordinamento degli studi organizzato in lauree di primo livello e in lauree specialistiche. Al suo interno appariranno anche le recensioni di nuovi libri sull'elettromagnetismo e le sue applicazioni e riferimenti sul materiale didattico, sia cartaceo che elettronico, che di volta in volta si rende disponibile.

Durante la stesura della struttura della rivista non si è voluto dimenticare che alcune tematiche connesse all'elettromagnetismo hanno oggi assunto un impatto tale nella vita quotidiana da meritare uno specifico approfondimento, magari meno tecnico, perché rivolto ad un pubblico non specializzato, ma tuttavia doveroso da parte di un organo che ha la qualifica per farlo. Di questo ci occuperemo prossimamente.

Da ultimo vogliamo ricordare che la rivista si farà promotrice di *numeri speciali* con lo scopo specifico di fungere da memoria delle attività di promozione scientifica cui hanno dato vita gruppi di ricercatori o unità che fanno parte della SIEm.

Il nome della rivista: *Quaderni della Società Italiana di Elettromagnetismo.*

A questo punto è doveroso fare l'elenco di tutti gli amici e colleghi che hanno accettato di spendere del proprio tempo per questa iniziativa: Fernando Bardati, Peppe di Massa, Paolo Lampariello ,Giuliano Manara, Giuseppe Mazzarella, Franco Moglie, Mauro Mongiardo, Giuseppe Pelosi. A loro deve andare il nostro ringraziamento per l'aiuto che hanno offerto fin dai primi passi di questa avventura.

Ovviamente la rivista è di tutti noi, dobbiamo sentircene responsabili e disponibili a fornire il nostro contributo per il suo successo.

Carlo Capsoni
Politecnico di Milano
(Direttore della Rivista)

Giornata di Studio

MEMS a Radiofrequenza
Stato della ricerca e della tecnologia in Italia

Perugia, 5 Dicembre 2003

Salone Conferenze
Hotel Giò Arte e Vini - Perugia

INDICE

Introduzione

I sistemi MEMS *MicroElectro-Mechanical Systems* sono dispositivi miniaturizzati, realizzati con processi tecnologici compatibili con quelli dei circuiti integrati, che combinano funzioni elettriche e meccaniche. I campi di applicazione vanno dalle membrane per i microfoni, ai sensori accelerometrici, ai micro-motori. Nel campo delle applicazioni a radiofrequenza, la tecnologia MEMS ha la sua applicazione specifica nella realizzazione di microinterruttori che potrebbero sostituire gli ormai consolidati dispositivi a stato solido. Per le loro ridottissime dimensioni, la totale integrabilità nei "front-end" dei moderni apparati di telecomunicazioni, l'alto isolamento a circuito aperto e le basse perdite d'inserzione a circuito chiuso e l'elevata linearità, i MEMS rappresentano una tecnologia innovativa di grandissimo interesse per le applicazioni nei circuiti a radiofrequenza e microonde, fino alle onde millimetriche (RF MEMS). La loro riconfigurablità meccanica li rende particolarmente interessanti per lo sviluppo di nuove funzionalità e per la realizzazione di circuiti di nuova concezione per sistemi mobili e le future generazioni di circuiti radio. L'uso dei MEMS è in effetti oggetto di crescente attenzione per la realizzazione di circuiti integrati RF riconfigurabili, operanti in campi di frequenza che arrivano fino a un centinaio di GigaHertz.

La tecnologia dei RF MEMS, tuttavia, è da considerarsi ancora in una fase di sviluppo: rimangono parzialmente irrisolti alcuni problemi riguardanti la loro affidabilità, il tempo di vita, la limitata potenza sopportabile ed il packaging. Inoltre, come sempre avviene con l'introduzione di nuove tecnologie, è carente la modellistica di tali dispositivi, la quale richiede sofisticati modelli elettromagnetici, meccanici e termici.

Anche in Italia, negli ultimi anni, si sta sviluppando notevole interesse nei confronti di questa nuova tecnologia: diversi laboratori universitari e industriali hanno intrapreso programmi di ricerca e di sviluppo tecnologico, in particolare su RF MEMS. Con questa Giornata di studio, promossa dalla SIEm, si è voluto fare il punto sulla ricerca e sullo sviluppo della tecnologia in Italia nel campo dei RF MEMS, costituendo un forum che favorisca integrazioni e sinergie tra laboratori universitari e industriali, attragga nuovi ricercatori e consenta il diffondersi delle conoscenze in questo settore in rapidissima evoluzione.

Il programma della giornata è mostrato nella pagina a fianco. Hanno partecipato all'incontro circa 50 ricercatori e tecnici provenienti da università e industrie italiane.

Nel seguito sono riportate le sintesi di alcuni degli interventi presentati.

Roberto Sorrentino
Università di Perugia

Programma

Giovedì 4 Dicembre
18:00 - Arrivo dei partecipanti
20:00 - Cena sociale

Venerdì 5 Dicembre
8:30 - Inizio lavori
Introduzione: Roberto Sorrentino, Università di Perugia

9:00 -   Progetto ESA/ESTEC *Microwave Electrostatic Micro-machined Devices for On-Board applications*, coordinatore: Francesco Vitulli, Alenia Spazio, Roma.

9:45 -   Progetto MIUR-COFIN *Modellazione elettromagnetica e meccanico-strutturale di dispositivi MicroElettromeccanici,* coordinatore Roberto Sorrentino, Università di Perugia:
• *Modellizzazione Elettromagnetica e Meccanico-Strutturale di dispositivi MicroElettro-Meccanici,* Paolo Mezzanotte, Claudio Rondini, Università di Perugia.
• *Analisi elettromagnetica e sintesi di circuiti integrati contenenti switch MEMS,* Marco Farina, Barbara Marchetti, Università Politecnica delle Marche.
• *Sviluppo di un algoritmo di uso generale per il CAD di circuiti integrati a microonde riconfigurabili a controllo micro-elettro-meccanico,* Paolo Arcioni, Università di Pavia.
• *Modelli non lineari per grandi segnali di MEMS e loro impiego nella simulazione di front-end a radiofrequenza,* Diego Masotti, Università di Bologna.

11:45 - *RF MEMS presso STMicroelectronics,* Chantal Combi, STMicroelectronics (*Nota: L'intervento è stato annullato per impedimenti della relatrice*).

12:15 - *Integrazione di MEMS in†Circuiti Integrati Monolitici su GaAs,* Claudio Lanzieri, Anna Maria Fiorello, Alenia Marconi Systems, Roma.

12:45 - Pranzo.

14:00 - *Micromachining e dispositivi MEMS per Applicazioni a Microonde ed Onde Millimetriche presso il CNR-IMM*, Romolo Marcelli, CNR-IMM, Roma.

14:20 - *Tecnologie realizzative di RF-MEMS presso ITC-Irst*, Benno Margesin, ITC-irst, Trento.

14:40 - *Sviluppo di RF MEMS in Alenia Spazio, Sergio Di Nardo*, Alenia Spazio, L'Aquila.

15:00 - Discussione

16:00 - Chiusura lavori

Sintesi di alcuni interventi

1. Progetto ESA/ESTEC Microwave Electrostatic Micro-machined Devices for On-Board applications
Francesco Vitulli

È stata illustrata l'attività di ricerca sviluppata nell'ambito del contratto ESA Nr. 14628/NL/CK dal titolo "Microwave Electrostatic Micro-machined Devices for On-Board applications". Scopo della ricerca è il progetto e la realizzazione di una matrice di commutazione a MEMS e di un micro-interruttore SPDT in tecnologia MEMS per applicazioni spaziali di potenza. I gruppi di ricerca coinvolti sono Alenia Spazio S.p.A. in veste di coordinatore del progetto, l'Università di Perugia e l'Università di Monaco di Baviera che hanno curato la progettazione dei dispositivi, il CNR-IMM che si è occupato delle misure RF e l'ITC-Irst che ha realizzato i dispositivi presso il proprio centro di ricerca di Trento.

L'interruttore SPDT, elemento chiave della matrice di commutazione, è stato progettato su linea complanare; è composto da due coppie di interruttori SPST disposti sui due bracci di uscita di una giunzione a T (Fig. 1). Ciascuna coppia è costituita da un interruttore parallelo capacitivo e da un interruttore serie con contatto ohmico. Questo abbinamento è stato ideato per garantire un buon livello di isolamento e basse perdite di inserzione sulla banda 1-30 GHz. In Fig. 2 è mostrato il confronto tra le misure e le simulazioni dei parametri di scattering della struttura.

I dispositivi sono stati realizzati su un substrato di silicio ad alta resistività mediante un processo composto da sette maschere, ciascuna delle quali prevede circa dieci passi intermedi.

Per la realizzazione delle linee di trasmissione e dei ponti mobili sono stati utilizzati strati di oro e oro-cromo, mentre per gli strati di passivazione è stato utilizzato LTO (Low temperature Oxide) o SiO_2, per la linea sotto il ponte un triplo strato composto da TiN-Al-TiN e infine polysilicon ad alta resistività per le linee di alimentazione. Sono stati inoltre discussi gli effetti indesiderati legati al processo tecnologico quali la rugosità delle metallizzazioni e dei dielettrici, gli stress termici, la formazione di ossidi indesiderati e il loro impatto sulle prestazioni elettriche dei dispositivi; sono state quindi illustrate le azioni correttive intraprese per limitare tali effetti.
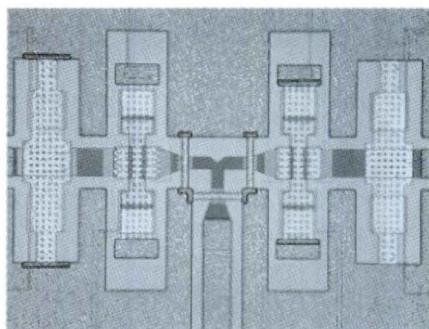
FIG. 1

Foto al microscopio del SPDT realizzato presso l'ITC-irst
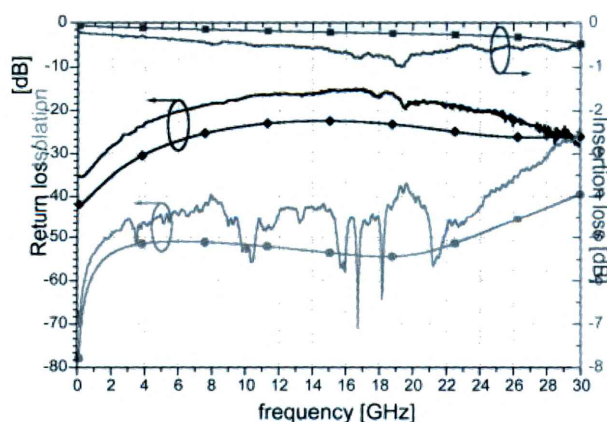
FIG. 2

Parametri di scattering della struttura di Fig. 1.
Confronto tra misure (linee senza simboli) e simulazioni (linee con simboli)

I dispositivi realizzati sono stati sottoposti a test di affidabilità e robu-
stezza; in particolare sono stati effettuati test di sopravvivenza dei circuiti a
10×10^6 cicli di attuazione; alcune prove in potenza sono state realizzate con
segnali di 1 W.

Infine è stato illustrato il package appositamente progettato per conte-
nere un singolo SPDT; la struttura è stata realizzata in tecnologia LTCC
presso lo stabilimento Alenia dell'Aquila.

2. Progetto MIUR-COFIN Sistemi Elettromeccanici Miniaturizzati (MEMS) per Circuiti Integrati a Radiofrequenza

ROBERTO SORRENTINO

Il progetto coinvolge quattro sedi universitarie, Perugia, Ancona, Pavia, Bologna, ed è finanziato dal Ministero dell'Istruzione, dell'Università e della Ricerca per promuovere lo sviluppo della tecnologia MEMS in Italia. Le unità sono coordinate, rispettivamente, da Roberto Sorrentino, Tullio Rozzi, Giuseppe Conciauro e Vittorio Rizzoli. Obiettivo specifico del programma è il progetto e la realizzazione di un tipico sottosistema circuitale basato su dispositivi MEMS, quale uno sfasatore digitale a quattro bit e, a partire dalla caratterizzazione di questo, lo studio del comportamento di circuiti complessi, quali ad esempio front-end RF, ottenuti dall'integrazione di sottosistemi anche basati su MEMS.

Le unità di Perugia e di Ancona si sono interessate principalmente dei singoli dispositivi MEMS, sia dal punto di vista progettuale-modellistico (elettromagnetico e meccanico), sia dal punto di vista sperimentale-realizzativo, mentre le unità di Bologna e di Pavia hanno concentrato maggiormente il loro interesse sulla progettazione lineare e non lineare di circuiti complessi contenenti MEMS.

Di seguito sono riportati le sintesi dei lavori effettuati dalle quattro unità di ricerca nel primo anno di attività.

2a. Modellizzazione Elettromagnetica e Meccanico-Strutturale di dispositivi MicroElettroMeccanici

PAOLO MEZZANOTTE
Unità di Perugia

Uno degli obbiettivi principali di questo progetto di ricerca è rappresentato dal progetto e dalla eventuale realizzazione di uno sfasatore digitale a 4 bit basato su dispositivi MEMS.

L'unità di Perugia ha concentrato i propri sforzi sul progetto del singolo micro-interruttore "single-pole single-throw" (SPST) sia per quanto riguarda le funzionalità elettriche che meccaniche. Facendo tesoro dell'esperienza maturata in un altro progetto di ricerca, sono state sintetizzate due tipologie di micro-interruttori SPST con ponte a doppio ancoraggio, uno con contatto capacitivo connesso in parallelo sulla linea e l'altro con contatto ohmico inserito in serie. Per il dimensionamento della struttura sono stati utilizzati software elettromagnetici sia commerciali (SONNET, MOMENTUM, CST MWS) che sviluppati in proprio (codice 3DFDTD).

Particolare attenzione è stata posta nel dimensionamento e posizionamento della rete di attuazione e alimentazione dei dispositivi; in questo difficile processo di ottimizzazione è stato fondamentale il contributo fornito dalle simulazioni meccaniche effettuate con il software commerciale ANSYS

basato sul metodo degli elementi finiti (FEM). In particolare è stata effettuata un'analisi elettromeccanica in grado di valutare la risposta capacitiva del dispositivo alla variazione dell'altezza del gap e di conseguenza la tensione di attuazione. Mediante un'elaborazione dei risultati ottenuti in termini di deformazione della struttura, è stato possibile visualizzare una mappa degli sforzi di Von Mises. Inoltre, a partire da misure effettuate su dispositivi sviluppati in precedenti progetti di ricerca, è stata effettuata una stima degli stress residui dovuti al processo di fabbricazione.

I dispositivi sviluppati sono stati impiegati nel progetto di due sfasatori in collaborazione con il Prof. P. Blondy dell' IRCOM di Limoges (Francia).

Il primo, una "true time delay network" a 3 bit su un substrato di allumina (Fig. 7) funzionante a 20 GHz, utilizza micro-interruttori serie di tipo cantilever (a singlolo ancoraggio) con contatto ohmico; sulla parte inferiore del ponte sono state poste due piccole protuberanze (dimples) per migliorare il contatto elettrico ed è stato praticato un foro per diminuire la tensione di attuazione. I dispositivi sono utilizzati per indirizzare il segnale su una linea di riferimento o su un'altra opportunamente sfasata rispetto alla prima. Le simulazioni, effettuate con ADS-Momentum, indicano ottime prestazioni per il circuito.
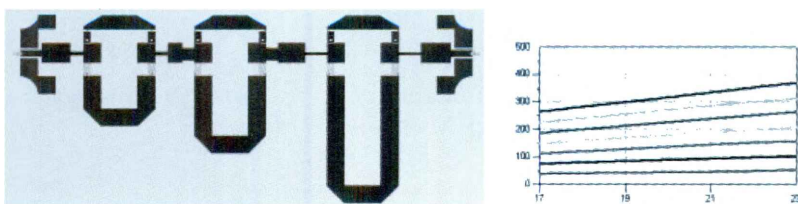
FIG. 7

Phase Shifter a 3 bit: a) layout del dispositivo; b) Simulazione
delle differenze di fase nei diversi stati in funzione della frequenza

Il secondo dispositivo è uno sfasatore a 2 bit funzionante a 40 GHz (Fig. 8), costituito da una microstriscia ad alta impedenza realizzata su un substrato di BCB (BenzoCycloButene) di soli 40 μm di spessore. La linea è periodicamente caricata con capacità variabili verso massa realizzate con microinterruttori MEMS in configurazione parallelo connessi in serie a capacitori fissi in microstriscia.

Entrambi i dispositivi sono in fase di realizzazione presso i laboratori dell'IRCOM.

Infine, utilizzando la telecamera ad infrarossi Delta Therm 1550, corredata con uno zoom avente risoluzione massima di 12 μm, sono state effettuate delle misure termografiche su un micro-interruttore capacitivo in possesso dell'unità di ricerca (Fig. 9).

	State 0,0	State 1,0	State 0,1	State 1,1
Phase Shift [degree]	0	92.77	180.8	273.9
Insertion loss [dB]	-1.22	-2.02	-1.38	1.79
Return loss [dB]	-12.88	-8.03	-27.27	15.24
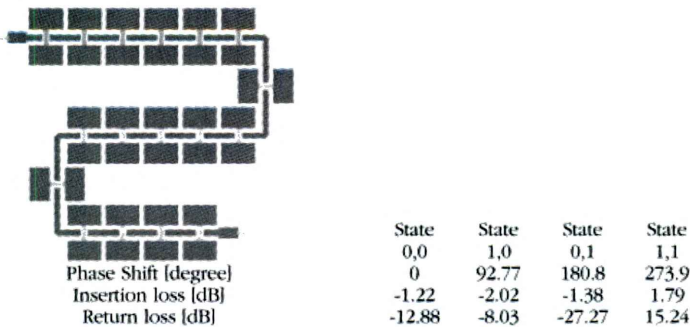
FIG. 8

Phase Shifter a 2 bit: layout del dispositivo con i risultati
delle simulazioni effettuate a 40 GHz.
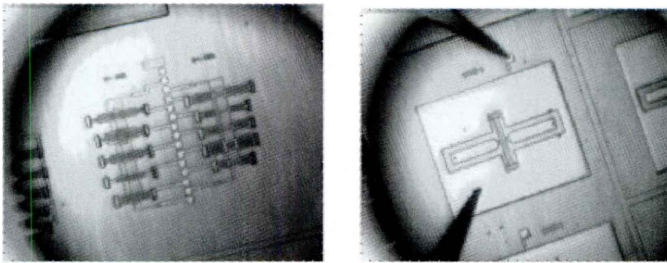
FIG. 9

Immagini termografiche su dispositivi MEMS
in possesso dell'unità di ricerca di Perugia.

2b. Analisi elettromagnetica e sintesi di circuiti integrati contenenti swich MEMS

MARCO FARINA
Unità di Ancona

Obiettivo finale della ricerca in corso presso l'unità di Ancona è la progettazione di nuovi dispositivi contenenti interruttori MEMS. Tale disegno è rivolto da una parte a realizzare circuiti con specifiche funzionalità, in particolare sfasatori a basse perdite, e dall'altra allo sviluppo di nuove topologie che consentano di aggirare limitazioni intrinseche dei singoli interruttori in tecnologia MEMS, come la limitata capacità di gestire segnali di potenza.

Propedeutico alla fase di progetto è lo sviluppo di sistemi di simulazione accurati e robusti, che consentano di valutare le prestazioni dei dispositivi tenendo conto di aspetti che, nella pratica, rivestono la massima importanza: quelli tecnologici. In tale contesto è stata messa a punto una procedura di analisi che integra le potenzialità dell'analisi elettromagnetica con quelle dell'analisi elettromeccanica, quest'ultima strettamente collegata

con aspetti tecnologici e proprietà tensili dei materiali. La tecnica di analisi è stata messa a punto con un processo iterativo di scambio dati con l'Università di Perugia, confrontando risultati attesi e misurati dopo l'effettiva realizzazione di alcuni campioni (Fig. 3). Al contempo sono state effettuate simulazioni di strutture più complesse come gli sfasatori DMTL (Fig. 4), confrontando i risultati con quanto disponibile in letteratura, e verificando un più che soddisfacente accordo.
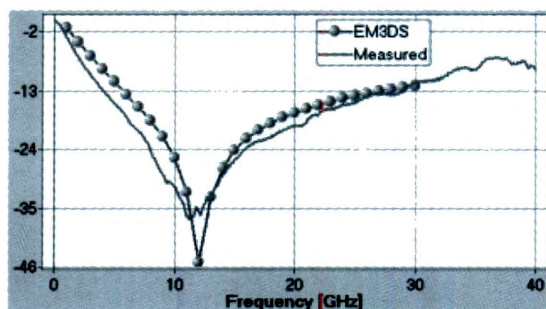
FIG. 3

Confronto tra la misura e la simulazione EM effettuata con il software proprietario EM3DS del coefficiente di trasmissione di uno switch capacitivo nello stato attuato.
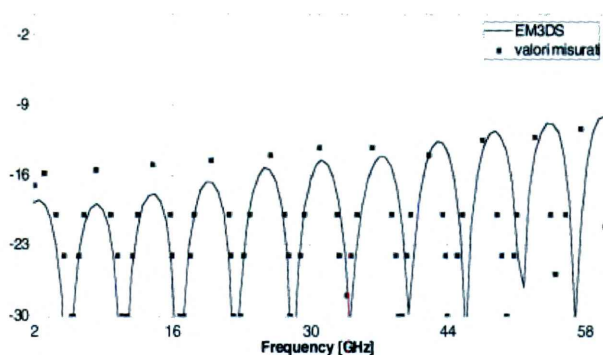
FIG. 4

Phase Shifter DMTL con 32 ponti; confronto tra misure e simulazione EM effettuata con EM3DS in termini di S_{11}.

Nell'ambito della progettazione è stata proposta una nuova topologia bilanciata per la realizzazione di interruttori SPDT che, facendo uso di ibridi planari, consente di ridurre le riflessioni in banda passante nelle due posizioni di funzionamento e di dimezzare la potenza che incide su ogni singolo interruttore (Fig. 5). Simulazioni preliminari hanno dimostrato le effettive potenzialità di tale nuova configurazione (Fig. 6).

Infine l'Ing. Marchetti ha illustrato il progetto, lo sviluppo e l'applicazione di un sistema di misura per la caratterizzazione dinamica di MEMS basato sulla vibrometria laser Doppler.
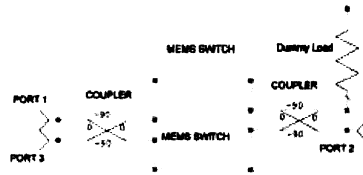
(a)
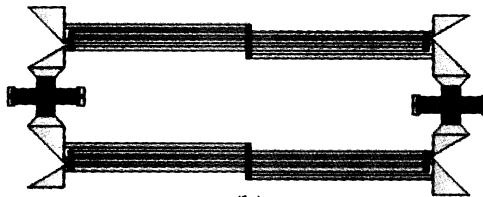
(b)

FIG. 5

SPDT in configurazione bilanciata: a) schema di funzionamento; b) possibile realizzazione con accoppiatori Lange e MEMS Switch capacitivi.
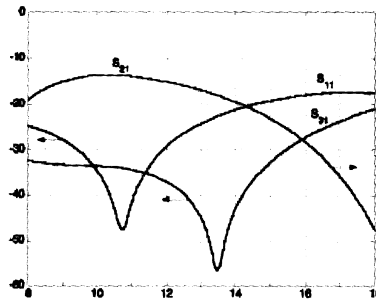
FIG. 6

Parametri di Scattering del circuito proposto in Fig. 5b.

È stato illustrato il principio di funzionamento del microvibrometro, le sue caratteristiche e sono stati mostrati alcuni risultati relativi all'analisi vibrazionale di micro-oscillatori meccanici (individuazione delle frequenze di risonanza e dei modi di vibrare) e alla correlazione di alcuni parametri fisici (pressione, temperatura) con il Quality Factor dei dispositivi.

Sono stati anche esposti risultati relativi all'individuazione di comportamenti non lineari nei sistemi, sempre utilizzando il microvibrometro laser Doppler costruito dall'unità di ricerca.

Roberto Sorrentino

2c. Sviluppo di un algoritmo "S-domain" di uso generale per il CAD di circuiti integrati a microonde riconfigurabili, a controllo micro-elettromeccanico

Paolo Arcioni

Unità di Pavia

Presso l'unità di Pavia è stato completato lo sviluppo teorico e la traduzione in un codice di calcolo di un algoritmo di analisi nel dominio della variabile di Laplace s (algoritmo SD) per il modellamento dei circuiti integrati a microonde.

L'algoritmo SD è stato poi reso più generale, introducendo la possibilità di considerare, oltre alle porte "esterne" originariamente previste (confinanti con la scatola metallica che contiene il circuito), anche porte "interne", opportunamente modellate come elementi superficiali di corrente magnetica, adatti a rappresentare generatori di tensione. Queste porte interne consentono il collegamento dei MEMS, modellizzati come elementi a costanti concentrate, al resto del circuito che costituisce la struttura a costanti distribuite. In particolare è stato sviluppato un originale metodo per il modellamento di interruttori utilizzanti MEMS capacitivi in parallelo, in cui parte del MEMS viene conglobato nel circuito a costanti distribuite, e quindi rappresentato con grande accuratezza del modello ottenuto dall'algoritmo SD. L'effetto di commutazione viene ottenuto variando una capacità tra due valori determinati con una procedura di "best fitting" di dati sperimentali relativi ad una semplice struttura di riferimento. Numerosi confronti con circuiti riportati in letteratura mostrano l'ottima accuratezza e l'efficienza numerica del metodo proposto.

L'algoritmo SD è stato infine completato, sviluppando un metodo originale di "deembedding", necessario per effettuare l'estrazione del modello del circuito, depurato degli elementi parassiti che vengono introdotti dal metodo di eccitazione ("delta-gap voltage excitation") usato nell'algoritmo di analisi. Il metodo sviluppato, sfruttando appieno le peculiarità dell'algoritmo SD, consente di effettuare un de-embedding a banda larga, e si è rivelato estremamente efficiente ed accurato.

2d. Modelli non lineari per grandi segnali di MEMS e loro impiego nella simulazione di front-end a radiofrequenza

Diego Masotti

Unità di Bologna

Una delle principali caratteristiche dei MEMS è la loro maggiore linearità rispetto ai corrispondenti componenti a semiconduttore. Nonostante ciò i MEMS presentano un complesso comportamento non lineare che può giocare un ruolo importante a livello di sistema, specialmente nel caso di forte eccitazione a radiofrequenza modulata. Infatti, a causa della presenza di

masse in movimento, l'inverso delle costanti di tempo associate ai MEMS è piccolo rispetto alle frequenze delle portanti a radiofrequenza, ma è comparabile con la frequenza del segnale modulante: la risposta del sistema elettromeccanico alle componenti a bassa frequenza causa distorsione dovuta ad intermodulazione nel circuito a RF.

Mediante un'estensione dell'ordinaria tecnica di Bilanciamento Armonico si è reso possibile il calcolo degli effetti distorcenti dovuti alle non linearità dei MEMS in circuiti a RF contenenti interruttori elettromeccanici. L'algoritmo risulta efficiente poiché le ordinarie equazioni circuitali sono risolte insieme alle equazioni elettromeccaniche.

Il metodo è stato applicato ad un'analisi di intermodulazione di un interruttore MEMS: il modello utilizzato è quello di Rebeiz, modificato mediante l'inserimento di una forza di contatto che limita lo spostamento verticale del ponte.

Lo strumento ottenuto si dimostra adatto ad investigare gli effetti della risonanza meccanica ed il fenomeno di auto-attuazione indotto dal segnale a RF, con tempi di calcolo contenuti.

3.   Micromachining e dispositivi MEMS per Applicazioni a Microonde ed Onde Millimetriche presso il CNR-IMM

ROMOLO MARCELLI

Le motivazioni fondamentali per l'utilizzo del *micromachining* come tecnica di microlavorazione del silicio per applicazioni ad alta frequenza hanno origine nella realizzazione di linee di trasmissione non dispersive a bassa perdita di propagazione e di antenne sostenute da membrane dielettriche per applicazioni fino ad oltre 100 GHz. Elevate frequenze di *cutoff* sono state dimostrate per elementi concentrati su Silicio e GaAs. Successivamente, applicazioni innovative come le interconnessioni verticali, le guide d'onda coplanari in versione *trenched* ed i microinterruttori (RF-MEMS switches) sono diventati veicoli dimostrativi per ulteriori applicazioni nel trattamento del segnale e verso una completa integrazione di componenti su silicio e/o GaAs.

In quest'ambito, il CNR-IMM è stato uno dei primi gruppi europei ad interessarsi di questa tecnologia, occupandosi di progettazione, realizzazione e test di configurazioni coplanari ad alta frequenza realizzate su membrane dielettriche. Sono stati sviluppati dimostratori di elementi concentrati, filtri ed antenne fin dal 1997, finanziati da accordi di cooperazione nazionali ed internazionali, seguendo i pionieristici risultati ottenuti negli USA all'inizio degli anni '90.

Le attività di ricerca condotte negli ultimi cinque anni sono state orientate ai seguenti obiettivi:

– *Risuonatori a film magnetico:* Risuonatori accordabili in frequenza, ottenuti mediante film di granato magnetico cresciuti presso il CNR-IMM

sono stati realizzati per applicazioni in filtri a banda stretta ed oscillatori a basso rumore di fase (2-40 GHz).

– *Magnetostatic Wave Devices* (MSWs). Programma finanziato dall'Agenzia Spaziale Italiana (ASI) e da Collaborazioni Bilaterali gestite dal Ministero per gli Affari Esteri.

– *RF-MEMS su Silicio e GaAs:* Elementi concentrati, flitri, antenne, ricevitori e sfasatori basati su microinterruttori RF-MEMS sono stati studiati ed in parte realizzati per applicazioni fino a 50 GHz ed oltre. Programma finanziato dall'Unione Europea tramite il progetto INCO-COPERNICUS "MEMSWAVE", l'accordo CNR-PAT (CNR-Provincia Autonoma di Trento), ASI, ESA/ESTEC e Collaborazioni Bilaterali gestite dal Ministero per gli Affari Esteri. Alcuni dimostratori ottenuti presso il CNR-IMM in collaborazione con altre unità di ricerca sono presentati nelle seguenti figure.
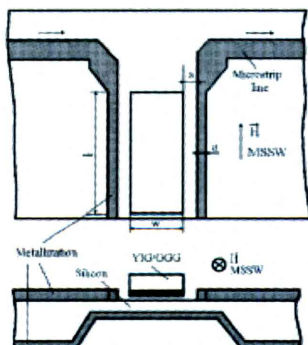
FIG. 10

Configurazione tipica di un risuonatore ad onda magnetostatica (MSW straight edge resonator - SER). Lo schematico è quello di un risuonatore ad onda superficiale su membrana di silicio, dove il SER è accoppiato ad un circuito in microstriscia.
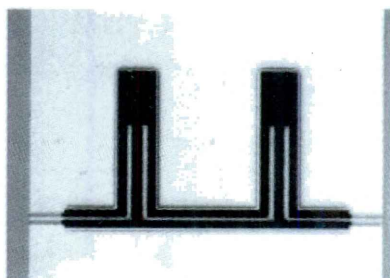
FIG. 11

Filtro a linee accoppiate realizzato su membrana dielettrica $SiO_2/Si_3N_4/SiO_2$, progettato mediante il metodo dei parametri immagine, con frequenza centrale di 38 GHz. (realizzato presso ITC-irst, Trento).
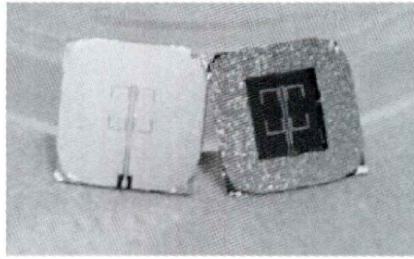
FIG. 12

Antenna a 38 GHz in guida d'onda coplanare su membrana $SiO_2/Si_3N_4/SiO_2$.
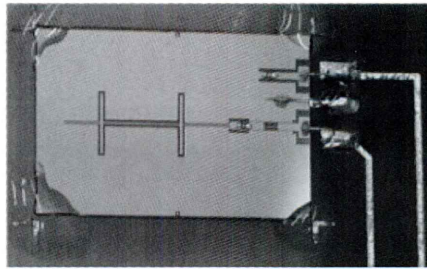
FIG. 13

Ricevitore ibrido a 38 GHz con diodo Schottky montato su wafer di silicio ed antenna su membrana. (in collaborazione con IMT, Bucharest).

Gli attuali interessi del CNR-IMM includono anche l'affidabilità dei dispositivi RF-MEMS e la loro progettazione circuitale. Vengono inoltre condotti test sul comportamento isteretico dei microinterruttori. Il *Work in Progress* include anche attività di ricerca su sfasatori basati su microinterruttori RF-MEMS (finanziata da ASI), dispositivi coplanari su membrane di SU8 e coplanari *trenched* (attività interna) e risuonatori micromeccanici a polisilicio, con potenziali interessi industriali fino ad oltre 100 MHz.

4.   Tecnologie realizzative di RF-MEMS presso ITC-irst
BENNO MARGESIN

L'ITC-Irst è parte dell'Istituto Trentino di Cultura la cui fondazione risale al 1976. L'Istituto, in parte finanziato dalla Provincia autonoma di Trento, vanta competenze nel campo dell'Information Technology, dei microsistemi, della fisica e della chimica delle superfici e delle interfacce.

In particolare i principali interessi della divisione Microsistemi sono:
- sensori ottici per la visione automatica;
- sensori biochimici per applicazioni biomediche e monitoraggio ambientale;
- sensori a raggi X e detector per particelle ad alta energia per applicazioni scientifiche e industriali;

- sistemi microelettromeccanici (MEMS);
- sviluppo di tecnologie non standard per produzioni prototipali e piccoli volumi;
- implementazione di sensori con elettronica di pre-processing.

All'interno della suddetta divisione è stato sviluppato un progetto denominato BioMEMS con le seguenti motivazioni:
- soddisfare la richiesta delle PMI di microsistemi e microsensori non-convenzionali;
- integrazione di nuove tecnologie di processo nelle tecnologie ITC-irst già disponibili per aumentare il valore aggiunto dei prodotti;
- rafforzamento delle collaborazioni della Divisione Microsistemi con le altre divisioni e le Università;
- esplorazione di nuove tecnologie e dispositivi innovativi.

Negli ultimi anni il gruppo BioMEMS ha studiato e implementato diversi procedimenti tecnologici che complementano la tecnologia planare:
- Etching Anisotropo del silicio con soluzioni TMAH/acqua;
- Membrane composite tensili;
- Etch-stop elettrochimico;
- Litografia con fotoresist spessi;
- Elettrodeposizione di oro;
- Wafer bonding a bassa temperatura.

Queste tecniche sono state impiegate nello sviluppo di svariati prototipi quali:
- Sensori chimici potenziometrici (ISFET e LAPS);
- Schiere di microelettrodi 2D e 3D per il monitoraggio dell'attvità elettrica di neuroni;
- Microbolometeri per la rivelazione di particelle ad alta energia;
- Sensori di pressione;
- Microriscaldatori per la rivelazione di gas;
- Guide d'onda per onde millimetriche su membrane dielettriche;
- MEM-switch per circuiti RF;
- Microfoni capacitivi;
- Colonne micro-gascromatografiche;
- Sensori di gas basati su fili di silicio submicrometrici;
- Sensori amperometrici per misure in vivo dell'acido lattico.

Nel campo dei microinterruttori per circuiti a radiofrequenza basati su tecnologia MEMS è stato sviluppato un processo di fabbricazione per MEM switch nella banda di frequenza da 1 a 30 GHz per applicazioni nello spazio con attuazione elettrostatica. Il componente di base sviluppato è il commutatore SPDT, che verrà utilizzato per la costruzione di una matrice di commutazione e per un commutatore di ridondanza. Il progetto è stato finanziato dall'Agenzia Spaziale Europea ed è già stato descritto nei paragrafi precedenti.

Microwave radiometry
and remote sensing applications

Rome, February 24-27, 2004

Faculty of Engineering,
University "La Sapienza" of Rome

INDEX

Preface

The 8th Specialist Meeting on Microwave Radiometry and Remote Sensing Applications (MicroRad04) was held on February 24-27, 2004 in Rome, Italy. The Meeting was an overwhelming success, much over any expectation. This exciting success can be summarized by few numbers such as 162 submitted abstracts, 152 participants, 85 oral presentations and 42 interactive posters along 4 full days of session works.

The MicroRad04 was held at the Engineering College, situated in one of the most beautiful sites of the Eternal City, between the Colosseum, the archaeological area and the early Christian Basilicas. It is worth mentioning the courtyard of the College (see Fig. 1), enriched by a piece of art dating back to Renaissance architecture: the ancient well designed by S. Mosca. The Engineering College occupied the area of an ancient Monastery, S. Pietro in Vincoli (St. Peter in Chains), situated on the gentle slopes of the Esquilino hill (one of the seven hills on which Rome was built). The Church of S. Pietro in Vincoli was built on the Empress Eudossia's buildings, to preserve St. Peter's chains. These can be found still nowadays in the Church, together with the large statue of Moses, sculpted by Michelangelo as part of the tomb of Pope Julius II.

The MicroRad04 Meeting is the latest of a series focusing on Microwave Radiometry and Remote Sensing of the Environment. The very first one dates back to March 1983, when it was organized and supported by the University "La Sapienza" of Rome, Italy, as a result of the initiative of Prof. G. d'Auria. The satisfactory outcome of the first Meeting stimulated an agreement among the participants to ensure the continuity in the form of a periodical meeting opportunity, the second of which, supported by IROE-CNR in Florence, Italy, occurred in 1988. Since then, more regular meetings, every 30 months approximately, have been scheduled and held in the US and in Italy, alternately. In 2001 the Meeting was hosted by NOAA in Boulder, Colorado.

The MicroRad04 Meeting was organized by the Department of Electronic Engineering of the University "La Sapienza" of Rome and was thought as an open invitation to convene again in Rome, after twenty years from the previous opportunity. The objective of MicroRad04 was to set up a common forum to report and discuss recent advances in the specific field

of microwave radiometry, thus gathering all parties belonging to the re-
search and industrial community, active in projects and studies in micro-
wave radiometry of atmosphere, ocean and land.

Contributions on topics of primary interest have been received.

When building up the program, the usually poor consensus towards paral-
lel sessions has been taken into account. The repartition of papers into both
oral and interactive sessions was therefore intended as a straightforward to
accommodate each author's wish to contribute to the Meeting with his/her
own work. The denomination "interactive", that identifies poster presentations,
reflected the concept of an open dialogue between the Authors and the
Audience, for mutual benefit and for a crosscheck of experiences and results.

FIG. 1

A picture of MicroRad04 participants in the old cloister
of the Engineering College.

The 15 sessions of the Meeting were focused on classical and new
advanced topics of environmental remote sensing by microwave radiometry,
emphasizing the methodological, instrumental, and application point of views.
Interdisciplinary and sensor synergy issues were also stimulated. The Meet-
ing was opened by the greetings of the Faculty Dean Dr. T. Bucciarelli and
of the Director of Electronic Engineering Dept. Dr. G. d'Inzeo as well as
by an introduction of the Scientific Chairman Dr. G. d'Auria. Two sessions,
chaired by Dr. A. Camps, Dr. S. Reising, Dr. A. Shibata and Dr. N. Skou,
were devoted to sea salinity, sea wind and ice. Following two sessions,
chaired by Dr. F.S. Marzano, Dr. Y. Kerr, Dr. M. Martin-Neira and Dr. E.
Njouku, dealt with missions and experimental campaigns. At the end of the
first day delegates of ESA, AIPAS and Alenia Spazio gave a presentation
on their activities during a session chaired by Dr. N. Pierdicca and F.S.
Marzano. A session, chaired by Dr. A. Shutko and Dr. S. Paloscia, was

devoted to soil and vegetation, while Dr. T. Hewison, Dr. C. Prigent, Dr. S. Crewell and Dr. N. grody chaired two sessions on clear-air and clouds applications. The second day was concluded by a session on snow cover, chaired by Dr. M. Hallikainen and Dr. P. Pampaloni. A session on electromagnetic models, chaired by Dr. D. Solimini and Dr. A. Voronovich, and a session on retrieval methodologies, chaired by Dr. R. Ware and Dr. E.R. Westwater, opened the third day. Two sessions, chaired by Dr. R. Ferraro, Dr. J. Turk, Dr. V. Chandrasekar and Dr. A. Mugnai, were dedicated to clouds and precipitation remote sensing. The last day of the Meeting was devoted to both sensor calibration and instrument and advanced techniques with chairpersons Dr. A. Gasiewski, Dr. G. Schiavon, Dr. P. Racette, Dr. H. Suess, Dr. I. Corbella and Dr. D. Le Vine.

Indeed, during the Meeting, special environmental "effects" were also foreseen, as pointed out by Dr. G. Calabresi, the scientific secretariat of the Meeting. As a matter of fact, the week was affected by a rigid weather with temperatures well below the seasonal average in Rome, northern winds and some showers. Nonetheless, the participants enjoyed both the Meeting and the city.

FIG. 2

Dr. G. d'Auria and Dr. D. Solimini with their wifes during the social dinner.

Last, but not least, the number of participants who attended the social dinner were 88, more than 55% of the Meeting attendees (see picture). The dinner was held in a typical Roman restaurant, called "Orazio", close to the Terme di Caracalla and Fori Romani. The meal was delighted by good local food and wine. At the end of the dinner a bus was offered for a memorable night sightseeing of Rome (in spite of the drizzle).

The Meeting was concluded by a MicroRad04 cake party (see Fig.3) and by the announcement of the next Specialist Meeting which will be held in Amherst at the University of Massuchessetts, MA, USA, chaired by Dr. S. Reising and planned on October 2005.

FIG. 3

Dr. N. Pierdicca, Dr. F.S. Marzano and Dr. G. d'Auria during
the MicroRad04 cake party on the last day.

The workshop proceedings will be published on a CD-ROM which
will be distributed to all participants and to those who will ask for. Full
papers are solicited for a MicroRad04 special issue of the IEEE Transac-
tions on Geoscience and Remote Sensing, whose deadline is on May 1st,
2004. See either the GRSS web site for details of the special issue or the
MicroRad04 web site at http://www.microrad04.org.

Many people and institutions made the MicroRad04 conference an
amazing success. The Meeting co-chairs, Dr. N. Pierdicca and Dr. F.S.
Marzano, would like to acknowledge the outstanding work of the local
organizing team, led by Dr. G. Calabresi and Dr. L. Pulvirenti with the
help of Mrs. S. Pongracz, Mr. M. Mazzetta and M. Fascetti. A thankful
acknowledgement goes to the session chairpersons and to the Scientific and
Steering Committee, composed by Dr. G. d'Auria, Dr. A. Gasiewski, Dr. B.
Greco, Dr. R. Guzzi, Dr. M. Hallikainen, Dr. M. Martin-Neira, Dr. A.
Mugnai, Dr. S. Paloscia, Dr. P. Pampaloni, Dr. D. Solimini, Dr. C.T. Swift,
Dr. J. Vivekanandan, and Dr. E.R. Westwater. A final acknowledgment is
addressed to the MicroRad04 sponsorship from IEEE-GRS-S, URSI, Univer-
sity "La Sapienza" of Rome Alenia Spazio, CETEMPS – University of
L'Aquila, ESA, AIPAS, AMS-Gematronik, ASITA, AIT, IEEE-GRS Central-
South Italy Section, CETEM and ASI.

Nazzareno Pierdicca
University of Rome "La Sapienza"

Frank Silvio Marzano
University of L'Aquila

Programma

SESSION 1
SEA SALINITY
(*Chairpersons*: A. Camps, S. Reising)

Passive synergy in the frame of sea surface salinity retrieval from microwave measurements at L-Band

EMMANUEL DINNAT, MARK DRINKWATER
ESA-ESTEC, Postbus 299, Keplerlaan 1, 2200 AG, Noordwijk, Netherlands

A key issue in the estimate of the sea-surface salinity (SSS) from L-band ($f = 1.4$ GHz) passive microwave radiometer brightness temperature (*Tb*) measurements is quantification of the influence of surface roughness: the wind-induced Tb (*Tbw*) is of the same order of magnitude as the expected salinity-induced Tb signal, and it is inaccurately predicted by emissivity models because of the uncertainty in sea state model predictions.

Conversely, radar cross-section (NRCS) measurements from scatterometers are much more sensitive to roughness than to temperature and/or salinity, and provide an independent estimate of the sea state. Such instruments could potentially be used to correct for *Tbw*, provided that the NRCS is influenced by the same scale ocean waves as the radiometer. A recent paper suggested that an empirically derived linear relation between Tbw and NRCS could help to refine the precision of the retrieved SSS from radiometric measurements at L-band. Moreover, electromagnetic theory suggests NRCS and *Tbw* of ocean surfaces to be strongly connected. Indeed, it is well known that the power backscattered by a slightly rough surface depends on ocean waves whose wavelength is similar in scale to the radar wavelength (at incidence angles larger than 20°). Similarly, it has been shown that the *Tb* induced by the small-scale roughness is mostly influenced by ocean waves whose wavelength is of the order of the radiometer's one, especially at small and moderate incidence angles. Nevertheless, the ocean surface is also composed of large waves, whose influence depends at the same time on polarization, incidence and azimuth angles but also differs according to the instrument (for example, at small incidence angles, the modulation by the large waves is dominant for the radar while it is negligible for the radiometer). Therefore, the SSS estimation from certain combinations of incidence/azimuth angles and polarization might also benefit from an estimation of the large-scale waves slope variance, derived for example from altimeters or a wave model. In the frame of the ESA Soil Moisture and Ocean Salinity (SMOS) mission currently in phase B, and of the future NASA Aquarius mission, we investigate active/passive synergy at L-band.

We use electromagnetic models to quantify the relative importance of the various ocean wave scales on the NRCS and *Tbw*, depending on polarization and incidence/azimuth angle. As the SMOS platform will not carry radar, we also assess the possibility of using external collocated instruments at other frequencies than L-band making some assumptions about the sea spectrum. A *Tbw* correction scheme is proposed, and the feasibility of the method is qualitatively evaluated using existing data at slightly higher frequencies than L band (i.e. C-band).

Salinity retrieval from SMOS brightness temperatures

ESTELLE-ANNE OBLIGIS, SYLVIE LABROUE, CHRISTINE BOONE, SABINE PHILIPPS
CLS, 8-10 rue Hermes, 31526 Ramonville St-Agne, France

Unlike classical radiometers, each point of the surface will be seen by SMOS with several incidence angles. All these informations will be used to retrieve salinity through an inverse process. The objective of this paper is to compare performances obtained with two different inversion methods to retrieve salinity from the SMOS measured brightness temperatures. Two kinds of inversion methods are compared in the same conditions: iterative and neural methods.

SMOS measurements can be modelized at different incidence angles with a direct model which takes into account the sea dielectric constant (depending on temperature and salinity), and the surface roughness (depending on the wind speed). Thus we constitute a complete global database containing a large number of geophysical parameters triplets (surface salinity, surface temperature, wind speed). This database must be as complete as possible to contain almost all geophysical situations.

The two inversion methods are compared through the following methodology:
1) Simulations of SMOS measured brightness temperatures on the database in two steps: i) for each triplet, simulation of the brightness temperatures using a direct model, ii) addition of a realistic noise to these brightness temperatures depending on the incidence angles.
2) Many studies have shown that the use of the brightness temperatures only will be insufficient to retrieve the salinity with enough accuracy to reach the GODAE requirements and that an a-priori knowledge of the surface (wind speed, temperature and eventually salinity) will be necessary. Once SMOS in flight, these values will come either from in-situ measurements (ARGO network) or other in-flight satellites (Quickscatt for the wind speed, Aquarius for the salinity...). The simulation of these ancillary parameters is performed adding a given noise on each geophysical triplet of the database to simulate the error on these a-priori

values (1°C for the temperature, 1psu for the salinity and 2 m/s for the wind speed).

3) Both inversion methods are developed and optimized (architecture of the network for the neural method, and use of a BFGS quasi-Newton inversion for the iterative method).

Application on the simulated measured brightness temperatures using simulated ancillary parameters. The accuracy of each inversion method is given by the standard deviation between the original salinity in the database and the one retrieved from the measured brightness temperatures.

Advantages of each method are pointed out in terms of accuracy, sensibility to noises and biases, computer time, flexibility, suitability in an in-flight context.

Uncertainties in the retrieval of sea salinity from L-Band radiometer measurements

NIELS SKOU
Building 348, Technical University of Denmark, DK-2800 Kgs. Lyngby, Denmark

An L-band radiometer can measure sea salinity from space. But the brightness temperature as seen by the radiometer depends also on a range of other geophysical parameters, and these dependencies must be identified so that proper countermeasures and corrections can be carried out. Note that the following only deals with external geophysical parameters. The radiometer itself is assumed perfect (no drift, no noise, perfect calibration).

Of fundamental nature is the fact that the radiated brightness temperature from the sea not only depends on salinity but also on sea surface temperature and surface roughness. The temperature dependence is not big, it is well understood and modeled, it is well measured by other sensors, and it varies slowly with time. Hence, it can be corrected for and it presents little problems. This is not the case for roughness issues! Classically, the roughness to be dealt with in this context, i.e. the roughness that perturbs the L-band radiometric signature, has been assumed a direct function of wind speed. This is certainly true at the higher microwave frequencies substantiated by the many microwave methods that can be used to yield meaningful wind speed data. These frequencies are through Bragg scattering sensitive to capillary waves, that again are directly dependent on wind speed (and direction). L-band, however, is with its 21 cm wavelength rather more sensitive to short gravity waves, that may not be directly dependent on wind speed, but may also depend on other circumstances that contribute to the development of the sea like swell and past wind speed and direction. It seems that these short gravity waves present a problem in several ways: concerning modeling and wave spectrum research,

longer gravity waves proper are much better understood - likewise for capillary waves. Concerning interaction with radio waves, the mechanisms are well understood from C-band and up through the microwave region. Present models predict even 21 cm waves to be in equilibrium with wind in a few seconds. Does this really hold true? But apart from these fundamental issues affecting the radiated brightness temperature, also modifications introduced by the intervening ionosphere and atmosphere, as well as sky radiation reflected in the sea surface must be accounted for. The ionosphere introduces Faraday rotation, which can be corrected for or circumvented by using the first Stokes parameter for salinity retrieval. In both cases this has significant impact on sensor design. The atmosphere introduces loss and emission due to water vapor (even at L-band) and oxygen, which can be corrected for. Galactic noise is reflected in the sea surface, and can in principle be corrected for as it is well mapped. However, to do the calculations it is really the bistatic scattering coefficient that is required, and is this readily available? Finally, reflected sun radiation enters a few pixels on occasion (scattering coefficient again), and the sun occasionally also directly enters a few pixels through aliasing. So, there is a range of issues to be discussed.

Foam-covered and rain-roughned sea surface emissivity at L-Band: results from the frog 2003 experiment

Adriano José Camps, Mercedes-Magdalena Vall-llossera, Ramon Villarino, Ignasi Corbella, Nuria Duffo, Francisco Torres, Rubén Rodriguez, Roberto Sabia, Sandra Monerris
Universitat Politécnica de Catalunya, Departamento de Teoria del Senyal i Comunicacions, c. Jordi Girona 1-3, 08034 Barcelona, Spain

Sea surface salinity can be measured by passive microwave remote sensing at L-band, where there is a reserved frequency band (1.400-1.427 MHz). This band is a compromise between the brightness temperature sensitivity to the salinity, small atmospheric perturbation, and reasonable pixel resolution (1). In May 1999 the European Space Agency (ESA) selected the Soil Moisture and Ocean Salinity (SMOS) Earth Explorer Opportunity Mission (2, 3), to provide global soil moisture and ocean surface salinity with three-day revisit time. SMOS will be the first two-dimensional (2-D) synthetic aperture radiometer for Earth observation and has been recently approved for phase C/D.

The ocean emission basically depends on two factors:

i) the sea water permittivity, which is a function of salinity, temperature and frequency, and

ii) the sea surface parameterization, which is given by the wind-in-

duced wave spectrum, swell and rain-induced roughness spectrum, and the foam coverage and its emissivity.

Theoretical (4) and experimental results (5) confirm a small, although non-negligible impact of the sea foam in the L-band brightness temperatures at wind speeds above 12 m/s. This paper presents the results of a controlled experiment to measure the foam emissivity vs. salinity and foam thickness, and the sea surface emissivity roughened by artificial rain. In addition, it presents the first experimental results to describe the effect of rain over the sea surface at this frequency.

The field experiment was carried out in support of the SMOS mission at the IRTA facilities at the Ebro river mouth during the April-May 2003. Fresh water from the Ebro river and salt water from the Mediterranean sea were mixed in a 3 m × 7 m pool to cover the range of salinities from 0 to 37 psu. The foam layer over the water surface was created by pumping a controlled air flow through a net of 104 air diffusers. The artificial rain was created by pumping fresh water up to 10-12 m height, and releasing it through a net of diffusers covering the whole pool. During the rain experiment the pool was filled with fresh water so that the artificial rain did not modify the water salinity during the experiment.

REFERENCE

(1) C.T. Swift, R.E. McIntosh, *Considerations for microwave remote sensing of ocean-surface salinity*, IEEE Trans. Geosci. Electron., **GE-21** (4), pp. 480-491, 1983.

(2) M. Martín-Neira, J.M. Goutoule, *A two-dimensional aperture-synthesis radiometer for soil moisture and ocean salinity observations*, ESA Bull. no. 92, pp. 95-104, Nov. 1997.

(3) P. Silvestrin, M. Berger, Y. Kerr, J. Font, *ESA's second earth explorer opportunity mission: The soil moisture and ocean salinity mission, SMOS*, IEEE Geosci. Remote Sensing Newslett., Mar. 2001.

(4) A. Camps, M. Vall-.llossera, J. Miranda, N. Duffo, *Emissivity of the sea surface roughned by rain: simulation results*, IGARSS 2001, Sydney, Australia, July 2001.

(5) R. Villarino, et al., *Sea surface emissivity at L-band. Results of the wind and salinity experiments WISE 2000 and 2001*, SPIE's 10th Intern. Symp.on Remote Sensing, Barcelona (Spain), 8-12 September 2003.

SESSION 2
SEA, WIND, ICE
(*Chairpersons*: A. Shibata, N. Skou)

WINDSAT Calibration and validation efforts at NOAA/NESDIS/ORA

Laurence Connor, Paul Chang, Zorana Jelenak, Nai-Yu Wang
NOAA-NESDIS, Office of Research and Applications, 5200 Auth Road, Camp Spring,
MD 20746, USA
Tim Mavor
Division Systems Technologies Inc., 7381 Calhoun Place, Suite 600, Rockville, MD 20855,
USA

Since the January 6, 2003 launch of the Naval Research Laboratory satellite Coriolis, the WindSat instrument onboard has provided several months of unprecedented polarimetric microwave measurements of the globe. The WindSat radiometer has five operating frequencies at 6.8, 10.7, 18.7, 23.8 and 37 GHz, with the 10.7, 18.7, and 37 GHz channels providing fully polarimetric signals. The primary mission of Coriolis is to exploit the unique information provided by WindSat's polarimetric capabilities to retrieve the complete ocean surface wind vector (speed and direction), though the retrieval of numerous other environmental parameters is being actively pursued as well.

As part of a pre-NPOESS risk reduction effort, the NOAA/NESDIS/ Office of Research and Applications has been collaborating with the Naval Research Laboratory's Remote Sensing Division in the calibration/validation of WindSat in preparation for the release of WindSat data products to the scientific and operational communities.

An extensive overview is presented of the WindSat calibration/validation effort being put forth at NOAA/NESDIS and the associated comparison databases constructed for that purpose. These databases include data of WindSat measurements colocated with measurements from oceanographic buoys, ships, other satellites, and global data assimilation models. The strengths and limitations of these various datasets will be discussed in detail. This includes a synopsis of the colocation strategies used in matchup database construction for comparing WindSat measurements with other satellite based measurements, focusing particularly on similar orbit SSM/I data and its use in brightness temperature calibration. In addition, the use of NCEP's Global Data Assimilation System (GDAS) as a powerful source of plentiful comparison data is explored, particularly with regard to WindSat model function development.

Estimated effects of foam on ocean surface microwave emission: inferences from passive polarimetric observations of reproducible breaking waves

STEVEN C. REISING, SHARMILA PADMANABHAN
Electrical and Computer Eng. Dep., University of Massachusetts Amherst, 151 Holdsworth Way, Amherst, MA 01003-4410, USA
WILLIAM E. ASHER
Air-Sea Interaction and Remote Sensing Dept., Applied Physics Laboratory, University of Washington, 1013 NE 40th Street, Seattle, WA 98105, USA
L. ALLEN ROSE, PETER GAISER
Naval Research Laboratory, 4555 Overlook Ave. SW, Washington, DC 20375, USA

WindSat was launched on January 6, 2003, to demonstrate near-daily global retrieval of both wind speed and direction using passive microwave measurements. This mission, accomplishing the first polarimetric microwave radiometer on orbit, also constitutes a pre-launch risk reduction for the development of the Conical Microwave Imager Sounder for the NPOESS satellites over the next five years. To date, aircraft and WindSat measurements, as well as modeling results, indicate that wind direction signals are small, on the order of 1-3 K peak-to-peak. Accurate wind vector retrieval requires quantitative understanding of the dependence of ocean surface emissivity on surface parameters, including roughness and foam.

Our recent open ocean observations from the R/P FLIP during the Fluxes, Air-Sea Interaction and Remote Sensing (FAIRS) experiment showed that the increase in brightness temperature related to foam depends on polarization and on incidence and azimuth angles with respect to wave breaking. In contrast with aircraft and satellite measurements, platform and tower experiments increase the number and reliability of   physical measurements available for comparison with the observed changes in polarimetric brightness temperatures. However, the inherent intermittency and relative sparseness of oceanic breaking waves strongly limits our ability to determine the effects of incidence and azimuthal angle variation reproducibly.

To overcome this limitation of oceanic experiments, we recently performed polarimetric microwave measurements of mechanically generated waves made to break repeatedly in the same location in a salt-water basin. Passive polarimetric measurements were performed at WindSat frequencies of 10.8, 18.7 and 36.5 GHz, at incidence angles of 45°, 53° and 60°, and each of those at four azimuth angles from 0° to 180°. The beam fill fraction of the foam produced by the breaking waves was estimated using a video camera bore-sighted with the radiometers. Void fraction probes and an underwater camera were used to measure the amount of entrained air and the bubble size spectrum, and pressure transducers measured the surface height of the

large-scale waves.

Results of this experiment were used to provide a quantitative assessment of the azimuthal dependence of the microwave emission due to wave breaking. These results show that the change in the measured microwave brightness temperatures was well correlated with the foam fraction in the field of view, but that the foam coverage in the field of view depends upon the azimuthal look angle, due to viewing different facets of the partially foam-covered water surface. These results constitute an important step toward quantitative determination of the errors in wind speed and direction retrieval caused by omitting the effect of foam from the surface modeling.

An anomalous microwave emission of ocean surface revealed by comparison with AMSR and seawinds data

AKIRA SHIBATA, KEIJI IMAOKA, HIROSHI MURAKAMI
Earth Observation Research and Application Center/JAXA, Harumi Island Triton square, Office Tower X 22F, 1-8-10, Harumi, Chuo-ku, Tokyo 104-6023 Japan

The microwave emission of calm ocean surface obeys the Fresnel equation, which can be calculated by giving several parameters, such as sea surface temperature (SST), salinity, and incident angle. Under windy conditions, the ocean surface becomes roughened, and the microwave emission changes. It is known that the change related with wind depends on both frequency and polarization. At the incident angle of around 55 degree, the emission of vertical polarization changes almost zero, and the horizontal one increases monotonously under weak wind less than about 7m/s. But, in rare cases, its behavior seems to be modified. Such an anomalous emission can be surveyed intensively by using composite data observed by two spaceborne microwave sensors. On ADEOS-II launched by JAXA (old NASDA) in Dec. 14, 2002, two microwave sensors are loaded; one is the Advanced Microwave Scanning Radiometer (AMSR) of JAXA, and the other is the SeaWinds of NASA's scatterometer. Both sensors measure ocean wind speed by different methods. AMSR measures the microwave emission change of ocean surface, and SeaWinds measures the microwave backscatter from the ocean surface. In most cases, two wind speeds agree well with each other in the global ocean. But, off California of US, strange relationships between AMSR and SeaWinds data are sometimes observed. A pattern of areas, where those anomalous relationships appear, coincides with the pattern of SST. Similar anomalous data are observed off Morocco of Africa. Possible mechanisms inducing anomalous relationships will be discussed.

The retrieval of gravity-capillary spectra by means of microwave radiometric techniques

Alexey Kuzmin, Michael Pospelov

Space Research Institute (IKI), 84/32 Profsoyuznaya Str., 117997 Moscow, Russia

This paper presents the results obtained during microwave remote sensing measurements carried out on the Black Sea coast in 1999 - 2001. The experiments were conducted from a pier in the South Department of the Shirshov Institute of Oceanology using microwave radiometers at wavelengths of 1.5, 0.8 and 0.3 cm. Surface wave spectrum parameters were retrieved from angular radiometric measurements using a novel approach. The evolution of spectrum parameters under unstable wind (ranged from 0.5 to 7 m/s) was investigated.

The determination of wavenumber spectrum of gravity-capillary waves is one of the most challenging tasks in the ocean surface study. Although a series of experiments have been undertaken over the last 20 years to collect suitable measurements by optical and radar technologies, general knowledge in this field is far from satisfactory. The variance of different models and published tank/field results is dramatically large for waves shorter than 10 cm, and the predicted spectral density can differ by one order of magnitude or more.

Currently, three main approaches are used for gravity-capillary wavenumber spectrum investigations. The first approach is based on the measurements by scanning laser slope sensors. The second one considers the sea surface radar backscatter with an adjustment of spectral parameters to provide the best fit with radar data. Our approach is based on microwave radiometric measurements. It has been demonstrated recently that a set of polarimetric measurements made at different angles can be converted to the mean squared slope of long waves and the curvature spectrum in the gravity-capillary interval.

Brightness contrasts at Ka-band (37 GHz) were used for measuring a curvature spectrum of gravity-capillary waves and a mean-square slope of large waves. It is shown that the position of a secondary spectral maximum is in the vicinity of wave numbers relevant to a minimum of a phase velocity. The range of a capillary cutoff where the mechanisms of a viscous dissipation start to play a dominant role is on wave numbers about 10 rad/cm.

The dynamics of the microwave brightness under alternating wind conditions has been explored in details. The new effect of the brightness delay was found. The delay of brightness variation relative to wind speed decreasing reached as large as 1-2 hours. The performed spectral analysis permitted to relate the observed brightness delay to short gravity-capillary surface waves, whereas longer gravity waves followed the wind practically

without any delay.

The obtained results can be used for interpretation of satellite data and development of new algorithms of wind speed measurements.

Sea ice remote sensing using AMSR 89 Ghz data

Georg Heygster, Lars Kaleschke, Gunnar Spreen
Institute of Environmental Physics, University of Bremen, P.O. Box 330440, 28334 Bremen, Germany

Recent progress in microwave remote sensing of sea ice has been stimulated by two new developments: First, the new sensors AMSR (Advanced Microwave Scanning Radiometer) aboard MIDORI-2 (formerly: ADEOS-2) and AMSR-E on TERRA have horizontal resolutions of 6×4 km at 89 Ghz. This is nearly three times the resolution of the standard sensor SSM/I (15×13km) at 85 GHz. The reason are the larger antenna reflectors of AMSR (2 m diameter) and AMSR-E (1.6 m) in comparison to SSM/I (65 cm). The sampling distance at the high frequencies is 12.5 km at SSM/I and 5 km at the AMSR and AMSR-E instruments, both together denoted AMSR(-E). The radiometric resolution of AMSR(-E) is enhanced by two separate receivers doubling the total integration time available for the A and B scans at 89 GHz. Second, it has become possible to correct the sea ice concentrations retrieved from the channels near 90 GHz for the atmospheric influence. This allows to fully exploit their horizontal resolution which is two to three times finer than the one of the channels near 19 and 37 Ghz. These frequencies are used by the most widespread algorithms for sea ice retrieval, the NASA Team and Bootstrap algorithms. Moreover, the polarization near 90 GHz is less sensitive to snow layering, and less influenced by refrozen melt ponds which both may cause interferences at the lower frequencies. These two developments have been combined to determine sea ice concentration maps. The used ASI (Artist Sea Ice) algorithm combines a model for retrieving the sea ice concentration from SSM/I 85 GHz data proposed by Svendsen et al. with an ocean mask derived from the 18- 23- and 37-GHz AMSR data using the Advanced Bootstrap Algorithm and a weather filter. The increased resolution reduces the errors due to mixed coastal pixels. This is particular useful when mapping coastal polynyas and smaller seas such as the Baltic Sea, Caspian Sea and the Okhotsk Sea of which examples will be demonstrated. For this purpose, the AMSR data are projected into grids of sampling sizes down to 3 km. Validation with data of the AMSR validation campaigns is in progress.

An empirical ocean surface wind vector retrieval from windsat polarimetric measurements

ZORANA JELENAK, NAI-YU WANG, LAURENCE CONNOR, PAUL CHANG
UCAR/NOAA/NESDIS, Office of Research and Applications, 5200 Auth Road, Camp Spring, MD 20746, USA
TIM MAVOR
Decision Systems Technologies, Inc., 7381 Calhoun Place, Suite 600, Rockville, MD 20855, USA
PETER GAISER
U.S. Naval Research Laboratory, 4555 Overlook Ave SW, Washington, DC 20375, USA

A new era in passive microwave remote sensing was started with the 6 January 2003 launch of the U.S. Naval Research Laboratory's Coriolis satellite, carrying the first spaceborne fully-polarimetric multi-frequency microwave radiometer specifically designed for the complete retrieval of ocean surface wind vector - WindSat. In a 845-km polar orbit, WindSat renders fore and aft swath measurements at five channels: 6.8, 10.7, 18.7, 23.8 and 37 GHz; with the 10.7, 18.7 and 37 GHz channels having full polarimetric capabilities. The 6.8 and 23.8 GHz channels are intended for estimation of the atmospheric and sea surface temperature contributions to the measured signals.

Polarimetric microwave radiometers directly measure naturally originating thermal microwave radiation from the wind-roughened ocean surface, which is in general partially polarized. The full characterization of the ocean surface emission polarization state by WindSat is achieved by measuring the full radiometric vector (four Stokes parameters) at the three fully polarimetric channels. Measured microwave thermal emission from the wind-induced ocean surface roughness shows small but a distinct signature with the respect to the wind direction relative to the radiometer's azimuth angle, especially in the third and fourth Stokes parameters. This allows for full ocean surface wind vector retrieval from these measurements.

The microwave thermal emission from wind-roughened sea surface is also affected by sea surface temperature, foam, salinity and the atmospheric state between the sensor and the surface. Using several months of WindSat measurements collocated with both the NCEP Global Data Assimilation System model field and the Special Sensor Microwave Imager (SSM/I) measurements, we have derived an empirical geophysical model that describes Stokes vector as a function of surface parameters (wind speed, wind direction, sea surface temperature) and atmospheric parameters (oxygen, water vapor and cloud liquid water amount). By applying regression techniques on multi-channel WindSat measurements the atmospheric and sea surface temperature influence on the observed signals were estimated, allowing the reduction in the number of geophysical model function parameters for ocean surface wind vector retrieval.

We present here an empirical based ocean wind vector retrieval algorithm from Windsat polarimetric measurements.

SESSION 3
MISSIONS AND EXPERIMENTAL CAMPAIGNS. PART I
(*Chairpersons: B. Greco, P. Waldteufel*)

Passive microwave imaging of hydrological variables during the 2003 AMSR-E calibration and validation campaign

MARIAN KLEIN, VLADIMIR LEUSKI
CIRES, University of Colorado, 216 UCB, Boulder, CO 80309-0216, USA
ALBIN J. GASIEWSKI, BOBA B. STANKOV, GARY WICK
NOAA/ETL, David Skaggs Research Center, 325 Broadway, Boulder, CO 80305-3328, USA
VLADIMIR IRISOV
Zel Technologies Inc., 55 West Queens Way, Suite 208, Hampton, VA 23669, USA
BOB L. WEBER
STC, Science and Techn. Corp., 325 Broadway, Boulder, CO 80305-3328, USA

The NOAA Environmental Technology Laboratory operated the airborne Polarimetric Scanning Radiometer (PSR) during several experiments in support of calibration and validation of the EOS AMSR-E sensor during 2003. The PSR system was flown in both one- and two-scanhead configurations during over 180 flight hours to provide high-resolution passive polarimetric imagery of raincells, snow cover, sea ice, and soil moisture signatures. The PSR system is based on conically scanning radiometers that are able to fully simulate the AMSR-E scanning geometry, polarizations, and frequencies. Due to the high spatial resolution on the data and the varied conditions encountered during the campaigns a unique database of brightness temperatures was obtained.

The first experiment (Wakasa Bay, Jan-Feb 2003) occurred over the Sea of Japan and western Pacific Japanese coast with the purpose to study the impact of melting level on passive microwave rain signatures. Imaging occurred during flight lines crossing both maritime and orographic precipitation. Cases of both snow and moderate to light rain were observed with melting levels from the surface up to ~8,000'. The Alaska sea ice experiment (AMSRIce03, March 2003) used two scanheads (PSR/CX and PSR/A) operating simultaneously, resulting in the first full polarimetric and spectral simulation of AMSR-E. Seven successful sea ice mapping missions were flown over a broad variety of ice classes with conditions ranging from open water to pack ice. The 2003 Cold Land Processes Experiments (CLPX03A, Feb 2003 and CLPX03B, March 2003) provided the first high spatial resolution (~0.4 km) microwave imagery of snowpack in mountainous areas

with observations occurring from the snowfall to melt stages. Inclusion of the PSR/CX scanhead for CLPX03B provided additional sensitivity to meltwater. The SMEX02 and SMEX03 experiments (June-July 2002 and 2003, respectively) used the PSR/CX for the first combined C- and X-band imagery of soil moisture in the presence of several types of vegetation canopies. Detailed spatial and temporal signatures of soil moisture variations were obtained on a ~1 km spatial scale.

Presented will be an overview of the PSR as configured for the 2003 AMSR-E experiments and a summary of the potential of airborne microwave hydrological imaging.

An image reconstruction and calibration approach for the SMOS aperture synthesis radiometer

Markus Peichl, Matthias Greiner, Volker Wittmann
DLR, Institute of Radio Frequency Technology, Oberpfaffenhofen, 82234 Wessling, Germany

The SMOS mission (Soil Moisture and Ocean Salinity) has the objective to observe two crucial variables, soil moisture over land and ocean salinity over sea. Both variables are used in predictive atmospheric, oceanographic and hydrologic models and may be important for extreme event forecasting. SMOS is based on an innovative 2-D L-band (1.4GHz), Y-shaped aperture synthesis radiometer to observe globally and with a revisit time of 3 days the brightness temperatures in H and V polarisation with a spatial resolution better than 50 km and with an angular coverage ranging from 0°-50°. A sun-synchronous (6 a.m. ascending), circular, 757 km orbit was proposed to ensure the requisite sampling, and at the same time to minimize signal perturbing effects such as Faraday rotation, sun glint, and thermal differences in soils and vegetation.

The basic idea of aperture synthesis is to replace the large real aperture antenna of a radiometer by a thinned array of single small aperture antennas and to correlate the input signals in pairs. The basic part of an aperture synthesis radiometer is a two-element interferometer. The measurements are carried out in the spatial Fourier domain in dependence of the single antenna distances, the baselines or spatial frequencies, and the brightness temperature distribution can be found by a discrete Fourier inversion assuming an ideal and perfect system. The initial FOV is given by the antenna pattern of the single antenna elements and all pixels of an image are measured at the same time.

In the real world situation an imaging system never is ideal and perfect. In the case of aperture synthesis the technical system is quite complex and consists of many single components, each one having a unique non-ideal

transfer function. As an example, the single receivers' frequency response in amplitude and phase, the single antenna patterns, and the single correlators' computations can be more or less different. Furthermore drifts in the electronics and deformations in the mechanics by temperature changes or aging can occur. Additionally the received signals can be disturbed on the path from the scene to be measured to the antenna terminals of the instrument.

This paper outlines an approach as being developed and investigated for the SMOS instrument. It is based on the in-space measurements of well-known calibration targets like point sources in a low-power background as it could be provided by the Sun or the Moon. The use of multiple scenes, where the point-source is located on different positions within the usable field of view, allows the determination of a G-matrix describing the whole imperfect system. Once determined, the matrix can be used to compute efficiently the corrected and calibrated brightness temperature map of the actually observed scene. Simulation results to assess the performance of the approach are shown and discussed.

The COST720 temperature, humidity, and cloud profiling campaign: TUC

DOMINIQUE RUFFIEUX, BEATRIZ ANDRADE
MeteoSwiss, Aérological Station, C.P. 316, Les Invuardes, CH 1530 Payerne, Switzerland
RETO NATER
Dept. of Physics, University of Fribourg, ch. Du Musee 3, CH-1700 Fribourg, Svitzerland
TIM HEWISON, CATHERINE GAFFARD
Met Office, Meteorological Bldg., University of Reading, Reading RG6 6BB, UK

Within the COST720 Action Integrated Ground-based Remote-Sensing Stations for Atmospheric Profiling and in connection with the COST720 Swiss project integrated remote sensing system for physical and chemical atmospheric parameters, MeteoSwiss is organizing the Temperature, hUmidity and Cloud profiling campaign (TUC) in Fall 2003 - Winter 2004. Various Meteorological Services and Universities from Europe and United States are participating to the experiment. The main goals of TUC are:
- to test ground-based temperature and humidity profiling systems (microwave radiometers), using the operational aerological soundings (performed at the same location of Payerne, Switzerland) with a high-quality humidity sensor as reference,
- to study in particular their ability to detect PBL phenomena like temperature inversion, presence of fog, fog dissipation, low clouds formation and evolution,
- to test cloud detection systems (passive and active ground-based systems),

- to provide a dataset for studying the possibility of system integration for improving temperature and humidity profiling with ground-based remote sensing systems.

The paper will focus on the general aspects of the TUC campaign. Various types of microwave radiometers as well as complementary systems (aerological soundings, wind profiler, ceilometer, cloud radar, surface meteorological stations) will be continuously operated from November, 2003 until end of January, 2004. The ability of microwave radiometers to detect inversion layers during stable high pressure conditions over Central Europe will be illustrated with case studies.

The 2004 north slope of Alaska arctic winter radiometric experiment

ED R. WESTWATER, MARIAN KLEIN, VLADIMIR LEUSKI
CIRES, University of Colorado, 216 UCB, Boulder, CO 80309-0216, USA
ALBIN J. GASIEWSKI
NOAA/ETL, David Skaggs Research Center, 325 Broadway, Boulder, CO 80305-3328, USA
JAMES LILJEGREN
OE/Argonne National Laboratory, 9700 South Cass Avenue, Argonne, Illinois 60532, USA

Measurement of water vapor during the arctic winter is very difficult because of uncertainties in radiosonde measurements of water vapor during these cold and dry conditions. Previously, at warmer locations such as the Department of Energy's Atmospheric Radiation Measurements (ARM) Program's field sites in North Central Oklahoma, USA, and in the tropics, scaling of radiosonde measurements of water vapor profiles by microwave radiometer (MWR) precipitable water vapor measurements, has led to substantial improvements in water vapor measurements. However, due to the lack of sensitivity of conventional MWR's to low amounts of water vapor, say below 2 or 3 mm, it is difficult to achieve this scaling and/or the associated quality control checks on radiosonde data. We plan to conduct an Intensive Operating Period (IOP) at the ARM field site near Barrow, Alaska, during February-March 2004. The major goal is to demonstrate that millimeter wavelength radiometers can substantially improve water vapor observations during the Arctic winter. Secondary goals include forward model studies over a broad frequency range, demonstration of recently developed calibration techniques, the comparison of several types of *in situ* water vapor sensors, and the application of infrared imaging techniques. During this IOP, we plan to deploy radiometers over a broad frequency range (18 to 380 GHz), including several channels near the strong water vapor absorption line at 183.31 GHz. These radiometers will be supplemented by 4-times-a-day radiosonde observations and other in situ observations, including several "Snow White" Chilled Mirror radiosondes. The radiometers deployed will also be useful in measur-

ing clouds during these cold conditions. Radiometers to be deployed include the Circularly Scanning Radiometer of NOAA's Environmental Technology Laboratory (several frequencies from 18 to 380 GHz), the MWR and Radiometric Profiler of ARM (frequencies from 22.235 to 60 GHz), a scanning 60 GHz radiometer from the Russian firm ATTEX. and an infrared imager operated by Montana State University. In addition, all of the ARM active cloud sensors (radar and lidars) will be operating. Preliminary results from this experiment will be presented.

Ground-based remote sensing of clouds during the Baltex Bridge campaigns

SUSANNE CREWELL, ULRICH LÖHNERT, CLEMENS SIMMER, VICTOR VENEMA
Meteorologisches Institut, Universität Bonn, Auf dem Hügel 20, 53121 Bonn, Germany

In order to improve modeling and forecasting of clouds in climate and numerical NWP models the BALTEX BRIDGE campaigns (BBC) were conducted in the Netherlands in August/September 2001 and Mai 2003. Both campaigns combined ground-based, airborne and satellites observations as well as modeling activities. Here, we focus on the ground-based activities performed at the central facility in Cabauw, the main experimental site of the Dutch Weather Service. For continuous monitoring of the atmospheric state, microwave radiometers, cloud radars, lidar ceilometers, infrared radiometers and many more instruments were operated. A synergetic retrieval algorithm which explicitly includes microwave radiative transfer calculations was applied to the whole data set to obtain cloud liquid water, temperature and humidity profiles. The integrated profiling technique (IPT) combines brightness temperatures measured at 19 frequencies by the microwave radiometer MICCY, cloud radar reflectivity profiles, cloud base height derived from lidar ceilometer, ground-level meteorological sensors and a-priori information within an optimal estimation framework. A priori information is taken from interpolated nearby radiosonde measurements for temperature and humidity while a cloud microphysical model is used for the liquid water content. An important point is the accurate error description of all input parameters since this determines their contribution to the retrieved product. Because the method is not applicable in cases when cloud liquid water is present within multiple layer clouds, a cloud classification scheme is applied first.

One cause of retrieval uncertainty can be the forward model, e.g. the assumed water vapor absorption model. The problem is addressed by comparing microwave radiometer measurements at frequencies between 20 and 90 GHz with simultaneous high quality radio soundings. These can also serve as a validation for the retrieved humidity and temperature profile.

While the measurements described above provide profile information at one point with high temporal resolution it is also of interest to observe the horizontal variability. This is especially true for clouds which quite obviously have a high variability. Therefore, azimuth scans at different elevation angles have been performed with the MICCY radiometer. The presentation will introduce the BBC campaigns and focus on the use of microwave radiometry for studying clouds.

Structural and cloud-physical characteristics of solid precipitation observed by Wakasa Bay field campaign 2003 (Wakasa 2003)

KAZUMASA AONASHI
Meteorological Research Institute, Tsukuba, Ibaraki, Japan

Passive microwave retrieval of solid precipitation requires accurate microwave radiative transfer models (RTMs) for solid precipitation clouds. For the development of the RTMs, it is necessary to know horizontal and vertical structure of solid precipitation and its cloud-physical characteristics in the real atmosphere. Wakasa Bay Field Campaign 2003 (WAKASA2003) was performed to observe solid precipitation over the Sea of Japan during Jan-Feb. 2003. In the present study, the structural and cloud physical characteristics of the observed solid precipitation are investigated using the observation data. The results show:

1. Solid precipitation was caused three types of disturbances (winter Monsoon outbreaks, extra-tropical lows, and an upper-cold low) for the period.
2. Solid precipitation observed with ground-based radars had large variability in profiles and horizontal inhomogeneity, depending on the disturbance types:
   • During the winter Monsoon outbreaks, meso-scale precipitation bands with strong echo cells (several kilometers in size) were observed. The precipitation top levels were around 2-3 kilometers.
   • Near the center of the upper-cold low on Jan. 29, a strong precipitation band with a width of 10-20 kilometer was found. The precipitation top levels were around 4.5-5.5 kilometers.
   • Around the extra-tropical lows, stratiform precipitation was mainly observed.
3. Precipitation top levels observed with the radars were related with depth of convective boundary layer estimated from the upper-air radiosonde observation during the winter Monsoon outbreaks.
4. Large amount (more than 0.5 kg m^{-2}) of cloud liquid water content (CLWC) was retrieved with ground-based microwave radiometers near the meso-scale precipitation bands during winter Monsoon outbreaks. The retrieved CLWC did not have correlation with the observed solid precipitation.

SESSION 4
MISSIONS AND EXPERIMENTAL CAMPAIGNS. PART 2
(*Chairpersons M. Martin-Neira, E. Njoku*)

Weather products and validation using AMSU

Antony Reale
NOAA/NESDIS, Office of Research and Applications, Washington, DC 20233, USA

The National Oceanic and Atmospheric Administration, National Environmental Satellite Data and Information Service (NESDIS) operates a fleet of civilian, polar orbiting satellites which provide users and researchers with a global suite of atmospheric and surface data on a global scale. On May 13, 1998, the Advanced TIROS Operational Vertical Sounder (ATOVS) radiometer configuration onboard NOAA-15 was successfully deployed into a morning orbit, replacing TOVS, followed by NOAA-16 into an afternoon orbit, on September 21, 2000, and NOAA-17 into a mid morning orbit (half way between NOAA-16 and NOAA-15) on June 22, 2002. The ATOVS features the Advanced Microwave Sounding Unit which replaced the Microwave Sounding Unit (and Stratospheric Sounding Unit) previously onboard TOVS, and includes AMSU-B which provides high (horizontal) resolution moisture data, a forefront piece of information in the operational weather satellite landscape.

This report summarizes the Online (orbital) and Offline (support) processing systems operated by NESDIS for atmospheric sounding products from the current (and unique) 3-satellite configuration of ATOVS operational satellites, and presents results. The orbital sounding products include the derived temperature and moisture soundings, clouds, and associated radiometric measurements. Offline support systems provide continuous compilation of data sets, for example, collocations of satellite and ground truth (radiosonde) observations, and coefficients used to validate and "tune" the orbital products. Results address projected accuracies and information content in the respective contexts of the collocated radiosondes, global weather forecasts, and meteorological consistency on a global and regional scale.

The report opens with a brief synopsis of how the global satellite weather community has gotten to where it is today, and concludes with where we might be headed in the future. The requirements for derived (sounding) products have weathered a storm which almost eliminated them from the satellite information landscape during the late 1990's. As a result, the current vision underlying their production has veered from that of the original pioneers of over forty years ago, with expanding applications in weather and climate in addition to the general problem of numerical weather prediction for which they were originally intended. Among the lessons learned is that although user needs tend to vary over time and among users, an overall fundamental requirement is for "well-behaved" products,

that is, data that are reliable, internally consistent and traceable. Another lesson concerns validation, that the problem of validation is not straightforward, and that the ultimate success of any product or application depends on the availability and integrity of ground truth data. Their impact on future operational systems, including a perceived shortcoming of current polar satellite programs which lack a dedicated global network of ground truth (validation) data, is presented.

The SMOS mission: status of the project

YANN KERR
CESBIO, 18 ave. Edouard Berlin, bpi 2801, 31401 Toulouse Cedex 9, France
JORDI FONT
ICM/CSIC, Institut de Ciences del Mar, 08039 Barcelona, Spain
PHILIPPE WALDTEUFEL
CNRS/SA, Institut Pierre Simon Laplace (IPSL), Service d'Aéronomie, 91371 Verrières le Buisson, France
MICHAEL BERGER
ESA-ESTEC/EOP/SML, Postbus 299, Keplerlaan 1, 2200 AG Noordwijk, Netherlands
JEAN PIERRE WIGNERON
INRA, Institut National de Recherche Agronomique, EPHYSE, BP 81, 33883 Villenave d'Ornon, France

Surface soil moisture is a key variable of water and energy exchanges at the land surface/atmosphere interface. But currently there are no means to assess it on a global and timely fashion. Similarly, our current knowledge of sea surface salinity is very reduced. One way to overcome this issue would be to use an adequate space-borne Instrument. The most promising instrument would then be L-band microwave remote sensing sensors as they are able to provide estimates of surface soil moisture and sea surface salinity, on spatial and temporal scales compatible with applications in the fields of climatology, meteorology and large scale hydrology.

The ESA Earth Explorer Opportunity mission SMOS is the first attempt to fulfil such a gap. SMOS is based upon an L-band 2-D interferometer. It is thus an innovative concept of bi-dimensional aperture synthesis method to obtain surface measurement with an appropriate resolution from a tractable (in terms of dimensions) space-borne instrument. Moreover, the sensor has new and very significant capabilities especially in terms of multi-angular view configuration.

This paper will describe the SMOS concept in terms of instrument (characteristics) and will investigate the main aspects of the retrieval capabilities of the 2-D microwave interferometer for monitoring soil moisture, vegetation biomass and sea surface salinity. The analysis is based on model inversion taking into account the instrument characteristics. The standard error of estimate of the surface variables is computed as a function of the sensor configuration system and of the uncertainties associated with the

spatial measurements. The inversion process is based on a standard minimisation routine that computes both retrieved variables and standard error associated with the retrievals.

Never the less, retrieving surface variables from such an instrument is not necessarily straightforward. Over the oceans, a very high sensitivity and accuracy are required. Over land the main issues are linked to mixed pixels and topography. Using other sensors/mission (such as Aquarius over the oceans) and assimilation techniques will be used to address these issues.

The potential of SMOS, depending on the view angle configuration and the use of the sole 1.4 GHz is thus investigated. These questions are key issues to define the observation configuration of SMOS that meets the scientific requirements and the technical constraints of the spatial missions. A special attention will be devoted to the calibration plan.

NOAA operational hydrological products derived from the advanced microwave sounding unit (AMSU)

RALPH R. FERRARO, FUZHONG WENG
NOAA/NESDIS, Office of Research and Applications, Washington DC 20233, USA

NOAA generates operational hydrological cycle products (e.g., rain rate, total precipitable water, cloud and ice water path, snow cover, sez-ice concentration, land surface temperature and emissivity) from the NOAA-15, -16 and -17 Advanced Microwave Sounding Unit (AMSU) as part of a product system known as the "Microwave Surface and Precipitation Products System (MSPPS)". The objective of this paper is to provide the current status of the MSPPS (originally reported at the 7th Meeting in 2001): algorithms utilized, products generated, validation/accuracy of these products and their applications. In addition, near-term enhancements to MSPPS will be discussed (e.g., snowfall detection and snow water equivalent products, upcoming launches, etc.) as well as long-term plans.

The proposed european GPM (EGPM) satellite

ALBERTO MUGNAI
CNR - ISAC, Via del Fosso del Cavaliere 100, 00133 Roma, Italy
PETER BAUER
The European Centre for Medium-Range Weather Forecasts (ECMWF), Shinfield Park, Reading, RG2 9AX, UK
PAUL JOE
Meteorological Service of Canada, 4905 Dufferin Str., Downsview M3H 5T4, Ontario, CA
CHRIS KIDD
University of Birmingham, School of Geography, Earth and Environmental Sciences, Edgbaston, Birmingham B15 2TT, UK
MARIA DEL CARMEN LLASAT

Dept. Astronomy and Meteorology, Faculty of Physics, University, 08028 Barcelona, Spain
GIORGIO ROTH
CIMA, Centro di Ricerca Interuniversitario di Monitoraggio Ambientale, Via Cadorna 7,
17100 Savona, Italy
JACQUES TESTUD
Novel Initiative for Meteorological and Environment Technologies (NOVIMET), 10-12
avenue de l'Europe, 78140 Vélizy, France
PAUL INGMANN
ESA-ESTEC, Postbus 299, Keplerlaan 1, 2200 AG, Noordwjik, Netherlands

At the beginning of January 2002, an international scientific consortium (the EGPM Science Team) constituted by numerous scientists involved in several disciplines related to precipitation, submitted to the European Space Agency (ESA) a proposal titled "EGPM: European contribution to the Global Precipitation Mission" in response to ESA's second call for proposals for Earth Explorer Opportunity Missions (EEOMs).

The principle objective of the EGPM proposal was to encourage ESA to directly engage in the international organization for the Global Precipitation Measurement (GPM) mission formulated by NASA and NASDA, by providing one member of the GPM constellation of satellites aimed at providing frequent global rainfall observations for an extended operations period starting in the time frame of 2007. Noteworthy, a large part of the European scientific and operational community is strongly interested in GPM. Especially, the operational community related to numerical weather prediction (NWP), nowcasting and hydrological hazards would take advantage of Europe being part of the constellation, because this would guarantee direct access to real-time data.

The proposed EGPM satellite should satisfy, as an integral and essential component of the GPM constellation, the following specific requirements:
• Improve rainfall estimation accuracy;
• Enhance the detectability of light rain and snowfall, specifically over land, as appropriate for Northern Europe and Canada and in mid-latitude oceanic perturbations;
• Provide a significant contribution to the monitoring and the understanding of hazardous and flash-flood producing storms along the Mediterranean coasts;
• Improve the forecast skill of global and regional NWP models through data assimilation of precipitation measurements;
• Provide near real-time as well as global data acquisition.

To this end, the scientific payload of the EGPM satellite would consist of an advanced conically scanning microwave radiometer and (as a very desirable option) of a three-beam nadir-pointing Ka-band rain radar. In this paper, we describe the characteristics of the EGPM constellation member, that is presently under Phase A study. In a companion paper, we investigate the potential contribution of the EGPM radiometer to precipitation measurements.

SESSION 5
LAND: SOIL AND VEGETATION
(*Chairpersons*: S. Paloscia, A. Shutko)

Soil moisture retrieval and algorithm evaluation for AQUA/AMSR-E

Eni G. Njoku, Tsz Chan
Jet Propulsion Laboratory, California Institute of Technology, 4800 Oak Grove Drive, Pasadena, CA 91109, USA
Peter Ashcroft, Frank J. Wentz
Remote Sensing Systems, 438 First Street, Suite 200, Santa Rosa, CA 95401, USA

The Advanced Microwave Scanning Radiometer (AMSR-E) is one of six instruments launched in May 2002 on the Aqua spacecraft as part of NASA's Earth Observing System (EOS). The AMSR-E instrument was developed by the National Space Development Agency (NASDA) of Japan. It operates at six frequencies in the 6.9 to 89 GHz range with coverage over a wide swath, providing global observations every 2-3 days. The low-frequency data channels provide a capability for estimating soil moisture at a spatial resolution of about 60 km, over land areas of limited vegetation cover, based on use of the 6.9 GHz frequency channels. The initial AMSR-E soil moisture algorithm emphasized use of the 6.9 GHz channels to maximize vegetation penetration while minimizing atmospheric effects. In post-launch evaluations the 6.9 GHz channel data were found to be contaminated by radio frequency interference (RFI) over many regions, especially in the United States. Calibration biases in the processed sensor data also hampered use of the low-frequency channel observations over land. Modifications to the soil moisture retrieval algorithm have been made that avoid the RFI problem by using 10.7 GHz and higher frequency data. A revised instrument calibration algorithm has also been implemented by the AMSR-E processing team. Limitations on the soil moisture sensing capability that result from eliminating use of the 6.9 GHz data are a reduction of soil moisture sensitivity in vegetated areas and an increase in sensitivity to atmospheric moisture. A benefit is the improved spatial resolution available at 10.7 GHz. Specific attention must be paid to the vegetation and roughness (topography) corrections since these effects have greater impacts at higher frequencies.

Updated AMSR-E soil moisture products using the revised calibration and soil moisture algorithm are currently being generated, and re-evaluations of the products are being carried out. In this paper we provide assessments of the revised products and an outlook on the utility of the AMSR-E soil moisture measurements.

AVE radiometric observations of bare soil with known type of moisture profile

Anatoly Shutko, Alexander Chukhlantsev, Sergey Golovachev, Evgeniy Novichikhin, Alexander Haldin
Institute of Radioengineering and Electronics, Russian Academy of Sciences, 1 Vvedensky sq. Fryazino, Moscow Regio, 141190 Russia
Tommy L. Coleman, Frank Archer,
Alabama Agricultural and Mechanical University, Center for Hydrology, Soil Climatology and Remote Sensing (HSCaRS), Alabama A, USA

Microwave radiometry is the most informative of the remote sensing technologies for soil moisture determination. The fundamentals of this approach have been established and near-surface soil moisture retrieval algorithms have been verified using ground based experiments and aircraft observations. By using an appropriate inversion algorithm, the fractional amount of water present in the contributing soil depth can be estimated.

There are several theories describing the emissivity resulting from different soil profiles with non-uniform features. Numerous field studies and modeling efforts have shown that a near surface layer with the depth of 1/10 to 1/4 of the wavelength dominates in forming land surface emissivity. It implies that single-wavelength microwave radiometric measurements provide moisture content in upper 0-2 cm or 0-5 cm layer. This follows from the results of direct comparison between the emissivity data at the selected wavelengths and averaged soil moisture content in different near-surface layers. Obviously, this is a rather shallow depth that hardly can satisfy the requirements of agronomists and hydrologists. The lasts usually need the data on soil moisture in the upper 0-100 cm layer or at least in the upper 0-20 cm layer of the root-zone.

Where is the solution?

We believe that solution is in dual-wavelength radiometric measurements and prior knowledge-based soil moisture profile modeling.

This paper discusses the peculiarities in spectrum of natural microwave radiation from a bare soil in a wavelength range from 2 to 30 cm as related to the peculiarities in soil moisture profile. Attention is focused on the profiles in a process of drying. It is shown that assessments of soil moisture profile parameters and average moisture content in a 20 cm to 100 cm upper layer can be obtained based on a strong correlation of moisture data along the soil depth, especially in the conditions of drying when a transition layer is forming. In warm climates, when lands are irrigated, surface soil moisture becomes a very dynamic parameter that changes quickly. Thickness of the transition layer increases in the drying process. Changes of soil moisture in the transition layer have sufficiently great gradient.

This approach results in plotting a dual-frequency diagram for emissivity of bare soil versus thickness of the transition layer and soil moisture at a lower border below this layer. The use of these diagrams allows one to get an assessment of the thickness of a transition layer and soil moisture at its bottom. Further, this moisture can be related to the average moisture of the root zone or, using statistical procedures, to determine the water content in a meter layer.

Recent advances on microwave radiometry of forests

Paolo Pampaloni, Giovanni Macelloni, Simonetta Paloscia
IFAC-CNR, Via Panciatichi 64, 50127 Firenze, Italy

Although about half of the forests that was present before the spread of human influence, has disappeared, mostly through the impact of man's activities, a large portion of the earth's surface is still covered with forests. In recent years, the interest in remote sensing observation of forest ecosystems both on local and global scale has significantly increased. Indeed, forests act as an interface between soil and atmosphere, and an efficient monitoring of natural and anthropic changes can help gain an understanding of the hydrological and biochemical processes of gas and water exchanges between soil and atmosphere through vegetation.

Despite the coarse ground resolution, microwave radiometry from satellite offers a unique opportunity to probe forests at a global scale by operating at different frequencies. On the other hand, airborne sensors make a much better resolution possible, and can be useful for detailed analyses of some particular areas and surveillance of forests subject to fires or other sudden damage. Theoretical studies have shown that the brightness temperature is significantly sensitive to woody biomass and saturates at a higher level of biomass than backscattering coefficient does.

At present, only few experimental data, mostly collected on conifer forests are available. Airborne microwave radiometric measurements in a frequency range from L- to Ka band were carried out by IFAC-CNR in June 1999 and January 2002 on six broadleaved forests, including: beech, Turkey oak and Holm oak. The average size of plots, of the order of some hectares, was large enough to contain several antenna footprints. The main purpose of this investigation was to evaluate the potential of multi-frequency radiometry in separating forest types, estimating woody biomass, and in identifying the differences between summer and winter features of trees.

The observations have indicated the sensitivity of multi-frequency microwave emission to forest type and biomass. The most significant interaction mechanism between microwaves and trees is absorption at low frequency or low biomass and scattering at high frequency and high biomass.

The use of the highest frequencies (Ka and X) was successful in distinguishing different forest types, whereas L-band was found to be the most significant frequency channel for estimating tree woody volume and basal area. A fairly good sensitivity to LAI was found mainly at Ka band. A further analysis demonstrated that microwave bands can also be suitable for monitoring the stress conditions of forests since the differences between normalized temperatures at different frequencies (Ka- and C- band) was found to be sensitive to the crown transparency, which is a parameter influenced by the health conditions of trees. Differences in emissivity between winter and summer were mainly due to presence of understory and leaves, and to variations in plant and soil moisture. Thus, these differences were more significant at low biomass and low frequency, where contributions from soil and from soil-trunk interaction were particularly important. For higher values of biomass and/or frequency, emission was mostly dominated by branches and less sensitive to season. An estimate of the relative weights of these components to total emission was made by model analysis. Simulations performed at L-band with a discrete element radiative transfer model were found to be in reasonable agreement with experimental data. A model analysis showed that total emission from trees is mainly due to crowns and that the main contribution to crown emission is due to primary and medium branches.

Attenuation spectra of trees fragments

ALEXANDER CHUKHLANTSEV, SVETOSLAV MARECHEK
Institute of Radioengineering and Electronics, Russian Academy of Sciences, 1 Vvedensky sq., Fryazino, Moscow Region, 141190 Russia

Forests play a vital role in humankind life since they represent about 90% of the standing biomass and determine the hydrological and biogeochemical cycles of the Earth system. Remote sensing techniques, in particular microwave radiometry, have the potential of monitoring forest canopies. However, interpretation of the microwave radiometric measurements requires a series of efforts such as developing an appropriate theoretical model of the forest canopy, establishing a relation between electrodynamic parameters of the forest medium and its biometric features, and estimating forest parameters from radiometric data. Knowledge of attenuation properties of forest canopies is extremely important in this respect. First of all, the propagation properties of the forest canopy play a central role in modeling microwave emission behavior of the canopy. Furthermore, attenuation values and their dependence on frequency, incident angle, polarization, as well as forest biometrical features, afford a basis for remote sensing retrieving algorithms.

Wide band waveguide transmission system is created and measuring technique is developed to obtain continuous attenuation spectra of vegetation fragments in the frequency range 0.8-8 GHz. The system consists of wide band rectangular waveguide, two horn antennas matched with the waveguide, and Vector Network Analyzer. The horn antenna transforms TEM-wave of coaxial cable into H_{10}-wave of rectangular waveguide. Since the divergence angle of antenna is not large, an excitation level of high-order waves is small. When H_{10}-wave passes through the camera it is attenuated by investigated object. The second horn antenna, in turn, transforms coming wave into TEM-wave of coaxial cable. Therefore, the antennas serve as the filters of spatial harmonics providing single-mode propagation regime in the waveguide and correct interpretation of attenuation measurements.

Attenuation spectra of aspen, birch, and maple trees parts are obtained. The following measuring procedure is applied. A big branch of the tree (or young tree) is cut. The branch is cut into smaller parts to fill the waveguide and to obtain attenuation spectrum of the branch as a whole. Then, the branch is cut into parts: thick branches with diameters of 3.5 cm, branches with diameters of 1.3 cm, and thin branches with leaves. Attenuation spectrum of every part is written down. After all, leaves are removed and attenuation by thin branches is measured to obtain the attenuation spectra of leaf component by subtracting attenuation by bare branches from attenuation by leafy branches. Attenuation measurements are accompanied by measuring the weight and gravimetric moisture of samples. Finally, attenuation values for every part are recalculated to find spectral dependences of specific attenuation for each of the tree components, i.e., attenuation per kg/m^2 of the component.

Microwave attenuation spectra of crops

SERGEY GOLOVACHEV, ALEXANDER CHUKHLANTSEV
Institute of Radioengineering and Electronics, Russian Academy of Sciences, 1 Vvedensky sq., Fryazino, Moscow Region, 141190 Russia

Retrieving biomass and soil moisture is considered as a fundamental application of passive microwave systems. Solving this problem meets a need of detailed experimental and theoretical studies on microwave attenuation properties of different crops. The paper summarizes the results of research in this field conducted by the authors during last two decades.

Several measuring techniques were proposed to obtain data on attenuation by crops. Measurements were fulfilled in the laboratory conditions under close control of biometric parameters, as well in the field conditions from the trucks and cars and from airplanes.

In the laboratory, passive microwave methods were used to obtain

attenuation spectra of crops models made of fresh cut plants to indicate the dependence of attenuation on the crop biomass, water content, and density. Different schemes of attenuation measurements were used (these measurements were conducted on the open test site):

1. Fresh cut crop samples were put on plane reflectors with reflectivity close to 1 and 0 (sheets of metal and absorbing microwaves material) and were measured using tunable microwave radiometers operating in the frequency band of 1.5-6 GHz and wideband antenna.

2. Crop samples were put in open horn (truncated pyramid) made of thick absorbing microwaves material and were measured using 2 cm radiometer.

In the laboratory room, active microwave methods were used to obtain attenuation spectra of crops:

1. Fresh cut crop samples were put on plane reflectors with reflectivity close to 1 and 0 and were measured using scalar network analyzers operating in the frequency band of 1.5-6 GHz and two wideband horn antennas (transmitting and receiving).

2. Waveguide transmission system was used to obtain continuous attenuation spectra of different types of crops in the 0.8-8 GHz band. This system consisted of two horn antennas matched with the waveguide, and Vector Network Analyzer.

On-truck field measurements were conducted with tunable microwave radiometer operating in the frequency band of 1.2 GHz and wideband antenna. In airplane measurements, microwave radiometers with operating wavelengths of 2.25, 6, 18, 21, 27 and 30 cm were used.

Results of measurements are presented in the form of frequency dependence of attenuation by different crops, such as corn, wheat, alfalfa, and others and compared with available experimental data obtained by other researchers and results of model simulations. The discrete model of vegetation canopy is used for calculation of attenuation values. The regression procedure is used to derive the simple formulas for estimating microwave attenuation by different crops.

Global soil moisture estimation: potential of available satellite observations from the infrared to the microwave

FILIPE AIRES
Dept. of Appl. Phys. and Appl. Mathem., Columbia University, NASA Goddard Inst. for Space Studies, 2880 Broadway, New York, N.Y. 100225, USA and CNRS/IPSL, Lab. de Météorologie Dynamique, Ecole Polythechinque, 91128 Palaiseau Cedex, France
CATHERINE PRIGENT
LERMA, Observatoire de Paris, 61 Avenue de l'Observatoire, 75014 Paris, France
WILLIAM B. ROSSOW
GISS/NASA, 2880 Broadway, New York, N.Y. 10025, USA

The sensitivity of available satellite observations to soil moisture is examined, at regional to continental scales for climatological applications. Satellite observations in the thermal infrared and in the microwave have shown some potential for soil moisture estimations. Soil moisture information can be inferred from the analysis of the diurnal cycle of surface skin temperature retrieved from infrared observations (e. g., Idso et al., JGR, 1975; Carlson et al., RSE, 1985). In the microwave region, changes of the dielectric soil properties with moisture induce measurable variations in the satellite microwave responses, for both passive and active observations (Owe et al., JGR, 1999; Vinnikov et al., JGR, 1999; Wagner et al., TGRS, 1999).

First, efforts have been to estimate the full diurnal cycle of Ts over continents, for clear and cloudy days. In clear sky conditions, Ts are estimated from thermal infrared measurements, from polar and geostationary satellite. The International Cloud Climatology Project provides clear sky estimates for the globe, with 30 km spatial resolution and a close to 3 h time sampling (Rossow and Schiffer, BAMS, 1999). A method has been developed to derive Ts under clouds, from combined infrared and passive microwave SSM/I observations (Aires et al., JGR, 2001). Statistical analysis of the Ts available estimate enables reconstruction of the full diurnal cycle (Aires et al., submitted JGR, 2003).

Second, land surface microwave emissivities have been calculated from the SSM/I observations (Prigent et al., JGR, 1997), by subtracting the atmospheric and cloud contributions. The ERS scatterometer observations have also been processed for a consistent estimate of the backscattering coefficients over the continents. In addition, the AVHRR relectances in the visible and near infrared have been collected and mapped to match the other satellite observations.

Sensitivity analysis of this suite of observations to the soil moisture is performed by comparison with two soil moisture data sets over two years (1993-1994):

– the Global Soil Moisture Data Bank (Robock et al., BAMS, 2000) that encompass in situ gravimetric measurements from XXXX stations;

– the soil moisture estimates from the Numerical Weather Prediction reanalysis of the European Center for Medium range Weather Forecast and National Center for Environmental Prediction.

The time records of the surface skin temperature (essentially the amplitude of the diurnal cycle), the passive microwave emissivities, the ERS backscattering and AVHRR visible and near IR reflectances are statistically examined as compared to the in situ soil moisture measurements and the NWP reanalysis values.

Preliminary results confirms the sensitivity of the Ts amplitude, passive microwave emissivities, and radar backscattering to the soil moisture content.

Soil moisture retrieval from two different vegetated sites -bare soil and fallow- with lewis 1.4 GHZ radiometer

MARIA JOSÉ ESCORIHUELA, YANN KERR, PATRICIA DE ROSNAY
CESBIO/CNRS/CNES, 18 ave. Edouard Berlin, bpi 2801, 31401 Toulouse Cedex 9, France
JEAN-CHRISTOPHE CALVET
Météo-France/CNRM, 42. Av. Coriolis, 31057 Toulouse Cedex 1, France
JEAN PIERRE WIGNERON
INRA - Bioclimatologie, Institut National de Recherche Agronomique, EPHYSE, BP 81, 33883 Villenave d'Ornon, France

The European Space Agency, in the frame work of the Earth Explorer Opportunity missions is planning to launch early 2007 the Soil moisture and Ocean Salinity (SMOS) mission. The project is a joint programme between ESA, the Centre National d'Etudes Spatiales (CNES) and the Centro para el Desarrollo Tecnológico Industrial (CDTI). In the context of the preparation of the SMOS mission over land, a field campaign (SMOSREX: for Soil Monitoring Of the Soil Reservoir EXperiment) is running since january 2003 in Mauzac, near Toulouse-France. The field campaign is a long term one and should last at least two years. It is based upon a ground based, dual polarised, high quality L-Band radiometer (LEWIS for L-band radiometer for Estimating Water In Soils) and a whole suite of ground measurements (vegetation and soil, meteorology, fluxes etc...). The aim of this campaign is to (i) contribute to a better understanding of the different processes affecting microwave signal including very specific events such a s interception and dew, freezing, etc. ...; (ii) improve the current algorithms; and (iii) to test the root zone soil moisture retrieval from dual polarized and multi-angular measurements for the preparation of the SMOS ground segment. The approach relies on using L-band brightness temperatures over long periods of time and for a variety of conditions. L-band microwave measurement are performed continuously at 40° inci-

dence angle over grass, and scanning up to 60° incidence angle over both bare soil and fallow every three hours (all dual polarised). We will present a method to retrieve soil moisture from multi-angular dual polarized L-band brightness temperatures applicable to SMOS data. The method is validated over a whole annual cycle on the two different surface types and including several perturbing effects.

Soil moisture sensing using AMSR

VENKAT LAKSHMI
Dep. Geological Sciences, University of South Carolina, Columbia, SC 29208, USA

Soil moisture has been shown to play a significant role in the hydrologic cycle as a boundary condition influencing infiltration, heat exchange and biogeochemical cycles. The launch of NASA's Aqua satellite on 4 May, 2002 provided the first opportunity for high temporal and large scale observation of global-wide soil moisture to be observed. The AMSR-E (Advanced Microwave Scanning Radiometer for the Earth Observing System) instrument onboard Aqua improves the spatial resolution and frequency range of earlier generations of passive microwave instruments. Brightness temperatures are simulated in an attempt to analyze heterogeneity effects and moisture retrieval methods for comparison with available observed AMSR-E data. The Ames, IA portion of the 2002 Soil Moisture Experiments (SMEX02) was successful in observing a large-scale rain event over the region. A semi-empirically-based radiative transfer model is used with the addition of surface and atmospheric parameters collected during the study. A description of the model simulation and heterogeneity effects will be given in addition to moisture retrievals and in-situ comparisons.

In addition, we will compare the simulated microwave brightness temperatures with those observed by the Polarimetric Scanning Radiometer - C-band (PSR-C) operated by NOAA-ETL. The soil moisture retrievals using the AMSR data over the SMEX02 region will be compared to the regional soil moisture observations. These studies will help us to gain confidence in using the AMSR derived soil moisture in regions of the world which lack in-situ observations.

SESSION 6
ATMOSPHERE: CLEAR AIR AND CLOUDS
(*Chairpersons*: *T. Hewison, C. Prigent*)

On the feasibility of using radiometrically-derived profiles of temperature and relative humidity for detecting cloud layers and amounts

PIERRE BOUCHARD
Earth-Space Propagation VPSAT, Communications Research Centre Canada, 3701 Carling Avenue, P.O. Box 11490, Station H, Ottawa, Ontario, Canada K2H 8S2

The Communications Research Centre Canada (CRC) in Ottawa, Ontario, has recently acquired a multifrequency microwave profiling radiometer to study and model the impact of clouds and water vapour on satellite links above 30 GHz. Among its numerous features, the instrument is capable of assessing the cloud base altitude of the lowest layer and the columnar cloud liquid water content continuously, unlike what can be achieved with radiosondes.

This paper will explore the possibility of using vertical profiles of temperature and relative humidity retrieved by this microwave radiometer to determine the bases and tops of clouds as well as amounts of individual layers (sky cover) using a technique originally developed by Chernykh and Eskridge (CE) for radiosonde profiles. Using radiometrically-derived profiles as input data to detect cloud layers and assess their sky cover would clearly provide several advantages over a radiosonde-based method: continuous and unattended measurements of the first 10 km of the troposphere made every few minutes, the use of true zenith profiles as input data (no uncontrolled horizontal drift through the atmosphere), to name a few.

The CE method determines the presence of cloud layers by monitoring the second order derivative of temperature $T(z)$ and relative humidity $R(z)$ vertical profiles. Conditions for detection of cloud layers are: $T''(z) >= 0$ and $R''(z) <= 0$. The cloud amount in percent is then estimated using the minimum dewpoint depression (i.e., the difference between the temperature at a given level and the corresponding dew point temperature) within the detected cloud layer and the corresponding temperature at that level. The dependence of cloud amount on dewpoint depression and temperature is presented in the form of the so-called Arabey diagram based on data from the former Soviet Union and the Indian Ocean.

Comparisons will be made between predictions based on the CE method using radiometric profiles and "ground truth" surface observations consist-

ing of our own co-located sky observations at CRC (based on the WMO International Cloud Atlas descriptions) supplemented by hourly cloud data from the Ottawa International Airport (a facility equipped with a ceilometer). These comparisons will include cases of low, middle and high cloud layers as well as cases of clear skies. Improvements to the CE method will also be described.

Monitoring inversions from ground-based remote sensing instruments during temperature, humidity, and cloud profiling campaign (TUC)

TIM HEWISON, CATHERINE GAFFARD, JOHN NASH
Met Office, Meteorological Bldg, University of Reading, Reading RG6 6BB, UK
DOMINIQUE RUFFIEUX, BEATRIZ ANDRADE
MeteoSwiss, Aérological Station, Les Invuardes, CP. 316, CH 1530 Payerne, Switzerland
RETO NATER
Dept. of Physics, University of Fribourg, ch. du Musee 3, CH-1700 Fribourg, Switzerland

Short-range weather forecasting of fog or stratus depends on accurate knowledge of boundary layer temperature inversions and hydrolapses. Such features develop rapidly, so they are not well represented by synoptic radiosonde profiles. Ground-based remote sensing instruments offer the potential to provide regular information on temperature and humidity profiles in real time. To investigate the capabilities of these systems to help forecasting these conditions, case studies will be examined.

During the Temperature, Humidity, and Cloud profiling campaign (TUC) of winter 2003-04, a number of sensors were operated at Payerne, Switzerland. For this study, we will use data from microwave radiometers: Radiometrics MP3000, Radiometer Physics HATPRO, Kipp & Zonen MTP5 and IAP's ASMUWARA. The accuracy of radiometer measurements can be assessed by comparison with forward modelled radiosonde profiles in clear sky conditions.

These radiometer are supplied with algorithms to retrieve profiles of temperature and/or humidity and/or liquid water cloud. In general, these retrievals combine observations near the 22 GHz water vapour line and in the 50-60 GHz oxygen band with prior information from a statistical climatology. Retrievals from these passive sounders typically have rather poor vertical resolution. This may be improved by combination with information from active instruments. During TUC, a cloud radar, UHF wind profiling radar and ceilometer were also available at Payerne, as well as operational and research radiosonde launches.

Case studies will be presented comparing radiometer retrievals to radiosondes and cloud radar profiles during the development of boundary layer inversions. The signal to noise ratio from wind profiling radar will also be examined during these cases to pursue the aims of COST Action

720 to integrate observations from different sensors.

The radiometers' ability to retrieve inversions will be tested to evaluate the benefits of elevation scanning and/or frequency scanning to obtain information on the vertical profile. We will also examine time series of retrievals for signatures that may be used to assist forecasting the formation or dissipation of fog or stratus.

Hurricane temperature structures obtained from satellite microwave measurements

FUZHONG WENG, TONG ZHU
NOAA/NESDIS, Office of Research and Applications, 5200 Auth Road, Camp Springs, MD 20746, USA

With the improved capability of radiative transfer modeling, we developed a new way of using satellite microwave sounding data for hurricane modeling and monitoring. Essentially, the satellite observations under cloudy and precipitation conditions are corrected to clear radiances by removing the cloud scattering and emission components from the measurements. To produce this correction, the radiosondes and dropsondes are collocated with satellite microwave measurements. The collocated data are first used to simulate the radiative components of atmospheric gases (e.g. oxygen and water vapor). The differences between satellite measurements and simulated radiances are used to determine a set of correction coefficients. At microwave frequencies, the brightness temperatures after correction can be directly utilized in one-dimensional variational retrieval to obtain temperature and water vapor profiles under cloudy conditions. This technique has been applied to NOAA-15, 16, 17 Advanced Microwave Sounding Unit (AMSU) and shown a great success in revealing a warm core structure of Hurricane Isabel. Formed in the tropical Atlantic Ocean on September 6, 2003, Hurricane Isabel rapidly intensified and became the fourth hurricane of the Atlantic region around 15:00 UTC September 7, 2003. At 0600 UTC September 12, Isabelle reached Category Five, centered at 56EW, 22EN, and had a maximum sustained wind of 160 mile per hour and a minimum sea-level pressure of 922 hPa. With the AMSU-A instrument on board NOAA-16 satellite, Isabel thermal structures are retrieved. At its mature state, Hurricane Isabel had an 8 K warm-core anomaly and a radius about 70 km, which is similar to Hurricane Bonnie in 1998 but its warm core size is somewhat smaller than that of Bonnie. The cold anomalies at lower levels (up to 10 K) are stronger than typically observed, partially resulting from inaccurate correction of strong scattering in heavy rainfall areas. This thermal-dynamic information obtained from the AMSU is being assimilated into NWP models to improve Isabel intensity and track forecasts.

Correlations between slant wet delays measured by microwave radiometry

Tobias Nilsson, Lubomir Gradinarsky, Gunnar Elgered
Onsala Space Observatory, Chalmers University of Technology, SE-438 92 Onsala, Sweden

A dense ground-based GPS receiver network and tomographic methods may be used to estimate the 3-dimensional distribution of the refractive index in the atmosphere. Given the geometry and the number of available GPS satellites it is necessary to apply constraints in space and time.

These constraints can be derived from models of the atmospheric turbulence. Here we address this problem by studying the correlation of the wet delay in two different directions using Water Vapor Radiometer (WVR) measurements at the Onsala Space Observatory from the period 2000-2003. By taking the squared difference between the measured wet delay (mapped to zenith) in two different directions we obtain a measure of how well the wet delays in the two directions are correlated. The time elapsed between the measurements of the two delays was not allowed to be too large (less than 200-300 s) so that the changes in the atmosphere during this time could be assumed to be small. It was investigated how the squared difference in the zenith mapped wet delay varies as function of the angle between the two directions. This was compared with what is expected in a turbulent atmosphere using the model from Emardson and Jarlemark (1). This model gives the expectation value of the difference in the zenith mapped wet delay as function of the angle difference and the elevations of the directions. By comparing the experimental results with the model, the turbulence parameter C_n could be estimated. This made it possible to investigate how the value of C_n changes under different conditions, for example how C_n changes as a function of the time of the year. We also assess C_n through analyses of 3-dimesional fields from numerical weather prediction models. In the beginning of 2003 the Onsala WVR was upgraded. A comparison of how well the measured delays agree with the model before and after the upgrade was made in order to assess the possible impacts of the instrumental uncertainties on the derived results.

(1) Emardson T.R., Jarlemark P.O.J., Journal of Geodesy, 73, 322, 1999

SESSION 7
ATMOSPHERE: CLEAR AIR AND CLOUDS. PART 2
(Chairpersons: S. Crewell, N. Grody)

Arctic stratospheric and mesospheric ozone and temperature profiles obtained with ground-based techniques

GIOVANNI MUSCARI, GIORGIO FIOCCO
Physics Dept., University of Rome "La Sapienza", P.le Aldo Moro 2, 00185 Rome, Italy
ALCIDE G. DI SARRA
ENEA C.R. Casaccia, Divisione Ambiente Globale e Clima, Via Anguillarese 301, 00060
S. Maria di Galiera, Roma, Italy
ROBERT DE ZAFRA
Physics Dept., State University of New York, USA

We present new ground-based measurements of polar stratospheric and mesospheric O_3 carried out from Thule (76.5° N, 68.8° W), Greenland, almost every day between January 21 and March 4, 2002, and between January 5 and February 22, 2003. We observe the rotational emission line of O_3 at ~277 GHz with a millimeter-wave receiver and two back-end spectrometers. The combination of the two spectrometers (a wide-band with 600 MHz of bandwidth and 1.2 MHz of resolution, and a narrow-band with 50 MHz of bandwidth and 65 KHz of resolution) allows retrievals of O_3 vertical profiles from 20 to 70 km altitude with an uncertainty of approximately ±10%, increasing to ±20% from 15 to 20 km and from 70 to 80 km.

During winter 2001/2002, temperatures in the Arctic stratosphere were unusually high, and only during a few days in December they reached values below the threshold for polar stratospheric cloud (PSC) formation. The absence over Thule of PSC particles during the entire duration of the measurements campaign is confirmed by concurrent backscattering measurements carried out with a Lidar system. As expected by such stratospheric conditions, our spectroscopic data show O_3 concentrations in the lower stratosphere larger than values usually observed in the Arctic stratosphere when chlorine and bromine compounds have been activated. However, the O_3 mixing ratios we observe in the lower stratosphere inside the polar vortex are lower by up to 40% (2 ppmv) than those measured outside the vortex only a few days before and after the passage of the vortex over Thule. Dynamics seems to play an important role in the formation of pockets of low O_3 concentration at high latitudes during both Arctic winters.

We also show upper stratospheric and mesospheric O_3 measurements combined with Lidar temperature profiles. The two sets of data can together

provide information on fast quasi-horizontal dynamical processes taking place across the polar vortex throughout the stratosphere, as well as on the slower vertical downward motion that characterizes the winter middle atmosphere over Polar regions. Although transport of air from the mesosphere to the stratosphere can be very important for the stratospheric budget of reactive nitrogen and therefore for ozone depletion, very few reliable estimates of vertical descent rates at upper stratospheric altitudes are available.

Precipitable water vapor and cloud liquid path retrieval from scanning microwave radiometer measurements during the 2003 cloudiness inter-comparison experiment

ED R. WESTWATER
CIRES, University of Colorado, 216 UCB, Boulder, Co 80309-0216, USA
VINIA MATTIOLI
DIEI, Facoltà di Ingegneria, University of Perugia, Via G. Duranti 93, 06125 Perugia

Ground-based microwave radiometers (MWR) are widely used to measure atmospheric Precipitable Water Vapor (PWV) and Cloud Liquid Water (CLW). Two dual-channel continuously scanning MWRs at 23.8 and 31.4 GHz were operated for two months (March and April 2003) during the Cloudiness Inter-Comparison Experiment (CIC IOP) at the Atmospheric Radiation Measurement (ARM) Program's Southern Great Plains site (SGP) in North-Central Oklahoma, USA. These scanning MWR measurements supplemented the operational SGP Central Facility MWR. The operational MWR scans continuously during clear conditions, but shifts to the zenith viewing Line Of Site (LOS) mode, during cloudy conditions. One of the additional MWRs scanned continuously in the same vertical plane as that of operational unit, while the second was scanning in a direction orthogonal to the other two. The primary goal of this work is the analysis of the MWRs data to derive a spatial distribution of PWV and CLW in the atmosphere, with the aim of improving the accuracy of parameterizations describing processes involved in the formation and evolution of clouds. Data from the three radiometers were compared during clear sky condition to assess their agreement. Differences of less than 0.5 K rms were obtained. Clear conditions were determined by combined radar/lidar measurements. Two different tipping calibration algorithms were considered (the original ARM calibration algorithm and the ETL calibration method), during clear and cloudy conditions. We evaluated the two calibration methods on the brightness temperature measurements as well as on PWV and CLW retrievals. Brightness temperatures and PWV were also compared with radiosonde (RAOB) computations. The RAOBs contained the Vaisala RS90 humidity sensor, and were launched at least four times a day on the same site. PWV and CLW

retrievals at each angle in presence of clouds were analyzed. We also compared the observed structures with optical and infrared cloud images, as well as ARM operational cloud boundary products.

Atmospheric humidity profiles over land from AMSU-B data

FATIMA KARBOU, LAURENCE EYMARD
CNRS/IPSL/CEPT, 10-12 Avenue de l'Europe, 78140 Vélizy, France
FILIPE AIRES
CNRS/IPSL/LMD, Ecole Polytechnique, 91128, Palaisseau, France
CATHERINE PRIGENT
LERMA, Observatoire de Paris, 61 Avenue de l'Observatoire, 75014 Paris, France
JUAN PARDO
Inst. Estructura de la Materia, Dpto Astrofisica Molecular e Infrarroja, Serrano 121, Madrid 28006, Spain

The Advanced Microwave Sounding Unit (AMSU-B) is a cross-track line-scanned humidity sounding system on board the new generation of the National Oceanic and Atmospheric Administration (NOAA) polar orbiting satellites.

The sounder has two window channels at 89 and 150 GHz and three other channels centred on the 183.31 GHz water vapor line. The instrument has a high geometric resolution (16 km at nadir) and samples 90 Earth views ranging from $-48.95°$ to $48.95°$ about nadir.

The 183 GHz AMSU-B channels enable deeper probing of the atmosphere as they measure the thermal emission of water vapor from different atmospheric layers. The AMSU-B window channels are sensitive to the lower troposphere water vapor and also to the Earth's surface. At these frequencies and over land, it is difficult to discriminate between the water vapor and the surface contributions. Consequently, the water vapor retrieval accuracies are better in the upper than in the lower troposphere.

Converting AMSU-B measurements to moisture profiles implies the resolution of non-linear processes. The humidity profile retrieval accuracies in the low troposphere could be enhanced by the knowledge of the land emissivity at AMSU-B window frequencies. We estimate microwave emissivities at 89 and 150 GHz over the globe and for different zenith angles by removing the contribution of the atmosphere, clouds, and rain using ancillary satellite data (the International Satellite Cloud Climatology Project (ISCCP) and the European Centre for Medium-Range Weather Forecast (ECMWF) products).

In this experiment, we focus on the tropical regions. The ECMWF temperature and humidity profiles collocated with ISCCP cloud free skin temperatures and previously calculated microwave emissivities at AMSU-B window channels are used to generate a learning dataset. A state of the art microwave

radiative transfer model is used to simulate AMSU-B observations. A neural network approach including first guess information is train on the learning data set to retrieve atmospheric humidity profiles from AMSU-B data. Our calculation scheme takes advantage of the knowledge of the land emissivity at lower frequencies as a first guess to constrain the inversion process.

In this study, the humidity profile retrievals using a neural network method is discussed. Preliminary results are presented and compared with available real atmospheric measurements (radiosondes).

The application of SSMI total precipitable water estimates to monitoring and assimilation in numerical weather prediction at the MET office

WILLIAM BELL, STEPHEN ENGLISH, BRETT CANDY
Satellite Radiance Assimilation Group, Met Office, FitzRoy Road Exeter, EX1 3PB, U.K.

Moisture plays a very important role in a wide range of thermodynamical, dynamical and radiative processes in the Earths atmosphere. In a global numerical weather prediction (NWP) model the accuracy of the representation of moisture is a powerful diagnostic tool which can be used to assess how well these processes are modelled. At the Met Office estimates of total precipitable water (TPW) are routinely derived from F13 and F15 SSMI radiances using a variational technique. These estimates have two main applications in NWP: firstly in passively monitoring the accuracy of the models representation of moisture, and secondly in the assimilation process in order to determine the initial conditions for the forecast model. For both applications it is important to understand the accuracy of the observed radiances from which the TPW estimates are derived.

An assessment of the long term stability and comparability of F13 and F15 SSMI radiances was carried out using daily minimum observed brightness temperatures. This approach uses measurements of radiance over cold, calm parts of the ocean surface as stable radiometric calibration points, and provides a model independent means of assessing observation quality. This analysis has shown the radiances to be stable and consistent to better than 0.6 K for all channels during the period July 2001-March 2003. The overall F13/F15 bias in the 22 GHz channel is less than 0.1 K. It is however not possible to estimate the absolute accuracy of the radiances using this approach. Given this level of consistency and probable accuracy, the observations have been used to study variable biases in the Met Office short term (T+6 hour) forecasts. Global average observed minus background (O-B) radiances during the period July 2001-March 2003 show the model to be biased dry relative to observations in August 2002 and wet relative to observations in November 2002. The model shows a consistent dry bias

relative to observations in the deep tropics and a variable extratropical bias. The changes in model bias relative to observations are partially attributable to recent changes in the model convection scheme.

Finally, the SSMI TPW estimates have been assimilated in the Met Office three dimensional variational assimilation scheme (3D-Var) to assess their impact on the accuracy of forecasts. In common with previous studies at the Met Office and elsewhere the SSMI TPW estimates trigger excessive convection in the tropics and the impact on the quality of tropical wind forecasts in this area is negative. The relative importance of observation error, the assimilation scheme and the model physics are discussed.

The effect of the half-width of the 22-GHz water vapor line on retrievals of temperature and water vapor profiles with a twelve-channel microwave radiometer

JAMES LILJEGREN
OE/Argonne National Laboratory, 9700 South Cass Avenue, Argonne, Illinois 60532, USA

The Atmospheric Radiation Measurement (ARM) Program has operated a twelve-channel microwave radiometer profiler (MWRP) built by Radiometrics Corporation since February 2000. This instrument provides real-time vertical profiles of temperature, water vapor, and limited-resolution cloud liquid water from the surface to 10 km in nearly all weather conditions at approximately 5-minute intervals.

Since its initial deployment, significant biases have been observed in the water vapor and temperature profiles retrieved from the MWRP in comparison with radiosonde data. The cause is systematic biases between the observed and model-calculated brightness temperatures at the five measurement frequencies between 22-30 GHz. The brightness temperature biases can be largely eliminated by replacing the air-broadened half-width of the 22 GHz water vapor line in the model (Rosenkranz, 1998; Liebe and Dillon, 1969) with the half-width from the HITRAN compilation (Rothman et al., 1992), which is 5% smaller. This finding contradicts a 6% increase in the Liebe and Dillon half-width recommended by Cruz Pol et al. (1998). An a priori statistical retrieval based on the revised absorption model yielded significant improvements in the accuracy and vertical resolution of the retrieved temperature and water vapor profiles.

Additional profiling improvements were achieved by combining the MWRP retrievals with those from the GOES-8 sounder.

of Chicago for the U.S. Department of Energy.

S.L. CRUZ POL, C.S. RUF, S.J. KEIHM, *Improved 20 to 32 GHz atmospheric absorption model*, Radio Sci., **33**, 1319-1333, 1998.

H.J. LIEBE, T.A. DILLON, *Accurate foreign-gas-broadening parameters of the 22-GHz H2O line from refraction spectroscopy*, J. Chem. Phys., **50**, 727-732, 1969.

P. ROSENKRANZ, *Water vapor continuum absorption: A comparison of measurements and models*, Radio Sci, **33**, 919-928, 1998.

L.S. ROTHMAN, ET AL., *The HITRAN molecular database: Editions of 1991 and 1992*, J. Quant. Spectrosc. Radiat. Transfer, **48**, 469-507, 1992.

Retrieval of mesospheric ozone profiles from airborne submillimeter measurements

ARMIN KLEINBOEHL, JAYANARAYANAN KUTTIPPURATH, HOLGER BREMER, MIRIAM SINNHUBER, HARRY KUELLMANN, KLAUS KUENZI

Institute of Environmental Physics, University of Bremen, P.O. Box 330440, 28334 Bremen, Germany

The Airborne SUbmillimeter Radiometer ASUR is a passive microwave receiver applying the heterodyne principle. It is operated on board an aircraft to avoid water vapor absorption. With its frequency range from 604 to 662 GHz it is capable to measure rotational lines of important stratospheric trace gases like Ozone, N_2O, HCl, ClO and HNO_3, among others. By analyzing the shape of the pressure broadened lines, vertical profiles of these species can be retrieved.

ASUR is equipped with an Acousto-optical spectrometer (AOS) with a band width of about 1.5 GHz and a resolution of about 1.5 MHz. The spectra taken with the AOS allow stratospheric profile retrievals.

In January 2002 a Chirp-transform spectrometer (CTS) with a band width of 178 MHz and a resolution of 278 kHz has been added. The resolution is significantly better than the Doppler width of the rotational lines measured by ASUR and hence the spectra of the CTS allow retrievals of middle atmospheric profiles well into the mesosphere.

During the Sciamachy Validation and Utilization Experiment (SCIA-VALUE) in fall 2002 and spring 2003 ASUR performed numerous measurements of several trace gases with this configuration in the northern hemisphere. An algorithm for mesospheric profile retrieval from the ozone line at 625.37 GHz has been developed. The retrieval shows a profile sensitivity reaching higher than 60 km altitude. The retrieval setup will be presented, its performance will be analyzed and error sources will be discussed. Mesospheric ozone profile retrievals from measurements before and after sunset will be presented. A significant increase in ozone mixing ratio is observed in the mesosphere after sunset. Comparisons with ozone profiles calculated by a mesospheric chemistry model show agreement with the observed diurnal variations.

SESSION 8
SNOW COVER
(*Chairpersons*: M. Hallikainen, P. Pampaloni)

AMSR-E snow water equivalent estimates in North America

Richard Kelly, Alfred T. Chang, James L. Foster, Dorothy Hall, B. Boba Stankov, Albin J. Gasiewski
NASA/Goddard Space Flight Center, Hydrological Sciences Branch, Greenbelt, Maryland 20771, USA

This paper describes the testing of SWE estimates from AMSR-E in North America for the 2002-2003 winter season. Satellite passive microwave observations have been used to estimate global snow depth and snow water equivalent (SWE) since 1979. The Advanced Microwave Scanning Radiometer-EOS launched in 2002 aboard NASA's Aqua platform, has improved spatial resolution capabilities compared with previous passive microwave instruments and, potentially, can be used to estimate snow depth and SWE with increased accuracy at the regional scale. We compare the performance of an updated retrieval methodology to estimate SWE with the AMSR-E baseline retrieval algorithm. Both algorithms use the observed brightness temperature difference between 18 and 36 GHz frequency channels to estimate snow depth and SWE. The baseline algorithm is parameterized from measured seasonal global average snowpack characteristics of snow grain size and density. The updated algorithm explicitly models changing snowpack properties and is coupled to a dense media radiative transfer model to estimate SWE. In both approaches an enhanced forest correction scheme is included. Testing of the approaches is performed using aircraft gamma survey estimates of SWE conducted by NOAA's National Operational Hydrologic Remote Sensing Center. We analyse the performance of the SWE retrieval algorithms from accuracy assessments at the regional spatial scale.

Multi-frequency microwave radiometry of snow cover: the microwave alpine snow melting experiment (MASMEX 2002-2003)

Giovanni Macelloni, Simonetta Paloscia, Paolo Pampaloni, Marco Tedesco
CNR-IFAC, Earth Observation Dept., Via Panciatichi 64, 50127 Firenze, Italy
Roberto Ranzi
Dept of Civil Engineering, University of Brescia, Via Branze 38, 25123 Brescia, Italy
Mauro Valt
ARPAV Centro Valanghe di Arabba, Via Pradat 5, 32020 Arabba (BL), Italy

The monitoring of the snow melting cycle is very important for the management of water resources, as well as for flood and avalanche forecasting. During the melting process, typical grains of dry snow are transformed into large rounded grains that rapidly grow up to dimensions of 1-2 mm. During the night-refreezing phase, which usually involves the first few centimetres of snow cover, the crystals aggregate in polycrystalline grains, thus forming hard surface crusts. This transformation impacts on the radiative properties of snow, which change in accordance with the daily melting and refreezing cycles.

An experiment aiming at studying the melting cycle of snow by combining microwave and micro-meteorological sensors with a hydrological model was carried out on the Italian Alps in 2002-2003. The site selected for the experiment was located at an altitude of 2030 m a.s.l. The measurements were carried out from mid March to early May in 2002, and from early February to mid May in 2003. Microwave radiometers at 6.8, 19, and 37 GHz) (V&H polarizations) operated 24 hours /day at an incidence angle of 55°. Angular scans between 30 and 70 degrees were carried out under specific conditions. A meteorological station, located close to the microwave equipment, included sensors for measuring wind speed and direction, air/soil temperature, air relative humidity, incoming and reflected solar radiation, net radiative flux in the snowpack, and heat flux into the ground. Conventional measurements of snow parameters were carried out along vertical profiles at each significant change during the daily cycles of snow melting and refreezing. A continuous simulation of the snow liquid water conteny (LWC) was performed by means of a physically based model. The melting rate was estimated on the basis of the energy balance equation and the meltwater flux within the snowpack was computed through a two-layer model.

Microwave emission at 37 GHz and 19 GHz was found to be in good agreement with the melting-refreezing cycles, the higher brightness temperatures T_b being related to melted snow and the lower ones to refrozen snow. In fact, T_b mostly depended on both the snow temperature and its LWC. When the latter increased, absorption and then brightness increased. The maximum value of T_b was usually reached when the snow wetness

attained a value close to 2%. Emission at 6.8 GHz was much less sensitive to changes in the snow cover. Indeed, at this relatively low frequency, penetration was high and the soil contribution was dominant.

A comparison between emission at 37 and 19 GHz LWC in the upper (0.1 m deep) and lower layers of snow showed that, in general, emission at 37 GHz was closely correlated to the liquid water content of the first layer, while the variations in Tb at 19 GHz appeared less marked and more correlated to the LWC of the deeper layers. This fact is explained by the different penetration depths of the two frequencies. However, when the first layer was dry and the lower layer was wet the 37 GHz channel was sensitive to the LWC of the latter and, consequently, Tb was high. A more detailed analysis showed that the steep increase in the Tb during the melting cycle was related to the increasing LWC in the upper layer, whereas the decrease in the brightness during the refreezing phase was better correlated to the wetness of the lower layer.

Experimental data were also compared with simulations performed with a two-layer radiative transfer model based on the Strong Fluctuation Theory (SFT) and on the Fluctuation-Dissipation Theorem (FDT). It is expected that inversion of this model with suitable methods will make it possible to use remote sensing data to initialize hydrological models.

Dense media modelling of local-scale snowpacks during the cold land processes experiment-1: a sensitivity analysis

MARCO TEDESCO
Cold Land Processes Working Group, NASA Earth Science Enterprise
EDUARD J. KIM
NASA Goddard Space Flight Center, Greenbelt, Maryland 20771, USA
DON CLINE
National Operational Hydrologic Remote Sensing Center, National Weather Service, 1735 Lake Drive W., Chanhassen, MN 55317, USA
TOBIAS GRAF, TOSHIO KOIKE
Dept of Civil Engr., School of Engineering, University of Tokyo, Bunkyo-ku, Tokyo 113-8656, Japan
RICHARD ARMSTRONG, MARY J. BRODZIK
National Snow and Ice Data Center, Univ. of Colorado, Boulder, CO 80309-0449, USA
JANET P. HARDY
Cold Regions Research and Engineering Lab., US Army Corp of Engineers, 72 Lyme Road, Hanover, New Hampshire 03755-1290, USA

The capabilities of the Dense Media Radiative Transfer model using the Quasi Crystalline Approximation with Coherent Potential (QCA-CP) to reproduce measured radiometric data were tested using ground-based mi-

crowave observations from the NASA Cold-land Processes Field Experiment (CLPX-1). The data were collected at the Local-Scale Observation Site (LSOS), a 0.8~ha study site consisting of open meadows separated by trees. Intensive measurements were also made of snow depth and temperature, density, and grain size profiles.

A DMRT model is desirable to describe radiative transfer in a medium such as snow because the assumption of independent scattering used in classical radiative transfer theory (CRT) is not valid. The DMRT takes the following into account: scattering of correlated scatterers, the pair distribution function of scatterer positions, and the effective propagation constant of a dense medium. The improved equations also preserve the advantage that the form of the equation remains the same as the Classical Radiative Transfer (CRT) equations so that numerical solutions can be calculated in the same manner. Validation of the DMRT approach requires a relationship between measured snow grain size and the DMRT approximation of snow grain radius as spherical particles with a mean radius of the log-normal particle-size distribution.

DMRT simulations were compared with observations of microwave brightnesses at 18, 36 and 89 GHz (V and H polarizations) collected in the spring of 2003. Observation angles ranged from 30 degrees to 70 degrees. Model inputs included measured snow parameters except mean grain size. Sensitivity analyses will be used to assess the variation of the DMRT predictions in response to variations in parameters such as snow temperature, fractional volume and depth, ice and soil permittivities, and particularly to snow grain size information. These sensitivities will help guide the choice of future snow retrieval algorithms and the design of future Cold Lands observing systems.

Observationally-based snow microwave emissivity model: its applications in global forecast system data assimilation system (GDAS)

BANGHUA YAN, FUZHONG WENG, JOHN DERBER
NOAA/NESDIS, Office of Research and Applications, 5200 Auth Road, Camp Springs, MD 20746, USA; STG Inc./DSTI, 11250 Waples Mill Rd., Fairfax, VA 22030, USA
KOZO OKAMOTO
NOAA/NCEP/EMC, 5200 Auth Road, Camp Springs, MD 20746, USA; UCAR, University Corporation for Atmospheric Research, P.O. Box 3000, Boulder, CO 80307-3000, USA; JMA, Japan Meteorological Agency, Otemachi 1-3-4, Chiyoda-ku, Tokyo 100-8122, Japan

The snow microwave emissivity model developed earlier by Weng et al., (JGR, 2001) has some deficiencies in its performance over the regions where snow is deep or multi-year aged. In general, simulated emissivity is much lower than the observed one over these conditions. This poor per-

formance seriously affects the direct uses of satellite measurements in the Global forecast system Data Assimilation System (GDAS). This study develops an improved model to simulate snow emissivity over a variety of surface conditions (16 surface types). For each snow, the emissivity spectrum is derived both from the ground-based measurements (Mätzler, 1994) and satellite retrievals.

The snow type and related emissivity spectrum over realistic snow surface is first specified using various discriminators that are derived from the measurements at 23, 31, 50, 80 and 150 GHz at the Advanced Microwave Sounding Unit (AMSU) on board NOAA-15,-16 and -17 satellites. And the emissivity at a certain frequency is interpolated or extrapolated from this snow emissivity spectrum. For more flexibility, we consider the availability of these window channel measurements. This is important because sometimes not all satellite window channels are available for surface classification. To further improve the performance of the emissivity model and the identification of snow types, we also use some additional information from forecast models such as surface temperature and snow cover and depth.

This new snow emissivity model is being implemented into the GDAS Spectral Statistical Interpolation (SSI) routine (Parrish and Derber, 1991). A preliminary analysis shows that the differences between simulated and observed brightness temperatures (TB) are significantly reduced. For example, with the previously developed emissivity model (Weng et al., 2001), the globally absolute mean biases (or TB) are 3 K at 52.8 GHz; 4K at 183.1 GHz; 11 K at 183.3 GHz; and 22 K at 183.7 GHz, respectively. With the new model, these biases are reduced to 1.5, 1.1, 2.2 and 3.8 K, respectively. Hence, it is anticipated that the new model will substantially improve the uses of satellite microwave sounding data over high latitudes in the numerical weather prediction models.

Passive and active microwave remote sensing of snow in Finland

MARTTI HALLIKAINEN, PEKKA HALME, JOUNI PULLIAINEN
Helsinki University of Technology, Laboratory of Space Technology, P.O. Box 3000, FIN-02015 HUT, Finland

Information on seasonal snow cover is vital for several applications ranging from management of water resources, including hydropower operations and flood prediction, to global studies involving the water and energy flux at the Earth's surface, the hydrological cycle of snow-covered areas, and the global change. Since seasonal snow mostly appears at high latitudes, microwave radiometer and radar, due to their nearly all-weather capability and independence of lighting conditions, are suitable for monitoring seasonal snow on various scales. However, interpretation of these data

in terms of snow cover characteristics is not straightforward.

In this paper we report results on using satellite data from passive and active microwave sensors for remote sensing of seasonal snow cover in Finland. Radiometer data are from the multi-frequency SSM/I sensor on the DMSP satellite and scatterometer data are from the Ku-band SeaWinds sensor on the QuikScat satellite. We discuss the feasibility of these data sets for monitoring snow cover characteristics especially during the snow-melting season. We have several test sites in Finland, representing the two main types of land-cover categories: forested and agricultural/forested areas. Satellite data for the winters of 1999-2000, 2000-2001 and 2001-2002 are employed along with daily maximum and minimum air temperatures and snow water equivalent values.

We have tested the feasibility of data from SeaWinds and SSM/I channels for determining the onset and end of the seasonal snow-melting period for each test site and, additionally, the snow-covered area in Finland during the melting season. Our results, based on daily satellite data for three winters, suggest that obtaining good accuracy may not be as straightforward as reported in previous studies. Behavior of the daily air temperature may substantially affect accuracy of the outcome. The use of reference values (snow-free terrain) from previous melting periods seems to cause systematic errors for the derived snow-covered area. We have obtained reasonable accuracy by using algorithms that employ satellite data for the winter of interest only.

Relationship between passive microwave measurements and snow parameters

NORMAN CHARLES GRODY
NOAA/NESDIS/Office of Research and Applications, 5200 Auth Road, Camp Springs, MD 20746, USA

Measurements from the Advanced Microwave Sounding Unit (AMSU) will be used to demonstrate the variations in emissivity due various snow parameters (e.g., snow depth, grain size, fractional volume and stratification). AMSU was first launched in 1998 aboard the NOAA-K operation satellite, and contains window channels at 23, 31, 89, 150 GHz. The AMSU measurements will be used to identify metamorphic changes in the spectral characteristics as the snow ages in addition to the effects of melting and re-freezing of the snow surface. Ice crusts on the surface and within the snow pack are also shown to affect the satellite measurements. The paper will also provide models to account for the satellite observations and develop relationships between the AMSU channel microwave measurements and snow parameters.

SESSION 9
ELECTROMAGNETIC MODELS
(*Chairpersons: D. Solimini, A. Voronovich*)

A new 3D polarized radiative transfer model
for microwave remote sensing in cloudy atmospheres

CORY DAVIS

Institute for Atmospheric and Environmental Science, University of Edinburgh, The King's Buildings, West Mains Road, Edinburgh EH9 3JG, UK

Cirrus clouds affect microwave limb sounder measurements; where there are large concentrations of large ice crystals, there will be a detrimental impact on trace gas measurements, and in other cases cloud information can be retrieved. Computational demands limit the detail in which the scattering problem can be treated in an operational forward model. This talk introduces a 3D polarized radiative transfer model that has been developed to assess the influence of cirrus clouds on radiances measured by the EOS-MLS instrument. EOS-MLS is on the Aura satellite, which is due for launch in March 2004. The radiative transfer model uses a reversed Monte Carlo algorithm and has been incorporated in the ARTS 1.1.x software package. The model will be used to study aspects of the scattering problem that are not considered in the existing operational EOS-MLS cloudy-sky forward model. These aspects include the influence of non-spherical, oriented hydrometeors and 3D inhomogeneous cloud structure. This talk covers the radiative transfer algorithm, example model results, and some expected implications for EOS-MLS measurements.

Rapid calculation of incremental brightness profiles

ALEXANDER VORONOVICH, ALBIN J. GASIEWSKI, REGINALD HILL
NOAA/Environmental Technology Laboratory,325 Broadway, Boulder, CO 80305-3328, USA
BOB L. WEBER
Science and Technology Corporation, 325 Broadway, Boulder, CO 80305-3328, USA

Assimilation of microwave radiometric data from satellite- and airborne sensors under all weather conditions is an important challenge in numerical weather prediction. Microwave radiances upwelling from the atmosphere depend strongly on frequency and carry a wealth of information on moisture and temperature profiles as well as clouds, rain, and surface param-

eters. Brightness temperatures generally depend on the electromagnetic scattering properties of hydrometeors through a well-described process. Statistically optimal retrieval of the environmental parameters requires accurate calculation of the derivatives of the brightness temperature with respect to all atmospheric and surface parameters. To accommodate the dense data stream from modern passive microwave satellites one requires calculations times of ~0.1 msec per profile or less.

In our approach the differential radiative transfer equation (RTE) for a planar stratified medium is used to model processes of emission and absorption by gases and particles as well as scattering by particles. Symmetry properties of scattering are very essential for building a fast solution, and the RTE is first cast into an explicitly symmetric form. Each layer is characterized by transmittance and reflection matrices that provide a complete description of its interaction with other layers. Accurate and stable calculation of those operators for arbitrary layer parameters is a non-trivial task since the opacity and scattering coefficients vary over a wide range. Moreover, the layer can be fairly transparent at steep incident angles and opaque at grazing angles. Computationally, this problem requires inversion of ill-conditioned matrices. We solve the inversion problem by first analytically factoring the matrix to be inverted into a product of five matrices. Four of them are regular, and only one diagonal matrix remains ill-conditioned. After explicit inversion the result includes only benign matrices and works well in all cases. Once the transmittance and reflectance operators for all layers are known, the overall brightness temperature field is built using the method of slab doubling via two profile sweeps. Calculation of incremental profiles generally requires only one extra sweep. Thus, the number of operations required is directly proportional to the number of layers.

This talk will present the above algorithm in the context of test data generated for a simulation of Hurricane Bonnie (1998). Methods for acceleration of the algorithm for low-albedo layers and connections between the radiative parameters of the atmosphere and prognostic variables of numerical weather models will be discussed.

Constant of pure and sea water from SSM/I, TMI and AMSR brightness temperature observations

THOMAS MEISSNER, FRANK J. WENTZ
Remote Sensing Systems

We provide an updated fit for the dielectric constant of pure and sea water that can be used in the theory of radiative transfer of ocean emitted microwave radiation and is valid within a larger frequency and temperature range than the model of Klein-Swift, which has been mainly used so far.

Our new fit uses two Debye relaxation frequencies: the lower one at around 20 GHz and the upper one at around 200 GHz. For pure water, we have used a large data set of laboratory measurements in the frequency range up to 500 GHz and in the temperature range between –20 C and +40 C, which includes supercooled water. Our fit smoothly interpolates the dielectric constant as a function of salinity between 0 and 40 ppt.

For sea water, our model is consistent with well established earlier results below 37 GHz and the recent measurements of the imaginary part of the dielectric constant by Guillou et al. (1) at 85 GHz.

We have validated our new model using an SSM/I, TMI and AMSR brightness temperature analysis. We have shown that below 100 GHz our dielectric model gives very accurate values for the ocean surface emissivities between –2 C and +30 C as well as the liquid cloud water absorption above –15 C. Due to the lack of measurements, uncertainties still remain for the emissivity of sea water above 100 GHz, the emissivity of fresh water above 37 GHz, the liquid cloud water absorption at supercooled temperatures for higher frequencies (above 100 GHz) and the liquid cloud water absorption at very cold temperatures (below –20 C).

(1) C. GUILLOU et al., Radio Science, 33, 649-667, 1998.

The microwave emission of a non-smooth periodic sea surface

ALEXENDER SELUNSKY, ALEXEY KUZMIN
Russian Academy of Science, Space Research Institute (IKI), 84/32 Profsoyuznaya Str., 117997 Moscow, Russia

The polarization effects at homogeneous sea wave were considered. The theory was developed and the experimental results obtained. The analysis was made and correlation verified. The set of new data was explained and the theoretical confirmation discovered.

The old data were revised. In particular, the Bragg equation for Laue case (Etkin's effect) was rediscovered and the new theory constructed. It's considered to be interesting that the precisions solution of the wave equation on the border sea-air can be obtained by absolutely different from traditional means. In this case, we developed a special method that is used to being in optics, but, in our opinion, is a little uncommon for microwave range. We had a very reasonable coincidence with our experiments and with older research.

Our results not only again confirmed the well-known Etkin's effect, but also added some new ones. In particular, we proposed some crucial conditions, which defined the emission behavior on different polarizations. We supposed that Etkin's effect could have various expressions by crucial

conditions. To be precise, we confirmed, that under definite conditions, Bragg diffraction dominates and defines microwave behavior, under another geometry Laue case is prevalent, and under the other Fresnel case is evident.

Let the border be of the type

[1]
$$z = a \times \sin(L \times x)$$

where L is the period of the shallow sea wave.

We consider the propagation of electro-magnetic wave

$$E = A_0 \exp(-i\omega t + ik_0 x - ik_0 z)$$

through this border. We'll develop the wave approach to the problem. The point is, that during such a process an infinite number arises of diffracted waves with the equidistant shift of wave number k by L.

By the appearance of the function on the border, we can conclude, that the series actually can't be cut at any finite value of n because of exponent's nonlinear property. No coefficients become zero and we observe the following effect at critical angle: the diffracted wave from reflected becomes adsorbed, that leads to bifurcation in refraction/adsorption indexes. It seems to be most interesting, that there is such a kind of critical angle. In the area of critical angle the reflection/adsorption indexes have a bifurcation that imply, taking into consideration the reversibility of the process (Kirchhoff law), the maximum of water emission in this direction.

Here we should emphasize the fact, that in optics the gitter indexes have almost the same kind of dependences (Wood anomalies).

At the experiments the bifurcation becomes (because of finite antenna polar pattern) obscure and the maximum smoothes.

Monochromatic radiative transfer model (Monortm): recent developments

KAREN CADY-PEREIRA, SID-AHMED BOUKABARA, SHEPARD A. CLOUGH
Atmospheric and Environmental Research, Inc., 131 Hartwell Ave., 02421 Lexington MA, USA

Monochromatic Radiative Transfer Model (MONORTM): Recent Developments MONORTM is a line-by-line radiative transfer model for calculations at specific monochromatic frequencies. It has all the physics of LBLRTM, including the CKD continuum (Clough et al, 1980). It also contains a cloud liquid water absorption model (Liebe et al, 1991). It was developed specifically for microwave applications but is physically valid

across the entire spectrum. Its applicability is in principle determined by the lines included in the spectral line file required as input. Its speed and accuracy has proven especially useful in water vapor and cloud liquid water retrieval schemes, and is currently been integrated into the Atmospheric Radiation Measurement (ARM) program's precipitable water vapor (PWV) and cloud liquid water (CLW) retrieval algorithm.

Accurate determination of atmospheric absorption in the microwave region is dependent on the inclusion of the significant spectral lines and accurate values for the line parameters (e.g., water vapor line width, line coupling, continuum coefficients). We have compared the brightness temperature values across the microwave spectrum generated from MONORTM and the MPMf93/s89 (Rosenkranz, 1998) models and determined which factors contribute most to the differences; among them are: the number of lines and species, line strengths and widths; the line shape model, Lorentz or Voigt; the continuum model; the inclusion or exclusion of the pressure induced wavenumber shift.

Since its release to the microwave community early in 2002, MONORTM has undergone many tests and a few changes. In an effort to improve speed a fast option has been added, which significantly reduces running time. This accomplished by defining a minimum set of spectral lines for the microwave region.

Several comparisons with microwave radiometer measurements from the ARM SGP site have been performed. The objective of our first analysis was to determine if MONORTM was spectrally consistent across the 23-32 GHz range. Water vapor was retrieved using the 23.8 GHz measurement and sonde profiles in a physical retrieval approach with MONORTM as a forward model. The profiles were then scaled to match the retrieved PWV and the brightness temperature at 31.4 GHz was calculated. The measurement-model RMS at 31.4 GHz was less than 0.3 K. Comparisons with MWRP measurements at five frequencies between 22 GHz and 31.4 GHz show good agreement at all frequencies. As a test of the sensitivity of the modeled brightness temperatures to the 22 GHz line width, we increased this line width by five percent, and noted that this introduced a linear dependence on BT in the measurement model difference, highlighting the importance of accurate determination of the spectral parameters. Finally, comparisons with MWRP measurement across the 20-60 GHz range revealed a problem in the 50-60 GHz region. By scaling the first order O_2 line coupling parameters by 0.87 and by setting the second order O_2 line coupling parameters to zero we were able to greatly reduce the measurement-model error.

The application of sea wave slope distribution empirical dependencies in estimation of interaction between microwave radiation and rough sea surface

BORIS KUTUZA, MIKHAIL DANILYTCHEV, ALEXANDER NICOLAEV
Inst. of Radio Engineering and Electronics, Russian Academy of Sciences, Mokhovaya St. 11/7, Moscow 125009, Russia

The development of simple and adequate procedure of utilization of the sea surface parameters distribution information in calculations of interaction between microwave radiation and rough sea surface is very significant both for the remote sensing theory and its applications.

Now this procedure in microwave radiometry is based as a rule on the next assumptions:
- sea surface roughness is a full developed wind waving;
- dispersion (variance) of the large sea wave slope distribution depends on the surface wind (at the standard altitude) in accordance with the Cox-Munk results. The influence of small and medium scale components (with lengths both less and about λ) of sea wave spectrum is ignored (within the quasi-mirror reflection region);
- the transition from Cox-Munk portion of the wind wave spectrum to the group of sea waves, large enough for the used radiowave with length λ (frequency *f*), is done as Hollinger and Wilheit implemented.

These assumptions represent the contemporary understanding of the Kirchoff method for practical calculations of interaction between microwave radiation and rough sea surface.

Now we have an opportunity to compare these assumptions and our experimental data. We ran a sea tower experiment (Catcively settlement, Crimea) to investigate the influence of solar microwave radiation on the radiometer antenna temperature after scattering it on rough sea surface. The experimental complex consisted of three main parts: a radiometric block (3 dual-polarized microwave radiometers at 0.8, 2.25 and 6.0 cm wavelengths), a recording and processing block and a block of contact measurements (the meteorological equipment set and the four-string wavegauge with 30 cm space matrix for measuring the variance of the large sea wave slope as well). We measured the contribution of reflected solar microwave radiation in the radiometer antenna temperature on horizontal and vertical polarization, wind power and direction on 19.5 m altitude, dispersion (variance) of the sea wave slope distribution along and across the wind direction or ripple and a classical set of meteorological parameters (pressure, humidity and temperature for surface air layer and water temperature for 1 m depth). The atmospheric state for experiments was chosen cloudless. The necessity of this experiment was the multifrequency control of Solar microwave flux. That was carried out by the data of Solar Service

radiotelescopes. The values of the contribution of scattered solar microwave radiation in the radiometer antenna temperature are large enough for using in the procedure of investigation of sea surface radiation characteristics. About 50 units of such Sun tracks and a great amount of the sea wave slope data were obtained.

Extended boundary condition method
for scattering from fractal surfaces

DANIELE RICCIO, GIORGIO FRANCESCHETTI, ANTONIO IODICE, GIUSEPPE RUELLO
Dipartimento di Ingegneria Elettronica e delle Telecomunicazioni, Università di Napoli "Federico II", Via Claudio 21, 80125 Napoli, Italy

It is widely recognized that fractal models are suitable to describe natural surfaces roughness. In particular, the fractional Brownian motion (fBm) and the Weierstrass-Mandelbrot (WM) functions provide reliable surface models in terms of few parameters.

In order to evaluate the scattered field from a natural surface, new electromagnetic methods have been recently proposed by employing the above introduced fractal models (1). Different scattering methods do not drive to the same scattering solution. This is because the exact solution to the scattering problem from a rough surface cannot be found in closed form and only approximate solutions are available: hence different approximations often lead to different solutions, applicable in different ranges of validity.

In particular, in a recent paper (2), the scattering solution has been obtained according to the Extended Boundary Condition Method (EBCM) rationale in conjunction with the WM surface description. Since the WM function is an almost periodic function (2), an exact solution can be obtained in the form of generalised Floquet modes, so that, in principle, this method does not have validity limits. However, the Floquet mode amplitudes are expressed in terms of infinite dimension matrixes, with elements written in terms of products of Bessel functions, whose arguments are proportional to the WM tone amplitudes normalised to the incident wavelength. Hence, in order to numerically evaluate the field, the infinite dimension matrixes have to be truncated, and this makes the solution approximate. In addition, matrix inversion is needed: for high roughness the matrixes to be inverted turn out to be ill-posed, and this in practice sets an upper bound on the surface roughness that cannot be analytically predicted.

The problem of truncation can be rather easily solved by using truncation criteria that lead to a highly accurate field solution (2). In order to solve the problem of matrix ill-conditioning, in this paper we present a new analytical recasting of the EBCM solution: since the exact matrix coefficient expression leads to ill-conditioned matrixes unless the surface

roughness is small, it is meaningful to use a small-roughness (i.e., small-argument) approximation of the Bessel functions. This leads to a faster field evaluation and dramatically reduces the ill-conditioning problem. Of course, an upper bound on the surface roughness exists, but it can be (at least approximately) analytically predicted. A technique to find significant WM tone combinations for each scattered mode is also shown, in order to neglect the terms that do not significantly contribute to the scattered field. The new solution will be presented, the validity limits and the reduction of the ill-conditioning problems discussed in the final paper version.

(1) G. FRANCESCHETTI, A. IODICE, D. RICCIO, *Fractal Models for Scattering from Natural Surfaces*, in: *Scattering*, ed. by R. Pike and P. Sabatier, Academic Press, London, U.K., 2000.

(2) G. FRANCESCHETTI, A. IODICE, D. RICCIO, G. RUELLO, *Fractal Surfaces and Electromagnetic Extended Boundary Conditions*, IEEE Trans. Geosci. Remote Sens., **40**, 1018-1031, 2002.

SESSION 10
RETRIEVAL METHODOLOGIES
(*Chairpersons*: R. Wave, E. Westwater)

Neural network inversion algorithms for satellite temperature and humidity profiling

GIOVANNI SCHIAVON, FABIO DEL FRATE, MICHELE FEDERICO IAPAOLO, DOMENICO SOLIMINI
Dip. Informatica, Sistemi e Produzione, University of Rome "Tor Vergata", Via di Tor Vergata 110, 00133 Roma, Italy

The Geostationary Observatory for Microwave Atmospheric Sounding (GOMAS) study is being carried out, partially funded by the Agenzia Spaziale Italiana (ASI). The purpose of GOMAS is to establish the feasibility of MW/Sub-mm sounding from geostationary orbit, to prove the applicability of such observation to frequent and nearly-all-weather atmospheric temperature and humidity sounding, and to estimate very frequently precipitation rate, associated to cloud liquid/ice water discrimination. In the framework of the GOMAS study, this paper reports on the development of neural network inversion algorithms for temperature and humidity profiling.

The GOMAS equipment is foreseen to operate in five millimeter-wave spectral bands. In each of the bands (centered at 55, 119, 183, 380 and 425 GHz), 6 to 10 narrow-bandwidth channels have to be implemented, by heterodyne spectrometers with quasi-optical band separation. The total number of channels will be around 40.

The algorithms have been configured with the choice of feed forward perceptrons as the type of neural networks to be used and with the choice of their topology, which means the number of hidden layers and of the neurons in each layer. The nets have been trained by means of the scaled conjugate gradient (SCG). Input data are the brightness temperatures in the GOMAS channels while the output ones are temperature and humidity values at different heights in the atmosphere.

Two statistically independent ensembles (training and test) of atmospheric profiles of temperature and humidity have been used, which will be the variables to be retrieved inverting the radiometric measurements. The brightness temperatures, which would be measured in each channels, have been evaluated by using Liebe's millimeter-wave propagation model (MPM), with the atmospheric profiles as inputs. A smooth ocean background has been considered at first. The coupled ensembles of profiles and the corresponding measurements form the output and input databases, respectively,

needed to train the nets. The algorithms performance have then been evaluated calculating the deviations of the profiles estimated by means of the retrieval algorithms from those used to generate the brightness temperatures with the propagation model.

Oceanic and atmospheric parameters retrieved from aqua AMSR-E using neural networks: theoretical and experimental error estimation

ELIZAVETA ZABOLOTSKIKH, LEONID BOBYLEV, OLA JOHANNESSEN
Scientific Foundation "Nansen International Environmental and Remote Sensing Centre" (NIERSC), Bolshaya Monetnaya 26/28, 197101 St. Petersburg, Russia
LEONID MITNIK
V.I. Il'ichev Pacific Oceanological Institute, Russian Academy of Science, FEB RAS, 43 Baltiyskaya Str., 690041 Vladivostok, Russia

Satellite passive microwave measurements are recognized for their ability to give reasonable estimates of such oceanic and atmospheric parameters as ocean surface wind speed (V), sea surface temperature (Ts), total atmospheric water vapor content (Q) and total cloud liquid water content (W). Aqua AMSR-E microwave radiometer ensures new possibilities for daily operative estimation of these parameters. Such estimations need well-calibrated parameter retrieval algorithms.

In this study AMSR-E parameter retrieval algorithms based on Neural Networks (NNs) are investigated using two consecutive approaches. During the first one the NNs-based algorithms were developed using simulated closed scheme of the numerical experiments. Simulated AMSR-E brightness temperatures (TBs) were used for the training NNs-based algorithms. Application of these algorithms to the independent simulated TBs made possible to calculate the theoretical errors of parameter retrieval (the radiometer noises were added to the TBs values). Those errors were compared with the errors of alternative algorithms.

The lowest retrieval errors were obtained when a single-output Neural Network with one hidden layer consisting of a few neurons had been used. At that various NNs should have been trained for the various atmospheric conditions characterized by different polarization difference at 36 GHz (DT36). 3 cases were considered: (1) DT36 > 50 K; (2) 35 K < DT36 < 50 K; (3) 15 K < DT36 < 35 K. The theoretical root mean square difference errors (rms) computed under different DT36 (without precipitation) were the following: $rmsQ1,2 = 0.4$ kg/m^2, $rmsQ3 = 0.7$ kg/m^2; $rmsW1,2 = 0.02$ kg/m^2, $rmsW3 = 0.03$ kg/m^2; $rmsV1,2 = 0.9$ m/s, $rmsV3 = 2.4$ m/s; $rmsTs1,2,3 = 0.4$ K. Comparison of these retrieval errors with the errors of other algorithms (nonlinear multiple regression, etc.) showed that NNs ensured 20-50% (dependently on the parameter and atmospheric conditions) lower

errors than the alternative algorithms.

But the second approach consisting of the application of the trained NNs algorithms to the measurements of the collocated in space and time aerological stations and oceanic buoys and obtaining the experimental retrieval errors showed that the developed algorithms needed to be corrected by means of additional tuning using in-situ data.

Duly tuned NNs algorithms can be used for the investigation of various weather systems (such as polar cyclones, atmospheric fronts etc.) taking advantage of the new possibilities of AMSR-E measurements.

On the regularization of inverse problems in imaging radiometry by aperture synthesis

ERIC ANTERRIEU, BRUNO PICARD
CERFACS, 42 Gaspard Coriolis, 31057 Toulouse Cedex, France
ALAN B. TANNER
Jet Propulsion Laboratory, California Institute of Technology, 4800 Oak Grove Drive, Pasadena, CA 91109, USA

Synthetic aperture imaging radiometers are potentially powerful instruments for high-resolution observation of the Earth at low microwave frequencies. Interferometric measurements, also called complex visibilities, are obtained by cross-correlating the signals collected by pairs of antennae which have overlapping fields of view. They are related to the radiometric brightness temperature of the scene under observation by a modeling operator which is a spatial Fourier-like integral. The corresponding inverse problem, which aims at inverting the modeling operator to retrieve the radiometric brightness temperature map from the complex visibilities, is often ill-posed unless a regularizing constraint is introduced in order to provide a unique and stable solution to the problem. Synthetic aperture imaging radiometers belong to the family of band-limited imaging devices because the finite physical size of a synthetic antenna results in a truncation of the visibility samples into the so-called experimental frequency coverage. Such a physical property should certainly be taken into account in the regularization of the imaging problem. However, other regularizing methods could lead to the same results, even if their physical meaning is somewhere hidden by the mathematical foundations.

This contribution makes a detailed review of standard methods for the regularization of inverse problems in imaging radiometry by aperture synthesis: the regularized solutions in the sense of Tikhonov, the solutions with minimal energy and those with band-limited properties are analyzed. The links between their physical and mathematical meanings are established. It is shown that the threshold of the truncated singular values decomposition

used to approximate the solutions with minimal energy is closely related to the regularization parameter of Tikhonov. Moreover, the number of spatial frequencies characterizing the solutions with band-limited properties in the experimental frequency coverage is equal to the number of singular values kept in the inversion of the modeling operator, while the number of singular values discarded prior to inversion is equal to the number of redundant visibilities. The stability of each reconstruction process is studied in depth, including the influence of the windowing function on the systematic error as well as the propagation of random errors from the complex visibilities to the reconstructed radiometric brightness temperature map. To support the theory and to illustrate the performances of these methods, in terms of accuracy and computational time, numerical simulations are carried out within the frame of the SMOS space mission, a project led by the European Space Agency and devoted to the remote sensing of soil moisture and ocean salinity from a low orbit platform.

Beam-filling correction with subpixel cloud fraction and inhomogeneity using neural network

DAMIEN LAFONT, BERNARD GUILLEMET
Laboratoire de Météorologie Physique (LaMP), Université Blaise Pascal, CNRS, OPGC, 24 Ave. des Landais, 53177 Aubière Cedex, France

The effects of cloud inhomogeneities on microwave retrievals are investigated. After an analysis of the beam-filling error with cloud types (precipitating and nonprecipitating), corrections schemes are presented. The objective of this work is to develop a scheme to correct this beam-filling error (BFE) with subpixel information and improve rain rate or liquid water path retrievals. We first determine some parameters which characterize the horizontal cloud inhomogeneity within the microwave radiometer field-of-view, and then we add them to simulated brightness temperatures as input of a neural network algorithm. In order to take into account for the spatial distribution of cloud within the field-of-view, textural-based parameters are also tested as additional subpixel information. It was found that cloud fraction within microwave pixels, is the main parameter in the BFE correction, but spatial distribution of cloud should be taken into account for more accurate retrievals. This technique requires accurate estimate of cloud fraction which can be given by colocated infrared or visible information. Convective-stratiform separation also plays an important role in this algorithm because the BFE is more pronounced for precipitating clouds. Finally, this neural network algorithm is tested on TRMM data (VIRS and TMI), in the case of nonprecipitating cloud.

Optimal linear spatial filtering of multi-resolution radiometric measurements

WILLIAM J. BLACKWELL
MIT Lincoln Laboratory, 244 Wood St., LL-S3-237, Lexington, MA 02420-9185, USA

A novel method for combining radiometric measurements at different spatial resolutions has been developed and evaluated. A spatial filter is derived that optimizes a "retrieved product" metric (for example, the mean-squared error of integrated water vapor over a specified region of interest) instead of a "beam quality" metric (for example, the width of the point spread function). The disadvantage of approaches that optimize beam quality (such as the Backus-Gilbert technique) is that the beam quality and the signal-to-noise ratio must be traded against one another, and it is often unclear which combination yields the best retrieval performance. In the present approach, retrieval performance is optimized directly.

The derivation of the optimal filter coefficients is composed of two steps. First, a neural network is used to retrieve the quantity of interest, using spatially co-located footprints of various resolutions. Second, the filter coefficients are found numerically by minimizing the retrieval error at a specified resolution over an area of interest. The neural network is a differentiable function, which greatly facilitates the search for the weights.

The method was evaluated using a high-resolution (1 km vertical, 2 km horizontal) three-dimensional "ground truth" scene generated by the PSU/NCAR mesoscale model (MM5). A cold front moving off the eastern coast of the United States on September 23, 2003 was modeled. A high degree of fine-scale spatial structure in atmospheric water vapor and cloud liquid water was evident in the scene. The sensor configuration that was used was the NPOESS Advanced Technology Microwave Sounder (ATMS), which has 23.8 and 31.4 GHz channels at a 5.2 degree spatial resolution, 14 channels near 50-90 GHz at a 2.2 degree spatial resolution, and six channels near 165-190 GHz at a 1.1 degree spatial resolution. All channels are co-located spatially with a 1.1 degree grid spacing. The neural network was trained with approximately 10,000 profiles from the model-generated data, and 30 filter coefficients were obtained using a numerical gradient search method.

The performance of the method compares favorably with traditional methods, such as the Backus-Gilbert technique, and several quantitative comparisons are presented.

Estimates of brightness temperatures from scanning radiometer data by means fo the Backus-Gilbert and TSVD procedures

Maurizio Migliaccio, Attilio Gambardella

Università di Napoli Parthenope, Ist. di Teoria e Tecnica delle Microonde, Laboratorio di Telerilevamento, Via Acton 38, 90133 Napoli, Italy

In this paper we consider two procedures to retrieve the brightness temperatures from scanning radiometer data and we compare the results. Our aim is to ameliorate the spatial resolution with respect to the intrinsic one. In fact, one of the limitation of microwave radiometer is the relatively low intrinsic spatial resolution; this is a limiting factor in application of radiometer measure in retrieval of geophiscal parameters and when radiometer data are used in multisensor data fusion techniques. For instance, in the next Meteorological Operational (MetOp) European Space Agency (ESA) mission a microwave radiometer and a radar scatterometer can be jointly used to best study the climatological/meteorological earth ecosystem. Within such a framework, the capability to generate microwave radiometric measurements with enhanced spatial resolution is a key element.

It is well-known that a microwave radiometer performs a set of multiple measurements scanning the Earth surface. This means that we have a set of partially correlated measurements of each scene. Such an occurrence can be exploited to enhance the intrinsic spatial resolution.

The physical link between the radiometer measures TA and the brightness temperature of the Earth surface TB belongs to the class of Fredholm integral equations of first kind whose kernel depends on the antenna pattern. Mathematically it is an ill-posed linear problem and must be carefully inverted.

The classical inversion method in microwave radiometry is the Backus-Gilbert technique. In this paper we illustrate this technique and a microwave radiometer resolution enhancement technique based on the Truncated Singular Value Decomposition (TSVD).

The second method is implemented via the combination of singular value decomposition and a variable regularization parameter. The key point is to use the regularization parameter dynamically depending on the features of the singular value spectrum.

This inversion method is attractive since it is simple and computer effective. In fact, if the scanning configuration is kept, the expression of TB is in terms of fixed weights of the measurements.

The study is conducted for the one-dimensional case, i.e. the scene is modelled by a brightness temperature profile and the radiometer antenna scanning is linear. Simulated radiometric measurements data are employed. The study is aimed at analyzing the performance of these inversion procedures in terms of sensitivity on the linear scanning configuration, i. e. we consider different antenna patterns and different measurement space sampling configurations.

SESSION 11
ATMOSPHERE: CLOUDS AND PRECIPITATIONS
(*Chairpersons: R. Ferraro, J. Turk*)

Submillimeter-wave radiometric measurements
of ice clouds with COSSIR

K. FRANK EVANS
University of Colorado, 1121 Monroe Dr., Unit C, Boulder, CO 80303, USA
JAMES R. WANG, PAUL E. RACETTE, GERALD M. HEYMSFIELD, LIHUA LI
NASA Goddard Space Flight Center, Greenbelt, Maryland 20771, USA

Theoretical analyses have shown the potential of employing submillimeter wave radiometry for measuring cirrus cloud parameters in order to obtain a more complete characterization of the physical properties of these clouds than is possible with visible and infrared remote sensing. An airborne Conical Scanning Submillimeter wave Imaging Radiometer (CoSSIR) was recently developed and flown during the Cirrus Regional Study of Tropical Anvils and Cirrus Layers-Florida Area Cirrus Experiment (CRYSTAL-FACE). The experiment provided the first opportunity to demonstrate the remote sensing of cirrus using CoSSIR. CoSSIR has 15 channels covering the frequency range of 183-640 GHz, although not all of the channels were available during the CRYSTAL-FACE. CoSSIR flew onboard the NASA ER-2 high altitude aircraft together with a suite of other instruments. Among these instruments is a new Cloud Radar System (CRS) that operates at the frequency of 94 GHz. The CRS reflectivity measurements are used to compare with the CoSSIR cirrus retrieval results.

Both the ice water path (IWP) and median mass equivalent sphere diameter (DME) of cirrus anvil clouds are retrieved with a Bayesian algorithm from the CoSSIR measurements. The retrieved values of IWP and DME are used to calculate the vertically integrated radar reflectivity which is compared with that derived from the CRS. The agreement is found to be very good between the CoSSIR calculated and CRS measured integrated radar reflectivities, usually within the error bars of the retrieval, 1 to 2 dB for thick anvils. These results and other experimental details will be discussed.

Preliminary comparison of AMSR-E observation and numerical
simulation with cloud resolving model for solid precipitation
in winter during the WAKASA 2003

HISAKI EITO, KAZUMASA AONASHI, G. LIU, CHIASHI MUROI, SYUGO HAYASHI, MASANORI YOSHIZAKI, TERUYUKI KATO

Meteorological Research Institute, Japan Meteorological Agency, 1-I Nagamine, Tsukuba, Ibaraki 305-0052, Japan

For improving the accuracy of passive microwave solid precipitation retrieval algorithm using the AMSR/AMSR-E, the field campaign (WAKASA2003) was conducted in the Fukui area, Japan, from January 12 to February 5, 2003. During the WAKASA2003, many active convective snowfall clouds frequently formed over the Sea of Japan due to cold outbreak. On 28-29 January 2003, broad cloud bands extending southeastward from the base of the Korean Peninsula to the Fukui area formed, and developed under the influence of the upper cold low. In this paper, high-resolution real simulations of these cloud bands are performed using a cloud resolving model with 1 km horizontal resolution. Some channels of AMSR-E simulated by microwave radiative transfer model (Liu, 1998) with model-derived precipitation are compared with observations. Our purposes are to check and improve the cloud microphysics scheme of the cloud resolving model, and to supply useful information from the model-derived 3-D structures of precipitation for improving the accuracy of the AMSR-E precipitation retrieval algorithm.

The cloud resolving model developed by Japan Meteorological Agency (JMA) is used in this study (JMA-NHM: JMA, 2003). The fully compressible equations with the conformal mapping are employed as the basic equations of the JMA-NHM. The bulk cloud microphysics scheme is employed in the JMA-NHM. This scheme predicts the mixing ratios of six water species (water vapor, cloud water, rain, cloud ice, snow and graupel). In the present study, the JMA-NHM on the Earth Simulator, which is the fastest supercomputer in the world, has a horizontal grid size of 1 km with 2000×2000×38 grid points. The initial and boundary conditions for the JMA-NHM are provided from output produced by Regional Spectral Model (RSM). The RSM with a horizontal grid size of about 20 km is a hydrostatic model used operationally in JMA.

The JMA-NHM successfully reproduced broad cloud bands over the Sea of Japan. Several cloud streets were also calculated around the cloud bands. Deepest convective clouds with the height of about 5 km formed in the developed stage (29 January 2003), while the height of deepest convective clouds was about 4 km in the moderate stage (28 January 2003). These model-simulated features almost agree with those of the observation used by a meteorological satellite, meteorological radars and an instrumented aircraft. The amount of model-calculated ice water path (IWP) in the developed stage was much larger than that in the moderate stage. These features were shown in the scattering index retrieved from AMSR-E 89 GHz data. The images of the scattering index retrieved from AMSR-E 89 GHz data were compared with those simulated by microwave radiative transfer model with model-derived precipitation. In the moderate stage, the model-derived value was almost equivalent to the observed one. However, model-calculated value was much lager in the developed stage. This result indicates that the JMA-

NHM overestimated the amount of solid precipitation perticles in the developed stage.

Geosynchronous microwave (GEM) sounder/imager observation system simulation

ALBIN J. GASIEWSKI, ALEXANDER VORONOVICH, BOBA B. STANKOV, JIAN-WEN BAO
NOAA/ETL, David Skaggs Research Center, 325 Broadway, Boulder CO, USA
BOB L. WEBER
NOAA/Environmental Technology Laboratory,325 Broadway, Boulder, CO 80305-3328, USA

Passive microwave sounding and imaging from geosynchronous orbit was first studied in the mid-1970's, although initial proposals using microwave channels at ~183 GHz and lower frequencies required prohibitively large antennas. In 1992 it was proposed that submillimeter-wavelength channels could be used for many of the sounding and cloud/precipitation imaging applications that previously were believed to require the use of microwave channels. The capabilities of submillimeter-wave channels for precipitation imaging were further demonstrated in 1994 using airborne imagery of clouds at the 325 GHz water vapor band. These studies suggested that the antenna costs for geosynchronous microwave precipitation imaging and temperature and moisture sounding could be significantly reduced while retaining good spatial resolution by using key submillimeter-wavelength water vapor and oxygen bands. It was with this notion that the Geosynchronous Microwave Sounder Working Group (GMSWG) was convened to develop a model for a practical submillimeter-wave geosynchronous microwave (GEM) sounder and imager. The current GEM concept is based on a ~2-3 meter center-fed reflector antenna and fast-scanning subreflector. The subreflector provides a narrow-field rapid scan capability with a wide-field scan provided by a slower motion of the entire antenna. As a result GEM will be capable of either intensively observing specific areas near severe weather or obtaining synoptic information over an extended environment.

In this study we illustrate the precipitation retrieval capabilities of GEM using an observation system simulation for a landfalling hurricane event (Hurricane Bonnie, August 1998). The system simulations are based on 6-km resolution, 60-level microphysical cloud data obtained from MM5 model runs for Hurricane Bonnie using the Reisner five-phase microphysical cloud model. A unique fast forward radiative transfer model based on the discrete-ordinate (DO) method and incorporating both scattering effects and fast calculation of the Jacobian of the forward transfer model is used to compute observed brightness temperature fields and their derivatives. Discussed will be the potential accuracy of rain rate and cloud liquid and ice water content retrievals, along with the impact of numerical weather model (NWP) phase-locking on retrieval accuracy. Phase-locking of an NWP onto the atmospheric state is facilitated using GEM rapid-update microwave im-

agery. Results from the observation system simulations and a program of concept validation using an airborne GEM simulator will be presented.

Simulated radiometric precipitation measurements from the proposed european GPM (EGPM) satellite

ALBERTO MUGNAI, BIZZARRO BIZZARRI, SABATINO DI MICHELE, ALESSANDRA TASSA
ISAC-CNR, V. del Fosso del Cavaliere 100, 00133 Roma
PETER BAUER
The European Centre for Medium-Range Weather Forecasts (ECMWF), Shinfield Park, Reading, RG2 9AX, UK
FRANK SILVIO MARZANO
Dip. Electrical Engineering, CETEMPS, University of L'Aquila, 67040 Monteluco di Roio
PEDRO P. BAPTISTA
ESA-ESTEC, Postbus 299, Keplerlaan 1, 2200 AG, Noordwjik, Netherlands
ERIC A. SMITH
NASA Goddard Space Flight Center, Code 912.1, Greenbelt, MD 20771, USA
GREGORY TRIPOLI
University of Wisconsin, Dept. of Atmospheric and Oceanic Sciences, 1225 West Daydon Str. Madison, WI 53706, USA

In a companion paper, we describe the characteristics of the proposed European constellation member of the Global Precipitation Measurement (GPM) mission - i.e., the so-called EGPM satellite, that is presently under Phase A study by ESA. The scientific payload of the EGPM satellite would consist of an advanced conically scanning microwave radiometer and (as a very desirable option) of a three-beam nadir-pointing Ka-band rain radar.

In its baseline version, the EGPM microwave radiometer would have four window frequencies (18.7, 36.5, 89.0, and 157.0 GHz) in double polarization (horizontal, H, and vertical, V), and one single-polarization (H or V) frequency (23.8 GHz) in a wing of the 22.235 GHz water vapor line. In addition, as a very desirable option, the EGPM radiometer could have a few additional single-polarization (H or V) channels within the 60 GHz oxygen complex (a strong oxygen absorption band between about 50-70 GHz) as well as near the strong oxygen line at 118.75 GHz.

These oxygen-sounding channels would offer in fact two main advantages over window channels for precipitation retrieval: **(1)** the lesser sensitivity to surface contributions and therefore the more global applicability; **(2)** the possibility of cloud-slicing caused by the increasing height of weighting function peaks with increasing clear-sky absorption. Their disadvantage would be a stronger dependence on temperature, so that hydrometeor retrievals would have to be constrained by temperature information. To explore the potential of coupled 50-60/118.75 GHz radiometric observations for precipitation retrieval, we are presently considering the lower four channel pairs of the NPOESS Aircraft Sounder Testbed-Microwave (NAST-M)

instrument (i.e., those channels that have the larger average penetration depths into the atmosphere) - i.e., 50.30, 51.76, 52.8 and 53.75 GHz for the NAST-M 54 GHz radiometer; and 118.75 ± 3.5, 118.75 ± 2.55, 118.75 ± 2.05, and 118.75 ± 1.6 GHz for the NAST-M 118 GHz radiometer.

In this paper, we investigate the potential contribution of the EGPM microwave radiometer to precipitation measurements, by simulating and analyzing both its observations and precipitation estimates for a series of different precipitation systems that have been simulated by means of a time-dependent, three-dimensional cloud/mesoscale model with explicit microphysics.

Application of ground polarimetric radar for cross-validating satellite observation of precipitation

CHANDRASEKAR V. CHANDRA, SANGHUN LIM
Colorado State University, Dept. Electrical and Computer Engineering, Fort Collins, CO 80523-1373, USA
EUGENIO GORGUCCI, LUCA BALDINI
ISAC-CNR, V. del Fosso del Cavaliere 100, 00133 Roma

Dual polarization observation of precipitation is used extensively in hydrometeor classification as well as estimation of parameters of raindrop size distribution. Dual polarization radars that have polarization agility on transmit, and diversity on receive, can measure the full covariance matrix of the hydrometeor volume. The full covariance measurements have been used as input to develop hydrometeor classification models. Specifically, dual polarization radar measurements of reflectivity, differential reflectivity and co-polar correlation between two polarization states, linear depolarization ratio and the specific propagation phase, have been used for hydrometeor classification applications by several researchers. Two independent models have been developed in the literature using fuzzy logic system to classify hydrometeor types based on dual-polarization radar measurements, namely the Colorado State University Model and the NCAR/NSSL Model. Similarly, dual-polarization radar data have been used to retrieve parameters of the raindrop size distribution.

Satellite observation of precipitation using microwaves can be classified into active (radar) and passive (radiometer) measurements. The satellite borne observation of precipitation is done typically at high frequencies such as Ku and Ka band where rain attenuation is very significant. The attenuation parameterization as well as characterization of the mixed phase precipitation are fundamentally important problems for interpreting space borne radar observations. Similarly, the radiometric observations are sensitive to the column of different type of precipitation along the radiometer observation column.

This paper specifically addresses the role of polarimetric radars in providing the column of hydrometeor path and drop size distribution parameters for validating the active and passive measurements of space borne observa-

tions. These validation principles will be described specifically in the context of Global Precipitation Mission (GPM) and European GPM (EGPM).

Cloud properties of Hurricane Erin estimated from active and passive observations

GAIL SKOFRONICK-JACKSON
NASA Goddard Space Flight Center, Greenbelt, MD 20771, USA

Cloud properties of Hurricane Erin (2001) were estimated using a physically-based retrieval algorithm employing active and passive microwave observations from the fourth Convection and Moisture Experiment (CAMEX-4) that was based in Jacksonville, Florida, USA during August and September of 2001. Cloud properties retrieved include vertical profiles of temperature, cloud water and size distributions for liquid and frozen hydrometeors. The iterative retrieval process ensures that the differences between the algorithm's computed brightness temperatures and reflectivities are comparable to the observed brightness temperatures and reflectivities. The retrieval algorithm is unique in that it uses wideband (10 to 183 GHz) brightness temperature observations to constrain the liquid and frozen hydrometeor properties. The higher frequency channels are essential for determining the particle size distributions of the frozen hydrometeors.

The CAMEX-4 field campaign included multiple instruments located on ground, on low and high altitude aircraft, and on satellites were used to observe convective and hurricane systems. This work focuses on measurements taken during Hurricane Erin on 10 September 2001 from the ER-2, flying at an altitude of approximately 20 km. The instruments of interest for this work are the High Altitude MM Integrated Circuit (MMIC) Scanning Radiometer (HAMSR) with passive channels between 50 and 183 GHz, the Advanced Microwave Precipitation Radiometer (AMPR) with passive channels between 10 and 85 GHz, and the ER-2 Doppler Radar (EDOP) with an active channel at 9.6 GHz. These ER-2 instruments measure atmospheric hydrometeors in the microwave region of the electromagnetic spectrum.

The retrieval results show that the liquid particle size distributions are more easily retrieved, while the frozen particle size distributions are somewhat noisy and more difficult to constrain using the available observations. These difficulties in estimating the frozen particles result from inadequacies in measuring and then modeling all the variations in size distributions, shape, and (ice-air-water) densities. The assumptions about these variations are direct inputs to determining the dielectric constants. The dielectric constant (or refractive index) is one of the variables used to determine the hydrometeor absorption, scattering, and asymmetry factors and therefore is an important component in the radiative transfer calculations used in the iterative retrievals. Further in situ measurements are required in order to make the best assumptions about frozen hydrometeor densities.

SESSION 12
ATMOSPHERE: CLOUDS AND PRECIPITATIONS. PART 2
(*Chairpersons*: V. Chandrasekhar, A. Mugnai)

Toward improving estimates of remotely-sensed precipitation with MODIS /AMSR-E blended data techniques

Joe Turk, Steven D. Miller
Naval Research Laboratory, Marine Meteorology Division, 7 Grace Hopper Avenue, Monterey, CA 93943, USA

The multispectral sensing capabilities afforded by the Moderate Resolution Imaging Spectroradiometer (MODIS) instruments aboard the Earth Observing System (EOS) Terra and Aqua satellites have the potential to improve satellite-derived cloud and precipitation products. The whiskbroom scanning MODIS radiometers feature 36 narrowband channels between 0.4 to 14.4 µm of the optical spectrum, with sub-track spatial resolutions between 250 to 1000 m. Included in this channel suite are spectral bands having particular sensitivity to both cloud vertical distribution and microphysics. EOS-Aqua, the local afternoon crossing satellite, carries in addition to MODIS the Advanced Microwave Scanning Radiometer for EOS (AMSR-E), a conically scanning passive microwave (PMW) instrument with 12 channels between 6.9 and 89 GHz and channel-dependent spatial resolutions between 5 and 56 km. AMSR-E provides the unique ability to sense the full profile of cloud water and detect the presence of rainfall.

Since many of the MODIS bands are comparable to those available from the Meteosat Second Generation (MSG: an operational geostationary platform) Spinning Enhanced Visible and Infrared Imager (SEVIRI), EOS-Aqua provides an ideal test bed for investigating operationally oriented, blended PMW/Optical-spectrum techniques related to clouds and precipitation. New methods for detecting and decoupling convective and stratiform precipitation regimes are now under development. For example, combining optically thin cirrus detection and deep convective diagnostics from MODIS with integrated cloud liquid/ice water path information from AMSR-E provides a superior characterization of the environment than either sensor can accomplish independently. In this paper, we present both the capabilities and limitations of multispectral MODIS/AMSR-E blended techniques for the screening of precipitation/non-precipitation regimes, and how these new metrics complement deficiencies in current techniques for satellite-based estimates of global precipitation.

Consistency check of drop size distribution in rain retrievals with a combination of TRMM microwave imager and precipitation radar observations

SHOICHI SHIGE, KEN'ICHI OKAMOTO
Department of Aerospace Engineering, Oasaka Prefecture University, 1-1 Gakuen-cho, Sakai 599-8531, Japan
SHUJI SHIMIZU
Earth Observation Research and application Center (EORC), Japan Aerospace Exploration Agency, Harumi Island Triton Square, Office Tower X, 1-8-10 Harumi, Chuo-ku, Tokyo 104-6023 Japan
NOBUHIRO TAKAHASHI, TOSHIO IGUCHI
National Institute of Information and Communications Technology, 4-2-1-Nukui-Kita-machi, Koganei Tokyo 184-8795, Japan
TOSHIAKI KOZU
Electronic Control Systems Engineering, Shimane University, 1060 Nishikawatsu-cho, Matsue 690-8504, Japan

The TRMM Microwave Imager (TMI) and Precipitation Radar (PR) have been providing distribution of rainfall throughout the Tropics and contributed significantly towards reducing uncertainty in satellite estimates of rainfall. Although differences in global averaged rainfall between the two sensors have been reduced, regional and seasonal differences still exist. Possible error sources are static model assumptions involved with individual retrieval algorithm. For example, the PR algorithm (2A25: Iguchi et al. 2000) uses a globally averaged drop size distribution (DSD) model, which strongly affects PR retrievals because information on the DSD enters radar echoes through the six moment of the DSD. In this study, the consistency between TMI and PR sensors is investigated focusing on the DSD model, similar to Viltard et al. (2000) but with increased numbers of cases. We obtain simulated brightness temperature from PR precipitation profiles at the same frequencies as those of the TMI, with a forward radiative transfer model (Liu 1998). Comparison of the observed and simulated brightness temperature, especially in low-frequency channels, is conducted, because TMI brightness temperatures in low-frequency channels are insensitive to DSD. We examine whether or not the DSD model assumed by the PR algorithm produces good or poor agreement between the observed and simulated brightness temperature.

Modeling and measurement of rainfall by ground-based multispectral microwave radiometry

FRANK SILVIO MARZANO, DOMENICO CIMINI, PIERO CIOTTI
CETEMPS, University of L'Aquila, Via Vetoio, 67010 Coppito, L'Aquila, Italy
RANDOLPH WARE
University Corporation for Atmospheric Research (UCAR), Boulder, CO 80307, USA
ERMANNO FIONDA
Fondazione Ugo Bordoni, Via Baldassarre Castiglione 59, 00142 Roma, Italy

Ground-based microwave radiometry has been mainly investigated for estimating temperature, water vapor and cloud liquid profiles in the absence of precipitation [Westwater, 1993]. However, the increasing use of multifrequency radiometers in ground-based stations has raised the question of their potential for retrieving also rainfall rate from ground [Marzano et al., 1999, 2001]. From an experimental point of view, one of the main problems of ground-based radiometry for rainfall retrieval is the possible impact of water layers on the receiving antenna whose measurements can be heavily contaminated [Jacobson et al., 1997]. From a modeling point of view, the modeling approach to rainfall signature characterization requests a thorough insight into the e.m. interaction between the microwave radiation and the scattering medium. The radiative transfer theory has been so far the most used approach to take into account multiple scattering and vertical inhomogeneity of the atmosphere in the presence of hydrometeor scattering [Tsang et al., 1985]. Following previous works [Marzano et al., 2002], the objective of this paper is to investigate about the rainfall signature on multispectral microwave measurements from ground. We develop inversion algorithms for ground-based retrieval of surface rainrate, adopting a model-based approach. For both stratiform and convective precipitation, we use a radiative transfer model (RTM), including spherical liquid, melt and ice hydrometeors. From the solution of the forward models, by varying the model parameters in a physically-based manner, it is derived a synthetic database made by the downwelling simulated brightness temperatures, the associated mean radiative temperature and the total path-attenuation. Non-linear statistical inversion algorithms are developed for different sets of frequency channels, observation geometries, cloud types, and precipitation intensities. A special care is devoted to set up robust estimators in presence of a random noise which can be attributed to various sources, first of all effects of possible water-films on the antenna reflector. A maximum a posteriori probability discrimination technique is applied to separate stratiform from convective raining clouds. Simulation results are shown to illustrate the potential of the proposed models by selecting, for this study, a wide range of frequencies from 22 to 60 GHz, representing the frequency set currently available on the ground-based radiometrics system. The latter in-

strument has been recently upgraded to minimize the effects of hydrometeors on the radiometric measurements, a circumstance experimentally proved as well. As a validation of the approach, we have analyzed rain events occurred in Boulder, Colorado and at the Atmospheric Radiation Measurement (ARM) Program Southern Great Plains (SGP) site. Results are illustrated in terms of comparisons between measurements and model data in order to show that the observed radiometric signatures can be attributed to rainfall scattering and absorption. Rain estimates are also compared with available rain gauge data.

Evaluation of detection and monitoring of precipitation techniques using multi-sensor observations

IREN GOLDHAR RUBINSTEIN
Laboratory for Industrial and Applied Mathematics, York University, 4700 Keele Street, North York, ON, Canada M3J 1P3

Weather radar provide precipitation information for regions close to populated areas. Thus, this information is limited for locations within radar mask. Precipitation information and precipitation type identification are required for areas where no radar installations exist. Remote sensing observations with different instruments capable of rain detection can extend capabilities for monitoring precipitation on regional and global scale. In addition, remote sensing can provide information for validation and calibration of forecast models by providing spatial distribution of precipitation several times per day.

Passive microwave sensors because of the multi-frequency observations have capabilities not only to detect precipitation but also provide information about the vertical distribution of hydrometeors within large precipitation cells. The retrieval algorithms currently used to process spaceborne passive microwave data require input of parameters describing cloud properties and vertical distribution of hydrometeors. In order to determine sensitivity of the retrieval algorithms to these parameters we have compiled case studies for several winter and summer precipitation events in Ontario and Quebec. Time and space collocated SSM/I brightness temperatures, Doppler weather radar, and AVHRR observations were analysed for these events.

We have observed that detection of precipitation for the winter case studies was not as reliable as for the extreme summer events but there was high correlation between radar returns from above 7 km and 85 GHz brightness temperatures measured by a spaceborne sensor.

Development of a forward biased Montecarlo
for microwave radiative transfer computations

ALESSANDRO BATTAGLIA
Dipartimento di Fisica, Università di Ferrara, Via del Paradiso 12, 44100 Ferrara, Italy
SIMONE MANTOVANI
ISAC-CNR, Via P. Gobetti 101, 40129 Bologna, Italy

A completely forward Montecarlo radiative transfer code has been developed with biasing techniques to efficiently solve the polarized radiative transfer equation for the full Stokes vector. The code has been adapted to accomodate plane parallel/3-D vertically/horizontally inhomogeneous scattering atmospheres. Particular attention has been paid in stochastically treating the propagation, the emission and the scattering through anisotropic media like for clouds containing perfectly or partially oriented particles. This modellization results very appealing because all the biasing techniques in it do not introduce unphysical Stokes vector. Several numerical results and comparison with benchmark tests are presented for verification.

The Montecarlo code is used to evaluate the polarization effects at high microwave frequencies (90, 150, 220 GHz) from multilayer plane parallel atmosphere composed by ice clouds. In particular a sensitivity study has been carried out to understand the impact of the ice content, of the crystal shape and of the orientation distribution on the polarimetric parameters.

To achieve this goal, different phase functions and extinction matrix are computed for population of perfectly and randomly oriented ice crystals modelled with different shapes. Results are promising in the direction of ice content retrieval and in the characterization of ice cloud microphysical properties.

Modeling of passive microwave responses over a cyclone using outputs from mesoscale models and comparison with TMI satellite observations

CATHERINE PRIGENT
LERMA, Observatoire de Paris, 61 Avenue de l'Observatoire, 75014 Paris, France
MARTINA WIEDNER
Physikalishes Institut, Universität zu Köln, Zülpicher Strasse 77, 50937 Köln, Germany
JUAN PARDO
Inst. Estructura de la Materia, Dpto Astrofisica Molecular e Infrarroja, Serrano 121, Madrid 28006, Spain
OLIVIER NUISSIER, JEAN-PIERRE CHABOUREAU, JEAB-PIERRE PINTY, PATRIK MASCART
Laboratoire d'Aérologie, 14 Avenue Edouard Belin, 31400 Toulouse, France

Outputs from a mesoscale cloud model are used as inputs to a microwave radiative transfer model and the simulated brightness temperatures are compared

with the Tropical Rainfall Measuring Mission (TRMM) satellite observations.

The first objective is to assess the strengths and weaknesses of the mesoscale cloud model. Comparisons between model outputs and observations have already been performed in the VIS and IR, but not extensively in the microwaves. Microwaves are expected to give more informations on the liquid and ice contents of the cloud structure.

Secondly, we want to evaluate the microwave radiative transfer model.

These two objectives are intermixed and cannot be isolated. It requires expertise from the two communities (cloud model and radiative transfer model) in order to diagnose the origins of the discrepancies and to suggest solutions.

The satellite observations are carried out with the TRMM satellite (http://trmm.gsfc.nasa.gov) which is equipped with 5 instruments. In this study, the TRMM Microwave Imager (TMI) observations are used: it measures the brightness temperatures at 10.7, 19.4, 21.3, 37 and 85.5 GHz in the vertical and horizontal polarizations (except for 21.3 GHz which is vertical polarization only).

The convective situations are modeled using Meso-NH. It is a 3D non-hydrostatic mesoscale code able to simulate a great variety of motions from the large meso-alpha scale down to the micro-scale, including the grid-nesting facility. It is currently initialized by ECMWF analyses to simulate real meteorological flows. Besides others, Meso-NH has an explicit cloud scheme which calculates the time evolution of several microphysical species: cloud droplets, raindrops, pristine ice crystals, snowflakes and graupels (http://www.aero.obs-mip.fr/mesonh). Two situations are presented in this study: the cyclone Bret (August, 1999 in the Gulf of Mexico) and a South Atlantic Convergence Zone case (off the Brazilian coast, February, 2001).

Radiative transfer calculations are performed with the Atmospheric Transmission at Microwaves (ATM) model (Pardo et al., JQSRT, 2002; Pardo et al., IEEE TGRS, 2001, Prigent et al., JGR, 2001). It includes atmospheric gaseous absorption, scattering by hydrometeors, and surface emissivity simulations to calculate the expected microwave brightness temperatures corresponding to the conditions simulated by Meso-NH.

In particular, we assumed that the hydrometeors are distributed according to the Marshall-Palmer distribution and calculated their size distribution. Further we refined the calculation of the refractive index, which takes size and density of the particles into account.

For both atmospheric cases, the spatial structure of the simulated brightness temperatures and the microwave observations agree very well. At high frequencies, surprisingly good agreement is obtained between the simulations and the observations, given the high sensitivity of these frequencies to the particle characteristics, especially in the ice phase. This gives a strong confidence not only in the radiative transfer model but also in the ice phase Meso-NH scheme.

It is planned to systematically evaluate the Meso-NH outputs by comparing the resulting microwave simulations with available satellite observations in the same frequency range.

SESSION 13
SENSOR CALIBRATION
(*Chairpersons*: A. Gasiewski, G. Schiavon)

**Status of mutual calibration and evaluation between ADEOS-II/
AMSR and AQUA/AMSR-E**

KEI SHIOMI
Remote Sensing Technology Center of Japan, (RESTEC), Uni-Roppongi Bldg. 7-15-17,
Roppongi Minato-ku, Tokyo 106, Japan
KEIJI IMAOKA, YASUHIRO FUJIMOTO, AKIRA SHIBATA
Earth Observation Research and Application Center/JAXA, Harumi Island Triton square,
Office Tower X 22F, 1-8-10, Harumi, Chuo-ku, Tokio 104-6023 Japan

The Advanced Microwave Scanning Radiometer (AMSR) is a newly developed multi-frequency microwave radiometer onboard the Advanced Earth Observing Satellite-II (ADEOS-II) of Japan Aerospace Exploration Agency (JAXA). It measures eight frequencies from 6.925 to 89.0 GHz with dual polarizations. The Advanced Microwave Scanning Radiometer for. EOS (AMSR-E) onboard NASA's EOS Aqua, which was launched 6 months before ADEOS-II, has almost the same characteristics on hardware as AMSR. Observation swath width of AMSR is 1600km, while that of AMSR-E is 1450 km. AMSR has 50.3 and 52.8 GHz vertical polarization channel, whereas AMSR-E does not. Observation of 50 GHz band by AMSR is the first attempt with conical scanning method different from conventional cross-track scanning. Since observation local times are different, both sensors make it possible to observe globally in short time.

To derive observation brightness temperature (TB) with simple two-point liner calibration, AMSR and AMSR-E have High Temperature noise Source (HTS), which gives a high temperature end target, and Cold Sky Mirror (CSM), which gives a low temperature one. HTS is controlled around 300 K with internal heater and CSM observes the deep space temperature 2.7 K. HTS has 8 thermometers attached on its outer and inner surface to measure the physical temperature. However, the temperature distribution in HTS structure is non-uniform and has its variation, thus those monitoring temperature cannot use as a determined high temperature target without arrangement. As a first step, effective HTS TB is calculated with multiple regression using 8 thermometer temperatures between TB of AMSR/AMSR-E and TB derived from Reynolds SST or transformed TB of SSM/I. Although HTS TB can be effectively calibrated on average, the detail fluctuation in orbit is not sufficiently simulated. As next step, HTS

TB is adjusted detail by the gains related to receiver (RX) and low noise amplifier (LNA) physical temperature variations with multiple regression using them over the scene data. As a result, HTS TB with this method is well simulated.

After calibration, compared with TBs between AMSR and AMSR-E, we evaluate the calibration method. We are to eliminate systematic difference and achieve equivalent accuracy to be able to process both data together. As for the 50 GHz band channels, which are measured by only AMSR, since they will give some information of atmospheric temperature, we evaluate with preexisting in-situ measurements. Thus, we make an effort to study the channels with insufficient correction. In this presentation, we show the current status of calibration and evaluation for AMSR and AMSR-E.

Calibration of fully polarimetric noise injection radiometer of miras

ANDREAS COLLIANDER, SIMO TAURIAINEN, TUOMO AUER, JUHA KAINULAINEN, MARTTI HALLIKAINEN
Helsinki University of Technology, Laboratory of Space Technology, P.O. Box 3000, FIN-02015 HUT, Finland
JOSU UUSITALO
Ylinen Electronics Ltd, Teollisuustie 9A, FIN-02700, Kauniinen, Finland
MARTTI TOIKKA
Inst. Toikka Engineering Ltd, Hannuntie 18, 02360 Espoo, Finland

An L-band noise injection radiometer (NIR) has been designed and implemented by the Helsinki University of Technology, Laboratory of Space Technology, for the SMOS (Soil Moisture and Ocean Salinity) mission of the European Space Agency (ESA). The work is performed as part of ESA's MIRAS Demonstrator Pilot Project-2 (MDPP-2) under a subcontract for EADS-CASA. The other partners in the MDPP-2 NIR project are Toikka Engineering Ltd. and Ylinen Electronics Ltd.

Fully polarimetric radiometers using digital correlator have been documented previously, but one using noise injection method for antenna brightness temperature measurement is unprecedented. The benefit of the method is high accuracy and stability of the measurements. However, the method affects the sensitivity and calibration of the instrument and these issues are discussed in this paper.

The NIR will work as part of the MIRAS (Microwave Imaging Using Aperture Synthesis) instrument. Its main purposes are (1) to provide precise measurement of the average brightness temperature scene for absolute calibration of the MIRAS image map and (2) to measure the noise temperature level of the internal active calibration source for individual receiver calibration. The NIR will be used also in the MIRAS array as a regular receiver

unit for interferometric image creation. The performance of the NIR is a decisive factor of the MIRAS performance.

One challenge in the implemented concept is the fact that there is additional noise in the correlated signal due to the noise injection method used in the brightness temperature measurement. However, we have shown with simulations and measurements that degradation of sensitivity is within acceptable limits.

A fully polarimetric radiometer has several parameters, which have to be considered in the calibration. We have applied a method of calibrating the correlators of interferometric radiometer so that the Stokes parameters can be solved using the same correlator. This means that the calibration network of MIRAS can be used for calibrating the correlator of NIR for both interferometric measurements and for fully polarimetric measurement. This kind of scheme has not been presented before.

An additional challenge in the NIR is the fact that the circuitry used for noise injection causes an offset in the correlation measurements, and also this offset needs to be calibrated. Sensitivity of the third and fourth Stokes parameter for this offset has been determined and our results indicate that the offset contribution has to be known accurately for fully polarimetric measurements. The previously presented methods have not addressed this issue, since a similar measurement condition has not been present.

We have developed and demonstrated a method for determining this offset so that the amount of correlated noise coupled between channels in the circuitry can be solved. However, by connecting the antenna in front of the receivers a new route for cross coupling is introduced. We have made preliminary measurements on this and more measurements will be carried out by the end of year 2003, so that a proper procedure for calibrating this effect can be defined.

Verification measurements of the chosen HUT-2D L-Band synthetic aperture radiometer technology

Kimmo Rautiainen, Robert Butora, Martti Hallikainen
Helsinki University of Technology, Laboratory of Space Technology, P.O. Box 3000, FIN-02015 HUT, Finland

An airborne L-band aperture synthetic radiometer (HUT-2D) for soil moisture and ocean salinity measurements is under construction at the Helsinki University of Technology, Laboratory of Space Technology. Currently all hardware design is frozen and a successful test campaign has been conducted with the prototype receiver subassembly to verify the chosen technology and instrument performance. The prototype subassembly is composed of four L-band receivers and one-bit digitising boards, a calibration

subsystem based on correlated noise injection, an external distributed local oscillator unit, and a digital correlator.

The test campaign was focused on the receiver on-board calibration measurements in laboratory conditions and on self-interference measurements in an RFI-free measurement facility (instrument surrounded with absorber material suitable for L-band. The expected complex correlation results (visibilities) for such a target are zero if the absorbers are in the same ambient temperature as the receivers.

Several improvements were made to the receiver unit during the campaign: The four-unit supporting structure ground plane was extended and vertical walls were built behind the ground plane to suppress any propagating waves at the backside of the construction. After the improvements the visibilities of the longer baselines became very close to zero, while a constant offset component between 20 to 50 correlation units (1cu = analogue correlation equal to 10^{-4}) remained in the shortest baselines. The antenna spacing in the HUT-2D instrument is 0.7 wavelengths. Based on the test results the constant offset term is very likely due to the receivers: the front-end isolator together with the antenna coupling attenuation is not sufficient to remove totally the effect of the correlated noise component coming out from each receiver. The offset remains constant and can be corrected. The correction was verified with measurements of a cold point target (liquid nitrogen-cooled absorber).

The improvements made to the four-unit subassembly can be included in a straightforward manner in the antenna supporting structure fairing of the final airborne instrument.

AMSR-E observed radio frequency interference and implications for passive microwave remote sensing

Eni G. Njoku, Li Li, Tsz Chan
Jet Propulsion Laboratory, California Institute of Technology, 4800 Oak Grove Drive, Pasadena, CA 91109, USA
Peter Ashcroft, Frank Wentz
Remote Sensing Systems, 438 First Street, Suite 200, Santa Rosa, CA 95401, USA

The AMSR-E instrument on the Aqua satellite measures the Earth's radiance in six frequency bands centered at 6.9, 10.7, 18.7, 23.8, 36.5 and 89 GHz, each with dual polarization. The Aqua satellite was launched in May 2002 into a polar, sun-synchronous orbit with Equator crossings at 1:30 am/pm local time. Any point on the Earth is viewed by AMSR-E at least once every three days in both ascending and descending orbits. The 6.9 GHz Earth-radiance data measured by AMSR-E are the first C-band observations from space since the Nimbus-7 SMMR instrument ended its mission in

August 1987. The primary uses of the C-band AMSR-E data are to provide sea surface temperature measurements over the ocean and soil moisture measurements over land. Unfortunately, no part of the C-band frequency range is protected exclusively for passive remote sensing, and the expanding use of this frequency range for telecommunications purposes has led to Radio Frequency Interference (RFI) that contaminates the remote sensing signals. Drawing on an archive of more than one year of AMSR-E data, we are developing a global survey of detectable RFI sources, focusing on the intensity, spatial, temporal, spectral and polarization characteristics of the RFI.

In many cases the RFI is easily recognizable, either by its intensity or its correlation with known population centers. While the obvious RFI (almost all of which is over land) can be identified and discarded in geophysical processing of the data, it is challenging to identify RFI when the signature is weaker and less pervasive. Various indices have been developed and tested with the AMSR-E data to identify RFI of different signal strengths and characteristics.

In this paper we review these indices and their results in characterizing RFI. Statistics of the RFI are compiled that will be useful for designers of future C-band radiometers, such as the CMIS sensor on the operational NPOESS satellites, and will provide early indications of the possible emergence of RFI at frequencies other than C-band.

A precision black body calibration target for operational meteorological microwave radiometers

MARK JARRETT
SULA Systems Ltd, Old Crown House, Market Street, Wotton under Edge, GL12 7AE, UK

The use of microwave radiometer sounders and imagers for the measurement of meteorological products is now well established. Recent developments in antenna feed and receiver component technology has led to significant improvements in radiometric resolution. However, users are also looking for improved radiometric accuracy performance for applications such as numerical weather prediction and climate monitoring and research, and this imposes increasing demands on the quality of the black-body target that is used to provide one of the in-flight calibrations. For cross-track sounders such as AMSU-B it is possible to use a target that is relatively large and heavy and to mount it within the instrument so that it is shielded from external thermal fluxes. However, for conical scanning radiometers that are used for both imaging and sounding, it is necessary to use a target design that is much lighter, yet which still provides high emissivity and which has good thermal stability and uniformity.

This paper describes the design, manufacturing and testing of a high

quality black-body target that has been developed for use on future conical scanning instruments over the frequency range 18 to 150 GHz. First, an exact EM design of the target was undertaken. This design process required the use of complex permeability and permittivity data, and a review of the literature showed that such data was not readily available. Therefore, the first stage was to undertake a measurement programme to obtain such a data. Another issue that had to be addressed was the measurement of the reflectivity of the target once it had been manufactured.

A further aspect of the target that was considered in detail was its thermal design. Detailed thermal modelling was performed taking into account the target itself, its thermal interfaces, including the thermal fluxes experiences in a typical polar LEO orbit, and the predicted gradients and stability assessed.

Analysis of ERS-2 and TOPEX microwave radiometer in-flight calibration and monitoring

Laurence Eymard, Fatima Karbou
CNRS/IPSL/CEPT, 10-12 Avenue de l'Europe, 78140 Vélizy, France
T. Ngan, Estelle-Anne Obligis
CLS, 8-10 rue Hermes, 31526 Ramonville St-Agne, France

The microwave radiometers on altimeter missions are specified to provide the wet troposphere path delay with an accuracy of 1 cm or better, at the location of the altimeter footprint. These instruments have 2 or 3 channels including one in the water vapour absorption line centred at 22.235 GHz in order to properly retrieve the path delay. The quality of the retrieval relies on an accurate in-flight calibration, both in term of absolute values and of time stability. The calibration of the measured brightness temperatures requires the exact knowledge of all the instrument parameters but within the on-ground calibration in vacuum chamber, the reflector cannot be included, so the instrument characterization is not fully representative of the situation in space. Moreover, it is very difficult to properly estimate the radiation emitted by the various sources in space (emission/reflection of the microwaves by the satellite itself, contribution of the earth in the side lobes). The reflector transmission is also poorly known (and often not measured), and is subject to degradation in space due to aging or collisions with debris or other small object particles. For all these reasons and because the mission requirements are high, it is not possible to be confident in the pre-launch calibration adjustment. So careful analysis, development of indirect methods of calibration, and correction when needed are required after launch.

We propose in this paper to do a comparison of the calibration of 2 microwave radiometers, EMWR on ERS-2 mission and TMR on TOPEX/

Poseidon mission by (1) presenting the specifications of each one and their in-flight calibration results after launch; (2) the different methods to monitor the stability of the instruments along their lifetime; and (3) the different methods used to externally absolute calibrate the instruments because contrary to conically scanning instruments, the in-flight calibration does not include the complete antenna circuit and so it is therefore impossible to achieve an absolute internal calibration.

MIRAS-SMOS end-to-end calibration scheme

IGNASI CORBELLA, FRANCISCO TORRES, NURIA DUFFO, ADRIANO JOSÉ CAMPS
Universitat Politécnica de Catalunya, Departamento de Teoria del Senyal i Comunicacions, c. Jordi Girona 1-3, 08034 Barcelona, Spain

SMOS is a mission of the European Space Agency (ESA) devoted to the measurement of soil moisture and ocean salinity maps at global scale from radiometric measurements at L-band. For the first time in space-borne Earth remote sensing, aperture synthesis techniques will be used, so that the single payload of the mission (MIRAS) is a Y-shaped L-band interferometric radiometer. Brightness temperature maps are obtained by cross-correlating the outputs of a large number of small antennas, effectively providing a spatial resolution similar to that of a real aperture antenna of similar overall dimension as the whole instrument. This technique does not require mechanical movement of the array since brightness temperature maps of large areas are retrieved by Fourier synthesis out of the measured cross-correlations.

One of the main difficulties of this approach is finding the appropriate means to correct for instrumental imperfections. The error correction process is usually referred to as "internal calibration" and its goal is to compute, from the raw output of the correlators, the corrected visibility samples, which in further steps will be inverted to get the brightness temperature map, or level-1 output. From it, single-pass sea surface salinity and soil moisture maps will be finally computed giving the level-2 output.

Internal error correction in MIRAS is performed in various steps. First, the basic correlator counts are preprocessed to give the so-called quadrature-corrected raw visibilities. This first step, which is common to both observation and calibration operation modes, can be referred to as autocalibration, since exclusively makes use of the intrinsic properties of the magnitudes. In a second step, uncorrelated noise is injected to compute the residual correlation offset. Finally, in a third step internal calibration is performed by injecting correlated noise at receivers' inputs. The correlation measurements while injecting noise provide an estimation of the instrument in-phase, amplitude and fringe-washing terms. These ones are later used to perform the correction needed while the instrument is in observation mode.

Obviously this procedure cannot deal with the imperfections of the antenna itself since the noise is injected between the antenna and the receiver input, therefore antenna pattern errors must be on-ground characterized and taken into account in the image reconstruction process. To avoid having a noise distribution network (NDN) exceedingly large, the approach relies on distributed noise injection, allowing less stringent network characteristics. Also, a relative calibration approach is envisaged to eliminate the contribution of the NDN itself.

Since the systematic errors depend basically on the receivers' physical temperatures, the rate at which the instrument must enter into calibration mode is related to the temperature variation with time, which is known to be deterministic along the orbit and along the year.

The presentation at rad 2004 will describe the present status of the MIRAS internal calibration approach using noise injection, including an insight on the time needed between calibrations.

SESSION 14
INSTRUMENTS AND ADVANCED TECNIQUES
(*Chairpersons*: P. Racette, H. Suess)

Faraday rotation correction using
the polarimetric brightness temperature matrix

Ribó Serni
Institute for Space Studies of Catalonia IEEC/CSIC, Despatx 201, Edifici Nexus, c/Gran Capità 2-4, 08034 Barcelona, Spain
Manuel Martín-Neira
ESA-ESTEC, Postbus 299, Keplerlaan 1, 2200 AG, Noordwijk, Netherland
Francisco Torres
Universitat Politécnica de Catalunya, Departamento de Teoria del Senyal i Comunicacions, c. Jordi Girona 1-3, 08034 Barcelona, Spain

Faraday rotation is an important issue to be taken into account in spaceborne L-band radiometers for earth observation as it may have a non-negligible effect on the retrieved physical parameters. This has been recently studied for ocean surface salinity by (1) and (2). Also different authors have proposed methods to compensate or measure the effect of Faraday rotation (3-5).

The method proposed in this paper consists in measuring the complete polarimetric brightness temperature matrix at the antenna frame. Its relationship with the polarimetric brightness temperature matrix of the observed target is a simple matrix product, where the rotation matrices are involved. These rotation matrices are due to the Faraday rotation, and may also arise if the target is viewed in an off-boresight direction of the antenna, as happens in imaging radiometers like MIRAS (6). For the case where the polarimetric brightness temperature matrix of the target is diagonal, that is, there is no correlation between H and V polarisations, this relationship becomes a simple diagonalisation equation and the H and V brightness temperatures are the eigenvalues of the polarimetric brightness temperature matrix at the antenna. In this way the H and V brightness temperatures of the target can be obtained without measuring separately the Faraday rotation. Furthermore, this rotation may be obtained from the eigenvectors of the polarimetric brightness temperature.

The presentation gives a detailed mathematical description of the method and also some simulation results that have been performed using this new method.

(1) D.M. Le Vine, S. Abraham, *The effect of inosphere on remote sensing of sea surface salinity from space: Absorption and emission at L-band*, IEEE Trans. on Geosci. and Remote Sensing, **40** (4), 771-782, Apr. 2002.
(2) S.H. Yueh, R. West, W.J. Wilson, F.-K. Li, E.G. Njoku, Y. Rahmat-Samii,

Error sources and feasibility for microwave remote sensing of ocean surface salinity, IEEE Trans. on Geosci. and Remote Sensing, **39** (5), 1049-1060, May 2001.

(3) A. CAMPS, N. DUFFO, M. VALL-LLOSERA, B. VALLESPÍN, *Sea surface salinity retrieval using multi-angular L-band radiometry: Numerical study using the smos end-to-end performance simulator*, in: Proc. IEEE Intern. Geosci. and Remote Sensing Symp., **2**, 1367-1369, June 2002.

(4) S.H. YUEH, *Estimates of Faraday rotation with passive microwave polarimetry for microwave remote sensing of earth surfaces*, IEEE Trans. Geosci. and Remote Sensing, **38** (5), 2434-2438, Sept. 2000.

(5) N. SKOU, *Faraday rotation and L band oceanographic measurements*, Radio Sci., **38** (4), 2003.

(6) M. MARTÍN-NEIRA, S. RIBÓ, A. MARTÍN-POLEGRE, *Polarimetric Mode of MIRAS*, IEEE Trans. Geosci. and Remote Sensing, **40** (8), 1755-1762, Aug. 2002.

Future prospects for airborne microwave remote sensing in the UK

DAVID POLLARD, JONATHAN. P. TAYLOR
Met Office, Fitwroy Road, Exeter, Devon, EX1 3PB, UK

The UK atmospheric research community will soon take delivery of a new atmospheric research aircraft. The new aircraft, a converted BAe 146-300, will be replacing the C-130 that was previously operated by the Met Research Flight (MRF).

As well as the suite instrumentation from the C-130 the new aircraft will also benefit from newly developed instruments, including a differential absorption water vapour and ozone lidar and potentially a cloud radar.

This presentation will give an overview of the new aircraft and its capabilities, as well as describing the microwave radiometers, MARSS and Deimos, which will be installed on the aircraft, and their scientific objectives.

The MARSS and Deimos instruments are both along track scanning total power radiometers with end-to-end calibration provided by ambient and heated black body targets. MARSS measures in 5 channels matching the AMSU-B channels at 89, 157 and 183 GHz with mixed polarisation, whilst Deimos can measure V and H polarisation at 22 and 59 GHz.

Both instruments complete a scan every 3 seconds during which time MARSS takes measurements in 18 directions, 9 up and 9 down, whilst Deimos will measure in 5 directions, either up or down depending on how it is installed on the aircraft.

These instruments have traditionally been used for validation of clear air radiative transfer models and surface studies. With the advent of the new aircraft, it is expected that they will be used in support of the assimilation of observations from current and anticipated satellite instruments. This will include the validation of scattering radiative transfer models and the representation of the cloud microphysics within them; and investigating large scale inhomogeneity and processes within precipitation affected fields of view in support of precipitation studies and the forthcoming GPM missions.

It is also hoped that the instruments can be used to validate and develop surface emissivity models as well as retrievals of surface quantities such as soil moisture and ocean salinity.

The NASA airborne earth science microwave imaging radiometer (AESMIR): A new sensor for earth remote sensing

ED KIM
NASA Goddard Space Flight Center, Greenbelt, Maryland 20706, USA

The Airborne Earth Science Microwave Imaging Radiometer (AESMIR) – a versatile new airborne imaging radiometer developed by NASA – recently completed its first flights. The AESMIR design is unique in that it performs dual-polarized imaging at all standard passive microwave frequency bands (6÷89 GHz) using only one sensor head/scanner package, providing an efficient solution for Earth remote sensing applications (snow, soil moisture/land parameters, precipitation, ocean winds, sea surface temperature, water vapor, sea ice, etc.), particularly when combined with other synergistic instruments. The microwave radiometers themselves incorporate state-of-the-art receivers, with particular attention given to instrument calibration.

Parallel filter banks allow AESMIR to simultaneously simulate the exact passbands of multiple satellite radiometers: SSM/I, TMI, AMSR, Windsat, SSMI/S, and the upcoming GPM/GMI and NPOESS/CMIS instruments – a unique capability among aircraft radiometers. And, all receivers except the 23 GHz sounding channels are configured for 4-Stokes polarimetric operation using both traditional analog detection and high-speed digital correlators.

The single-package design of AESMIR makes it compatible with a variety of aircraft, including high-altitude platforms. The arbitrary 2-axis gimbal can perform conical and cross-track scanning, as well as fixed-beam staring. This compatibility with high-altitude platforms coupled with the flexible scanning configuration, opens up previously unavailable science opportunities, as well as providing wider swath coverage for all science applications.

In another role, AESMIR is serving as a ready-made testbed for spaceflight radiometer technology development. Examples involving a calibration source for polarimetric or interferometric spaceborne radiometers and high-speed digital correlators will be highlighted.

The capabilities and unique design features of AESMIR will be described, and example imagery from test flights will be presented. Finally, the AESMIR/COSMIR – super-instrument – concept will be presented.

SiGe technology and radiometric applications: present possibilities and future trends

FEDERICO ALIMENTI, STEFANIA BONAFONI, VALERIA PALAZZARI, LUCA ROSELLI, ANDREA SCORZONI, PATRIZIA BASILI
DIEI, University of Perugia, Via G. Duranti 93, 06125 Perugia, Italy

Sensing of the environment has improved dramatically in recent years thanks to the evolution of ground-based and space-based microwave radiom-

eters. Reliable weather forecasts, global climate studies and Earth's surface property detection over a wide range of spatial and temporal scales create an increasing demand of networks of high-reliability low-cost systems (1). These apparatuses should satisfy stringent power consumption as well as size/weight requirements. To solve the above problems several monolithic design have been published in the past, ranging from simple Tuned Radio-Frequency (TRF) receivers (2), (3), to complex heterodyne architectures (4). All these circuits were implemented in GaAs since, similarly to other III-V semiconductor compounds, the high charge-carrier mobility and saturation velocity can be exploited to realize high-frequency and low-noise devices (5). During the last decade a great effort has been made in order to develop the Silicon-Germanium (SiGe) Heterojunction Bipolar Transistor (HBT). In such a device the base region is formed by an epitaxially grown SiGe layer between adjacent silicon layers. Due to the lower band-gap of the base region, even in the case of high base doping, a high emitter efficiency is achieved. This allows one to combine a small base width with a low base series resistance (6). As a result, performances similar to that of GaAs devices can be achieved in terms of both cut-off frequency and noise figure (7). Nowadays the SiGe option is commercially available in a number of foundries: a typical $0.4 \mu m \times 12 \mu m$ HBT is characterized by a cut-off frequency of about 60 GHz and a noise figure less than 3 dB at 15 GHz (8). Another advantage offered by such a technology is the complete compatibility with classic silicon based processes (e.g. CMOS and BiCMOS) and, therefore, the possibility to integrate, on the same chip, a complete radiometric system (both the front-end and the data processing unit). Such a philosophy, known as System-on-a-Chip (SoC) approach, could significantly impact on the design of radiometric systems. For example, easy and effective thermal stabilization strategies can be pursued at chip level, thus reducing the measurement errors due to the drift of the circuit parameters. Purpose of this contribution is to report the state-of-the-art achieved by the SiGe technology and discuss the feasibility of a single-chip radiometric receiver. To this purpose, present possibilities and future trends will be investigated.

(1) S. CREWELL et al., *Boreal Environment Research*, 7, 235-245, 2002.
(2) S. WEINREB, IEEE Intern. Microwave Symp., 405-407, 1991.
(3) B. KANE et al., IEEE Microwave and Millimeter Wave Monolithic Circuit Symp., 59-62, 1995.
(4) U. GUTTICH et al., IEEE Microwave and Millimeter Wave Monolithic Circuit Symp., 145-148, 1996.
(5) G. RAGHAVAN et al., IEEE Spectrum, 37, 47-52, Oct. 2000.
(6) P. CRESSLER, IEEE Spectrum, 32, 49-55, Mar. 1995.
(7) P. RUSSER, IEEE Trans. Microwave Theory Tech., 46, 590-603, May 1998.
(8) D.L. HARAME et al., IEEE J. of Solid State Circuits, 48, 590-603, Nov. 2001.

Initial results from the 2d-star synthetic aperture radiometer

DAVID M. LE VINE
NASA Goddard Space Flight Center, Greenbelt, Maryland 20771, USA
MICHAEL HAKEN
Science Systems Applications (SSAI), 10210 Greenbelt Road, Suite 600, Lanham, Maryland 20706, USA

The 2D-STAR is a new airborne interferometric radiometer that images using aperture synthesis in two dimensions. It is a research instrument built under NASA's Instrument Incubator Program (IIP) as part of work to extend this technology for passive microwave remote sensing to include synthesis in two dimensions. Examples will be presented of the first images from this instrument obtained during test flights in June, 2003 over the Delmarva Peninsula.

The 2D-STAR antenna consists of a rectangular array of dual polarized, patch antennas tuned to L-band (1.413 GHz). Each patch is connected to its own receiver that filters, amplifies and mixes to a common IF. The IF signal then goes to the digital processor where it is digitized, phase shifted to produce I and Q signals, and then multiplied by the signal from the other antennas. Each (complex) product is proportional to the Fourier transform of the brightness temperature of the scene at spatial frequencies determined by the spacing between the antennas. Together, these products form a sampling of the Fourier transform that is inverted in the signal processing stage to obtain an image of brightness temperature. The digital processor averages for a minimum time (10 ms) and then passes the products to the data system which averages and stores the data. In the current configuration, 10 samples are averaged to form one record and three records are taken at each polarization before switching polarization.

The antenna array consists of a fully populated, rectangular array of patches; however, only some of the patches are connected to a receiver. In the current configuration the instrument operates as an array thinned into the shape of a cross ("+") with 11 elements (patches) in each arm. Each patch is square and about 6.86 cm on a side. The patches are dual polarized and separated by 0.5 wavelength (10.6 cm at L-band).

The instrument was completed in fall, 2002. Problems with the data flow through the correlator were corrected and 2D-STAR was successfully test flown in June, 2003 prior to the SMEX-03 soil moisture campaign. Images from these test flights, which represent the first images from this instrument and are among the first images from an aircraft instrument using this technology, will be presented.

Filter bank radiometers for atmospheric profiling

THOMAS ROSE, HARALD CZEKALA
Radiometer Physics GmbH (RPG), Birkenmaarstrasse 10, 53340 Meckenheim, Germany

Microwave radiometers are used for remote sensing of atmospheric variables such as integrated water vapor (IWV), liquid water path (LWP) and vertical profiles of temperature and humidity. While IWV and LWP are often observed by radiometers with two distinct frequencies and separate receivers for each channel, profiling radiometers need to observe several frequencies along the wings of spectral lines. Although a simultaneous observation of all such frequencies should be preferred in order to obtain consistent measurements, some profiling radiometers use synthesizer controlled receivers: The detection frequency of only one receiver is sequentially tuned to the specified observation frequencies. Such designs have technical advantages (a simplified receiver layout), but scientific drawbacks: If short term fluctuations (such as clouds) occur during the measurement cycle, the samples along the wing of the observed line become inconsistent and thus the retrieved profiles will be less accurate. Furthermore, it is often desirable to use the profiler with its set of multiple channels for the retrieval of IWV and LWP. The sampling rate for these variables will be significantly reduced when they are observed with a synthesizer controlled profiling radiometer instead of a standard two channel radiometer. As a consequence, RPG-profilers perform simultaneous direct detection of all profiling channels by using a filter bank design. The RF band is directly amplified and split into 8 channels for each profiler. In this way all frequencies are recorded at the same time (100% duty cycle) and the repetition rate of measurements are only limited by the integration time of a single detector (typically one second). Improving the duty cycle by using the filter bank design allows for observation of rapid changes in the atmosphere, for example humidity bubbles and turbulent transport phenomenon. All calibration procedures are several times faster compared to synthesizer receivers. The direct detection technique contributes to higher accuracy and stability of observed brightness temperatures (no mixers, no sideband suppression necessary, no drifting local oscillators) and makes the receivers less sensitive to intermittances by telecommunication links (e.g. cell phones). In contrast to previous generation instruments, improvements in technology allow for small and precise low-cost instruments. The hardware design is optimized for durability and offers many additional sensors which make the instruments ideal for measurement campaigns. The software design provides full access to all sensors and allows also for unattended measurement periods of several weeks. High accuracy and long term stability together with high sampling rate are essential features of the filter bank receiver design. Due to the receiver layout the system is also capable of measuring high resolution (50 m, $h<1000$ m) boundary layer temperature profiles.

SESSION 15
INSTRUMENTS AND ADVANCED TECNIQUES. PART 2
(Chairpersons: I. Corbella, D. Le Vine)

SPIRA - A scanning polarimetric imaging radiometer in w-band

Alexandar Duric, Andreas Magun
Institute of Applied Physics, University of Bern, Sidlerstrasse 5, 3012 Bern, Switzerland

SPIRA is a fully polarimetric imaging radiometer at 91 GHz whose developement started in November 2002 at the Institute of Applied Physics in Bern. The aim of the project is to design and build an imager for obtaining signatures of the brightness temperature distribution of the Earth surface in all four Stokes parameters. SPIRA will be transportable by 2 persons and achieve an imaging-ready status in a short time. In this paper we present the concept as well as the current status of the SPIRA-project.

Due to the required size and weight limits, compatible with maximum angular resolution, a half power beamwidth of 0.5 deg was chosen. For a scan angle range of 30×30 degrees an image consists of 125×125 pixels. As the imaging distance will be approximately 30 m imaging will be done in the near field. A radiometric sensitivity of 0.5 K will be achieved with a bandwidth of 2 GHz, millisecond sampling time, an interlaced calibration and post-measurement digital integration. Because significant absorption changes in the earth atmosphere can occur due to changes in meteorological conditions, the scan time has to be made as short as possible - for SPIRA a limit of approximately 600 s is planned.

The antenna design has been completed. The aim was to maximize the main-beam efficiency, keeping at the same time the cross-polarisation as low as possible. This will guarantee minimum measurement errors due to side lobes and cross-polarisation. As the transportability of the system puts an upper limit on the antenna size the design of the imager had to be compact. This is achieved with a single reflector 90 deg offset antenna that is rotated around the horizontal axis of a fixed horn connected to the polarimeter. The rotating antenna, that scans in vertical direction, and the polarimeter are mounted on a horizontal table. Rotating the latter around the vertical axis provides also scans in the horizontal direction.

Two sub-harmonic mixers with a common local oscillator downconvert the orthogonally polarized signals, received by a dual polarized horn, to a frequency band between 2 and 4 GHz. They are correlated by a broadband correlator consisting of several hybrids and quadratic detectors, providing all four Stokes parameters. The receiver is calibrated with two switchable

noise diodes (noise adding) and an external hot load at ambient temperature. Data acquisition and control of scanning and calibration are done at millisecond rates. All raw data are immediately displayed and stored for the post-processing of images.

The ESA Envisat microwave radiometer mission two years after launch

PIERRE FÉMÉNIAS
ESA/ESRIN, Via G. Galilei, 00044 Frascati (Roma), Italy
ANNALISA MARTINI
Serco S.p.A., Via Sciadonna 24/26, 00044 Frascati (Roma), Italy

The Envisat satellite was launched on March 1, 2002. It carries on-board a large number of sensors among which a two-frequency Microwave Radiometer (MWR).

The Envisat MWR has evolved from the instruments previously flown on ERS-1 and ERS-2. For Envisat the design of the MWR had to be modified in some areas compared to its ERS predecessors to comply with the different platform and mission requirements. The structure is a new design using CFRP technology having the old deployable antenna replaced by nondeployable one fully integrated into the instrument structure.

The main objective of the microwave radiometer (MWR) is the measurement of the integrated atmospheric water vapour column and cloud liquid water content, as correction terms for the radar altimeter signal. In addition, MWR measurement data are useful for the determination of surface emissivity and soil moisture over land, for surface energy budget investigations to support atmospheric studies, and for ice characterization.

Over the last two years, the MWR sensor on-board Envisat has been commissioned and is now nominally operational since January 2003.

Next generation spaceborne microwave radiometers for meteorological applications

JANET CHARLTON, MARK JARRETT
Sula Systems Ltd, Old Crown House, Market Street, Wotton under Edge, Gloucestershire GL12 7AE, UK
PAT FOSTER
MAAS, 16 Peachfield Road, Malvern, Worcestershide WR14 4AP, UK
NIGEL ATKINSON
Met Office, FitzRoy Road, Exeter EX1 3PB, UK
ULF KLEIN
ESTEC, Keplerlann 1, PO Box 299, 2200AG Noordwijk, Netherlands

AMSU-A, AMSU-B and MHS represent the current generation of microwave radiometers that are used to support operational meteorology. The ATMS instrument currently being developed by NASA aims to combine the main functions of AMSU-A and AMSU-B in one instrument, but does not offer any improvement in performance.

In the last two years the European space industry has undertaken a number of studies for ESA to define the requirements for and initial designs of the next generation of meteorological microwave radiometers for flight in 2015 and beyond. This paper describes the instrument designs produced by the study teams led by Sula Systems.

The first task was to identify and consolidate the expected user requirements for the timescale under consideration for numerical weather prediction (NWP), nowcasting and very short term forecasting, and climate monitoring. This task was undertaken by a team of meteorologists led by the Met Office in the UK. Consideration was given to the desire to maintain the capabilities of the current systems, and also to the expected developments in tools available to the users.

The user requirements were used to produce mission and instrument requirements for systems operating in low earth orbit (LEO), medium earth orbit (MEO) and geostationary equatorial orbit (GEO). Different instrument concepts were developed for each case and trade-offs performed to select the most appropriate for realising the user requirements. The paper describes each of the selected instrument designs, and identifies critical design features of the antenna, receiver and scanning subsystems. The technology developments needed to support these instruments are also discussed. Finally, the improvements in performance compared to the current systems are addressed.

Fully polarimetric measurements of brightness temperature distri-butions with a quasi-optical radiometer system at 90 GHz

HELMUT SUESS

DLR, Institute of Radio Frequency Technology, Oberpfaffenhofen, 82234 Wessling, Germany

The thermal radiation of our environment includes besides the widely used horizontal and vertical polarization information two further independent polarimetric information sources, which can be expressed by the third and fourth component of the Stokes vector. Experimental observations and theoretical models have shown the existence of these effects in the application field of sea surface wind speed determination. High resolution fully polarimetric radiometer measurements of complex, real objects can help to learn more about polarimetric effects and to reveal possible new applications. One reason for the rarely used fully polarimetric information is the necessity of considerable experimental efforts and the complex relations between the realistic object characteristics and the modeling of the polarimetric effects. A high resolution radiometer measurement system was designed and realized at DLR. In contrast to fully polarimetric correlation radiometers, a quasi-optical measurement system was developed to measure the complete Stokes vector of stationary targets on the basis of a conventional, single channel total power radiometer at 90 GHz.

This quasi-optical system was designed with the goal to carry out two-dimensional measurements of the four Stokes vector components from stationary targets of interest. The selection of the operating frequency was driven by an already existing receiver with a very high sensitivity (less 0.1 K at 0.5 s integration time), the long-time stability and the geometrical beam dimensions of the polarimetric devices influencing the mechanical manufacturing process. Besides the reflecting parabolic mirrors, the polarisation selective device is a key element which has to be manufactured with a very high polarimetric purity. The measured transmitted cross polarization in W-band is -38 dB, which agrees with theoretical expectations.

A complete polarimetric system calibration can be achieved with only three independent and known incident Stokes vectors. Definite Stokes vectors can be generated from a smooth dielectric plate used as a calibration target observed under different observation angles. The calibration signatures can be modelled analytically and also be determined by measurements. The calibration analysis shows a statistical deviation of about 0.8 K between the model and the measurement. This corresponds to an average error of about 1.5% for the polarimetric system coefficients which demonstrates the unique system performance.

As an artificial target for the determination of the polarimetric signature a periodic surface of plastic material was constructed mechanically. The brightness temperature distribution in dependence on the observation angle

the complete Stokes vector was modelled numerically. With the quasi-optical system the brightness temperature signature was measured and compared with the model computations. The agreement is very well and shows the following interesting effects: the third component of the Stokes vector has a very high dynamic range up to 60 K; the fourth component goes up to 10 K in agreement with the theory. Further targets like antipersonal landmines have been investigated.

0-1 correction of comparator threshold in 1-bit interferometric radiometers

Manuel Martín-Neira
ESA-ESTEC, Postbus 299, Keplerlaan 1, 2200 AG, Noordwijk, Netherland
Ribó Serni
Institute for Space Studies of Catalonia IEEC/CSIC, Despatx 201, Edifici Nexus, c/Gran Capità 2-4, 08034 Barcelona, Spain
Kimma Rautiainen
Helsinki University of Technology, Laboratory of Space Technology, P.O. Box 3000, FIN-02015 HUT, Finland

Within the frame of the Soil Moisture and Ocean Salinity (SMOS) mission of the European Space Agency, an L-band Microwave Imaging Radiometer with Aperture Synthesis (MIRAS) is being developed. One of the main features of MIRAS is that it digitises the signals of the interferometer elements with 1 bit for further correlation. Threshold offsets in the comparators which quantify the signals are translated into correlation errors and have to be calibrated out. Moreover the threshold offsets may change with temperature and aging over the SMOS mission life.

A method to correct the effect of the comparator threshold offsets in 1-bit interferometric radiometers as MIRAS is described. The method is based on measuring the unbalance between zeroes and ones of the signals, this being related to the threshold offset of the quantizer. For this reason it has been called the "zeroes-minus-ones" or "0-1 correction". An important advantage of the 0-1 correction is that it can be applied without interrupting the observations, that is, in parallel while measuring the scene. Test results are shown that verify the concept.

CoSSIR: a new instrument for exploring the utility of submilleterwave radiometry for earth observation

Paul E. Racette, J.R. Wang, Bryan Monosmith, Zhaonan Zhang
NASA Goddard Space Flight Center, Greenbelt, Maryland 20771, USA
K. Frank Evans
1121 Monroe Dr., Unit C, University of Colorado, Boulder, CO 80303, USA

The Conical Scanning Submillimeter-wave Imaging Radiometer (CoSSIR) has been developed to study the application of submillimeter-wave radiometry for remote sensing of cirrus clouds and humidity sounding. Measurements of the global distribution of ice cloud mass and particle size are important for understanding the Earth's energy budget and for evaluating global climate models. The spatial variability and the wide variety of cloud particle shapes and sizes make ice clouds particularly difficult to measure. Ice clouds are essentially undetectable at microwave frequencies due to the low dielectric constant of ice and small size of the particles relative to wavelength. However, submillimeter wavelengths demonstrate significant response to the presence of ice clouds thus this frequency regime is applicable to measuring ice clouds. Another potentially viable application for submillimeter-wave radiometry is humidity and temperature sounding. The principle of sounding at submillimeter wavelengths is similar to that at microwavelengths. Submillimeter-wave radiometry has the advantage of achieving finer spatial resolution using a smaller antenna aperture which is an important consideration for spaceborne observatories. Submillimeter-wave radiometry also offers the potential of sounding over land and as a surrogate measurement for precipitation. CoSSIR is a new instrument to explore these applications.

The CoSSIR is designed to fly aboard the ER-2 aircraft and its modest size (~100 kg) permits it to be configured for other aircraft. A dual-axes gimbals mechanism provides conical, across-track, and along-track scanning capability. In its present configuration CoSSIR has fifteen channels between 183 GHz and 640 GHz. Three channels are centered about the 183 GHz water vapor absorption line, four channels are centered about the 380 GHz water vapor absorption line, and three dual-polarized channels are centered about the 487 GHz oxygen absorption line. Two channels are located in atmospheric windows at 220 GHz and 640 GHz. All channels are single-linear polarized with the exception of those near 487 GHz. Calibration is achieved by periodically observing two blackbody radiators; one blackbody is heated to ~325 K and the other is ~250 K during flight. Details of the instrument design as well as measurements from the Cirrus Regional Study of Tropical Anvils and Cirrus Layers - Florida Area Cirrus Experiment will be presented.

Giornata di Studio
su

Schiere riflettenti stampate

Rende (Cosenza), 27 Febbraio 2004

Laboratorio di Microonde
Dipartimento di Elettronica, Informatica e Sistemistica
Università della Calabria, Rende (Cosenza)

INDICE

Presentazione

Il 27 Febbraio 2004 presso il Laboratorio di Microonde dell'Università della Calabria si è svolto un workshop sui risultati del progetto *schiere riflettenti stampate* cofinanziato dal MIUR, Politecnico di Torino, Università di Siena, Università di Roma Tor Vergata, Università di Napoli Parthenope, Università di Napoli Federico II ed Università della Calabria. Il progetto, della durata di 24 mesi, ha potuto contare su un finanziamento di Euro 334.144,00 corrispondente al 99% di quanto a suo tempo richiesto dai proponenti.

Il progetto, coordinato dal Prof. Giuseppe Di Massa dell'Università della Calabria, ha prodotto risultai scientifici di notevole interesse in un settore fino ad ora poco conosciuto in Italia. In più, alcune sedi hanno acquisito attrezzature e capacità di misura e realizzazione prototipali.

Gli oratori intervenuti hanno illustrato l'attività delle sedi coinvolte nel progetto:

I risultati scientifici presentati, per la loro ampiezza, sono difficilmente sintetizzabili in poche righe. Si riportano nel seguito i risultati teorici raggiunti per l'analisi e la sintesi delle *Schiere Riflettenti Stampate* (SRS):

- algoritmi e codici di calcolo per l'analisi nel dominio del tempo;
- analisi con la tecnica SFX (funzioni sintetiche), e con la rappresentazione multi-risoluzione (MR);
- tecnica ibrida di analisi FDTD-SFX;
- teoria incrementale della diffrazione per funzioni di Green di *reflectarray* planari;
- metodo ibrido equazioni integrali/metodi asintotici per l'analisi di *reflectarray* planari;
- coefficienti di diffrazione per interruzioni brusche di periodicità
- algoritmo di sintesi in potenza di antenne riflettenti stampate a fascio sagomato;
- algoritmo di sintesi di sola fase.

Allo scopo di verificare le tecniche messe a punto sono stati realizzati e misurati diversi prototipi:

- un *reflectarray* a 18 GHz, off-set, composto da 21x21 elementi;
- un *reflectarray* costituito da 15x15 elementi riflettenti, operante alla

frequenza di 14.15 GHz;
  • numerosi prototipi in banda X.

  La ricerca ha prodotto inoltre risultati non previsti nel progetto a suo tempo presentato:
  • l'implementazione di un nuovo algoritmo FDTD per calcolare l'irradiazione da trombini rettangolari o circolari;
  • progettazione di SRS come scatteratori permanenti per applicazioni di Interferometria SAR;
  • integrazione degli elementi radianti con diodi a capacità controllabile.

Giuseppe Di Massa
Università della Calabria

Programma

GIUSEPPE DI MASSA, Università della Calabria
Attività e risultati del progetto

GAETANO MARROCCO, Università di Roma "Tor Vergata"
Analisi a larga banda per componenti di Reflectarray

GIUSEPPE D'ELIA, Università di Napoli "Federico II"
Tecniche di analisi e sintesi di schiere riflettenti stampate

FRANCESCA VENNERI, Università della Calabria
Tecniche di controllo della fase per la sintesi di antenne riflettenti stampate

LADISLAU MATEKOVITS, Politecnico di Torino
Analisi efficiente di antenne riflettenti stampate

PAOLA PIRINOLI, Politecnico di Torino
Modelli a complessità ridotta

STEFANO MACI, Università di Siena
Effetti di bordo in strutture periodiche

Convegno
su

Interazione tra campi elettromagnetici e soggetti esposti

Roma, 1-2 Aprile, 2004

Centro Ricerche Casaccia, ENEA
S. Maria di Galeria - Roma

INDICE

Presentazione

È oggi sempre più diffusa la consapevolezza che l'utilizzazione delle nuove tecnologie e lo sviluppo industriale e sociale, che da esse traggono origine, devono avvenire in forma controllata, tenendo conto in modo prioritario delle esigenze di salvaguardia dell'ambiente e di protezione sanitaria dell'uomo. Sulla base di tali considerazioni, il Ministero della Ricerca, in applicazione della Legge 95/95, ha individuato come settore di rilevante interesse per lo sviluppo del sistema nazionale di ricerca quello della "Salvaguardia dell'uomo e dell'ambiente dalle emissioni elettromagnetiche", indicando come Enti istituzionalmente competenti a proporre un piano coordinato di ricerche in detto settore il CNR e l'ENEA. Il Programma, di durata triennale, avviato nel 2001, prevede un piano di ricerche mirate alla valutazione dell'impatto ambientale di sistemi, impianti e apparati che producono e immettono campi elettromagnetici nell'ambiente, ed è diretto alla messa a punto di strumenti per la predizione, controllo e mitigazione del campo elettromagnetico prodotto nell'ambiente e all'approfondimento delle conoscenze sulle interazioni del campo elettromagnetico con i sistemi biologici.

In particolare, le ricerche da sviluppare si articolano in quattro Linee aventi per oggetto rispettivamente:

1) lo sviluppo di tecniche di predizione per valutare l'impatto ambientale dei sistemi elettromagnetici su vasti territori e/o in ambienti complessi (quartieri urbani densamente popolati, aeroporti, mezzi di trasporto, siti centralizzati di tele-radiodiffusione, interno di edifici);

2) la realizzazione di sensori e di strumentazione per il controllo e il monitoraggio dei livelli di campo elettromagnetico con collegamento in rete per la utilizzazione e la gestione dei dati raccolti;

3) lo sviluppo di tecniche di valutazione delle reali condizioni di esposizione umana in presenza di vari scenari operativi, dell'assorbimento del campo nei soggetti esposti, degli effetti biologici dei campi elettromagnetici;

4) lo sviluppo di tecniche di protezione realizzate con nuovi dispositivi, materiali, metodologie progettuali, procedure costruttive, nonché lo studio di tecniche e procedure di valutazione di conformità ai requisiti di protezione umana e infine una linea di attività (la Linea 5) in cui, oltre alle attività di coordinamento delle ricerche sviluppate nelle varie Linee, è stata prevista la messa in atto di iniziative di disseminazione dei risultati e l'individuazione di

possibili sinergie con altri programmi affini a livello nazionale e internazionale.

In questo Convegno vengono esposti i risultati della attività svolte dalle Unità partecipanti nei quattro temi in cui si articola la linea di ricerca 3 "Interazione tra sorgenti e soggetti esposti":

- Misure sperimentali di accoppiamento tra sorgenti e soggetti esposti.
- Modelli per la valutazione del campo elettromagnetico assorbito in soggetti esposti in presenza di sistemi per la comunicazione mobile.
- Individuazione dei meccanismi di interazione del campo elettromagnetico con i biosistemi.
- Effetti biologici *in vitro* ed *in vivo*.

L'obiettivo generale di questa linea del progetto è di approfondire la conoscenza della reale esposizione dei biosistemi alle emissioni elettromagnetiche e valutarne le condizioni di rischio attraverso la messa a punto di procedure di misura standardizzate, valide entro livelli contenuti di incertezza, lo sviluppo di modelli di calcolo numerico per l'analisi del campo interno ai sistemi biologici (uomo, animali); il raccordo tra i risultati dosimetrici, e infine l'esecuzione, sulla base delle conoscenze acquisite nei precedenti items, di esperimenti *in vivo* ed *in vitro* alle basse (ELF) e alte frequenze (RF) con esposizioni prolungate, per evidenziare possibili effetti cancerogeni, mutageni, citogenetici e funzionali, utilizzando tutti i test biologici garantiti e mutuati dalle ricerche tossicologiche in generale al fine di valutare i reali rischi per l'uomo.

Le attività presentate si inseriscono nel quadro internazionale della ricerca sugli effetti dei campi elettromagnetici, richiamato da alcuni interventi: Progetto Interphone, 5° Programma Quadro; Azione Coordinata EMF-NET, 6° Programma Quadro; Progetto Nazionale francese; intervento del Presidente ICNIRP.

Questo Convegno Nazionale, inoltre, segue i primi due Convegni inerenti al progetto, svoltisi a Roma nell'aprile 2002 (codici di calcolo per la valutazione dell'impatto ambientale) e a Firenze nel maggio 2003 (reti di monitoraggio e strumenti di misura), e rappresenta una prima conclusione del programma di attività della Linea 3, a cui si aggiunge un preliminare sintetico bilancio dell'intero Programma.

Il Comitato Scientifico

PAOLO BERNARDI, *Università "La Sapienza"/CNR - Roma*
MARCO BINI, *IFAC-CNR - Firenze*
GUGLIELMO D'INZEO, *Università "La Sapienza"/ICEmB - Roma*
GIORGIO A. LOVISOLO, *BIOTEC-ENEA - Roma*
CARMELA MARINO, *Chair, BIOTEC-ENEA - Roma*
FRANCESCO MAURO, *Ferrovie dello Stato*
DONATELLA TIRINDELLI, *BIOTEC-ENEA - Roma*

Programma

SESSIONE 1
Caratterizzazione dei sistemi espositivi e dosimetria sperimentale

PINTO R., ARDOINO L., MANCINI S., LOVISOLO G.A., *Sistemi espositivi per sperimentazione biologica e test per dispositivi radiomobili.*

LIBERTI M., APOLLONIO F., PAFFI A., PELLEGRINO M., D'INZEO G., *Sistemi espositivi in vitro per sperimentazione in tempo reale.*

MARROCCO G., BARDATI F., BANDINELLI M., *Simulatore elettromagnetico per la caratterizzazione di sistemi espositivi.*

RAVAZZANI P., EMF-NET - *Effects of the exposure to electromagnetic fields: from science to public health and safer workplace. A Coordination Action in the 6th FP of the European Commission.*

SESSIONE 2
Valutazione del campo EM assorbito per soggetti esposti ai sistemi di comunicazione mobile

BERNARDI P., CAVAGNARO M., CRISTOFORETTI L., LOPRESTO V., PISA S., PIUZZI E., PONTALTI R., SANDRINI L., *Dosimetria nei sistemi di telefonia cellulare.*

PONTALTI R., SANDRINI L., VACCARI A., MALACARNE C., CRISTOFO-RETTI L., *Sviluppo di fantocci numerici per dosimetria elettromagnetica: confronto uomo-donna in onda piana.*

CAORSI S., MASSA A., PASTORINO M., RANDAZZO A., *Tecniche numeriche innovative per la caratterizzazione del campo emesso da terminali per la telefonia mobile ai fini della valutazione del SAR in soggetti esposti.*

SESSIONE 3
Effetti biologici dei campi EM: sistema neurosensoriale

MAZZANTI M., *Studio parallelo della stimolazione elettromagnetica a 50 Hz e 900 MHz sul firing neuronale in singole cellule di neuroni sensoriali.*

ZECCA L., COSTI P., PIVA F., DONDI D., ZUCCA F., *Effetti dell'esposizione cronica a CEM di 50 Hz su neurotrasmettitori e recettori nel cervello di ratto.*

GALLONI P., LOVISOLO G.A., MARINO C., PINTO R., PISCITELLI M., *Effetti dei campi elettromagnetici associati alla telefonia cellulare sul sistema uditivo del ratto.*

LAGORIO S., *Progetto Interphone - Studio epidemiologico internazionale su tumori cerebrali ed uso del cellulare.*

SESSIONE 4
Effetti biologici dei campi EM: proliferazione e differenziamento

GATTA L., PINTO R., NASTA F., PACE L., GALLONI P., LOVISOLO G.A., MARINO C., PIOLI C., *Effetti dei campi elettromagnetici generati da dispositivi di telefonia mobile sul sistema immunitario.*

LISI A., LEDDA M., CIOTTI M.T., PIERI M., ZONA C., RIETI S. MERCANTI D., GRIMALDI S., *Precoce espressione dei recettori dell'Acido Glutammico in cellule nervose di ratti neonati esposte a radiazioni non ionizzanti.*

SANTINI M.T., FERRANTE A., ROMANO R., RAINALDI G., DONELLI G., VECCHIA P., INDOVINA P.L., *Evidenza di apoptosi precoce nella linea cellulare eritroleucemica umana K562 esposta a un campo magnetico sinusoidale a 50 Hz rilevata da 1H-NMR a 700 MHz.*

SANTINI M.T., RAINALDI G., FERRANTE A., DONELLI G., VECCHIA P., INDOVINA P.L., *Effetti dei campi magnetici sinusoidali a 50 Hz sull'espressione delle molecole di adesione su due linee cellulari umane di osteosarcoma (MG-63 a Saos-2).*

VENTURA C., MAIOLI M., MESIRCA P., AGOSTINI C., BERSANI F., *Influenza di campi magnetici ELF sul differenziamento di cellule staminali murine.*

DEL RE B., GAROIA F., MESIRCA P., AGOSTINI C., BERSANI F., GIORGI G., *Differenti segnali di campo magnetico ELF influenzano in modo diverso l'attività di trasposizione e la sopravvivenza in Escherichia coli.*

SESSIONE 5
Effetti biologici dei campi EM: citogenetica

CAPRI M., MESIRCA P., CAROSELLA S., BIANCHI E., FRANCESCHI C., BERSANI F., *Effetti delle radiofrequenze (900-1800 MHz) sulla proliferazione dei linfociti umani e dei fibroblasti murini.*

SCARFI' M.R., ZENI O., SARTI M., PERROTTA A., ROMANO' M., SANNINO A., DI PIETRO R., LIOI M.B., BARBIERI R., *Valutazione dell'induzione di effetti genotossici in colture cellulari di mammifero esposte a campi elettromagnetici di bassa e di alta frequenza.*

STRONATI L., APOLLONI M., CORDELLI E., FRESEGNA A.M., MARINO C., TESTA A., VILLANI P., *Valutazione degli effetti genotossici in cellule di sangue periferico umano indotti dall'esposizione alle radiofrequenze (935 MHz).*

SESSIONE 6
Modellistica dell'interazione

RAMUNDO ORLANDO A., LIBERTI M., MATTIA F., MORBIDUCCI U., SCHIAVO R., D'INZEO G., *Effetti indotti da esposizione a campi a bassa frequenza ed a bassa intensità sulla permeabilità di membrana.*

BIANCO B., GIORDANO S., MOGGIA E., *Metodologie per una microdosimetria in ambiente non lineare.*

D'INZEO G., APOLLONIO F., LIBERTI M., DOMINICI L., PAFFI A., CAPPELLI M., GIANNI' M., *Modellistica dell'azione dei campi elettromagnetici sui processi bioelettrochimici.*

VECCHIA P., *Valutazione e percezione del rischio alla luce dei risultati nazionali.*

National Worokshop
on

Special material and metamaterials
for electromagnetic applicacions and TLC

Roma, 5 Aprile 2004

Aula Magna del Rettorato
Università di "Roma Tre"

INDICE

Preface

In the past few years, there has been a renewed interest in using artificial structures to develop composite materials that mimic known material responses or that qualitatively have new, physically realizable response functions that do not occur, or may not be readily available, in nature. The word itself "metamaterial" recalls this interdisciplinary aim of physicists, chemists and engineers of going beyond the limits that natural materials present at different frequencies. This renewed interest is witnessed also by the Special Issues that important scientific international journals have dedicated or have scheduled to dedicate to this topic in the last months (e.g., Optics Express, IEEE Transactions on Antennas and Propagation and Progress in Electromagnetics Research).

The history of fabricated materials traces back to the late part of the nineteenth century, when J. C. Bose published his work on the rotation of the plane of polarization by man-made twisted structures, which are currently well known as artificial chiral structures. Also K.F. Lindman in 1914 studied artificial chiral media formed by a collection of randomly-oriented small wire helices. Afterwards, there were several other investigators in the first half of the twentieth century who studied various man-made materials. In the 1950s and 1960s, artificial dielectrics were explored for light-weight microwave antenna lenses and for building plasma-like materials at microwave frequencies for several applications. The interest in artificial chiral materials was resurrected in the 1980s and 1990s and they were investigated for microwave radar absorber and other applications.

Recent examples of engineered material activities include double negative (DNG) materials, which are artificial materials with simultaneous, effective negative real permittivity and permeability parameters, and are also known as negative index of refraction (NIR) materials or left-handed materials (LHM) due to their anomalous wave interaction; electromagnetic band gap (EBG) structured materials; and complex surfaces such as high-impedance ground planes. The qualitatively new response functions of these metamaterials are often generated by artificially fabricated inhomogeneities embedded in host media or connected to or embedded on host surfaces. The DNG materials involve elements, and distances between them, that are much smaller than the operating wavelength and consequently they may be

described by the effective medium theory. On the other hand the EBG materials involve distances that are of the order of half a wavelength or more, and are therefore described by the periodic media concepts.

The IX Workshop on Microwave Engineering - *Metamaterials and special materials for electromagnetic applications and TLC* held in the Aula Magna of the "Roma Tre" University on 5 April 2004, was intended to present recent research advances in the metamaterials area. Theoretical, numerical, and experimental contributions to the understanding of the behavior of several classes of metamaterials and to their potential applications in components, devices, and antennas were reported.

The first session, chaired by Prof. Giuseppe Schettini from the "Roma Tre" University, presented the work of several international research groups in the theoretical and modeling aspects of metamaterials. The talks of this session primarily focused on the theoretical properties of isotropic and anisotropic metamaterials, on their potential applications at microwave and optical frequencies, and also on their experimental verification.

The next session and the last one, chaired respectively by Prof. Giuliano Manara from the University of Pisa and Prof. Nader Engheta from the University of Pennsylvania, primarily focused on the applications of metamaterials, complex surfaces and EBG structures, showed numerical and experimental results for their active employment in the electromagnetic applications of a near future.

Finally, the third session, chaired by Prof. Fabrizio Frezza from the "La Sapienza" University of Rome, focused in particular on the space applications of complex materials.

We profit by the occasion to thank all those who made possible this event, the contributors and the attendees for coming and for the very interesting works they presented in Rome. Moreover we wish to thank the members of the organizing committee (Andrea Alù, Filiberto Bilotti, Lara Pajewski, and Alessandro Toscano). Last, but not least, the patronage (SIEM, Italian Society of Electromagnetics, IEEE Central and South Italy Section, IEEE AP-S and MTT-S Joint Chapter), Microwave Engineering Center for Space Applications (MECSA) and the sponsors (Alenia Spazio, Ansoft e CST).

Finally, special thanks to the journal "Atti della Fondazione Giorgio Ronchi".

Lucio Vegni, Giuseppe Schettini
"Roma Tre" University

SESSION I
METAMATERIALS: THEORETICAL ASPECTS AND MODELING

Properties and characteristics of indefinite metamaterials

ARI SIHVOLA (*)

SUMMARY. – *The characteristics of indefinite metamaterials are described. A special emphasis is put on the manner how the combination of anisotropy and negative parameters in some of the permittivity components affects the way mixtures are homogenized. It is shown that even if the depolarization factors display apparently strange behavior, energy conservation in the material model is conserved.*

1. Introduction

The electromagnetic response of matter, although very elementary on the basic level where a charged unit experiences a force due to the electric field, can become quite involved and complicated when the elements are macroscopic and react in interference with their neighbors. The variety of this response is reflected in names and labels that we encounter in today's discussion of complex materials: anisotropic, gyrotropic, magnetic, non-reciprocal, ferroelectric, conducting polymers, chiral, omega, bi-anisotropic, non-linear, dispersive (both temporally and spatially dispersive), impedance surfaces, FSS (frequency-selective surfaces), SHS (soft and hard surfaces), periodic materials, band-bap structures, photonic crystals, EBG, media with negative parameters, Veselago media...

A common broad class of media carries the name metamaterials, and their characteristic property is indeed the simultaneously negative values for permittivity and permeability. Quite often theoretical studies dealing with such "left-handed", or Veselago media focus on the particular case that the parameters are $\varepsilon = -1$ and $\mu = -1$ at a certain frequency, in order to study the salient electromagnetic effect of these media. But certainly matematerials

(*) Dept. of Electrical and Communications Engineering, Electromagnetics Laboratory, P.O. Box 3000, Helsinki University of Technology, Otakaari 5 A, Espoo, FIN-02015 HUT, Finland

offer quite much larger spectrum of possibilities when the parameter space is expanded. Especially if we relax the assumption of isotropy, there are six parameters, three for both ε and μ, that define the constitutive character of the material. And indeed, the present-day fabrication of metamaterials comprising metal posts and split-ring resonators, for instance, makes the material rectangularly anisotropic in its effective description (see the groundbreaking studies, e.g. (1)).

In this presentation, the focus on particular type of anisotropic metamaterials, such for which the permittivity and permeability components are alternately positive and negative, for example the *xyz*-components of ε being (−1,−1,+1) and those of μ (−1,+1,+1). Such media have also been called *indefinite* media (2). One of the special properties of such media is that depending on the direction of the propagation of the wave, it can display "left-handed" or "right-handed" character (or even evanescent propagation), unlike the isotropic "ordinary" metamaterials, which are left-handed (how unfortunate name! Remember chiral media!) independently of the direction of propagation. In the following, I shall discuss such indefinite metamaterials. In particular, special treatment is needed when heterogeneities are modelled macroscopically involving indefinite material parameters. This is to be expected, of course, because the step to indefinite media is quite a large generalization from ordinary anisotropic materials, and in the analysis one needs to tackle the difficulties in both Veselago media and anisotropy.

2. Microscopic response of random matter

Like Fig. 1 shows, the macroscopic response of matter ultimately is an averaged effective reaction which hides behind itself a fantastic amount of detailed microsopic functional variation. There the random sample of matter is divided by a dense grid into small elements and the Laplace equation is solved by element method. By integrating the resulting fluxes, an estimate for the effective permittivity is found.

But mixing rules give us estimates for the effective permittivity without having to solve the full-field behavior within the matter. For example, given the permittivities of the components that compose the mixture in Fig. 1 (which are 10 for the inclusions and 1 for the background) and their fractional volumes (inclusion volume fraction 0.39), the Maxwell Garnett estimate (3) for the relative permittivity is 2.25 and the Bruggeman estimate 2.96. The computational simulation gives a value that falls inbetween these two classical predictions.
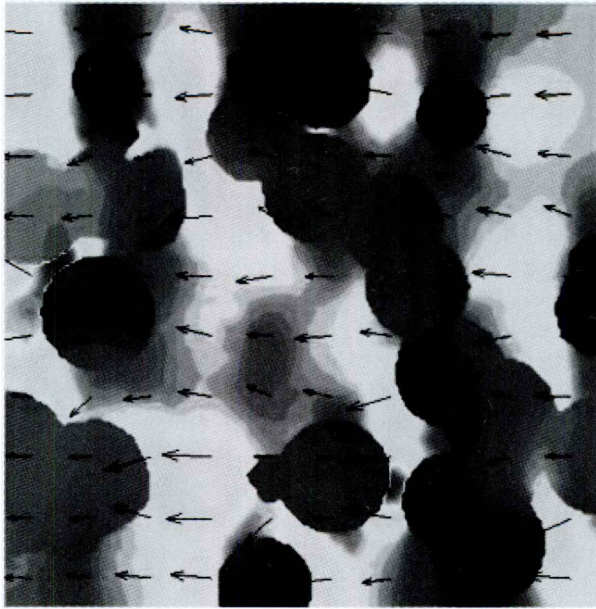
FIG. 1

Numerically solved (element method) electric field pattern in a cut from a pseudorandom cubical cell where spherical inclusions with permittivity 10 relative to the background are randomly positioned. The volume fraction of the inclusion phase is 0.39, and the computational evaluation of the macroscopic permittivity gives the value 2.8. The picture is taken from the diploma work (M.Sc.Tech. thesis) of my assistant Liisi Jylhä.

3. Depolarization factors for anisotropic matter

It is very generally known that the manner how the dipole moments are created into inclusions of matter are mainly determined by the shape of the inclusion (and of course, by its permittivity). The polarizability of a scatterer can be calculated from the depolarization factors.

But what is less known is that the depolarization factors are also functions of the anisotropy of the host material in the mixture (Ref. 3, Sect. 5.5). For simplicity, let us consider a uniaxially anisotropic host medium, with permittivity e_z in the z direction and e_t in the x and y directions. Then there are two depolarization factors, one for the axial, the other for the transversal direction, for a geometrically spherical scatterer.

These are shown in Fig.2, which displays the depolarization factors for the case of uniaxially anisotropic host medium. The abscissa is the permittivity ratio (z-component to t-component of the permittivity of the environment), including the special case of isotropy. In the isotropic case (permit-

tivity ratio equal to unity) depolarization factors are real, and of magnitude 1/3 as should be in case of ordinary spheres. But differing ratios give then different depolarization factors, and these are in fact the same functions as for oblate and prolate spheroids (ellipsoids of revolution). There is a connection between the anisotropy and the axial ratio (being the square root of the permittivity ratio) of the effective ellipsoid.

However, the depolarization behavior for orthogonal field excitations bifurcates strongly if the permittivity ratio is large compared to one (or small compared to one). The depolarization may vanish or become very large. And what is after all not very surprising is that most peculiar depolarization characteristics come in the case when the anisotropy is that of indefinite metamaterial, in other words, the ratio of the permittivity components is negative.

When the permittivity ratio of the environment becomes negative, both depolarization factors attain imaginary parts. This is quite peculiar. But certainly complex-valued permittivities are not unheard of in material modeling. And surely they do not represent stranger phenomena than those that come with negative-index materials that we are dealing with in the first place. And another phenomenon that may raise the eyebrows of materials modelling people is the narrow region for negative values of the permittivity ratio where the real part of the z-component of the depolarization factor is negative. *Repolarization* instead of depolarization! But again, no restrictions broken yet. However, we should be careful to analyze what kind of repercussions these complex-valued depolarization factors may cause with respect to the effective parameters of the mixture. At least no well-known restrictions dictated by physical laws should be violated.

4. Conclusions

Space not permitting here, we must leave further analysis. But let us content ourselves with the observations that even if the depolarization factors may display such peculiar behavior as illustrated in Fig. 2, all numerical results that have been calculated using those have produced results in accordance with energy conservation. A more detailed analysis on those results can be found in the report (4).
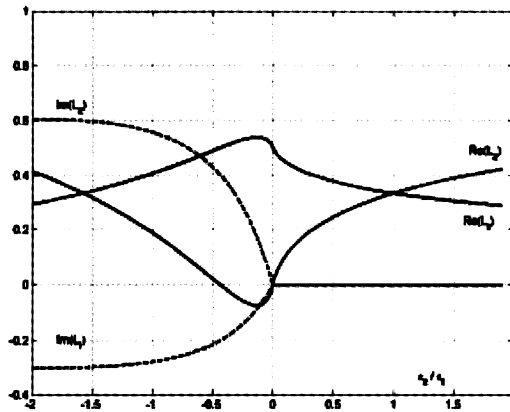
FIG. 2

The depolarization factors of spheres in anisotropic material as functions of the ratio of the permittivity components of the anisotropic host. (The isotropic special case – permittivity ratio unity – gives the ordinary depolarization factors 1/3.) Note that for negative values of the permittivity ratio, the two depolarization factors become complex. However, regardless of this ratio, always the condition $L_z + 2L_t = 1$ is met.

REFERENCES

(1) R.A. SHELBY, D.R. SMITH, S. SCHULTZ, *Experimental verification of a negative index of refraction*, Science, **292**, 77-79, 2001.

(2) D.R. SMITH, D. SCHURIG, *Electromagnetic wave propagation in media with indefinite permittivity and permeability tensors*, Phys. Rev. Letters, **90** (7), 077405, 21 February 2003.

(3) A. SIHVOLA, *Electromagnetic mixing formulas and applications*, The Institute of Electrical Engineers (Electromagnetic Waves Series, **47**), London, 1999.

(4) A. SIHVOLA, *Metamaterials and depolarization factors*, Helsinki University of Technology, Electromagnetics Laboratory Report Series, **425**, February 2004.

Near-field imaging and amplification in double polariton-resonant grids or arrays

STANISLAV MASLOWSKI (*), SERGEI TRETYAKOV (*),
PEKKA ALITALO (*)

Since the revolutionary paper of Pendry (1) there have been many scientific groups involved in a race after getting a system capable of amplification of evanescent fields. Indeed, having such a system at hands means a possibility of improving the resolution of optical or electromagnetic devices operating, in many cases, already at their limits. For example, in optical discs used for data storage the maximum disk capacity is limited by the resolution of the beam forming optics. Decreasing the size of elementary pixels brings reduction to the level of optical signal read out from the disk. It would be undoubtedly useful if something (passive!) placed in between the disk and the reading optics could increase the signal level.

Only a couple of theoretical possibilities of evanescent field enhancement in passive systems were known until recently. The Pendry's idea of making use of Veselago's backward-wave (also called double-negative) materials for that purpose has not been confirmed experimentally yet, as far as we know. There are certain difficulties in realization of isotropic Veselago media.

In this presentation we show that a system of two electromagnetically coupled polariton resonant grids or arrays can be used as a near-field imaging device, i.e. as a device which enhances evanescent field components of a source. The system under study is a pair of planar surfaces possessing surface mode (polariton) resonances.

The surfaces are placed in free space parallel to each other and separated by a certain distance. Using transmission matrix approach a general theory of near field behavior in the system is developed. General

(*) Radio Laboratory/SMARAD, Helsinki University of Technology, Finland

requirements on electromagnetic grids or arrays realizing the surfaces are found. As a special case, arrays of weakly interacting resonant particles are studied.

In the presentation, we discuss a structure not involving any bulk material layers (double-negative or whatever) yet possessing the necessary evanescent field growth.

The idea behind it is very simple and based on the known behavior of coupled resonators: The field enhances because of a resonant interaction of an incident evanescent wave with surface modes (polaritons) of the proposed double-grid system.

We have developed a theory that allows to analyze the evanescent field behavior in the structure and find the conditions under which the near field amplification can be achieved. Based on the theoretical findings, we have developed an experiment that approved the reality of evanescent field resonant enhancement in passive linear systems. Our microwave experiment is based on the use of arrays of metal resonant particles. The experiment has confirmed our theoretical predictions of a possibility of evanescent field enhancement in the considered structures.

REFERENCES

(1) J. PENDRY, *Negative refraction makes a perfect lens*, Phys. Rev. Lett., **85**, 3966, 2000.

Selected features of metamaterials and plasmonic media

NADER ENGHETA (*), ANDREA ALÙ (**)

SUMMARY. – *We have been investigating a variety of theoretical problems of electromagnetic wave interaction with several structures involving DNG metamaterials and exploring optical theories of wave manipulation with SNG plasmonic nanostructures. Here we report a short summary of some of these results. In particular, we have found that cavities and waveguides formed by pairing some of these media may support resonant and propagating modes even when they have very small lateral dimensions (i.e., below the diffraction limit) compared with the operating wavelength. Furthermore, our theoretical work has shown that the cylindrical and spherical nanostructures containing these media may be "compact" resonant or "anti-resonant" scatterers, despite their very small physical cross sections.*

1. Introduction

The electromagnetic properties of complex media in which both permittivity and permeability attain negative real parts in a given band of frequencies have become the subject of research interest for many groups in recent years (1-12). Various names, such as "double-negative (DNG)" media (2), "left-handed (LH) materials (1), "backward-wave (BW) media", "negative index materials (NIM)", have been coined for this class of metamaterials. These particulate composite media, which may be formed by period arrangements of many small inclusions with certain particular geometries (3), possess interesting electromagnetic features such as negative refraction and backward wave propagation, in which the direction of the

(*) Dept. of Electrical and Systems Engineering, University of Pennsylvania, 19104 Philadelphia, PA, USA
(**) Dept. of Applied Electronics, University of Roma Tre, Via della Vasca Navale, 84, 00146 Roma, Italy

Poynting vector of a plane wave is antiparallel with the direction of its phase velocity (1, 2). These may lead to some exciting unconventional electromagnetic characteristics with potential applications in various devices and components involved in radiation, guidance and scattering of electromagnetic waves. In addition, the "single-negative (SNG)" media (5), i.e., the materials in which only one of the material parameters of permittivity and permeability, but not both, can be negative, also exhibit certain interesting properties such as plasmonic interaction in nanostructures.

We have been investigating a variety of theoretical problems of electromagnetic wave interaction with several structures involving DNG metamaterials and exploring optical theories of wave manipulation with SNG plasmonic nanostructures (4-12). We have found that cavities and waveguides formed by pairing some of these media may support resonant and propagating modes even when they have very small lateral dimensions (i.e., below the diffraction limit) compared with the operating wavelength (4, 7-8, 11). Furthermore, we have shown theoretically that the cylindrical and spherical nanostructures containing these media can be "compact" resonant or "anti-resonant" scatterers, even though they may have very small physical cross sections (6, 9). These properties may offer potential applications in high-resolution near-field imaging and microscopy, RF and optical energy transport below the diffraction limit, enhancement or reduction of polaritonic wave interaction with nano-particles, and many more. We are also developing theories and ideas for optical nano-circuits in the form of nanospheres as effective "nano-inductors" and "nano-capacitors". These may be extended to more complex circuits with several nanostructures acting as nano-inductors and nano-capacitors arranged in many different ways.

In the following, we review some of these works, showing some anomalous interesting properties of metamaterials and plasmonic media.

2. Planar conjugate slabs

Pairing two planar lossless slabs of media with "conjugate" properties, for instance, standard DPS media with DNG metamaterials, or ENG media with MNG materials (5) leads to anomalous scattering properties, in the sense of anomalous tunneling, growing evanescent fields and zero reflection. Although the wave interaction with each slab by itself has its usual features, it can be shown that the juxtaposition and judiciously pairing of such conjugate slabs may lead to an anomalous response, revealing resonance, complete tunneling, zero reflection and total transparency. A condition on the bilayer for achieving these phenomena for a given plane wave excitation has been derived and a more stringent condition for having "total transparency" for every propagating and evanescent wave impinging on the bilayer has also been found in (5). It is worth to underline that such conditions

do not depend on the surrounding environment in which the bilayer is embedded, but only on the materials employed, since they are based on an "interface resonance" present on the plane interface between the two layers. Using equivalent transmission-line circuital models, further insights and a justification for the field behavior in these resonant paired structures have been given, and salient features such as the sensitivity to the material parameters, slab thicknesses, dissipation, and angle of incidence have also been explored.
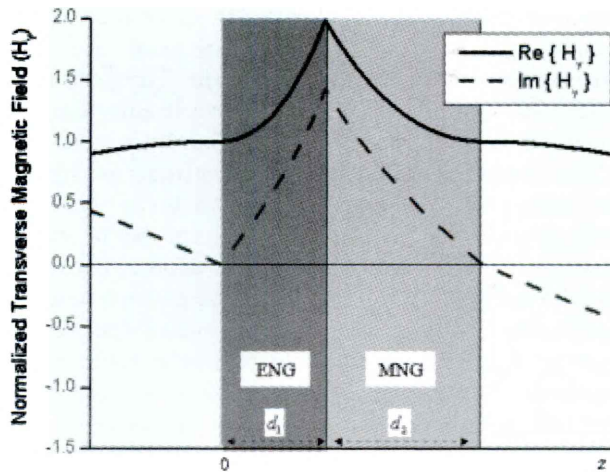
FIG. 1

Total transmission and anomalous tunneling through a planar bi-layer of "conjugate" slabs (from (5))

In a similar way, this anomalous resonance at the interface between the two conjugate materials may be employed in guiding problems. When the planar bilayer, in fact, is delimited by metallic plates, the intrinsic resonance at the bilayer interface induces the possibility of making very compact cavities and waveguides, overcoming the diffraction limit typical of these structures. We have shown in (4, 7-8, 11) how sub-wavelength waveguides with no cut-off TE and/or TM modes may be in principle possible by judiciously pairing metamaterials with conjugate behavior.

3.Anomalous scattering in tiny cylindrical and spherical shells

Some of the peculiar scattering properties of metamaterials can also be investigated in problems involving coaxial shells made of DNG and/or SNG metamaterials. For instance, when we have an electrically thin cylin-

drical scatterer made of a conventional dielectric, it is well known that the scattering cross section of such a structure is low due to its electrically small radius. However, if the same structure with the same radius is formed by a pair of DNG-DPS coaxial layers (or a pair of ENG-MNG coaxial layers), a condition for the existence of anomalous scattering resonance peaks may be obtained. We have theoretically shown that in the case of small radii the scattering coefficients may reach their resonant peaks when specific ratios of the shell radii for this coaxial structure are achieved, in principle regardless of the value of the outer radius (6, 9). In other words, although the circular cross section of such DPS-DNG or ENG-MNG co-axial shells may be electrically very thin, its scattering width may become significantly large for certain specific ratio of radii. This feature may lead to interesting possibilities for the design of sub-wavelength resonant scatterers whose physical cross sections are much smaller than the wavelength of operation, but for certain applications their scattering widths need to be large. Such structures may have unusual polarizability tensors and may also be used as resonant inclusions in forming novel composite media. It is also important to note that in the case of small radii another set of ratio of radii for these DNG-DPS or ENG-MNG coaxial shells may provide certain oppo-site effects, namely, low scattering cross section, which can lead to reduction of radar cross section (6). This effect would be similar to an "anti-resonance" of the whole structure and it may be interesting in applications devoted to reduction of the total scattering from objects or obstacles.
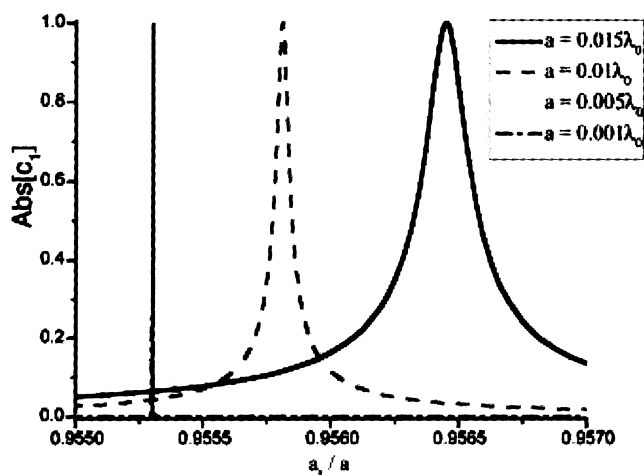
FIG. 2

Scattering peaks in tiny spherical particles with metamaterials, varying their filling ratio (from (6))

Similar phenomena may also be shown in the scattering from sub-wavelength concentric spheres. As in the cylindrical case, a suitably designed pairing of conjugate metamaterials may induce a significant increase in the scattering cross section of electrically small concentric spheres. Our theoretical analysis has shown, for instance, how an electrically small dielectric sphere, which conventionally has a small radar cross section, can provide very large scattering cross section when it is coated by some SNG metamaterials. This phenomenon is consistent with the plasmonic resonance in metallic nanoparticles in the visible and IR regimes. Conversely, our theoretical investigation has revealed that in the limit of small radii for a dielectric sphere with notable scattering cross section, one may reduce the scattering by putting an appropriate concentric layer of metamaterial layer either inside or outside the sphere. Figure 2 shows, as an example, the scattering peaks achievable with a suitable pairing of metamaterial shells in a tiny spherical particle. An equivalent circuit approach is applicable also to this problem, and it indeed leads to extremely useful physical insights into the underlying phenomenon. In particular, the nanospheres constructed to induce these anomalous resonances and anti-resonances may represent bulk nano-inductors and nano-capacitors in an effective nano-circuit. This may allow building an effective guiding circuit for light propagation at frequencies for which the optical diffraction represents a major limitation.

4. Conclusions

We have here briefly reviewed some recent results in a variety of theoretical problems of electromagnetic wave interaction with several structures involving DNG metamaterials and SNG plasmonic nanostructures. In particular, we have briefly presented sub-wavelength cavities and waveguides formed by pairing some of these media, cylindrical and spherical nanostructures forming "compact" resonant or "anti-resonant" scatterers, despite their very small physical cross sections

REFERENCES

(1) V.G. VESELAGO, *The electrodynamics of substances with simultaneously negative values of ε and μ,* Soviet Physics Uspekhi, **10**, 509-514, 1968.

(2) R.W. ZIOLKOWSKI, E. HEYMAN, *Wave propagation in media having negative permittivity and permeability,* Physical Review E, **64**, 056625, 2001.

(3) R.A. SHELBY, D.R. SMITH, S. SCHULTZ, *Experimental verification of a negative index of refraction,* Science, **292**, 77-79, 2001.

(4) N. ENGHETA, *An idea for thin subwavelength cavity resonators using metamaterials with negative permittivity and permeability,* IEEE Antennas and Wireless Propagation Letters., **1**, 10-13, 2002.

(5) A. ALÙ, N. ENGHETA, *Pairing an epsilon-negative slab with a mu-negative slab: resonance, tunneling and transparency*, IEEE Transactions on Antennas and Propagation., Special Issue on Metamaterials, **51**, 2558-2571, 2003.

(6) A. ALÙ, N. ENGHETA, *Peculiar radar cross section properties of double-negative and single-negative metamaterials*, Proceedings of IEEE Radar Conference, Philadelphia, PA, April 26-29, 2004.

(7) A. ALÙ, N. ENGHETA, *Mono-modal waveguides filled with a pair of parallel epsilon-negative (ENG) and mu-negative (MNG) metamaterial layers*, Digest of IEEE MTT Int. Microwave Symp. (IMS'03), Philadelphia, PA, June 8-13, 2003, **TU2D-2**, 313-316, 2003.

(8) A. ALÙ, N. ENGHETA, *Guided modes in a waveguide filled with a pair of single-negative (SNG), double-negative (DNG) and/or double-positive (DPS) media*, IEEE Transactions on Microwave Theory and Techniques, **52**, 1-13, 2004.

(9) A. ALÙ, N. ENGHETA, *Resonances in Sub-wavelength Cylindrical Structures Made of Pairs of Double-Negative and Double-Positive or ε-Negative and μ-Negative Coaxial Shells*, in Proc. of ICEAA'03, Turin, Italy, September 8-12, 2003, pp. 435-438.

(10) A. ALÙ, N. ENGHETA, *Distributed-Circuit-Element Description of Guided-Wave Structures and Cavities Involving Double-Negative or Single-Negative Media*, in Proc. of the SPIE Annual Meeting 2003, Complex Mediums IV: beyond Linear Isotropic Dielectrics, Vol. 5218, San Diego, CA, USA, August 3-8, 2003, pp. 145-155.

(11) A. ALÙ, N. ENGHETA, *Mode Excitation by a Line Source in a Parallel-Plate Waveguide Filled with a Pair of Parallel Double-Negative and Double-Positive Slabs*, in Proc. of 2003 IEEE AP-S International Symposium, Columbus, OH, USA, June 22-27, 2003, Vol. III, pp. 359-362.

(12) A. ALÙ, N. ENGHETA, *Anomalous Mode Coupling in Guided-Wave Structures Containing Metamaterials with Negative Permittivity and Permeability*, in Proc. of IEEE Nanotechnologies 2002, Washington DC, USA, August 26-28, 2002, pp. 233-234.

Modal properties of surface and leaky waves on metamaterial grounded slabs

PAOLO BACCARELLI (*), PAOLO BURGHIGNOLI (*),
FABRIZIO FREZZA (*), ALESSANDRO GALLI (*),
PAOLO LAMPARIELLO (*), GIAMPIERO LOVAT (*),
SIMONE PAULOTTO (*)

SUMMARY. – *In this paper some recent results concerning guidance and radiation phenomena in a double-negative (DNG) metamaterial grounded slab are presented. The dispersion behavior of TM and TE modes supported by this structure is studied and conditions have been derived which ensure the suppression of surface waves in certain frequency ranges. Particular attention has been devoted to the excitation of such structure by means of dipole sources. With reference to leaky modes, it has been shown that proper leaky modes are responsible for backward radiation from DNG slabs, and that frequency scan of the radiated beam may be achieved by properly choosing the physical and geometrical parameters of the structure.*

1. Introduction

Waveguiding structures involving metamaterial media have received considerable attention in recent years, due to their surprising propagation features (1)-(4). In the present paper, we first analyze the modal properties of surface waves supported by double-negative (DNG) grounded slabs: two different kinds of waves are known to exist in such structures, i.e., *ordinary waves* (transversely attenuating only in air) and *evanescent waves* (transversely attenuating also inside the slab). Moreover, the dispersion and radiation properties of complex (leaky) modes supported by these grounded metamaterial slabs are investigated.

In section 2, a simple analysis and discussion of the dispersion equations of TE and TM modes supported by such structures allows us to

(*) "La Sapienza" University of Rome, Electronic Engineering Dept., Via Eudossiana 18, 00184 Roma, Italy.

present conditions which ensure suppression of surface waves of both polarizations and kinds. Numerical results on the dispersion properties of a specific DNG grounded-slab structure are reported here, which confirm the existence of such ranges.

In section 3, the field excited by a dipole source is examined and radiation patterns of specific structures are reported in order to illustrate the nature of radiation from the considered leaky modes.

2. Structure description and analysis

The structure considered here is a grounded slab of height h, made of an ideal linear, stationary, isotropic, homogeneous, lossless metamaterial medium, with permeability $\mu = \mu_0 \mu_r$ and permittivity $\varepsilon = \varepsilon_0 \varepsilon_r$, both of which are negative (see Fig. 1, where the relevant coordinate system and a horizontal magnetic dipole source placed on the ground plane are also shown).
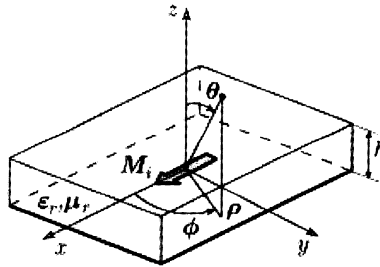
FIG. 1

Three-dimensional view of the metamaterial grounded slab studied here, excited by a horizontal magnetic-dipole source placed on the ground plane, with the relevant coordinate system, and geometrical and physical parameters.

We consider here TE and TM modes excited by a dipole source and propagating in the xy plane along the radial ρ direction with propagation constant k_ρ. As is well known, based on a transverse-resonance approach, the dispersion equation for both TE and TM modes is:

[1]
$$Z_0^{TE/TM} + jZ_s^{TE/TM} \tan\left(k_{zs}h\right) = 0$$

where $Z_0^{TE/TM}$ and $Z_s^{TE/TM}$ are the transverse modal characteristic impedances in the air and in the slab regions, respectively, whereas

$$k_{zs} = \sqrt{k_0^2 \mu_r \varepsilon_r - k_\rho^2}$$

is the transverse wavenumber inside the slab and k_0 is the free-space wavenumber.

As a result of a graphical analysis of Eq. [1], sufficient conditions may be derived for the *absence* of *any proper surface wave* (5):

[2] $\mu_r, \varepsilon_r > 1,\ |\mu_r| < 1,\ |\varepsilon_r| > 1,\ h < \dfrac{1}{k_0\sqrt{\mu_r\varepsilon_r - 1}}\min\left\{\arctan\dfrac{1}{|\mu_r|},\sqrt{\dfrac{1}{|\mu_r|^2} - 1}\right\}$

[3] $\mu_r, \varepsilon_r < 1,\ |\mu_r| < 1,\ |\varepsilon_r| < 1,\ h > \operatorname{arctanh}(|\varepsilon_r|)\dfrac{1}{k_0\sqrt{\mu_r\varepsilon_r - 1}}$

In order to verify the possibility of achieving surface-wave suppression, we consider here a DNG grounded slab with relative permeability and permittivity given by:

[4] $\mu_r = 1 - \dfrac{F\omega_0^2}{\omega^2 - \omega_0^2},\ \varepsilon_r = 1 - \dfrac{\omega_p^2}{\omega^2}$

with $F = 0.56$, $\omega_0/2\pi = 4$ GHz, $\omega_p/2\pi = 10$ GHz (parameters chosen as in (4)). In Fig. 2(a) it can been checked that both the relative permeability and the relative permittivity are negative in the shown frequency range. Since $\mu_r, \varepsilon_r > 1$, by choosing conditions [2], a surface-wave suppression can be obtained: in Fig. 2(a) the dashed line represents an upper limit for the slab height imposed by [2] and therefore the choice $h = 20$ mm ensures the surface-wave suppression in the range from 5.1 GHz to 5.2 GHz (*shaded area*). In Fig. 2(b) a dispersion diagram for both TE and TM modes is reported: as it can be seen, in the above-mentioned range no real proper mode (*solid line*) can propagate.

(a)   (b)
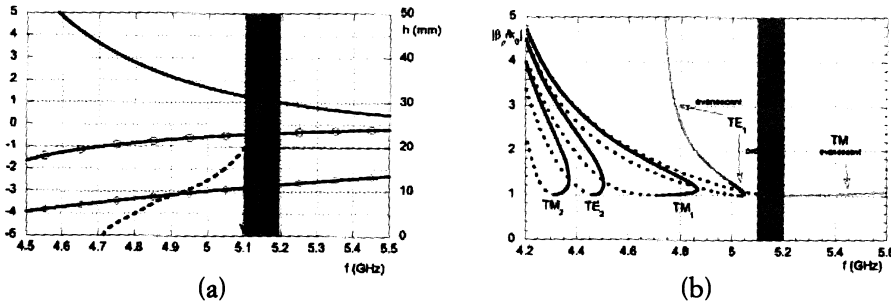
FIG. 2

(a) Relative permeability μ_r (*solid line with circles*), relative permittivity ε_r (*solid line with diamonds*) and their product $\mu_r\varepsilon_r$ (*solid line*) as a function of frequency f for a structure with material parameters as in Eq. [4]. The maximum slab height to have surface-wave suppression is reported with a *dashed line*. (b) Normalized phase constant as a function of frequency f for both TE and TM modes of the considered structure ($h = 20$ mm).

3. Conical beam scanning and radiation at broadside

In order to illustrate the effects of the presence of the metamaterial grounded slab on the radiation properties, we have studied the beam-scanning features of the far field radiated by a finite source (Fig. 3a), namely a horizontal magnetic dipole placed on the ground plane along the x axis in the presence of the same structure as in Fig. 2, with $h = 60$ mm. It can be observed (Fig. 3b) that the normalized phase constants $|\beta_p/k_0|$ of all the shown leaky modes (that result to be *proper* on a DNG slab) span almost completely the range (0, 1). Moreover, the low values of the normalized attenuation constants α_p/k_0 of the TE_1 and TM_1 modes give rise to radiation of a directive beam in a wide angular range.

In Fig. 3(a), radiation patterns in the E plane ($\phi = 90°$) are shown for this structure at different frequencies, where only one couple of leaky modes, i.e., the couple TE_1 and TM_1, contributes appreciably to radiation and thus a single beam is radiated. The beam is scanned toward broadside as frequency is increased, due to the backward nature of this complex mode, which is related to its proper character. An excellent agreement between the far field of the TE_1 and TM_1 leaky modes and the total far field can be observed. In Fig. 3(b) it can also be observed that the normalized phase constants of the TE_1 and TE_2 leaky modes are almost superimposed to those of the TM_1 and TM_2 leaky modes, respectively, over a wide frequency range. By taking into account that leaky modes contribute in all the ϕ-constant planes, this phase-constant equalization determines equal pointing angles of the radiated beams in the E and H planes. This implies that the 3D radiation pattern of the considered dipole has a conical shape with an almost-circular cross section, as it can be observed in Fig. 4(a), which represents the normalized radiation pattern at $f = 5.8$ GHz. The directions of maximum radiation are located in an annular region of al-most-perfectly circular shape, corresponding to a pointing angle $\theta_1 \approx 17.3°$. In Fig. 4(b) the level of power density radiated at broadside is reported as a function of frequency. Two peaks are visible, at $f = 5.479$ GHz and $f = 5.943$ GHz, respectively; it has analytically been proved that these maxima occur at the frequencies at which the phase and attenuation constants of the couple of leaky modes, which are responsible of radiation, are equal. It has also been proved that, when $|\mu_r|$ is small, the power density radiated at broadside at the peak frequencies is proportional to the ratio $|\varepsilon_r|/|\mu_r|$; this explains why the second peak is much higher than the first one.

(a)   (b)
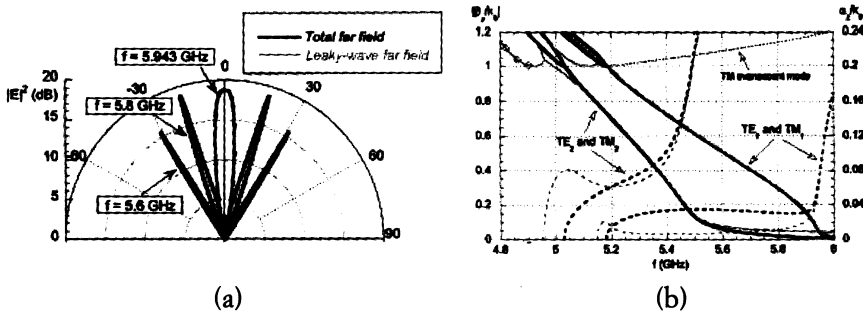
FIG. 3

(a) Radiation patterns as a function of the elevation angle θ in the plane φ = 90°.
(b) Normalized phase and attenuation constants for the TE and TM modes as
functions of frequency f for a slab modeled as in Fig. 2 with $h = 60$ mm.

(a)   (b)
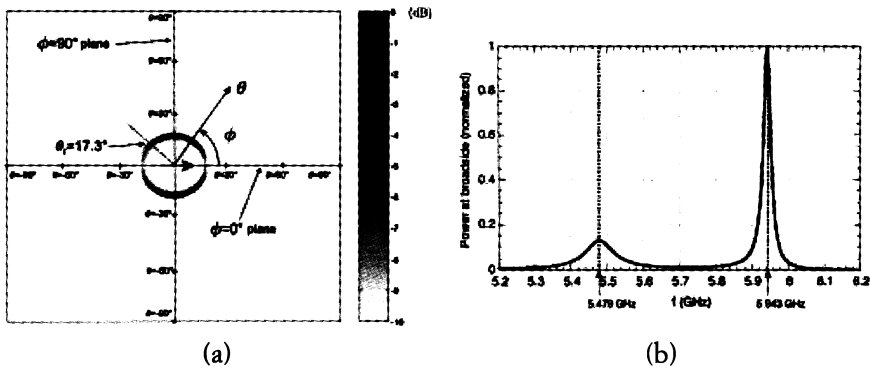
FIG. 4

(a) Gray-scale map (in dB) of the normalized radiation pattern at $f = 5.8$ GHz for
a structure as in Fig. 2(a). The radial coordinate is proportional to the spherical
angle θ; the angular coordinate is equal to the spherical angle φ (see Fig. 1 for
the definition of the spherical angles). (b) Normalized power density radiated at
        broadside as a function of frequency for the same structure as in (a).

REFERENCES

(1) A. ALÙ, N. ENGHETA, *Guided modes in a waveguide filled with a pair of single-negative (SNG), double-negative (DNG), and/or double-positive (DPS) layers*, IEEE TRANS.
MICROWAVE THEORY TECH., **52**, 199-210, Jan. 2004.
        (2) I.S. NEFEDOV, S.A. TRETYAKOV, *Waveguide containing a backward-wave slab*, RA-
DIO SCI., **38**, 1101-1109, Dec. 2003.
        (3) B.-I. WU, T.M. GRZEGORCZYK, Y. ZHANG, J.A. KONG, *Guided modes with imagi-
nary transverse wave number in a slab waveguide with negative permittivity and permeabil-
ity*, IEEE ANTENNAS WIRELESS PROPAGAT. LETT., **93**, 9386-9388, 2003.
        (4) I.W. SHADRIVOV, A.A. SUKHORUKOV, Y.S. KIVSHAR, *Guided modes in negative-
refractive-index waveguides*, PHYS. REV. E, **67**, 57602-1-57602-4, May 2003.
        (5) P. BACCARELLI, P. BURGHIGNOLI, G. LOVAT, S. PAULOTTO, *Surface-wave suppression
in a double-negative metamaterial grounded slab*, IEEE ANTENNAS WIRELESS PROPAGAT.
LETT., **2**, 269-272, 2003.

Miniaturized guiding structures based on evanescent waveguide filled with anisotropic single-negative meta-material

SILVIO HRABAR (*)

SUMMARY. – *This paper reports miniaturized guiding structure based on evanescent waveguide filled with anisotropic uniaxial meta-material with transversal negative effective permeability. Since this structure supports propagation of backward wave below the cut-off frequency, the waveguide width can be arbitrarily smaller than a half of the wavelength. Several experimental miniaturized waveguides filled with different resonant meta-materials in 7 GHz and 350 MHz frequency bands have been designed, fabricated and tested.*

1. Introduction

From basic electromagnetics it is very well known that transversal dimension of the rectangular waveguide should be at least one half of a wavelength in the filling material. If this constrain is not obeyed, there is no propagation of electromagnetic energy along the waveguide and energy is stored in the evanescent field. Very recently (1), the propagation below cut-off frequency of a waveguide loaded with split-ring resonators was demonstrated. This waveguide was interpreted as one-dimensional meta-material with both negative permeability and negative permittivity (1). Different interpretation, based on uniaxial anisotropy of magnetic meta-material filling was given in (2,3). In this paper, the mathematical background as well as the intuitive explanation of phenomenon of backward propagation below the cut-off frequency are presented. Application of this phenomenon for waveguide miniaturization is demonstrated experimentally.

(*) Dept. of Radiocommunications and Microwave Engineering, Faculty of Electrical Engineering, University of Zagreb, Unska 17, Zagreb, HR-10 000, Croatia

2. Theoretical analysis

Let us consider the waveguide with square cross section (Fig. 1), filled with one row of split-ring resonators (SRR's). The row is placed along the waveguide line of symmetry (1,2,3).
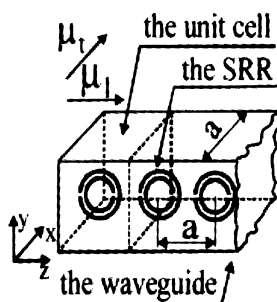
FIG. 1

The waveguide filled with SRR's
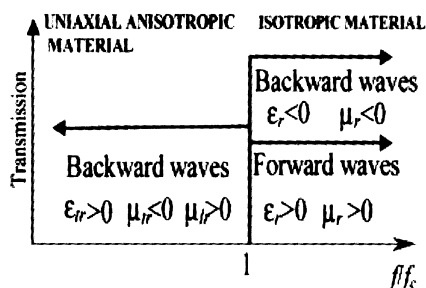
FIG. 2

The influence of waveguide filling on propagation

The waveguide filling behaves as uniaxial meta-material (2) described by permeability tensor:

[1]
$$\overline{\mu} = \mu_0 \begin{bmatrix} \mu_{tr} & 0 & 0 \\ 0 & \mu_{lr} & 0 \\ 0 & 0 & \mu_{lr} \end{bmatrix} = \mu_0\, \overline{\mu}_r.$$

In [1] μ_0 is absolute permeability and μ_{tr} and μ_{lr} stand for relative permeability in transversal (x) and longitudinal (y and z) directions of the waveguide, respectively. Only μ_{tr} may have negative sign due to properties

of propagation in the waveguide explained in detail in (2). Briefly, if one assumes the TE mode, only x component of the magnetic field (H_x) is perpendicular to the SRR and it will give rise to the induced current eventually yielding negative relative permeability.

The dispersion equation for this waveguide was derived in (3) and it reads

[2] $$\frac{k_x^2}{\mu_{lr}} + \frac{k_z^2}{\mu_{tr}} = \varepsilon_r k_0^2, \quad k_x = \left(\frac{m\pi}{a}\right), \quad m = 1, 2, 3, \ldots$$

The symbol k_0 stands for free space propagation factor, ε_0 is absolute permittivity and ε_r is relative permittivity. The symbols k_x and k_z stand for propagation constants in transversal and longitudinal directions, respectively whereas the symbol a stands for the waveguide width (Fig. 1). From [2] one easily finds the expression for longitudinal propagation factor:

[3] $$k_z = \pm \sqrt{\varepsilon_r \mu_{tr} \left(k_0^2 - \frac{k_x^2}{\varepsilon_r \mu_{lr}}\right)}.$$

One should note that there are always two different solutions for square root in [3] and therefore two different solutions for propagation factor k_z. The physically meaningful solution can be chosen by introduction of losses (i.e. the imaginary part of the permeability). One must choose the solution that gives attenuated waves, since every physical flow of energy must decay away from the source in media with loss. In the limiting case of loss-free material [3] can be rearranged into the compact, more convenient form given by:

[4] $$k_z = \pm k_0 \sqrt{\varepsilon_r \mu_{tr} \left[1 - \left(\frac{f_c}{f}\right)^2\right]}, \quad f_c = \frac{f_{c0}}{+\sqrt{\varepsilon_r \mu_{lr}}}, \quad f_{c0} = \frac{mc}{2a}.$$

Here, f stands for frequency of the signal, whereas f_{c0} and f_c are the cut-off frequency of an empty waveguide and waveguide filled with material, respectively. Now one can analyze the influence of different filling on propagation in the waveguide (Fig. 2).

In familiar case of waveguide filled with isotropic double positive material, $(\varepsilon_r > 0, \ \mu_{tr} = \mu_{lr} = \mu_r, \ \mu_r > 0)$ one must chose positive sign in [4]. This yields very well known high-pass behavior (Fig. 2). Above the cut off frequency there is propagation in form of forward waves $(k_z > 0)$. Below the cut-off k_z becomes imaginary and there is no propagation along the waveguide.

In the case of waveguide filled with isotropic double negative material $(\varepsilon_r < 0, \ \mu_{tr} = \mu_{lr} = \mu_r, \ \mu_r < 0)$ (Fig. 2) one must choose negative sign in front of the square root in [4]. Now, k_z is negative $(k_z < 0)$, indicating propagation in the form of the backward waves.

Very interesting, counter-intuitive case occurs if the waveguide is filled with uniaxial material with negative transversal permeability ($\mu_{tr} < 0$ and $\mu_{lr} > 0$). One can see that the expression under the square root in [4] is now positive for frequencies below cut-off (due to $\mu_{tr} < 0$). The meaningful physical solution is now given by negative sign in front of square root in [4]. Thus k_z is negative ($k_z < 0$), again indicating backward wave propagation, but now at the frequencies below cut-off frequency. Hence, this waveguide shows low-pass behavior (Fig. 2) and it can be considered as a dual of an ordinary waveguide. The waveguide width can be arbitrarily smaller than half of the wavelength in filling material ($a < c/(2f_{c0}\sqrt{\varepsilon_r \mu_{lr}})$, c being the speed of light).

3. Transmission line model of the waveguide

The propagation in the waveguide filled with uniaxial negative permeability material can be explained in simpler, intuitive way using the transmission line model. The rectangular waveguide can be thought of an ordinary, two- wire TEM transmission line loaded with infinite number of short-circuited stubs (Fig. 3).
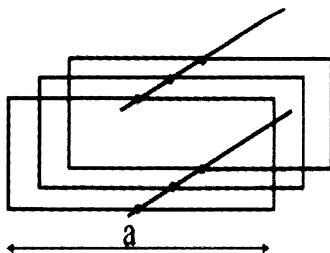
FIG. 3

Transmission line presentation of rectangular wavwguide
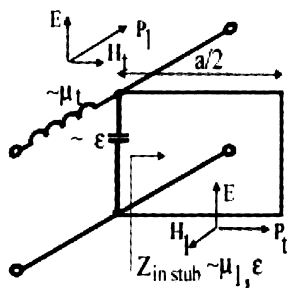
FIG. 4

Explanation of distributed inductances and distributed capacitance
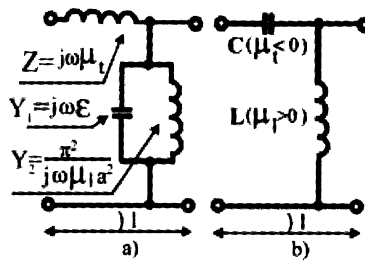
FIG. 5

a) Equivalent transmission line circuit b) Equivalent C-L line

The main two-wire transmission line can be modelled with the distributed series inductance and distributed shunt capacitance (Fig. 4). The distributed capacitance of the main line is associated with the permittivity of the filling material ε. The transversal magnetic field vector H_t is caused by energy flow along the main line (longitudinal flow along the waveguide defined by E, H_t, P_l). Due to this, the distributed inductance is associated only with the permeability in transversal direction of the waveguide (μ_t). On contrary, the energy flow down the stub causes existence of non-zero longitudinal magnetic field vector H_l. Thus, the distributed series inductance of the stub is associated with the permeability in longitudinal direction (μ_l). Bearing in mind that input admittance of a short circuited stub can be modeled as a parallel tank circuit, one ends up with equivalent circuit of the differential section of the waveguide (Fig 5a). Here, Z stands for the series impedance while Y_1 and Y_2 represent shunt admittances.

If the waveguide is filled with the isotropic double positive material, the series reactance Z will have positive value (caused by positive sign of μ_t). Below the cut-off frequency, the stubs are shorter than one quarter of the wavelength, and the shunt admittance Y_2 has inductive character (since $\mu_l > 0$). Since the tank circuit formed by shunt capacitance and shunt inductance operates below the resonance (f_c), the overall shunt admittance $Y_1 + Y_2$ has inductive character. Thus, the waveguide behaves as transmission line where both series impedance and shunt admittance are inductive (L-L transmission line). This type of line does not support propagation of electromagnetic waves. Above the resonance (f_c), parallel admittance exhibits capacitive behavior, the transmission line has usual form (series inductance and parallel capacitance, L-C line) and propagation is in the form of ordinary forward waves.

In the case of uniaxial anisotropic material, the reactance Z behaves as a negative inductance (due to $\mu_t < 0$). At any single frequency below the cut-off, one can think of the series negative inductance Z as the ordinary capacitance. This leads to the equivalent circuit that comprises series capacitance and the shunt inductances (C-L transmission line) (Fig. 5b). It was shown in (5) that this type of line supports the backward waves. This is the simple explanation of the origin of backward-wave propagation below cut off.

4. Experiment

The experimental uniaxial meta-material was based on the inclusions in the form of double ring (4). The rings were designed to have f_0 of 7.8 GHz and fabricated using standard etching process on the CuClad substrate with double copper cladding (substrate thickness of 0.7 mm, copper thickness of 0.02 mm, $\varepsilon_r = 2.6$). The rings had inner diameter of 4 mm with the tracks width of 1 mm and the slit width of 0.5 mm. The experimental waveguide was made out of copper, with the length of 60 mm and square cross section of 12 mm × 12 mm ($f_{c0} = 12.5$ GHz). The transmission coefficient of the waveguide was measured using HP 8720B network analyzer. The measurement results (Fig. 6) show propagation pass-band located well below the cut-off frequency, similarly to the results given in (1).

The backward wave propagation was verified by measurement of the phase of transmission coefficient for two waveguides of different length (60 mm and 90 mm). Results (Fig. 7) show that increase of the length is accompanied with the increase of the phase angle of transmission coefficient. One concludes that phase of the electromagnetic wave increases along the waveguide i.e. the propagation is indeed in the form of backward waves.
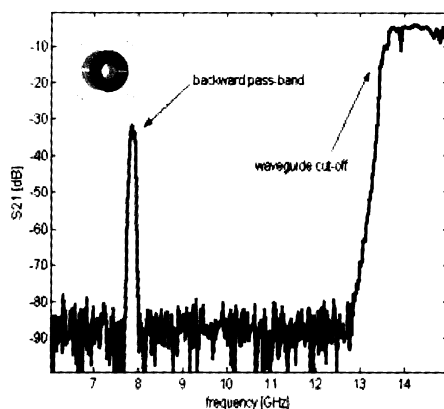
FIG. 6

Measured S_{21} parameter of miniaturized filled with meta-material based on double rings. Insert: the double ring inclusion

The experimental waveguide has transversal width that is approximately 30% of the width of the standard J-band waveguide. In principle, the reduction in size can be arbitrary large if it is possible to fabricate appropriate meta-material which has negative transversal permeability at some lower frequency below cut off. In order to test proposed approach, the laboratory model of different meta-material was fabricated. It comprised

twelve solid copper rings (inner radius of 6 mm, outer radius of 8 mm, thickness of 1 mm, slit width of 1 mm). Each ring was loaded with 33 pF chip capacitor (size of 2mm × 2mm × 1mm).

This inclusion behaves similarly to the SRR (6). The rings were mounted on a foam with lattice constant of 8 mm and inserted along the line of symmetry of 115 mm long waveguide (cross section of 16 mm × 16 mm, f_{c0}=9.4 GHz). Measurement of S_{21} parameter revealed pass-band located at the frequency of 350 MHz (Fig. 8). The transversal dimension of this waveguide is only 3.7% of half of the wavelength.
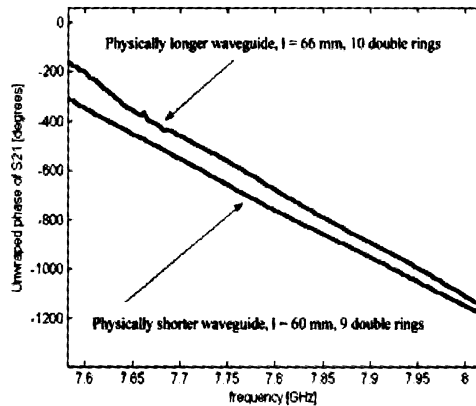
FIG. 7

Measured phase of S_{21} parameter across the pass-band for waveguides filled with meta-material based on double rings
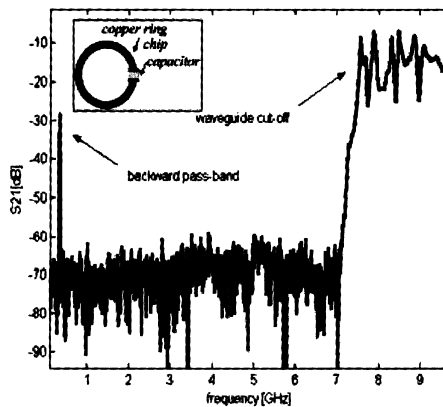
FIG. 8

Measured S_{21} parameter of waveguide filled with meta-material based on capacitively loaded rings; Inset: the inclusion

5. Conclusions

It has been shown that waveguide filled with uniaxial negative permeability material supports propagation of backward waves below the cut-off frequency of the dominant TE mode providing that transversal permeability is negative. The transversal width of such a waveguide can be in principle arbitrarily small, which may be used for waveguide miniaturization.

REFERENCES

(1) R. Marques, J. Martel, et. al., *Left-handed-media Simulation and Transmission of EM waves in Subwavelength Split-Ring-Resonator-Loaded Metallic Waveguides*, Phys. Rev. Lett., October 2002.

(2) S. Hrabar, J. Bartolic, *Backward-Wave Waveguide Based on Uniaxial Anisotropic Negative Permeability Meta-Material*, Proc. of ICECOM 2003, Dubrovnik 2003.

(3) S. Hrabar, J. Bartolic, Z. Sipus, *Miniaturization of Rectangular Waveguide using Uniaxial Anisotropic Negative Permeability Meta-Material*, Proc. of MELECON 2004, Dubrovnik 2004.

(4) R. Marques, F. Medina, R. Rafii-El-Idrissi, *Role of Anisotropy in Negative Permeability and Left-handed Metamaterilas*, Phys. Rev., **B65**, 1-6, 2002.

(5) C. Caloz, T. Itoh, *Application of the Transmission Line Theory of Left-handed Materials to the Realization of a Microstrip LH Line*, Proc. IEEE MTT-S, 412-415, 2002.

(6) S. Hrabar, J. Bartolic, *Capacitively Loaded Loop as Basic Element of Negative Permeability Meta material*, Proc. on European Microwave 2002, 357-361, Milan, 2002.

Metamaterial monolayers and bilayers for enhanced transmission through a sub-wavelength aperture in a flat perfectly conducting screen

ANDREA ALÙ (*), FILIBERTO BILOTTI (*),
NADER ENGHETA (**), LUCIO VEGNI (*)

SUMMARY. – In *this paper, we will provide an overview of our theoretical work on the role of metamaterial covers in dramatically enhancing the wave transmission through a subwavelength aperture over a perfectly conducting flat screen. It is well known that a low-permittivity or a low-permeability grounded slab may support surface polaritons. In our problem these natural modes are exploited to collect and redirect the impinging radiation into the tiny hole and to reshape the radiation pattern at the exit side of the screen towards an observer. The sum of these two effects may potentially lead to a dramatic increase in the total power transmission through the aperture. Moreover, we show how this effect may be further increased and optimized by employing bilayer covers with "conjugate" materials, i.e., materials with oppositely signed constitutive parameters. In some earlier works, we have indeed utilized such a coupling to induce a compact "interface" resonance, suggesting several microwave and optical applications. Here, the same resonant phenomenon can lead to the transmission enhancement together with a reduction of the required cover thickness. We provide some insights into the physical basis of this effect, and we speculate some potential applications.*

1. Introduction

The challenge of transporting optical information in a structure with lateral dimensions below the diffraction limit is currently an exciting topic in the scientific community, due to the increased attention in science and technology of nanoscales, and optical computation (see, e.g., [1]). One such

(*)Dept. of Applied Electronics, University of Roma Tre, Via della Vasca Navale, 84, 00146 Roma, Italy
(**) Dept. of Electrical and Systems Engineering, University of Pennsylvania, 19104 Philadelphia, PA, USA

problem has been the study of techniques to enhance wave transmission through sub-wavelength apertures, which are being investigated by several groups worldwide [2-4].

In this work, we report and summarize our recent theoretical work on the role of metamaterial covers in dramatically enhancing the wave transmission through a subwavelength aperture over a perfectly conducting flat screen. It is well known that a low-permittivity or a low-permeability grounded slab may support surface polaritons, which are commonly used in leaky-wave antenna applications [5]. In our problem these natural modes are exploited to collect and redirect the impinging radiation into the tiny hole and to reshape the radiation pattern at the exit side of the screen towards an observer. The combination of these two effects may potentially lead to a dramatic increase in the total power transmission through the aperture.

Moreover, we show here how this effect may be further increased and optimized by employing bilayer covers with "conjugate" materials, i.e., materials with oppositely signed constitutive parameters. In some earlier works (see, e.g., [6-7]), some of us have indeed utilized such a coupling to induce a compact "interface" resonance, suggesting several microwave and optical potential applications. Here, the same resonant phenomenon may lead to the transmission enhancement and a reduction of the required cover thickness.

The huge enhancement effect in the wave transmission through tiny holes may offer several interesting potential applications. It has been suggested in the literature that such enhancement may be used to spatially filter the electromagnetic radiation, avoiding the diffraction limitations [8], for tunable optical filters [9], for photolithography, for near-field microscopy or to extract light from LED [3]. In the following, we provide some insights into the physical basis of this effect. We also address the sensitivity of our designs to losses and to a few other realistic limitations.

2. Theoretical analysis

The geometry we refer to in the following is depicted in Figure 1, and consists of a flat perfectly conducting and infinitely thin metallic screen embedded in a suitable Cartesian reference system. The screen is placed on the plane $y = 0$ and an electrically tiny aperture, with arbitrary cross section, is positioned at the origin. Let the region that the hole occupies on the screen be denoted by A. An $e^{j\omega t}$-monochromatic source is placed somewhere in the region $y < 0$, far from the hole, illuminating the structure. The screen is covered on both sides by layers of isotropic material, with complex constitutive parameters ε and μ at the operating frequency $f = \omega/2\pi$, and with thicknesses d_{in} and d_{out}, respectively for the $y < 0$ and $y > 0$ sides. The covered screen is surrounded by vacuum, with permittivity and permeability ε_0 and μ_0, respectively.
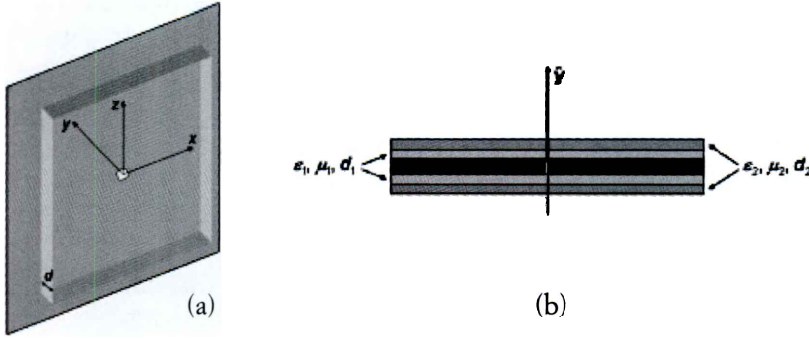
FIG. 1

Geometry of the problem: a) a sub-wavelength hole in a perfectly electric conduct-
ing (PEC) flat screen covered by a metamaterial slab (entrance face), b) cross-
sectional view of the setup with bilayer covers in the entrance and exit faces

According to Bethe's theory [10], we should first calculate the field
induced by the excitation in the region A, neglecting the presence of the
hole, since its small dimensions should not sensibly affect the field on the
entrance face. Then, we may calculate the equivalent magnetic sources to
be put on the other side of the screen, again in the region A, in order to
solve the radiation problem on the exit face. As shown by Bethe, these
magnetic sources are directly proportional to the amplitude of the field in
A when the hole is closed, and for an observer far from the hole on the
exit side they are represented by an electric and a magnetic dipole as
follows:

[1]
$$p = \alpha_1 E_0$$
$$m = -\alpha_2 \cdot H_0,$$

where the electric polarizability $\boldsymbol{\alpha}_1$ and the magnetic polarizability tensor $\underline{\boldsymbol{\alpha}}_2$
depend on the shape of the hole and, due to the small dimensions of A,
they may be evaluated using the static limits. The fields E_0 and H_0 repre-
sent, respectively, the uniform electric and magnetic fields present in region
A when the hole is closed, which implies the normal component of the
total electric field and the tangential component of the total magnetic field
in formula (1).

It may be shown that an efficient way to dramatically increase the
electromagnetic field on the hole, which corresponds to a proportional
increase of the equivalent radiating dipoles from the hole, as justified by
formula (1), is to use at the entrance face of the screen a cover with:

[2]
$$|\mu| \leq \mu_0, \quad d_{in} = \frac{(2N-1)\pi}{2\sqrt{k^2 - \bar{k}_t^2}},$$

where N is a positive integer, $k=\omega\sqrt{\varepsilon\mu}$ and $\bar{k}_t$ is the transverse wave number of the plane wave impinging at the angle from which most part of the radiation is expected to come. This condition, in fact, implies that the grounded slab at the entrance face supports a natural mode (leaky wave) with transverse wave number $k_t \simeq \bar{k}_t$, with a very small imaginary part taking into account the typical radiation losses of such modes, which couples very well with the incoming radiation. This polariton easily collects power from the entrance side into the tiny hole, drastically increasing the total power transmission.

Correspondingly by reciprocity, placing a similar cover at the exit side of the hole, induces a parallel increase of transmission towards the observer, similar to the effects shown in another setup by Enoch *et al.* [5].

3. Numerical results

Figure 2 shows the normalized radiation patterns of a setup with a monolayer cover, designed following Eq. 1. The main drawback of this setup is that the required cover may easily become relatively thick, since the wavelength in the cover material is larger than in the free space (in the example here shown $d \leq 8\lambda_0$). A way to overcome this problem is to utilize cover bilayers constituted by conjugate materials, in the sense reported in [6-7]. In this case, a compact interface resonance may be induced in the cover, which allows designing a thin cover still supporting a material polariton. The optimized design gives a total power enhancement of about 90 dB with a cover thick less than a wavelength in free space.

Clearly, the results here reported are ideal numerical simulations, whereas in practice we should take into account several intrinsic limitations: material losses, sensitivity to a variation in the material parameters, cover and screen finiteness in the transverse plane, finiteness of the screen conductivity and longitudinal thickness. We have considered also these realistic limitations in our work, even though the results are not reported here for lack of space. However, it is interesting to underline that still promising results are obtained also in these cases, which in the optimized setups lead to major enhancements of power transmission through tiny subwavelength apertures.
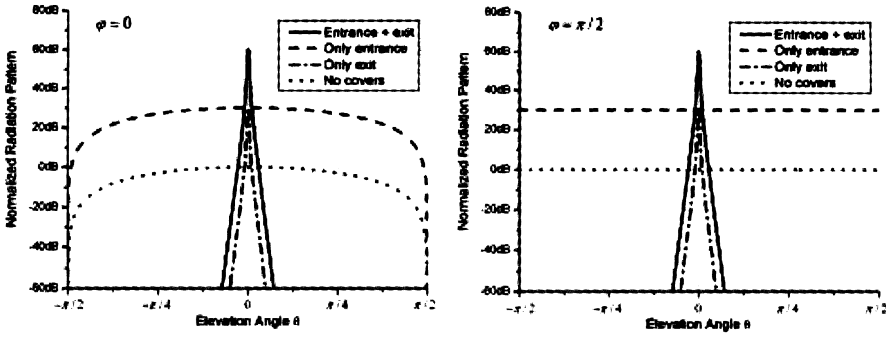
FIG. 2

Radiation patterns in the E and H planes for covers with $\varepsilon = \varepsilon_0$, $\mu = 10^{-3}\mu_0$, $d_{in} = d_{out} = \pi/2k$, normalized to the peak of the pattern with no covers, compared to those with only the entrance slab, only the exit one, and the one with no covers.
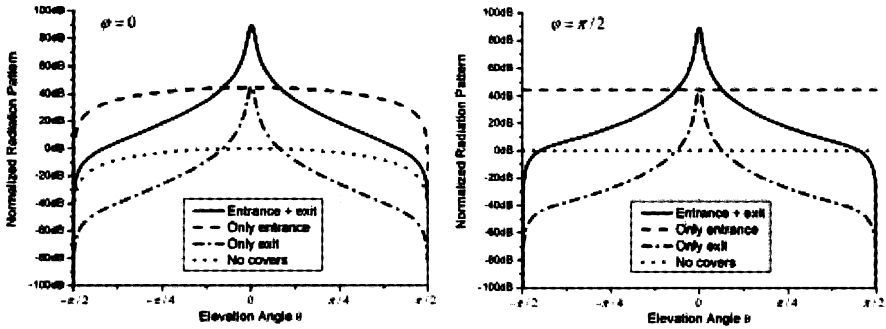
FIG. 3

Radiation patterns in two planes $\phi = 0°$ and $\phi = 90°$, normalized to the pattern with no covers. Cover bilayers are employed with $\varepsilon_1 = 9.957\varepsilon_0$, $\mu_1 = 0.034\mu_0$, $\varepsilon_2 = 5.747\varepsilon_0$, $\mu_2 = -0.283\mu_0$, $d_1 = d_2 = 0.36\lambda_0$

REFERENCES

(1) S.A. MAIER, P.G. KIK, H.A. ATWATER, S. MELTZER, E. HAREL, B.E. KOEL, A.A.G. REQUICHA, *Local detection of electromagnetic energy transport below the diffraction limit in metal nanoparticle plasmon waveguides*, Nature Materials, **2**, 229-232, 2003.

(2) T.W. EBBSEN, H.J. LEZEC, H. F. GHAEMI, T. THIO, P.A. WOLFF, *Extraordinary optical transmission through sub-wavelength hole arrays*, Nature, **391**, 667-669, 1998.

(3) D.E. GRUPP, H.J. LEZEC, T. THIO, T.W. EBBSEN, *Beyond the Bethe limit: tunable enhanced light transmission through a single sub-wavelength aperture*, Advanced Materials, **11**, 860-862, 1999.

(4) A.A. OLINER, D.R. JACKSON, *Leaky surface-plasmon theory for dramatically enhanced transmission through a sub-wavelength aperture, Part I: Basic features*, Proceedings of IEEE Antennas and Propagation Society Symposium, Columbus, OH, **2**, 1091-1094, 2003.

(5) S. ENOCH, G. TAYEB, P. SABORNOUX, N. GUERIN, P. VINCENT, *A metamaterial for directive emission*, Physical Review Letters., **89**, 213902, 2002.

(6) A. ALÙ, N. ENGHETA, *Pairing an epsilon-negative slab with a mu-negative slab: resonance, tunneling and transparency*, IEEE Transactions on Antennas and Propagation., Special Issue on Metamaterials, **51**, 2558-2571, 2003.

(7) A. ALÙ, N. ENGHETA, *Peculiar radar cross section properties of double-negative and single-negative metamaterials*, Proceedings of IEEE Radar Conference, Philadelphia, PA, 2004, to appear.

(8) R. SAMBLES, *More than transparent*, Nature, **391**, 641-642, 1998.

(9) T.J. KIM, T. THIO, T.W. EBBSEN, D.E. GRUPP, H.J. LEZEC, *Control of optical transmission through metals perforated with subwavelength hole arrays*, Optics Express, **24**, 256-258, 1999.

(10) H.A. BETHE, *Theory of diffraction by small holes*, Physical Review, **66**, 163-182, 1944.

SESSIONS II AND III
METAMATERIALS AND COMPLEX MATERIAL: APPLICATIONS

Characterization of chirowaveguides by a new development of the coupled mode method

ÁLVARO GÓMEZ (*), ÁNGEL VEGAS (*),
MIGUEL ÁNGEL SOLANO (*)

SUMMARY. – *The application of the coupled mode method (CMM) for the calculation of the propagation constants and the electromagnetic field distribution in chirowaveguides is well known. The CMM is a method of moments in which the basis and test functions are the modes of an ideal guide with the inside media removed (i.e., an empty waveguide). The usual formulations of the CMM involves the electric field E and the magnetic filed H as unknowns (EH-formulations), When the media inside the waveguide is anisotropic or bi-isotropic, the normal components on the perfect electric conductors of the waveguide are not zero, but in these formulations they become zero because the basis functions vanish on these walls. Then, in this paper we will develop a new formulation of the CMM which obeys the appropriate boundary conditions by using the magnetic induction B as unknown instead of the H field (EB-formulation). The results for this formulation are more accurate than those obtained by the EH-formulations.*

1. Introduction

The propagation of electromagnetic waves in chiral media has received considerable attention in the last few years, due to its potential applications at microwave and millimeter wave frequencies (1). A chiral object is defined to be a three-dimensional body that is not superimposible with its mirror image by translation and rotation (2). At microwave frequencies, the most relevant property of chiral media concerning the propagation of electromagnetic waves is the rotation of its plane of polarization. One of the problems commonly studied in the literature is the propagation of electromagnetic waves through guided structures, which are called chirowaveguides.

(*) Dept. De Ingenieria de Comunicaciones, Universidad de Cantabria, Avda de los Castros s/n, 39005 Santander, Spain.

This paper presents a new formulation of the coupled mode method (3). The coupled mode method is a moment method in which the basis and test functions are the components of the electromagnetic field of an empty parallel plate waveguide. Several papers using this numerical technique have been published. In all of them the electric field $\vec{E}$ and the magnetic field $\vec{H}$ are expanded as a function of the same fields of an empty waveguide. They are called *EH-formulations*. Two types of *EH-formulations* (direct and indirect formulations) have been proposed in the literature, depending on the different ways in which the longitudinal components of the electromagnetic field can be expressed as functions of the transverse ones. A good discussion about these two formulations can be seen in (4). In the *EH formulations* for chirowaveguides the normal components of $\vec{H}$ vanish at the perfect electric walls because they are expanded in terms of functions that are zero on these walls. Analytically, this is incorrect. What should vanish at the walls is the normal component of the magnetic induction $\vec{B}$. Then, if the components of the electric field $\vec{E}$ and the magnetic induction $\vec{B}$ are expanded, we obtain a new formulation, which we call the *EB formulation* (4).

The goal of this paper is to extend the EB formulation to parallel plate waveguides partially filled with chiral media. We also propose a way of finding the magnetic field distribution $\vec{H}$ from the *EB formulation* which is not directly obtained as in *EH formulations*. Finally, we discuss the advantages and disadvantages and point out a common error found in the literature about EH formulations.

2. Theory

Let us consider the problem illustrated in Fig. 1, where the planes $y = 0$ and $y = a$ are perfect electric walls, thereby constituting a parallel-plate waveguide. Inside this waveguide there is a chiral material characterized by the constitutive relations

$$[1] \qquad \vec{D} = \varepsilon \vec{E} - j\kappa\sqrt{\mu_0\varepsilon_0}\,\vec{H}; \quad \vec{B} = \mu\vec{H} + j\kappa\sqrt{\mu_0\varepsilon_0}\,\vec{E},$$

where ε is the dielectric permittivity, μ the magnetic permeability and κ is the Pasteur parameter. By means of the well-known Galerkin method, the CMM for either formulation (EH or EB) leads to an algebraic system of equations.

The expansion in the *EB-formulation* for the unknown components, which are the electric field and the induction magnetic, are

$$[2] \qquad E_x(y,z) = \sum_{j=1}^{\infty} V_{[j]}(z)\frac{\partial T_{[j]}(y)}{\partial y}; \quad E_y(y,z) = \sum_{i=0}^{\infty} V_{(i)}(z)\frac{\partial T_{(i)}(y)}{\partial y}$$
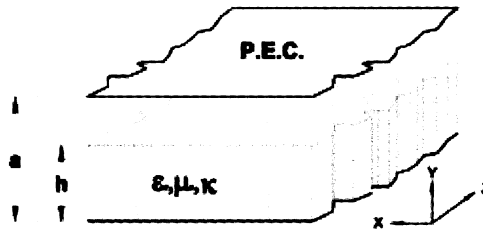
FIG. 1

Parallel plate waveguide partially filled with a slab of chiral medium. PEC means Perfect Electric Conductor.

[3] $B_x(y,z) = -\mu_0 \sum_{i=0}^{\infty} b_{(i)}(z)\dfrac{\partial T_{(i)}(y)}{\partial y};\quad B_y(y,z) = \mu_0 \sum_{j=1}^{\infty} b_{[j]}(z)\dfrac{\partial T_{[j]}(y)}{\partial y}$

[4] $E_z(y,z) = \sum_{i=1}^{\infty} k_{c(i)} V_{(i)}^z(z) T_{(i)}(y);\quad B_z(y,z) = \mu_0 \sum_{j=1}^{\infty} k_{c[j]} b_{[j]}^z(z) T_{[j]}(y) + \mu_0 b_0(z)$

where $V_{[j]}(z)$, $V_{(i)}(z)$, $V_{(i)}^z(z)$, $b_{[j]}(z)$, $b_{(i)}(z)$ and $b_{[j]}^z(z)$ are the coefficients of the expansion, whose dependence on the z-coordinate is $V_{(i)}\exp(\Gamma_k z)$ with $k = 1, 2, ..., \infty$, $V_{(i)}$ is a constant and Γ_k are the propagation constants for the proper modes. Analogous expressions can be written for the other coefficients. The T-potentials, which give the solutions for the *TEM*, *TE* and *TM* modes inside an empty parallel-plate waveguide, are given in (5). Also, it is necessary to express the components of the displacement electric vector $\vec{D}$ and the magnetic field $\vec{H}$ as a function of the components known by their expansions (electric field $\vec{E}$ and magnetic induction $\vec{B}$). Using [1] we can write

[5] $\quad \vec{H} = \dfrac{1}{\mu}\vec{B} - j\kappa\sqrt{\mu_0\varepsilon_0}\,\vec{E};\quad \vec{D} = \left(\varepsilon - \dfrac{\kappa^2}{\mu}\mu_0\varepsilon_0\right)\vec{E} - \dfrac{j\kappa}{\mu}\sqrt{\mu_0\varepsilon_0}\,\vec{B}.$

Substituting [2]-[4] into curl Maxwell's equations for the transverse components, using the relations given by [5] and applying the Galerkin method, the Telegraphist's equations for the *EB-formulation* are obtained in matrix form as

[6]
$$\dfrac{d}{dz}\begin{bmatrix} V_{(n)} \\ V_{[m]} \\ b_{(n)} \\ b_{[m]} \end{bmatrix} = -\begin{bmatrix} 0 & T_{(n)[j]}^V & \Psi_{(n)(i)}^{TM} & 0 \\ 0 & 0 & 0 & \Psi_{[m][j]}^{TE} \\ \Phi_{(i)(n)}^{TE} & 0 & 0 & T_{(i)[j]}^B \\ 0 & \Phi_{[j](m)}^{TE} & T_{[j](i)}^B & 0 \end{bmatrix}\begin{bmatrix} V_{(i)} \\ V_{[j]} \\ b_{(i)} \\ b_{[j]} \end{bmatrix},$$

$n,i = 0,1,2,...,ntm,$

$m,j = 1,2,...,nte,$

The eigenvalues of the matrix of [6] are the propagation constants and the eigenvectors are the coefficients of the expansions [2]-[4].

This formulation has two main disadvantages. Firstly, its mathematical development is much more complicated than the *EH formulations*. Secondly, and perhaps more significantly, if one wants to study structures which are not uniform in the z-direction by means of a mode matching method, it is essential for the field $\vec{H}$ to be known; however, it can not be obtained directly. Therefore, in order to get the magnetic field, we must find the expansion of each component. From the constitutive relations, we can write

$$
[7] \quad
\begin{aligned}
\vec{H} = {} & \left(-\sum_{i=0}^{ntm} I_{(i)}^x \frac{\partial T_{(i)}}{\partial y} - \sum_{j=1}^{nte} I_{[j]}^x \frac{\partial T_{[j]}}{\partial y} \right) \vec{a}_x + \left(\sum_{i=1}^{ntm} I_{(i)}^y \frac{\partial T_{(i)}}{\partial y} + \sum_{j=1}^{nte} I_{[j]}^y \frac{\partial T_{[j]}}{\partial y} \right) \vec{a}_y \\
& + \left(\sum_{i=1}^{ntm} k_{c_{(i)}} I_{(i)}^z T_{(i)} + \sum_{j=1}^{nte} k_{c_{[j]}} I_{[j]}^z T_{[j]} + h_0 \right)
\end{aligned}
$$

where the coefficients I's are obtained by the habitual procedure of applying Galerkin Method and the term h_0 is obtained in similar way as b_0. In accordance with the *EH formulations*, h_0 is not null.

3. Results

First, the results obtained for a fully loaded waveguide will be compared with the analytical ones. Fig. 2 shows the convergence diagram of the propagation constant normalized to the vacuum wavenumber for the fundamental mode of the chirowaveguide. It can be seen that the results of the *EB formulation* converge to the analytical value faster than those of either one of the *EH formulations*. For example, taking only 20 basis modes, the propagation constant given by the *EB formulation* is almost equal to the analytical solution. For the indirect *EH formulation*, the convergence is slower, but acceptable. However, the convergence for the direct *EH formulation* is very poor. Fig. 3 shows the y-component of the magnetic field against y-coordinate given by the *EB* and *EH indirect formulation* using 20 basis modes and the exact values. The results provided by *EB formulation* are very acuracce, while the solution given by the *EH formulation* would need more basis modes to minimize the ripple. Also it can be seen that the *EH formulation* does not verify the boundary conditions on the PEC. However, the magnetic field component given by the *EB formulation* yields the analytical one.
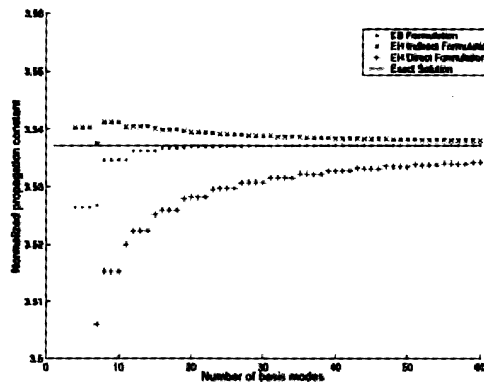
FIG. 2

Convergence diagram for the fundamental mode of the fully loaded parallel-plate chirowaveguide. Dimensions in mm: $b = a = 10$, $\varepsilon r = 5.142$, $\kappa = 1.5$ and $f = 11$ GHz.
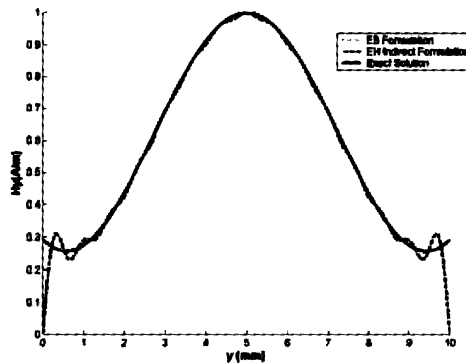
FIG. 3

Field distribution of the H_y component for the third mode in fully loaded chirowaveguide Dimensions in mm: $b = a = 10$. $\varepsilon r = 8.553$, $\kappa = 0.754$ and $f = 11$ GHz.

4. Conclusions

This paper presents a generalization of the *EB formulation* of the CMM for a parallel- plate waveguide partially filled with slabs of chiral media. A new expansion for the H-field is also proposed. Its knowledge is essential when a structure with discontinuities in the propagation direction has to be analyzed. The *EB formulation* is mathematically more complicated than the *EH formulation*, but the results obtained for the magnetic field verify the boundary conditions on the PEC's.

Acknowledgments

REFERENCES

(1) I.V. LINDELL, A.H. SIHVOLA, *Plane-Wave Reflection from Uniaxial Chiral Interface and Its Application to Polarization Transformation*, IEEE Trans. on Antennas and Propagat., **43**, 1397-1404, 1995.

(2) D.L. JAGGARD, A.R. MICKELSON, C.H. PAPAS, *On Electromagnetic Waves in Chiral Media*, Appl. Phys., **18**, 211-216, 1979.

(3) P. PELLET, N. ENGHETA, *Coupled-mode theory for Chirowaveguides*, J. Appl. Phys., **67**, 2742-2745, 1990.

(4) Y. XU, R. G. BOSISIO, *A Study on the Solutions of Chirowaveguides and Bianisotropic Waveguides with the use of the Coupled-Mode Analysis*, Microw. and Opt. Tech. Letters, **14**, 308–311, 1997.

(5) A. GOMEZ, M.A. SOLANO, A. VEGAS, *New Formulation of the Coupled Mode Method for the Analysis of Chirowaveguides*, Proc. of SPIE, **4806**, 290–301, 2002, (Seattle, USA).

Application of metamaterials to the design of planar microwave filters

FERRAN MARTÍN (*), JORDI BONACHE (*),
FRANCISCO FALCONE (*), JOAN GARCÍA-GARCÍA (*),
JESÒS MARTEL (***), RICARDO MARQUÉS (***),
MARIO SOROLLA (**)

SUMMARY. – *In this work, the design and optimization of planar microwave filters based on the concept of artificially fabricated materials (metamaterials) is envisaged. Specifically, the designed structures are based on a key particle (i.e., the split rings resonator -SRRs), that possesses unique electromagnetic properties. Namely, when arranged in an effective medium, SRRs behave as a magnetic plasma for properly polarized radiation, with negative valued permeability in the vicinity of resonance. Thanks to this property, by properly etching SRRs in CPWs or microstrip transmission media, it will be shown the possibility to achieve stop band and band pass structures with a high level of frequency selectivity and very low in-band losses.*

1. Introduction

The miniaturization of planar microwave and millimeter wave circuits is a key issue for the full integration and/or compactness of communication transceiver front-ends. In these subsystems, present solutions either use off-chip mechanically resonant components such as crystals and SAW devices (with an eye towards achieving high-Q factors), or waveguide and transmission line based filters, where volume and cost are the bottleneck against front-end optimization. In this work we introduce a new approach, based

(*) Departament d'Enginyeria Electrònica, Universitat Autònoma de Barcelona, 08193 Bellaterra (Barcelona). Spain.
(**) Departamento de Ingeniería Eléctrica y Electrónica. Universidad Pública de Navarra. 31006 Pamplona (Navarra). Spain.
(***) Departamento de Electrónica y Eletromagnetismo. Facultad de Física, Universidad de Sevilla. Av. Reina Mercedes s/n. 41012 Sevilla (Spain).

on the concept of metamaterials, for the design of miniature planar filters with potential application in future communication transceivers. The approach make use of key constituent particles which are planar and electrically very small, i.e. the split ring resonators (SRRs). Apart from the high-Q factor at microwave frequencies, the most relevant characteristics of the cited resonators (proposed some time ago by Pendry (1)) are their dimensions, which potentially can be more than one order of magnitude smaller than free space wavelength at the resonant frequency. The typical topology for a SRR is depicted in Fig. 1 (rectangular or other polygon geometries are also possible).
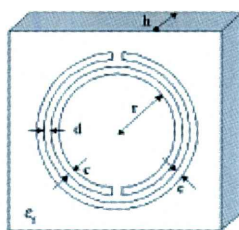
FIG. 1

Topology of the SRRs and relevant dimensions

Essentially, a SRRs consists on a pair of concentric metal rings with splits etched in opposite sides. At resonance, when these rings are excited by a time varying magnetic field with a non-negligible component applied parallel to the ring axis, current loops are generated in the rings that are closed through the distributed capacitance between concentric rings (2). This means that SRRs behave as an LC tank externally driven by a magnetic field. It has been previously demonstrated that a periodic array of SRRs illuminated by a properly polarized radiation (i.e. with the magnetic field vector in the direction of the ring axis) inhibits signal propagation in the vicinity of resonance (3). This result has been interpreted as due to the properties of the structure, that can be considered as an effective medium provided signal wavelength is very high compared to SRRs diameters and relevant dimensions (period). Specifically, SRRs make the structure to behave as a magnetic plasma, with negative valued permeability in a narrow band above resonance. Below the resonant frequency, the effective permeability of the medium is highly positive and this explains the well known property that signal propagation is forbidden in the vicinity of the resonant frequency of SRRs. It has been also demonstrated that by combining these SRRs with metal posts, the stop band behavior can be switched to a band pass characteristic. To this end, the posts should provide a negative effective permittivity to the medium up to a frequency (plasma frequency) located above the resonant frequency of SRRs. By a proper design of the

posts and electric field polarized along posts axis, this condition is achieved and the structure exhibits a narrow band with backward (left-handed) wave propagation above the resonant frequency of the rings.

In this work, it is demonstrated that these ideas can be translated to planar implementations with the possibility to design high performance filters with miniature dimensions. As will be shown, since SRRs are high-Q particles, few stages suffice to obtain highly selective structures.

2. Design of SRRs stop and band pass filters and results

Stop band filters have been designed and fabricated in CPW technology by etching SRRs in the back substrate side, underneath the slots. By this means, the orientation of the rings is adequate to achieve high magnetic coupling between line and rings, and signal propagation is expected to be inhibited in the vicinity of SRRs resonance. Figure 2 shows the layout of a fabricated stop band filter at C band. Ring dimensions (see Fig. 1) necessary to obtain a certain resonant frequency can be estimated from the model described in (4), although tuning is required since the presence of the strip and ground plane metals on the opposite substrate side is not accounted for in such model. For the circuit of Fig. 2, ring dimensions have been set to $c=d=0.2$ mm and $r=1.3$ mm, the period of the structure is $l=5$ mm and strip and slot widths ($W=5.4$ mm and $G=0.3$ mm) have been determined to achieve a 50 Ω host line (the parameters of the *Arlon 250-LX-0193-43-11* substrate, i.e., dielectric constant $\varepsilon_r=2.43$, thickness $h=0.49$ mm, have been considered). The frequency response of the structure is also depicted in Fig. 2. As expected, a narrow rejected band centered at the resonant frequency of the rings ($f_0=7.7$GHz) appears, with a rejection level near 40 dBs and negligible insertion losses in the allowed band. It has been also demonstrated (results not shown) that the stop band can be widened by tuning adjacent rings at slightly different frequencies. Remarkable in Fig. 2 is the significant rejection level achieved with only four SRR stages. Due to the small dimensions, these structures are of interest for the elimination of frequency parasitics or undesired frequencies in planar microwave circuits.

We have also designed band pass filters by using SRRs inductively coupled to CPW structures. To this end, electric shorts between signal and ground at the positions of the rings have been added to the layout of Fig. 2. The resulting structure and its frequency response is depicted in Fig. 3. The metal wires (width $w=0.2$mm) make the structure to behave as a microwave plasma up to a frequency beyond f_0, and an allowed band starting at f_0 arises, where signal propagation is negative (left handed filter). Frequency selectivity is significant and the level of losses acceptable. This latter aspect has been optimized by using a bi-layer SRR structure, where SRRs have been etched on both substrate sides of a buried CPW (Fig. 4).
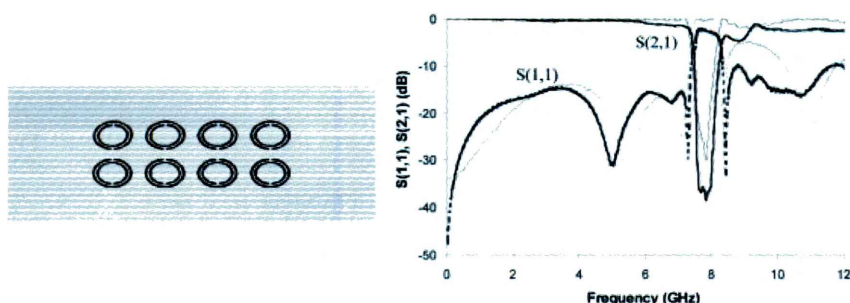
FIG. 2

Layout of the 4-stage SRR-CPW stop band filter drawn to scale (actual device length is 3.5cm) and frequency response. Simulations are depicted in thin line while measurements are depicted in bold line.
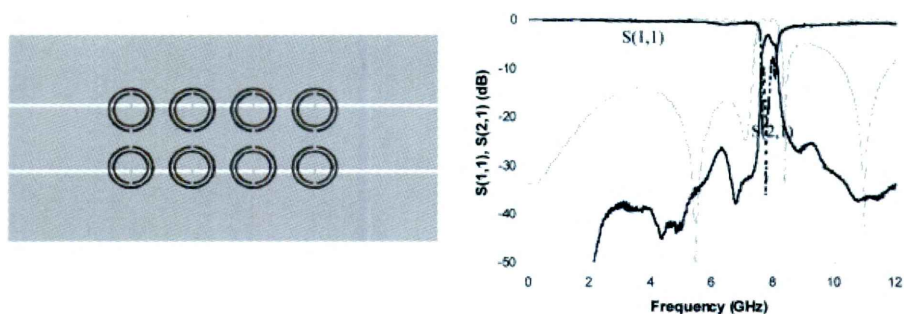
FIG. 3

Layout of the SRR based left handed CPW structure drawn to scale (actual device length is 3.5 cm) and frequency response. Simulations are depicted in thin line while measurements are depicted in bold line.

It is worth mentioning the small dimensions of the circuit of Fig. 4. The active region of the device, namely excluding access lines, is approximately one fifth signal wavelength at the central frequency of the allowed band. These are very small dimensions in comparison to those that result from conventional distributed approaches.

Finally, we would like to show the layout and frequency response of a microstrip band pass filter with open SRRs (OSRRs) cascaded with the central strip in a series configuration (Fig. 5). In terms of in-band losses this approach is very promising while dimensions are still very small (28.5mm in length, excluding access lines). With this design, bandwidth can be easily controlled by varying the distance between adjacent rings.
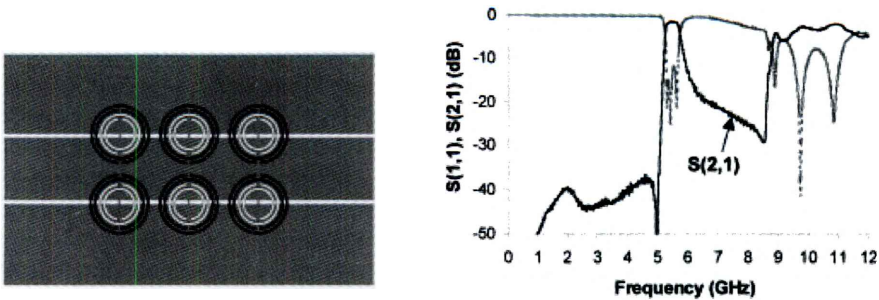
FIG. 4

Layout of the bi-layer SRR left handed CPW structure drawn to scale and frequency response.
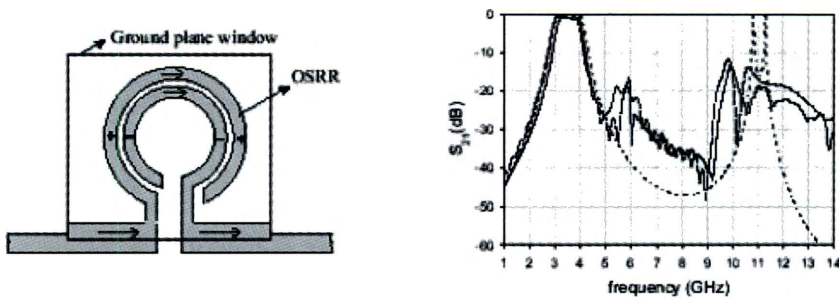
FIG. 5

Elemental cell of the OSRR 3rd-order filter, measured frequency response (solid line), electromagnetically simulated (dashed line) and circuit simulated frequency response (dot and dashed line).

3. Conclusion

In conclusion, the potentiality of SRRs for the design of planar microwave filters with reduced dimensions has been pointed out by providing several illustrative examples of fabricated prototypes. Impact and application of these structures on future communication transceivers is expected. These results are patent pending.

Acknowledgement

REFERENCES

(1) J.B. PENDRY, A.J. HOLDEN, D.J. ROBBINS, W.J. STEWART, *Magnetism from conductors and enhanced nonlinear phenomena*, IEEE Trans. Microw. Theory Tech., **47**, 2075-2084, 1999.

(2) R. MARQUÉS, F. MEDINA, F. MESA, J MARTEL, *On the electromagnetic modeling of left-handed metamaterials*, in: *Advances in electromagnetics of complex media and metamaterials,* edited by S. Zouhdi, A. Shivola and M. Arsalane (Kluwer, Dordretch, 2002), p. 123.

(3) D.R. SMITH, W.J. PADILLA, D.C. VIER, S.C. NEMAT-NASSER, S. SCHULTZ, *Composite medium with simultaneously negative permeability and permittivity*, Phys. Rev. Lett., **84**, 4184-4187, 2000.

(4) R. MARQUÉS, F. MESA, J. MARTEL, F. MEDINA, *Comparative analysis of edge- and broadside-coupled split ring resonators for metamaterial design – theory and experiments*, IEEE Trans. Antennas and Propagat., **51**, 2572-2581, 2003.

Artificial metamaterial surfaces and applications

JOHN C. VARDAXOGLOU (*), ALEXANDROS P. FERESIDIS (*), GEORGE GOUSSETIS (*)

SUMMARY. – *Novel designs of artificial metamaterial surfaces are presented here and an application is proposed. Miniaturised metamaterial surfaces are produced using single layer arrays with complex element geometries. Further miniaturisation is achieved by close coupling two layers. The application of a compact electromagnetic band gap surface to the performance enhancement of a mobile telephone antenna is presented.*

1. Introduction

The term "metamaterials" refers to a large variety of complex structures that possess electromagnetic properties not readily available in nature. At microwave frequencies, metamaterials typically consist of periodic arrays of dielectric and/or conducting elements. Passive metallic arrays have been used over the last few decades as Frequency Selective Surfaces with numerous applications in antennas for fixed and mobile communication systems (1). During the last few years the Electromagnetic Band Gap (EBG) properties of passive metallodielectric arrays have been studied (2). Metallic EBG (MEBG) structures have been used for the performance enhancement of mictrostrip antennas and circuits. Furthermore, metallic arrays printed on a grounded dielectric substrate have been presented as artificial magnetic conductors (AMCs). Such surfaces fully reflect incident waves with a near zero degrees reflection phase. Another property of complex materials that has attracted particular attention recently is left-handed (LH) propagation. According to this property, waves propagate with the phase and group velocity in opposite directions.

(*) Department of Electronic and Electrical Engineering, Loughborough University, Loughborough, LE11 3TU, UK.

Miniaturisation of microwave components and antennas has become increasingly important in recent years, due to the requirement for high level integration into compact light-weight systems. With respect to metamaterials, the importance of miniaturisation also reflects the requirement of an equivalent effective medium description. This is only valid when the unit cell of the array is considerably smaller than the wavelength. Novel miniaturized metamaterials structures are presented here. Closely coupled double layer surfaces have resulted in significant size reduction of EBG arrays (3). Furthermore, complex elements have been investigated and utilized to implement miniaturized surfaces (4). The application of compact EBG surfaces to the performance enhancement of a mobile handset antenna has been studied. An EBG surface conformal to a slim handset isolates the antenna from the human hand, reduces the antenna detuning and improves the efficiency.

2. Complex elements

In this section we investigate complex element geometries and their effect on the reduction of the physical size of EBG structures. Left-handed (LH) propagation, where group and phase velocities run in opposite directions (5), is also demonstrated. The study starts with 1D elements (dipoles) and 2D symmetrical elements are subsequently investigated. Fig. 1 shows the TE dispersion diagram for the dipole (15.5mm by 0.5mm) array on grounded dielectric with rectangular unit cell dimensions 16mm by 5mm. On the same Figure the dispersion relation for the end-loaded dipole array and the periodically loaded dipole array for identical lattice topologies are also presented.
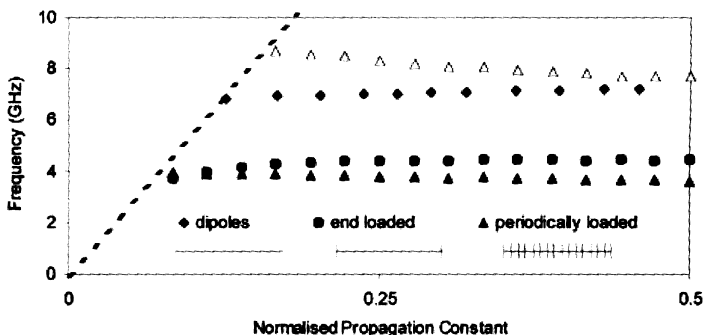
FIG. 1

TE Dispersion relation for the GX direction of propagation for dipole, end loaded dipole and periodically loaded dipole array on grounded dielectric substrate. In mm dipole 15.5×0.5, unit cell 5.0×16.0

As shown, the 1st TE cutoff for the unloaded case is more than 7GHz while it drops to 4GHz and below for the end-loaded and periodically loaded respectively, which corresponds to 60% size reduction. Furthermore, it is instructive to see how the slope of the dispersion relation for the first resonant modes reduces as we move to the periodically loaded dipole. In fact for the periodically loaded dipole the frequency derivative with respect to propagation constant is negative. This is an indication for the existence of left-handed surface wave TE modes, as phase velocity of bounded TE surface waves runs now opposite to the group velocity (5). The left-handed propagation bandwidth is 10%.
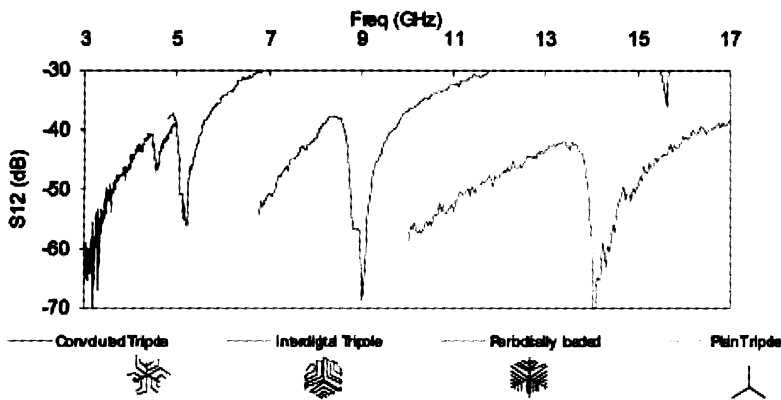
FIG. 2

Measured EBG performance for TE waves for periodically loaded, interdigital and convoluted tripole

Following thorough investigation on dipole designs, three mechanisms for the miniaturisation of the resonant elements based on 2D symmetrical tripole geometries were considered and compared. The EBG properties of periodic loading, interdigital elements and convoluted elements for grounded arrays were assessed experimentally. The unit cell is now hexagonal with diameter 6.2mm. Fig. 2 shows the measured TE surface wave bandgaps for the arrays with elements shown as insets. The EBG response of the plain tripole array in the same lattice is also shown for comparison. The convoluted tripoles are more compact (~70% miniaturisation) whereas the interdigital tripoles have a better bandwidth (~20% fractional bandwidth), in accordance with the findings of the 1D case.

3. Closely coupled MEBGs

The concept of Closely Coupled MEBG (CCMEBG) surfaces can be used to achieve miniaturisation of MEBG arrays (3). The design is based on a double layer array configuration with the two layers positioned in close proximity and shifted with respect to each other in order to produce maximum element coupling. The small spacing and overlapping of the elements of the two layers increases the capacitance values in an equivalent circuit representation of the structure, which results in significant lowering of the band gap frequency. Tripole arrays have been used as 2D elements with good symmetry properties. When a tripole array is arranged on a hexagonal lattice, the irreducible Brillouin zone of the reciprocal lattice is small (Fig. 3). This suggests that common band gap performance could be achieved for any direction of surface wave propagation on the plane of the array. We have used a tripole array geometry with the following dimensions: $L = 5$ mm, $W = 0.5$ mm, and periodicity $D = 12$ mm (Fig. 3). A CCMEBG array design has been implemented using two tripole arrays printed on either side of a 0.1 mm thin dielectric layer with dielectric constant 3 and supported on a dielectric slab of thickness $S_{sub} = 1.13$ mm and permittivity 2.2. The tripole CCMEBG configuration is shown in Fig. 1a.
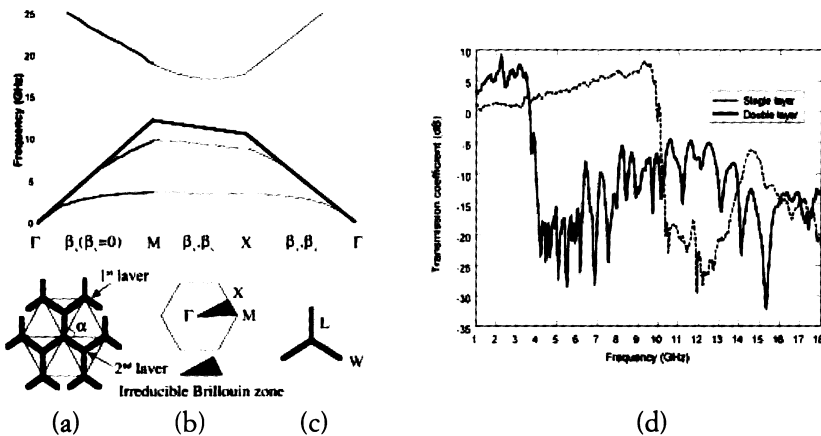
FIG. 3

Dispersion diagram of tripole CCMEBG array; (a) Direct lattice, (b) Reciprocal lattice and its irreducible Brillouin zone, (c) Tripole (d) Measured surface wave transmission response.

The dispersion diagram showing the first few TE modes of the double layer tripole CCMEBG is shown in Fig. 3. The simulation results show a TE band gap of 2.3 GHz, starting from 3.7 GHz. to 6 GHz. The next

band gap starts at 10 GHz extending to 17.4 GHz. The tripole CCMEBG surface has been fabricated and measured. Surface wave measurements have been obtained using a pair of wideband antipodal Vivaldi antennas printed on either side of the array. The measured transmission response is shown in Fig. 3(d). The measured surface wave response of the single-layer tripole array of same dimensions is also shown. A reduction of the resonant frequency from 10GHz to less than 4GHz has been achieved. This corresponds to a miniaturisation factor of more than 2.5.

4. Reduction of Handset Antenna Detuning

The de-tuning effect of the hand on the performance of a handset antenna is initially demonstrated. A permittivity of 40 has been used to model the hand. Fig. 4(a) shows the return loss of a handset antenna designed at 2.64 GHz centre frequency. For the simulation we have used handset dimensions 90×20×25 mm with a permittivity of 10, while we have omitted other circuitry of the handset for simplicity. A simple wire model of a dipole has been used as the antenna embedded in the handset case. The return loss of the antenna when a volume simulating the hand holds the handset is also shown in Fig. 4(a). We can clearly see that the antenna now resonates at 2.51 GHz, as an effect of the hand. The relative detuning of the antenna due to the hand is approximately 5.2%.

We now introduce a miniaturised tripole CCMEBG structure printed on the case of the handset as a means of suppressing the surface waves. The CCMEBG has been designed using the tripole dimensions of the previous section. However, the separation distance between the two arrays has been reduced to 0.05 mm, so that the surface wave bandgap covers the antenna operating frequency. Upon introducing the MEBG, we needed to optimise the antenna design to achieve good matching. This was achieved by means of altering its input impedance. Fig. 4(b) shows the return loss for the handset with the CCMEBG now embedded. The same figure shows the antenna return loss with a similar volume simulating a hand around it. As can be seen, the de-tuning is now significantly reduced at 0.8%. This result suggests that the major coupling of the antenna with the user's hand occurs due to the surface waves and demonstrates the benefit of embedding the MEBG in the handset's case.

(a)   (b)
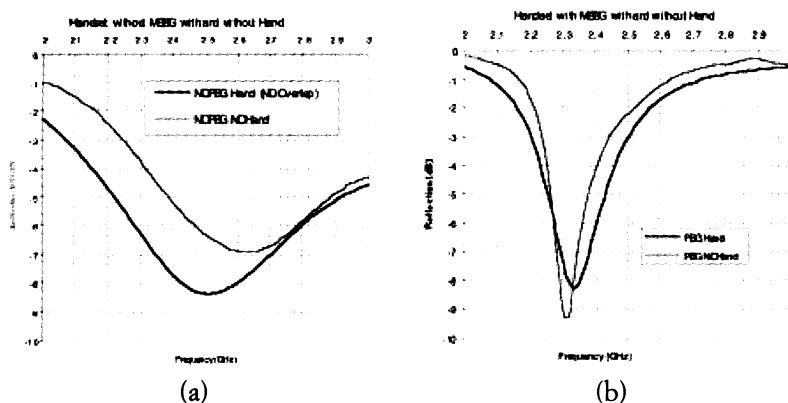
FIG. 4

(a) Return loss of handset antenna without MEBG
(b) Return loss of handset antenna with MEBG

REFERENCES

(1) J.C. VARDAXOGLOU, *Frequency Selective Surfaces: Analysis and Design* (Somerset, UK, Res. Studies Press; New York, Wiley, 1997)

(2) P. DE MAAGT, R. GONZALO, J.C. VARDAXOGLOU, J.M. BARACCO, *Photonic Bandgap Antennas and Components for Microwave and (Sub)millimetre wave Applications*, Special issue on *Metamaterials*, IEEE Trans. on Antennas and Propagation, **51** (10), 2667-2677, Oct. 2003

(3) A.P. FERESIDIS, G. APOSTOLOPOULOS, N. SERFAS, J.C. VARDAXOGLOU, *Closely Coupled Metallodielectric Electromagnetic Band Gap (CCMEBG) Structures Formed By Double Layer Dipole and Tripole Arrays,"* IEEE Trans. Antennas and Propagation, to appear

(4) G. GOUSSETIS, A.P. FERESIDIS, J.C. VARDAXOGLOU, *Periodically loaded 1-D Metallodielectric Electromagnetic Band Gap Structures*, submitted to IEE Proc Microwave Antennas Propagat.

(5) A. GRBIC, G. ELEFTHERIADES, *Dispersion Analysis of a Microstrip-Based Negative Refractive Index Periodic Structure*, IEEE Microwave and Wireless Components Letters, **13** (4), 155- 157, April 2003

Efficient modeling of planar Electromagnetic Band-Gap (EBG) structures by the MoM/BI-RME method

MAURIZIO BOZZI (*), SIMONE GERMANI (*),
LUCA PERREGRINI (*)

SUMMARY. – *This paper presents an efficient method for the modelling of metallo-dielectric planar periodic structures, operating as electromagnetic band-gap (EBG) structures. These structures are characterized through the phase of the reflection coefficient under plane wave illumination, and the dispersion diagram of the modes propagating along the periodic structure. In our approach, the electromagnetic problem is formulated in terms of an integral equation, which is solved by using the Method of Moments (MoM) with entire domain basis functions. The basis functions are calculated numerically by using the Boundary Integral-Resonant Mode Expansion (BI-RME) method. In the calculation of the dispersion diagram, a novel technique has been developed for the solution of the homogeneous matrix problem arising from the application of the integral equation method: this technique, based on the tracking of the matrix eigenvalues in the complex plane, proved to be more efficient and reliable than standard techniques usually adopted to solve this problem. The classical Uniplanar Compact Photonic Band-Gap (UC-PBG) structure is used to validate the proposed approach.*

1. Introduction

Metallo-dielectric periodic structures are widely used for improving the electromagnetic performance of printed antennas (1,2). They consist of metal patches patterned on a grounded dielectric substrate (Fig. 1), possibly connected to the ground plane through metal pins. These structures can exhibit two kinds of performance. On the one hand, they can be used to prevent the propagation of substrate waves in a frequency band (electro-

(*) Dept. of Electronics, University of Pavia, Via Ferrata, 1, I 27100 Pavia, Italy.

magnetic band-gap, EBG). On the other hand, they can behave as a perfect magnetic conductor (PMC), reflecting an incident plane wave without phase reversal.

In this paper, we present a novel approach for the efficient characterization of planar metallo-dielectric EBG structures (Fig. 1). We discuss the calculation of the phase of the reflection coefficient under plane-wave illumination, and the determination of the dispersion diagram (DD) of the guided modes. Instead of searching the zeros of the determinant of the MoM matrix for the determination of the dispersion diagram, our approach is based on the tracking of the eigenvalue path in the complex plane. This approach is more reliable and reduces dramatically the computing time.

(a)   (b)
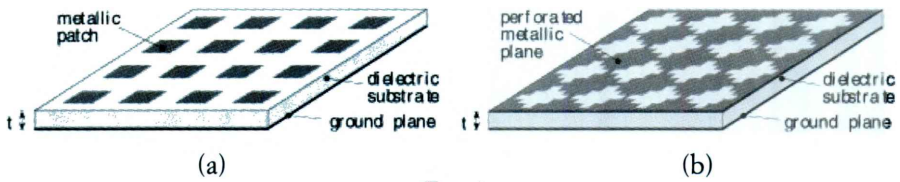
FIG. 1

Uniplanar EBG structures consisting of an array of metal patches on a grounded dielectric substrate: *a*) isolated patches; *b*) interconnected patches.

2. Analysis of planar EBG structures

The full-wave analysis of planar EBG structures can be efficiently performed by using an integral equation method. In the case of isolated metal patches (Fig. 1*a*), the unknown quantity is usually the electric current density on the patches, whereas in the case of interconnected patches (Fig. 1*b*) the unknown quantity is usually the magnetic current density on the holes.

In the calculation of the reflection coefficient, the formulation of the problem is similar to the one adopted in the determination of the scattering from frequency selective surfaces, and can be efficiently performed by using the MoM/BI-RME method (3, 4).

In the calculation of the DD, the integral equation is obtained by imposing the proper boundary condition to the fields on the surface S of the patch/hole, considering the periodicity condition corresponding to a value $\boldsymbol{\beta}=\beta_x\boldsymbol{x}+\beta_y\boldsymbol{y}$ of the propagation vector in the irreducible Brillouin zone (1). At a given frequency f and propagation constant $\boldsymbol{\beta}$, the integral equation is solved by using the Method of Moment (MoM) in the Galerkin form, thus obtaining the following homogeneous matrix equation:

[1] $A(f,\boldsymbol{\beta})\,X=0$

When using the MoM/BI-RME method, entire-domain basis functions are used to represent the unknown current density (3, 4), thus leading to a small matrix A. The electromagnetic problem is satisfied only if the matrix equation [1] presents non-trivial solutions, *i.e.*, if the determinant of A vanishes. Therefore, the calculation of the DD is based on an iterative procedure, with a double loop in frequency and propagation constant: the pairs $\{f, \beta\}$ which satisfy [1] determine a point in the DD.

The most common strategy to solve [1] is based on the calculation of the frequency points where the determinant of A vanishes. Hoverer, this approach requires a fine frequency scan, and, in many cases, the selection of zeros needs human intervention.

Conversely, the proposed approach is based on the tracking of the path of the eigenvalues of A in the complex plane when varying the frequency. By setting β and scanning the frequency range $f_{min} \div f_{max}$ with a given frequency step Δf, this method permits to identify those frequencies where one (or more) eigenvalues cross the origin of the complex plane. For a pair of frequencies f_1 and $f_2 = f_1 + \Delta f$, eigenvalues Λ and eigenvectors V of A are calculated

$$[2] \qquad A(f_1, \beta) = V_1^{T^*} \Lambda_1 V_1 \qquad A(f_2, \beta) = V_2^{T^*} \Lambda_2 V_2$$

where the eigenvectors matrices are normalized according to $V^T V^* = I$ (identity matrix). The correspondence between eigenvalues at f_1 and f_2 is obtained by using the matrix

$$[3] \qquad P = V_1^T V_2^*$$

which exploits the correlation between the eigenvectors. In fact, if Δf is small enough, the entries of P are close to unity for correspondent eigenvalues, and close to zero otherwise. In such a way, the path of each eigenvalue can be tracked, and its zero-crossing can be detected. The frequency corresponding to the zero-crossing is then estimated by a linear interpolation.

Moreover, the correlation of the eigenvectors can be also exploited to find a link between the points on the DD, calculated at different values of β, thus permitting an automatic drawing of the curves of the DD.

3. Numerical Results

The classical UC-PBG structure (2, 5) has been used for validating the proposed method (Fig. 2*a*). The DD was calculated by considering 30 basis functions for representing the unknown magnetic current density on the holes, and 1200 Floquet modes. The calculation was performed in 30

points on the boundary of the irreducible Brillouin zone, and the frequency step adopted in the zero-searching was $\Delta f = 1$ GHz (thus resulting in a total of 900 analyses). The DD obtained with our method is shown in Fig. 2*b* and compares very well with data reported in (2). The overall computing time for obtaining the whole dispersion diagram was about 18 min on a PC Pentium IV @ 2.4 GHz. The phase of the reflection coefficient in the case of normal incidence (30 basis functions and 1200 Floquet modes) is shown in Fig. 2*c*. The reference plane was set to the top side of the dielectric layer, and this required to shift the measured phase reported in (5), where the reference plane was set to the ground plane. Also in this case, a very good agreement is found with the measurement results. The overall computing time for calculating the reflection coefficient in 70 frequency points was 9 sec.

To better appreciate the robustness of the proposed method, we applied different methods for the calculation of the mode frequencies in the critical M-branch ($\beta_x = \beta_y = \pi/a$) of the dispersion diagram, where three modes are almost degenerate. When using the standard approach, based on the determination of the zeros of the determinant of A, a frequency step of 10 MHz is required for identifying the zeros, in particular those corresponding to the 4th and 5th modes (see Fig. 2*d*). With regard to the technique based on the tracking of the eigenvalues, it is preliminary observed that the eigenvalues are pure imaginary in this branch, since A is an anti-hermitian matrix below the light line. Fig. 2*e* shows the imaginary part of the first eigenvalues versus the frequency. It is observed that the path of the eigenvalues can be easily identified by using a frequency step $\Delta f = 1$ GHz, even when their frequencies are almost coincident. Moreover, Fig. 2*f* shows the relative error in the calculation of the mode frequencies in the M-branch of the dispersion diagram, when varying the frequency step Δf. The reference value used for calculating the relative error is taken at $\Delta f = 0.1$ GHz. The first six modes are found even with $\Delta f = 4$ GHz, and an accuracy better than 0.5% in the determination of the frequencies is obtained with $\Delta f = 1$ GHz.

4. Conclusions

This paper presented a novel method for the efficient, reliable, and fully automated calculation of the dispersion diagram of planar electromagnetic bandgap structures. The novel technique based on the tracking of the eigenvalues in the complex plane takes advantage of some information on the correlation between the eigenvectors at different frequencies, which are not exploited in the classical direct search of the determinant zeros. This permits to detect and accurately determine the zeros, even with a large frequency step.

Furthermore, the information on the correlation of the eigenvectors

also permits to interconnect the points of the dispersion diagram at different values of the propagation constant, thus automatically obtaining the curves of the dispersion diagram.

The use of the MoM/BI-RME method permits to reduce the dimension of the matrix problems, thus improving the numerical efficiency of the method.

(a)

(b)

(c)

(d)

(e)

(f)
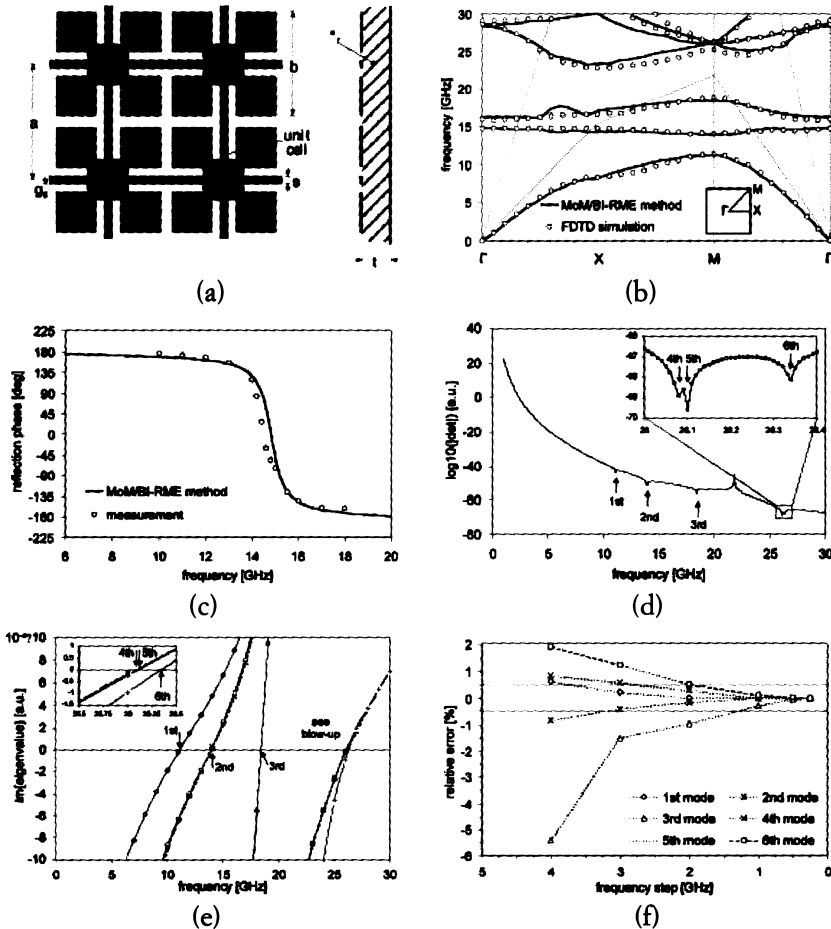
FIG. 2

Analysis of the UC-PBG structure (2,5): *a*) geometry of the unit cell (dimensions in mm: $a = 3.048$, $b = 2.794$, $g = s = 0.254$, $h = 0.6985$, $t = 0.635$; $\varepsilon_r = 10.2$); *b*) dispersion diagram; *c*) phase of the reflection coefficient; *d*) determinant of A in the M-branch ($\Delta f = 10$ MHz); *e*) path of some eigenvalues versus frequency in the M-branch ($\Delta f = 1$ GHz); *f*) relative error in the calculation of the DD vs. Δf (M-branch).

REFERENCES

(1) D. SIEVENPIPER et al., *High-Impedance Electromagnetic Surfaces with a Forbidden Frequency Band*, IEEE Trans. on Microwave Theory & Tech., **47**, 2059-2074, 1999.

(2) F.R. YANG et al., *Planar PBG Structures: Basic Properties and Applications*, IEICE Trans. Electron., **E83-C**, 687-696, 2000.

(3) M. BOZZI, L. PERREGRINI, J. WEINZIERL, C. WINNEWISSER, *Efficient Analysis of Quasi-Optical Filters by a Hybrid MoM/BI-RME Method*, IEEE Trans. on Antennas & Propagat., **49**, 1054-1064, 2001.

(4) M. BOZZI, L. PERREGRINI, *Analysis of Multilayered Printed Frequency Selective Surfaces by the MoM/BI-RME Method*, IEEE Trans. on Antennas & Propagat., **51**, 2830-2836, 2003.

(5) F.R. YANG et al., *A Novel TEM Waveguide Using Uniplanar Compact Photonic-Bandgap (UC-PBG) Structure*, IEEE Trans. on Microwave Theory & Tech., **47**, 2092-2098, 1999.

3D considerations on light propagation in planar photonic crystal waveguides

STEFANO BOSCOLO (*), MICHELE MIDRIO (*)

Last year, at the first edition of the Workshop on metamaterials and special materials for electromagnetic applications and telecommunications that was held in Firenze, our research group presented a novel way of studying light propagation in photonic crystals (PhC) waveguides. This was based on an equivalence between PhC guides and conventional transmission lines.

The model and the examples we considered mainly referred to 2D photonic crystal waveguides, either realized by etching infinitely long air holes in an high index dielectric substrate, or by placing infinitely long high-index dielectric pillars in air.

Since the last year, we have developed an accurate and fast numerical tool that permitted us to extend our analysis from the 2D case to the full 3D one. This way, we were able to study more realistic devices, where finite-height holes or pillars are embedded in a proper substrate. We analyzed a wide set of effects that take place in real photonic crystal waveguides and that may have a major role when realizing integrated optical devices for telecommunication systems. The most interesting among these are polarization effects, and coupling of guided waves to the continnum of radiating modes, which leads to out-of-plane scattering losses.

At the Workshop, we will first illustrate the basic principle of the numerical technique we use to study 3D photonic crystal waveguides. Later on, we will discuss the role of the effects we mentioned above on the performance of realistic devices, and we will show which strategies may be considered to mitigate their impact.

(*) Dipartimento di Ingegneria Elettrica Gestionale e Meccanica, Università degli Studi di Udine, Viale delle Scienze 208, 33100 Udine, Italy.

Interaction between electromagnetic waves and metamaterials:
The case of PEC cylinders coated by multiple elliptic layers

SALVATORE CAORSI (*), MATTEO PASTORINO (**),
MIRCO RAFFETTO (**), ANDREA RANDAZZO (**)

SUMMARY. – *The interaction between plane waves and multilayer elliptic cylinders made of metamaterials is considered. An analytical solution is proposed, which extends to double-negative metamaterials an efficient recursive procedure for double-positive media. Two cases are considered: multilayer dielectric cylinders and perfectly conducting cylinders with a multilayer coating made up of metamaterials. Numerical results and comparisons are provided concerning both the internal field and the scattering cross section per unit length, allowing a significant assessment on the scattering properties of metamaterials.*

1. Introduction

In recent years, one of the most challenging area of electromagnetics has been represented by the study of metamaterials. These media exhibit several interesting features that cannot be found in common matters. Their theoretical properties were first studied by Veselago in 1960 (1), which considered materials characterized by negative values of both dielectric permittivity and magnetic permeability. This assumption leads to some "strange" effects, such as a negative refraction index and an anti-parallelism between Poynting vector and phase velocity (1). Since these media could not be produced with the technology of such years, their study was abandoned until '90s, when Shelby, Smith, and Schultz were able to create them by embedding arrays of small metallic wires and split ring resonators (2) in

(*) Dept. of Electronics, University of Pavia, Via Ferrata 1, I 27100 Pavia, Italy.
(**) Dept. of Biophysical and Electronic Engineering, University of Genoa, Via Opera Pia 11A, I 16145 Genova, Italy.

common media.

Nowadays, the class of metamaterials is composed by various elements, classified with different names. Common examples are plasmas, double negative materials (DNG), single negative materials (ε-negative and μ-negative) and chiral media.

Recently, there has been a growing interest in proposing the application of these material to design a wide number of components and apparatuses, such as absorbers, lens, microwave components and antennas (a lot of references can be found in the papers included in (3)).

In parallel to the development of approaches devoted to applying metamaterials toward practical realizations, there is the need for further evaluating the effects of this kind of materials on the propagation and scattering of electromagnetic waves.

To this end, the present paper proposes an analytical solution to the electromagnetic scattering by: 1) an infinite cylinder whose cross section is constituted by confocal dielectric elliptic layers possibly made up of left-handed metamaterials and 2) a perfectly conducting (PEC) elliptic cylinder multi-coated by dielectric layers of standard media or metamaterials.

A TM plane wave illumination is always considered. The solutions, which are based on the field expansion in Mathieu functions, which are the eigenfunctions of the elliptic cylinder, extend the techniques previously proposed in (4)(5).

The results presented demonstrate the unusual properties of metamaterials, mainly in terms of the radar cross section per unit length. The proposed results are validated by verifying that they tend to coincide with those obtained in the case of a circular cylinder and by comparing them with those numerically obtained by a hybrid MOM-FEM electromagnetic simulator.

Beside the practical interest related to the study of scattering properties of coating materials, the multilayer elliptic cylinder also represents an important canonical object. First of all, it constitutes quite a complex scatterer since it is inhomogeneous and its cross section is relatively "irregular". Thus this solution can be used as a test case for computational procedures (e. g., numerical methods involving spatial discretizations). Moreover, elliptic cylinders are used to approximately model several real structures, like aircraft fuselage and other cylindrical bodies.

The scattering by the single elliptic cylinder has been solved for the first time by Yee, who developed a series solution in terms of Mathieu functions. The scattering by elliptic cylinders have been also studied by other researchers, whereas the multilayer elliptic cylinder was considered a rather difficult case, since the sets of eigenfunctions in each layer are not orthogonal sets. However, a recursive procedure to deals with multilayer dielectric cylinders was proposed in (4) and extended in (5) to the case of PEC cylinders multiple coated.

The paper is organized as follows. In Section II the problem configuration is described and the mathematical formulation is very briefly outlined. In Section III some results are reported, allowing an assessment of the scattering properties of metamaterials when used as coating layers and an "exact" evaluation of the interaction between electromagnetic waves and dielectric cylinders of elliptic cross section possibly made up of inhomogeneous double-negative materials.

Finally, comparisons are provided as consistency checks for validating the analytical solution.

2. Mathematical formulation

Let us consider a dielectric cylinder made of N layers. The i-th layer is bounded by the elliptic cylinders $u = u_{i-1}$ and $u = u_i$, $i = 1, ..., N$. Two cases are assumed. In the first case, all layers are of dielectric materials, consequently $u_0 = 0$. In the second case, the innermost cylinder is a PEC cylinder and $u_0 = u_{\text{PEC}}$. The semi-major and semi-minor axes of the cylinder $u = u_i$ are denoted by a_i and b_i. The semi-focal distance is indicated by d. We consider time-harmonic fields and the time-dependence $\exp\{j\omega t\}$ is suppressed.

The dielectric permittivity and the magnetic permeability of the i-th layer are indicated by ε_i and μ_i, respectively, which are here assumed to be real parameters. If a layer is constituted by a double-negative dielectric, it has $\varepsilon_i < 0$ and $\mu_i < 0$ and the corresponding layer has a negative refraction index.

A uniform unit plane wave of transverse magnetic kind normally impinges to the cylinder with an angle α with respect to the x axis. In each layer, the electric and magnetic field vectors are given by:

[1] $$E^i(u,v) = E_z^i(u,v)\mathbf{z}$$

[2] $$\mathbf{H}^i(u,v) = H_u^i(u,v)\mathbf{u} + H_v^i(u,v)\mathbf{v} = -\frac{j}{\omega\mu_i h}\left[\mathbf{u}\frac{\partial}{\partial v} + \mathbf{v}\frac{\partial}{\partial u}\right]E_z^i(u,v)$$

where $h = d(\cosh^2 u - \cos^2 v)^{1/2}$. Following the Yeh's solution (4), the z-component of the electric field can be expressed in terms of Mathieu functions

[3] $$E_z^i = \sum_{m=0}^{\infty}\left[e_{m,1}^i Mc_m^{(1)}(q_i,u) + e_{m,2}^i Mc_m^{(2)}(q_i,u)\right]ce_m(q_i,v) +$$
$$\sum_{m=1}^{\infty}\left[o_{m,1}^i Ms_m^{(1)}(q_i,u) + o_{m,2}^i Ms_m^{(2)}(q_i,u)\right]se_m(q_i,v)$$

where $q_i = 0.25(k_i d)^2$, k_i being the wavenumber of the i-th layer. In the external $(N+1)$-th layer, the incident field can be expressed in terms of Mathieu functions, as follows

$$E_z^{inc} = E_0 e^{jk_{N+1}(x\cos\alpha + y\sin\alpha)} =$$

[4]
$$= 2\pi \sum_{m=0}^{\infty} \frac{j^m Mc_m^{(1)}(q_{N+1},u)ce_m(q_{N+1},v)ce_m(q_{N+1},\alpha)}{\int_0^{2\pi}\left[ce_m(q_{N+1},v)\right]^2 dv} +$$

$$+ 2\pi \sum_{m=0}^{\infty} \frac{j^m Ms_m^{(1)}(q_{N+1},u)se_m(q_{N+1},v)se_m(q_{N+1},\alpha)}{\int_0^{2\pi}\left[se_m(q_{N+1},v)\right]^2 dv}$$

Finally, in the same layer, the scattered electric field can be expressed in terms of the Mathieu functions of the fourth order

[5]
$$E_z^{scat} = \sum_{m=0}^{\infty}\left[e_m^{N+1}Mc_m^{(4)}(q_{N+1},u)\right]ce_m(q_{N+1},v) +$$

$$\sum_{m=1}^{\infty}\left[o_m^{N+1}Ms_m^{(4)}(q_{N+1},u)\right]se_m(q_{N+1},v)$$

In the case of a fully dielectric cross section, it results $e_{m,2}^1 = o_{m,2}^1 = 0$. If a PEC core is present, the boundary equation is

[6]
$$E_z^1 = 0 \quad \text{for} \quad u_0 = u_{PEC}$$

For the other layers, the boundary conditions concerning the continuity of the tangential component of the electric and magnetic field vectors (i.e., E_z^i and H_v^i) are applied. All the unknown expansion coefficients can be determined by the efficient recursive procedure described in (4), which involves a single matrix inversion, as in the Yeh's solution, independently of the number of layers. Finally, the radar cross section per unit length (echo width) can be obtained by the following equation

[7]
$$W = \lim_{\rho\to\infty} \frac{2\pi\rho\left|E_z^{scat}\right|^2}{\left|E_z^{inc}\right|^2}$$

where ρ denotes the distance from the coordinate center and, for $\rho\to\infty$, a simple expression is available in terms of the asymptotic formulas for the radial Mathieu functions (5).

3. Analytical results

Some results are reported in this section. In the first example, we consider the computation of the radar cross section per unit length in the case of a dielectric cylinder (Fig. 1), illuminated by a unit plane wave polarized along the z axis and propagating along the x axis ($\alpha = \pi$). The

dielectric parameters and the semi-major axes are given by $\varepsilon_1 = \varepsilon_0$, $\mu_1 = \mu_0$, $a_1 = 0.05$ m, and $a_2 = 0.10$ m, respectively, and for the double-positive case $\varepsilon_2 = 9.8\,\varepsilon_0$ and $\mu_2 = \mu_0$, while for the double-negative case $\varepsilon_2 = -9.8\,\varepsilon_0$ and $\mu_2 = -\mu_0$.
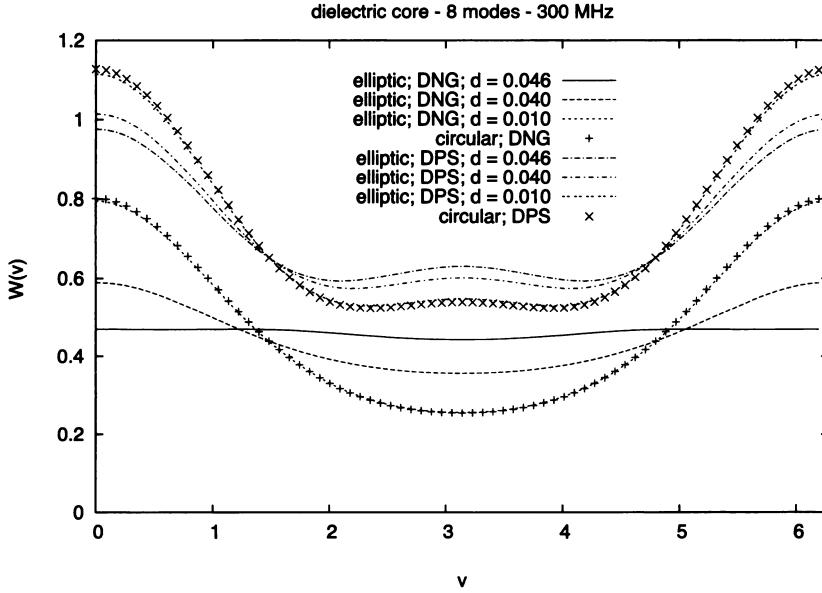
FIG. 1

Radar cross section per unit length for a two-layer elliptic cylinder.

The plots of Fig. 1 concern different values of the semi-focal distance, *d*, and are compared with the corresponding circular cylinder. It should be noted that, when $f = 1$ GHz, the analytical simulations have been proven to be in excellent agreement with the results published in (6) concerning a circular PEC cylinder coated with a DNG material.

In particular, results concerning a PEC cylinder coated by a dielectric layer are reported in Fig. 2 (DPS) and Fig. 3 (DNG). They provide the total electric field (amplitude) computed along the *x* axis, under the same illumination conditions of the previous examples. The dielectric parameters of the dielectric layer are the following: DPS: $\varepsilon = 9.8\,\varepsilon_0$, $\mu = \mu_0$; DNG: $\varepsilon = -9.8\,\varepsilon_0$, $\mu = -\mu_0$. The semi-major axis are given by $a_1 = 0.05$ m, and $a_2 = 0.10$ m. Fig. 2 and Fig. 3 provide a comparison with the results obtained by a hybrid MOM-FEM electromagnetic simulator. The consistency check is very successful.
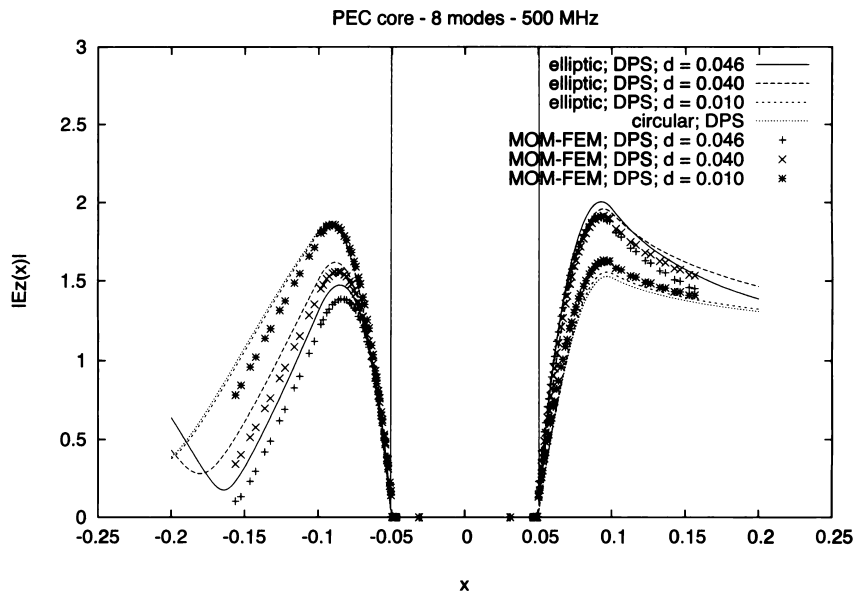
FIG. 2

Total electric field (amplitude). Coated PEC elliptic cylinder (DPS).
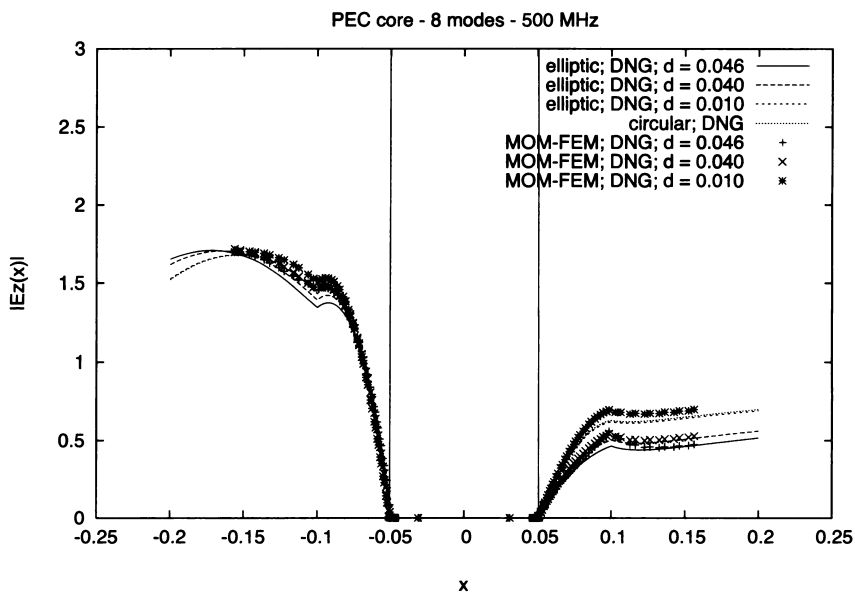
FIG. 3

Total electric field (amplitude). Coated PEC elliptic cylinder (DNG).

4. Conclusions

In this paper, the interaction between electromagnetic plane waves and multilayer elliptic cylinders made even of metamaterials has been considered. In particular, an efficient recursive procedure has been applied in order to evaluate the scattering properties in terms of fields and radar cross section. Coated PEC and dielectric cylinders have been considered. The proposed results clearly shown the impressive changes in the scattering properties due to the presence of metamaterials, which open new grounds in the development of devices and systems that are based on the electromagnetic interaction between waves and matter.

REFERENCES

(1) V.G. VESELAGO, *The electrodynamics of substances with simultaneously negative values of e and m*, Sov. Phys. Uspekhi, **10**, 509-514, 1968.

(2) R.A. SHELBY, D.R. SMITH, S. SCHULTZ, *Experimental verification of a negative index of refraction*, Science, **292**, 77-79, 2001.

(3) IEEE Transactions on Antennas and Propagation, Special Issue on Metamaterials, **51**, 2003.

(4) S. CAORSI, M. PASTORINO, M. RAFFETTO, *Electromagnetic scattering by a multilayer elliptic cyliner: series solution in terms of Mathieu functions*, IEEE Trans. Antennas Propagat., **45**, 926-935, 1997.

(5) S. Caorsi, M. Pastorino, M. Raffetto, *Scattering by a conducting elliptic cylinder with a multilayer dielectric coating*, Radio Sci., **32**, 2155-2166, 1997.

(6) C. LI, Z. SHEN, *Scattering by a conducting elliptic cylinder with a multilayer dielectric coating*, Progress in Electromagnetics Research, PIER, **42**, 91-105, 2003.

Modeling of three-dimensional Electromagnetic Band-Gap (EBG) structures

LARA PAJEWSKI (*), GIUSEPPE SCHETTINI (*)

SUMMARY. – *In this paper we present a three-dimensional Fourier modal method for the characterization of three-dimensional electromagnetic band-gap materials. The proposed technique, originally developed for the analysis of doubly-periodic finite-thickness gratings, is fast, accurate and versatile.*

1. Introduction

Electromagnetic band-gap (EBG) materials (1) are a subject of considerable interest for their important applications in the microwave region, such as high-quality resonant cavities, filters, waveguides, planar reflectors, antenna substrates.

In EBGs, periodic implants of material with a specific permittivity are embedded in a homogeneous background of different permittivity; the implants are comparable in size to the operation wavelength, and the involved materials are typically dielectrics. Such periodically structured electromagnetic media generally possess stop-bands: ranges of frequency in which light cannot propagate through the structure.

Electromagnetic crystals can be periodic in one, two and three directions. Only a three-dimensional (3D) periodicity can support an omnidiretional stop-band, but the electromagnetic characterization of 3D-EBGs is a heavy and difficult task.

In this paper we suggest that a fast and accurate modeling of the transmission and reflection properties of 3D-EBGs can be performed by exploiting a Fourier modal method (2) developed for the characterization of

(*) Applied Electronics Dept., "Roma Tre" University, v. Vasca Navale 84, 00146 Rome, Italy.

doubly-periodic diffractive optical elements. We implemented it with the correct Fourier factorization rules for discontinuous functions (3). For a numerically stable treatment of the evanescent waves at the boundaries we used the S-matrix algorithm (4) in the solution of the boundary problem. We present the basic theory and some preliminary results concerning binary three-dimensional surface-relief profiles. We discuss the computational requirements and the convergence of the method.

2. Theoretical approach

An EBG material can be considered as a stack of diffraction gratings separated by homogeneous layers, as pointed out in (5) where we presented an accurate, versatile, and fast modeling of two-dimensional (2D) finite-thickness (i.e., infinitely extending only in two dimensions) EBGs. Our approach exploited a full-wave method developed for the characterization of diffraction gratings. We have shown that, taking advantage of recent calculation techniques, the approach proposed in (5) can be employed to study, in a stable and rapidly convergent way, 2D electromagnetic crystals with rods having an arbitrary cross-section; the implanted rods can be arranged in whatever kind of lattice, and they can be made of isotropic or anisotropic dielectric, as well as metallic materials. Losses can be taken into account and EBGs with periodic defects can be characterized.

A 3D-EBG is actually a stack of doubly periodic gratings, also known in the literature as crossed or three-dimensional gratings. The electromagnetic analysis of such diffractive elements have been a heavy problem even with the use of up-to-date computers, leaving almost the whole resonance domain (grating period comparable in size to the operation wavelength) unexplored except for periods near the optical wavelength.

The most efficient prevailing rigorous technique for crossed gratings is the three-dimensional Fourier modal method (3DFMM) (2), which is based on the use of the waveguide modes of the structure, instead of numerically more laborious and less efficient approaches.

Consider the grating configuration illustrated in Fig. 1(a): two semi-infinite homogeneous half spaces with refractive indices n_1 and n_2 are separated by a doubly periodic layer located in $0 \leq z \leq h$. The periods of the grating are d_x and d_y in the x and y directions, respectively. A unit-amplitude monochromatic plane-wave impinges from the negative direction of the z-axis, with a wave vector k_0 and a polarization vector $\hat{u}$ shown in Fig. 1(b): we denote with θ the incidence angle, with φ the azimuthal angle, and with ψ the angle between the incidence plane and the polarization vector.

(a)

(b)
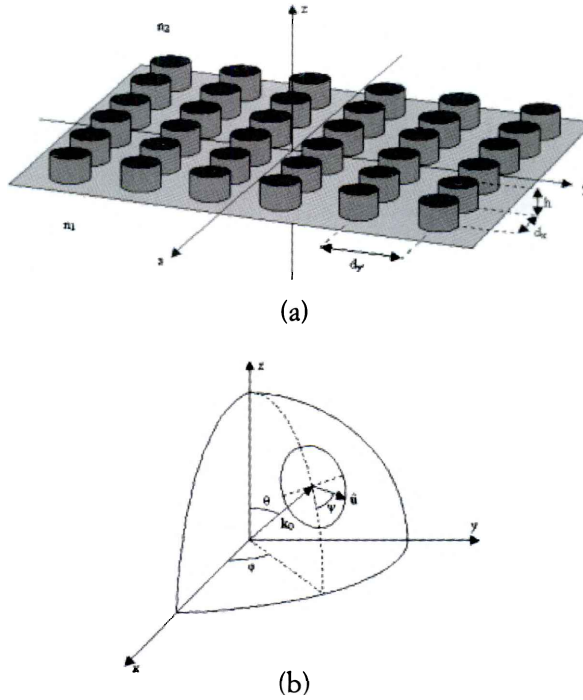
FIG. 1

(a) A three-dimensional grating configuration.
(b) Wave vector k_0 and polarization vector u of the incident plane-wave.

For the scattered field in the homogeneous regions we use Rayleigh expansions. In the periodic layer we use modal expansions, moreover we expand in a Fourier series the permittivity $\varepsilon(x,y) = \varepsilon_0 \varepsilon_r(x,y)$ and its reciprocal:

[1]
$$\varepsilon(x, y) = \varepsilon_0 \sum_{p=-\infty}^{+\infty} \sum_{q=-\infty}^{+\infty} \varepsilon_{pq} \exp\left[2\pi i \left(\frac{px}{d_x} + \frac{py}{d_y}\right)\right]$$

$$\left[\varepsilon(x, y)\right]^{-1} = \varepsilon_0^{-1} \sum_{p=-\infty}^{+\infty} \sum_{q=-\infty}^{+\infty} \zeta_{pq} \exp\left[2\pi i \left(\frac{px}{d_x} + \frac{py}{d_y}\right)\right]$$

We also introduce the following quantities:

$$\left\lceil \varepsilon \right\rceil_{mn} = \frac{1}{d_x} \int_0^{d_x} \varepsilon_r(x,y) \exp\left[-i(m-n)2\pi \frac{x}{d_x} \right] dx$$

$$\left\lfloor \varepsilon \right\rfloor_{mn} = \frac{1}{d_y} \int_0^{d_y} \varepsilon_r(x,y) \exp\left[-i(m-n)2\pi \frac{y}{d_y} \right] dy$$

[2]

$$\left\lceil \varsigma \right\rceil_{mn} = \frac{1}{d_x} \int_0^{d_x} \varepsilon_r^{-1}(x,y) \exp\left[-i(m-n)2\pi \frac{x}{d_x} \right] dx$$

$$\left\lfloor \varsigma \right\rfloor_{mn} = \frac{1}{d_y} \int_0^{d_y} \varepsilon_r^{-1}(x,y) \exp\left[-i(m-n)2\pi \frac{y}{d_y} \right] dy$$

and

$$\left\lfloor \left\lceil \varepsilon \right\rceil \right\rfloor_{mn,pq} = \left\lfloor \left\{ \left\lceil \varsigma \right\rceil^{-1} \right\}_{mp} \right\rfloor_{nq} = \frac{1}{d_y} \int_0^{d_y} \left\{ \left\lceil \varsigma \right\rceil^{-1} \right\}_{mp}(y) \exp\left[-i(n-q)\frac{2\pi y}{d_y} \right] dy$$

[3]

$$\left\lceil \left\lfloor \varepsilon \right\rfloor \right\rceil_{mn,pq} = \left\lceil \left\{ \left\lfloor \varsigma \right\rfloor^{-1} \right\}_{nq} \right\rceil_{mp} = \frac{1}{d_x} \int_0^{d_x} \left\{ \left\lceil \varsigma \right\rceil^{-1} \right\}_{nq}(x) \exp\left[-i(m-p)\frac{2\pi x}{d_x} \right] dx$$

Starting from Maxwell equations, and using the correct Fourier factorization rules for discontinuous functions (3), we derive the following eigenvalue problem:

[4]

$$k\gamma E = F \cdot H \quad F = \begin{pmatrix} \alpha_q \left[\left[\varepsilon\right]\right]^{-1} \beta_m & k^2 \delta_{nq}\delta_{mp} - \alpha_q \left[\left[\varepsilon\right]\right]^{-1} \alpha_n \\ -k^2 \delta_{nq}\delta_{mp} + \beta_p \left[\left[\varepsilon\right]\right]^{-1} \beta_m & -\beta_p \left[\left[\varepsilon\right]\right]^{-1} \alpha_n \end{pmatrix}$$

$$k\gamma H = G \cdot E \quad G = \begin{pmatrix} -\alpha_q \beta_p \delta_{nq}\delta_{mp} & -k^2 \left\lceil\left\lfloor\varepsilon\right\rfloor\right\rceil + \alpha_q^2 \delta_{nq}\delta_{mp} \\ k^2 \left\lfloor\left\lceil\varepsilon\right\rceil\right\rfloor - \beta_p^2 \delta_{nq}\delta_{mp} & \alpha_q \beta_p \delta_{nq}\delta_{mp} \end{pmatrix}$$

where E and H are the eigenvectors, γ the eigenvalues, $k = 2\pi/\lambda$ is the vacuum wavenumber, α and β are the vectors of the lateral propagation coefficients according to the Floquet-Bloch theorem, and δ_{nq} is the Kronecker symbol.

The tangential electric and magnetic field components have to be matched at the boundary surfaces $z=0$ and $z=h$. The resulting equation system has to be solved for the reflected and transmitted field amplitudes, so that the diffraction efficiencies can be determined.

For a numerically stable treatment of the problem, when the periodic region is divided into z-invariant different layers we use the S-matrix algorithm (4) to solve the boundary value system.

3. Numerical results

In Fig. 2(b) we present a comparison with results available in the literature, for a checkerboard structure (which top view is sketched in Fig. 2(a)) with $d_x = d_y = 2.5\lambda$, $h = \lambda$, normally incident illumination ($\theta = \varphi = 0$), polarization along x axis ($\psi = 0$), $n_1 = 1.5$, $n_2 = 1$. The transmission efficiency is shown as a function of L^2, being $L = L_x = L_y$ the number of diffracted orders considered in each periodic direction. Markers correspond to our results, dotted lines to the results obtained in (3). It can be seen that the agreement is very good. Both the standard eigenvalue solution and the improved one, that uses the correct Fourier factorisation rules, are considered: it can be appreciated that the convergence of the improved method is faster.

Generally, the cross-section of the dielectric element composing the grating is a not separable function of the x and y coordinates. In order to use the improved eigenvalue formulation it is therefore necessary to make a discretization of the cross-section by a zigzag contour, consisting of n_{div} line segments of the grid parallel to the x and y axes, as sketched in Fig. 3 for an elliptic pillar grating. For such a structure, with $d_x = d_y = 2.5\lambda$, $r = 0.625\lambda$, $h = \lambda$, $n_1 = 1.5$, $n_2 = 1$, and $\theta = \varphi = \psi = 0$, we report in Table I the diffraction efficiency values of the (0,0), (1,0), (1,1) transmitted and (0,0) reflected orders, calculated with both the standard and improved eigenvalue solutions, for different values of L.

(a)   (b)
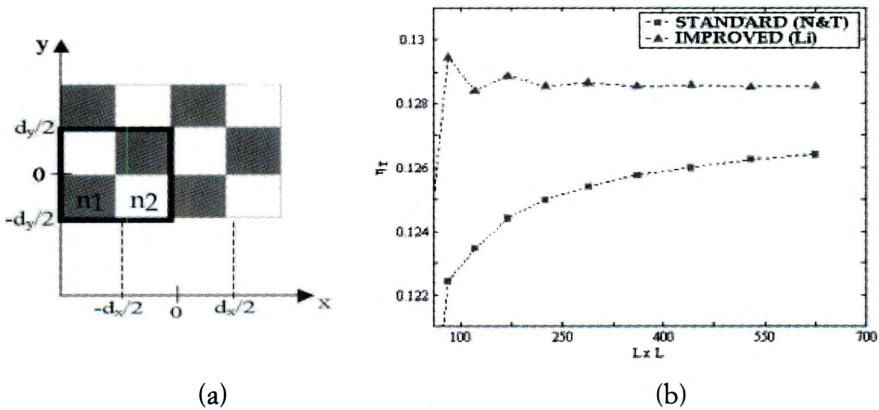
Fig. 2

(a) Checkerboard structure, top view. (b) Comparison with the literature, for a checkerboard structure with $L = L_x = L_y$, $d_x = d_y = 2.5\lambda$, $h = \lambda$, $\theta = \varphi = \psi = 0$, $n_1 = 1.5$, $n_2 = 1$. Markers: our results; dotted lines: results reported in (3).
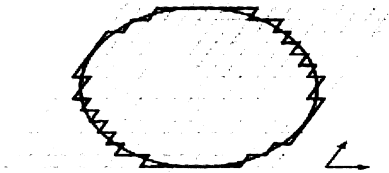
FIG. 3

Discretization of the cross-section in the unit-cell.

Table I

Standard				
L	(0,0)t	(1,0)t	(1,1)t	(0,0)r
3	24.434	12.052	5.017	3.1194
5	27.962	9.604	3.5393	4.171
7	26.523	10.327	3.1541	3.6092
9	25.838	10.573	3.2274	3.566
11	26.042	10.691	3.2613	3.5251
13	26.009	10.728	3.2723	3.5172
15	26.13	10.774	3.2889	3.5047
17	26.142	10.789	3.2946	3.5019
19	26.214	10.813	3.3042	3.4965
21	26.229	10.821	3.3079	3.495
23	26.278	10.836	3.3142	3.4922
25	26.292	10.841	3.3169	3.4913

Improved, $n_{div}=500$				
L	(0,0)t	(1,0)t	(1.1)t	(0,0)r
3	31.257	10,796	4.807	2.3227
5	31.328	9.5999	3.8108	3.9422
7	29.116	10.228	3.2438	3.709
9	27.727	10.562	3.3229	3.6725
11	27.51	10.663	3.3222	3.6153
13	27.273	10.723	3.3284	3.5953
15	27.191	10.758	3.3281	3.5741
17	27.1	10.782	3.3299	3.5639
19	27.055	10.799	3.3299	3.553
21	27.01	10.812	3.3307	3.5467
23	26.983	10.823	3.3309	3,54
25	26.955	10.831	3.3314	3.5357

REFERENCES

(1) J.D. JOANNOPOULOS, R.D. MEADE, J.N. WINN, *Photonic Crystals: Molding the Flow of Light*, Princeton University Press, Princeton, NJ, 1995.

(2) E. NOPONEN, J. TURUNEN, *Eigenmode method for electromagnetic synthesis of diffractive elements with three-dimensional profiles*, J. Opt. Soc. Am., **A11**, 2494-2502, 1994.

(3) L. LI, *Use of Fourier series in the analysis of discontinuous periodic structures*, J. Opt. Soc. Am., **A13**, 1870-1876, 1996.

(4) L. LI, *Formulation and comparison of two recursive matrix algorithms for modelling layered diffraction gratings*, J. Opt. Soc. Am., **A13**, 1024-1035, 1996.

(5) F. FREZZA, L. PAJEWSKI, G. SCHETTINI, *Characterization and design of two-dimensional electromagnetic band-gap structures by use of a full-wave method for diffraction gratings*, IEEE Trans. on Microw. Theory Techn., **51**, 941-951, 2003.

Design of single and double negative metamaterials by using uniplanar frequency selective surfaces

AGOSTINO MONORCHIO (*), SEBASTIANO BARBAGALLO (*), GIULIANO MANARA (*)

In this communication, the behavior of planar Frequency Selective Surface as Single and Double Negative (SNG and DNG) Metamaterials is investigated. The design procedure is based on a proper inversion of the equation relating the reflection and transmission coefficients (Γ and τ) of the screen with the value of the effective permittivity and permeability of the structure considered homogenous. In order to avoid the problem of multiple solutions, a procedure based on the continuity of the dispersion relations in the frequency domain is employed when the thickness of the slab under test is greater than the wavelength inside it. The values of Γ and τ) are therefore used in the fitness function of a Genetic Algorithm used to design the corresponding FSS. In this way, some structures are designed that behaves like a metamaterial for a certain range of frequency from a macroscopic point of view. Since one of the required characteristic of a metamaterial is the homogeneity at least along the direction of propagation, further analysis has been performed on the resulting structures in order to consider this aspect. It will be shown that the proposed structure behaves as a DNG or SNG at different bands by changing the number of the cascaded layers without modifying the shape of the FSS. This, in turn, can be used as a parameter to tune the frequency behavior. Finally, we investigate the possibility of obtaining backward wave vectors and negative angles of refraction in properly modified SNG metamaterials, whose optimized structure is to be determined once again by the Genetic Algorithm. We observe that, in this case, complete three dimensional homogeneity must be provided for the elementary cell.

(*) Microwave and Radiation Laboratory, Department of Information Engineering, University of Pisa, Via Diotisalvi 2, I-56126 Pisa.

Double-dipolar artificial dielectrics as radiofrequency absorbing materials

ROBERTO OLMI (*), MARCO BINI (*),
CRISTIANO RIMINESI (*), GIUSEPPE PELOSI (**)

SUMMARY. – *An artificial dielectric consisting of a bidimensional lattice of electric and magnetic minimum scattering antennas is proposed. The lattice can be geometrically arranged in several ways, for example as a Yee-like cell where a repeated structure is realized with a matched magnetic loop placed at the center of four matched electric dipoles occupying the corners of a rectangle. Such a planar array can be designed to constitute a virtually perfect absorber for a monochromatic wave impinging at normal incidence. The artificial dielectric is studied by means of a mixed microscopic/macroscopic approach allowing to compute the equivalent permittivity and permeability of the metamaterial automatically taking into account dipole-dipole interactions. It is demonstrated for a dilute double-dipolar medium that both permittivity and permeability have a unitary real part and imaginary parts such to allow a full absorption of the impinging electromagnetic power. The dependence of the absorbed electromagnetic power on the lattice geometry is investigated in terms of the ratio between the total power incident on a given surface of the dielectric and that absorbed by it, showing that an interval of lattice spacings is available where that ratio is close to one.*

1. Introduction

Materials capable of absorbing electromagnetic (EM) energy are requested in several contexts, from military applications (where absorbing screens prevent a target from radar recognition) to EM compatibility tests, where measurement accuracy demands for the availability of anechoic environments. The absorbing walls of anechoic chambers are realized by different techniques, depending on the frequency band of interest, for example by means of ferrite bricks between 30 and 300 MHz, and by means of

(*) Institute for Applied Physics "N. Carrara", CNR, Via Panciatichi, 64, I 50127 Firenze, Italy.
(**) Dept. of Electronics and Telecommunications, University of Florence, Via S. Marta, 3, I 50134 Firenze, Italy.

absorbing pyramids made of carbon loaded foams in the upper range, say 300 MHz – 18 GHz. Ferrite absorbers, in particular, have several short-comings: sensitivity to the wave direction of incidence, high cost and weight, just to mention the principal ones.

A perfectly absorbing material should exhibit zero reflection in the frequency band of interest, independently of the direction of incidence of the impinging wave and of its polarization. Moreover, such an ideal material should absorb all the incoming power in a finite slab. The above requirements are clearly too stringent to be physically realizable. A physical absorber could be realistically required to have negligible reflection in a given range of incidence angles and to exhibit a nearly flat frequency response. This work describes a metamaterial based on a lattice of electric and magnetic dipoles closely resembling the microscopic structure of a natural dielectric. Such a material will be shown to possess interesting characteristics which make it worth to be considered as a potential future alternative to ferrite absorbers.

2. The double-dipolar material

An artificial dielectric consisting of a bidimensional lattice of electric and magnetic dipoles can be geometrically arranged as in Fig. 1. That arrangement, resembling the Yee cell used in finite difference EM models, consists in a repeated structure where a magnetic dipole is at the center of a rectangular cell whose corners are occupied by electric dipoles. Such geometry maximizes space filling, meanwhile minimizing the interaction between electric and magnetic dipoles. Magnetic dipoles are straightforwardly realized as small loops in the yz plane. Both dipoles and loops are matched for maximum power transfer, with the further property of being minimum scattering antennas (1).
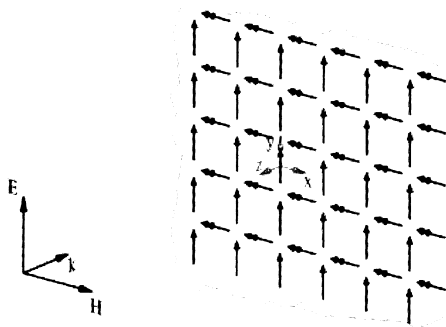
FIG. 1

Geometry of the double-dipolar medium

In order to compute the constitutive parameters of the medium, both electric and magnetic dipole moments must be evaluated. The current on a matched electric dipole is computed in terms of its Thevenin equivalent circuit, consisting in an open-circuit voltage generator: $V_{oc} = E \cdot h$, where h is the vector effective length of the antenna, with a source impedance Rd (the radiation resistance of the dipole), closed on an equal load resistance. For normal incidence ($h = L/2$, L being the physical length of the antenna) the dipole moment:

[1]
$$\left| \vec{p_e} \right| = \frac{IL}{2j\omega} = \frac{V_{oc}L}{2j\omega R_d} = \frac{L^2 E}{8j\omega R_d}$$

If dipole density is v^{-1}, the electric polarization – given by p_e/v – allows computing the electric susceptibility χ_e and eventually the relative permittivity:

[2]
$$\varepsilon_r = 1 + \chi_e = 1 - j\frac{L^2}{8\omega\varepsilon_0 v R_d} = 1 - j\varepsilon''$$

A similar reasoning on a small loop of vector area S exposed to an incident magnetic field H, i.e. with dipole moment IS for normal incidence, brings to the following expression for the magnetic permeability:

[3]
$$\mu_r = 1 + \chi_m = 1 - j\frac{\omega\mu_0 S^2}{2v R_m} = 1 - j\mu''$$

where R_m is the radiation resistance of the small loop.

A perfect absorber should not reflect incident EM energy, i.e. its wave impedance should be equal to that of vacuum, meanwhile having high electric and magnetic losses. For a medium with constitutive parameters as [2] and [3], the following relationship between ε'' and μ'' must hold:

[4]
$$\varepsilon'' = \mu''$$

Substituting in [2] and [3] the expressions for the radiation resistance of short dipoles and small loops, that are respectively (2):

$$R_d = \frac{\pi}{6}\eta_0\left(\frac{L}{\lambda}\right)^2 \qquad R_m = \frac{8\pi^3}{3}\eta_0\left(\frac{S}{\lambda^2}\right)^2$$

the following relevant property is eventually determined:

[5]
$$\varepsilon'' = \mu'' = \frac{3\lambda^3}{8\pi^2 v}$$

Equation [5] shows that a dilute lattice of electric and magnetic dipoles behaves as a transparent medium for a plane wave normally incident, with power absorption directly proportional to the medium density.

3. Dipolar interactions

Dipole-dipole interactions have been investigated by evaluating the input impedance of the central dipole of an $N{\times}N$ array. The impedance seen at the input of the kth dipole can be computed by means of the impedance matrix (Z_{ij}) of the array, by adding the pertinent load impedance values to all diagonal elements of (Z_{ij}) except the kth. Denoting by (Z'_{ij}) the modified matrix:

$$[6] \quad \underline{\underline{Z'}} = \begin{pmatrix} Z_{11} + Z_{L1} & Z_{12} & \cdots & Z_{1k} & \cdots & Z_{1N} \\ Z_{12} & Z_{22} + Z_{L2} & \cdots & Z_{2k} & \cdots & Z_{2N} \\ \vdots & & & & & \\ Z_{1k} & Z_{2k} & \cdots & Z_{kk} & \cdots & Z_{kN} \\ \vdots & & & & & \\ Z_{1N} & Z_{2N} & \cdots & Z_{kN} & \cdots & Z_{NN} + Z_{LN} \end{pmatrix}$$

and by (Y'_{ij}) its inverse, the required input impedance is given by:

$$[7] \qquad Z_{k,in} \equiv \frac{V_k}{I_k} = Z_{kk} + \frac{1}{Y'_{kk}} \sum_{j \neq k} Z_{kj} Y'_{kj}$$

The input resistance of the central element of a 9×9 array of dipoles, all matched for isolated conditions, is shown in Fig. 2a, as a function of the lattice cell size. Dipole resistance tends to the isolated dipole value for diluted lattices, oscillates for decreasing cell sizes and rapidly increases for very dense lattices. The input reactance changes less than one part per thousand in the "accessible" region (un-touching dipoles).

Dipole current can also be computed by means of the (Z_{ij}) matrix for the central element, resulting in the behaviour reported in Fig. 2b. The current on the central dipole oscillates slightly about a unitary value for dilute arrays, while it changes more sensibly for decreasing cell sizes. Dipole-loop interaction has also been investigated for a geometry like that of Fig. 1, showing that loop and dipole currents are practically unperturbed until the lattice cell size is greater than about $3\lambda/4$.
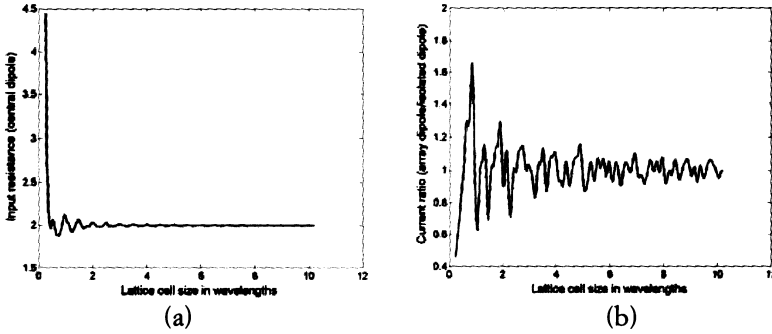
FIG. 2

Dipolar interaction as a function of the lattice cell size. (a) Input impedance of the central dipole of a square array; (b) Current on an array dipole referred to the same dipole in isolated conditions.

4. Results

The absorbing performances of the material have been investigated in terms of the ratio between the power absorbed by the central element, $R_L|I|^2/2$, and the incident power, i.e. the flux of Poynting vector through the surface A of a lattice cell, $A|E|^2/2\eta$. Fig. 3a reports the computed power ratio for an array of 0.1λ matched electric dipoles, as a function of lattice cell size for a square lattice. The average power ratio is about 0.4 for cell sizes d up to about one wavelength, straightforwardly tending to $3(d/\lambda)^2/8\pi3$ for large cell sizes – which holds for an isolated dipole. Note that the above power only refers to dielectric absorption, the magnetic component (loop array) being absent in the above computation.

Furthermore, a square lattice does not appear to be the best choice for the double-dipolar medium. The dependence of the power absorbed by the full artificial material has been investigated (though not in a systematic way, at present) by computing the power ratio for an array consisting in 5×5 electric dipoles and 4×4 loops, using the method of moments. The best power absorption comes out when the cell size ratio (y over x, with reference to Fig. 1) is about 2. Fig. 3b shows the power ratio as a function of the lattice cell size. The presence of ratios greater than one can be ascribed to the small array size, but the results confirm the possibility of absorbing all the incident power with a single layer screen.

5. Oblique incidence

The material just described is anisotropic. An incident wave having the electric field parallel to the electric dipoles and the magnetic field in the

plane of incidence (TE case) – as shown in Fig. 4a – always has a maximum electric coupling, while magnetic field coupling depends on $\cos\theta$. Denoting by α the magnitude of dielectric (and magnetic) losses, the constitutive parameters of the medium in the TE case are:

[8] $$\varepsilon_r = 1 - j\alpha, \quad \mu_r = 1 - j\alpha\cos\theta$$

The wave impedance is thus given by [9], electric absorbed power is always maximum and magnetic absorbed power depends on $\cos\theta$.

[9] $$\eta = \eta_0 \sqrt{\frac{1 - j\alpha}{1 - j\alpha\cos\theta}}$$

Figure 4b clearly shows that for TM incidence – electric field in the plane of incidence, magnetic field parallel to the electric dipoles – both electric and magnetic coupling are zero and the medium is transparent.

(a)   (b)
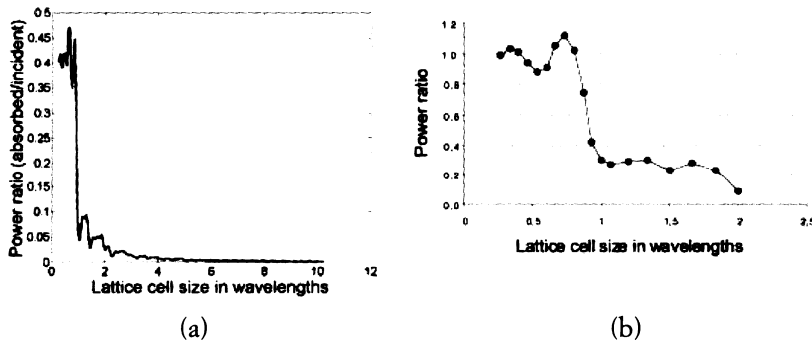
FIG. 3

Power absorbed: (a) lattice of electric dipoles. (b) Double-dipolar material

Denoting the double-dipolar material as DL (dipole-loop), the DL medium can be complicated by adding cross electric and magnetic dipoles to form a DL^2 medium, as Fig. 5a shows for the case of TE incidence. This last can be further complicated by a third set of orthogonal dipoles to give a DL^3 medium, as shown in Fig. 5b for the same polarization. By reasoning as in the cases of Fig. 4, the DL^2 medium appears be identical to DL for TE polarization, while its constitutive parameters and wave impedance for the TM case are:

[10] $$\varepsilon_r = 1 - j\alpha\cos\theta, \quad \mu_r = 1 - j\alpha, \eta = \eta_0 \sqrt{\frac{1 - j\alpha\cos\theta}{1 - j\alpha}}$$

DL^3 can be easily demonstrated to be isotropic and perfectly absorbing, in the ideal case of negligible interaction between dipoles and loops, i.e. $\eta = \eta_0$ and $\varepsilon'' = \mu'' \neq 0$.
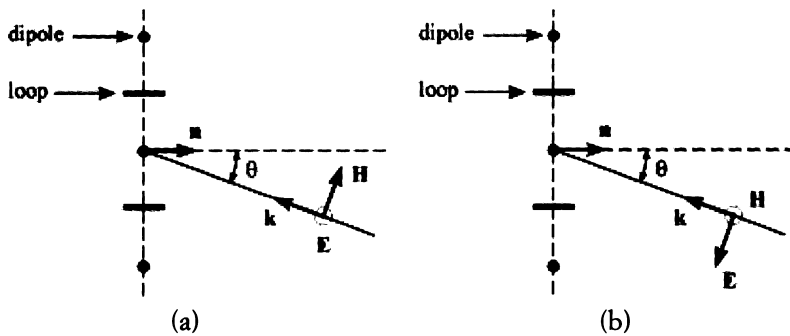
FIG. 4

DL material with oblique incidence: (a) TE case, (b) TM case
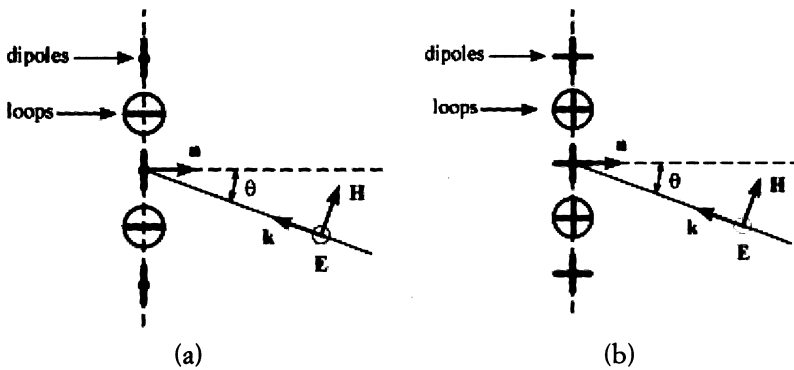
FIG. 5

TE incidence: (a) DL^2 medium, (b) DL^3 medium

6. Conclusions

A preliminary study of an artificial material employable for realizing EM absorbing screens has been proposed. This double-dipolar material, which closely resembles a natural medium at the microscopic level, exhibits no reflection and maximum absorption for normal incidence when all dipoles are matched for maximum power transfer. A simple qualitative analysis for oblique-incidence suggests the possibility of improve the material making it isotropic and in principle perfectly absorbing for every direction of the incident EM wave. A more systematic study of the dependence of power absorption by the lattice geometry is currently in progress for the LD medium, which will be also experimentally verified in the near future. The first theoretical findings concerning LD^2 and LD^3 mediums must be supported by studies on realistic numerical models. Work is in progress

also on this last topic. As a last important point, in the effort of widening the material bandwidth – very narrow at present – several solutions are under investigation: from the use of lossy conductors for building dipoles and loops, to an adaptive filtering of load impedances to obtain wide-band matching.

REFERENCES

(1) R.E. COLLIN, *The receiving antenna*, in Antenna Theory, 93-137, McGraw Hill, New York, 1969.
(2) R.F. Harrington, *Time Harmonic Electromagnetic Fields*, McGraw Hill, New York, 1961.

Resonant trapping in a fiber
with photo-induced gap in wave-number

GAETAN VAN SIMAEYS (*), STEPHANE COEN (*),
MARC HAELTERMAN (*), SILVIA VALENTINI (**),
GAETANO BELLANCA (**), STEFANO TRILLO (**)

SUMMARY. – *We show that the nonlinear response of a standard telecom fiber can be exploited to induce a traveling-wave (dynamic) grating by means of illumination with a beat signal. When other two pulses at different frequency are resonant with the grating and sufficiently intense, they can be trapped as a single localized wave, i.e. a resonance soliton, that leads to cancel the group delay experienced by the pulses in the absence of the grating.*
This phenomenon is representative of systems that exhibit a gap in wavenumber.

1. Introduction

Periodic dielectric structures that exhibit a band-gap in their frequency response have remarkable properties that can be exploited in several photonic and microwave applications. When the nonlinear response of such dielectric becomes effective, an entire host of new phenomena can take place (1,2). Optical fibers with permanently built-in longitudinal Bragg gratings can be regarded as 1D band-gap structures (transversally the light sees the standard modal structure), and have served as an extremely valid test-bed for the investigation of the nonlinear propagation regime, which in turn could help the understanding of higher dimensional structures (3,4). In this work we exploit the nonlinear response of a standard telecom fiber to photo-induce a dynamic (moving) grating of refractive index that couples resonantly two forward-propagating modes of the fiber, that experience group-delay (originating in our case simply from the fiber group-velocity dispersion, GVD).

(*) Service d'Optique et d'Acoustique, Université Libre de Bruxelles, 50 Av. F.D. Roosevelt, CP 194/5, 1050 Brussels, Belgium.
(**) Dept. Of Engineering, University of Ferrara, Via Saragat 1, 44100 Ferrara, Italy.

In contrast with a permanent Bragg grating that involves counter-propagating modes, the co-propagating nature of the coupling (common to other possible schemes (5-7)) results into a dispersion relation with a forbidden gap in wave-number (8), thus allowing to consider the fiber as a 1D wave-number photonic crystal. When the power of the coupled modes is increased, the nonlinearity affects their propagation too. Under these conditions, the propagation with in-gap values of wave-number becomes allowed in the form of localized envelopes, so-called resonance solitons, which have been predicted earlier for a static long-pitch grating (9) but never observed to date. The most relevant signature of such phenomenon is the grating-induced suppression of the group-delay between the two modes.

2. Theory

In our arrangement, a traveling-wave periodic perturbation is induced by illuminating the fiber with two intense (each with power P_g) monochromatic laser lines at frequencies $\omega_g \pm \Omega$. The beating of these frequencies can be ideally described by a complex electric field $E_g(z,t)\exp[ik(\omega_g)z - i\omega_g t]$, where $E_g(z,t) = 2P_g^{1/2}\cos[\Omega(t - z/k'_g)]$ represents the envelope associated with a sinusoidal intensity pattern traveling at group-velocity $k'_g = dk/d\omega|_{\omega_g}$. This intensity modulation gives rise, through the fiber nonlinear response, to a traveling-wave refractive index change (henceforth the dynamic grating), which can be experienced by other two frequencies $\omega_s \pm \Omega$ (henceforth the signal) co-propagating with the grating. The grating can couple efficiently the signal components when the well-known resonance condition $k(\omega_s + \Omega) - k(\omega_s - \Omega) = k_g$ is fulfilled. By using the expression for the wave-number of the sinusoidal intensity pattern $k_g = 2\Omega/k'_g$, as well as the second-order expansion $k(\omega_s \pm \Omega) = k(\omega_s) \pm k'_s\Omega + k''_s\Omega^2/2$, where $k''_s = d^2k/d\omega^2|_{\omega_s}$ is the signal GVD, it is easy to verify that the resonance requires $k'_g = k'_s$, i.e., synchronous group-velocities (at central grating and signal frequencies, ω_g and ω_s, respectively). This can be achieved by carefully tuning the two frequency pairs on opposite sides of the zero dispersion frequency of the fiber.

The interaction of the signal with the grating can be conveniently described by means of the time-dependent coupled-mode approach. Under the simplifying hypothesis of grating waves propagating unchanged, Maxwell equations reduce to the following coupled equations for the two resonant pulse envelopes $E_1(z,t)$ (slow mode, at frequency $\omega_s - \Omega$) and $E_2(z,t)$ (fast mode, at frequency $\omega_s + \Omega$)

$$[1] \quad i\left[\partial_z + \delta k'\partial_\tau + i(k'_s/2)\partial_\tau^2\right]E_1 + \Gamma E_2 + \chi\left(|E_1|^2 + 2|E_2|^2\right)E_1 = 0$$

$$[2] \quad i\left[\partial_z - \delta k'\partial_\tau + i(k''_s/2)\partial_\tau^2\right]E_2 + \Gamma E_1 + \chi\left(|E_2|^2 + 2|E_1|^2\right)E_2 = 0$$

where $\tau = t - k'_g z$ is the retarded time, $2\,\delta k' = 2 k''_s \Omega$ is responsible for the GVD-induced group-delay between the modes, and $\Gamma = 2\chi P_g$ is the linear coupling coefficient, χ being the fiber nonlinear coefficient.
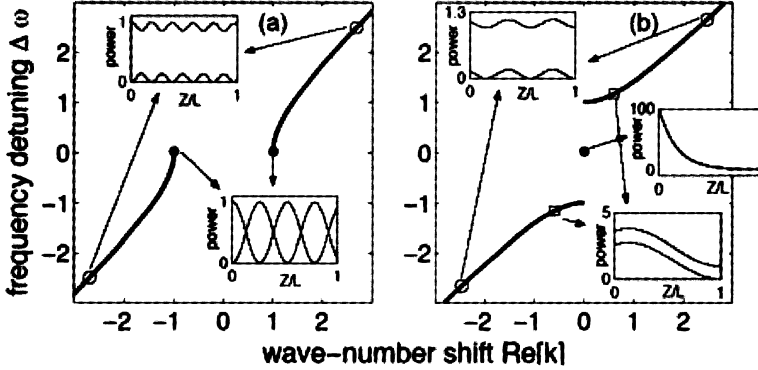
FIG. 1

(a) Dispersion relation $\Delta\omega$ vs. wave-number k for our grating scheme. The insets show the normalized modal power evolutions $P_{1,2}(Z)/P_1(0)$ for marked values of $|\Delta\omega|$ when mode 1 is launched (Z is given in units of grating length L, and we set a grating figure of merit $|\Gamma|L=6$). For comparison we report in (b) the dispersion relation $\Delta\omega$ vs. wave-number $Re[k]$ characteristic of counter-propagating modes in a Bragg grating (here the insets are relative to excitation of the forward mode 1, and the modal powers $P_{1,2}$ are given in units of $P_1(L)$, with fixed figure of merit $|\Gamma|L=3$).

In the linear ($\chi=0$) regime, the dispersion relationship $K(\Delta\Omega)$ associated with Eqs. (1-2) features two branches $K^{\pm}=\pm[\Gamma^2+(\delta k'\Delta\Omega)^2]^{1/2}$ separated by a forbidden gap in wave-number whose aperture 2Γ can be tuned by means of the grating power P_g. Here $\Omega\omega$ is the frequency detuning from resonance and K is the related wave-number shift. This gap, displayed in Fig. 1(a) in terms of normalized quantities $k=K/\Gamma$ and $\Delta\omega=\Delta\Omega(\delta k'/\Gamma)$ is characteristic of the forward coupling process, and is markedly different from the case of a permanent Bragg grating (reported in Fig. 1(b) for comparison) where the gap appears in frequency. In fact, in the latter case, the gap is associated with solutions of the coupled-mode equations that become exponentially damped, thus entailing strong energy transfer to the back-propagating wave (or in other words, strong reflection). Conversely, for co-propagating modes, the solutions are always of the oscillatory type, and the K-gap reflects the fact that the spatial frequency of the coupling is bounded from below by the value $|K(0)|=\Gamma$ that it takes on-resonance (no matter whether the resonance is approached from above or below). This diversity has a major consequence in the *full nonlinear regime*, which in our scheme becomes easily accessible by raising the power of both signal components (excited by means of end-firing), without experiencing the major

drawback of permanent fiber Bragg gratings, where the strong reflectivity hampers the observation of nonlinear effects on-resonance.
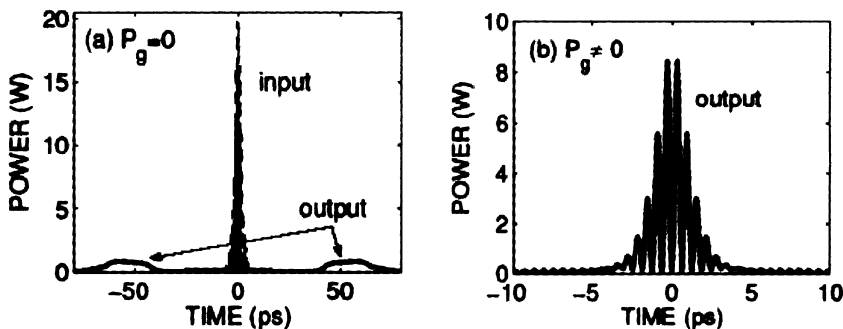
FIG. 2

Output temporal profiles of the total signal envelope after propagation in a 1 Km long fiber: (a) in the absence of grating ($P_g=0$); (b) in the presence of the grating ($P_g \neq 0$) that sustains the soliton. In both cases the input is an ideal soliton of Eqs. (2-3), composed by a fast and a slow component with the frequency offset $\pm\Omega = \pm 1.64\pi$THz characteristic of our experiment.

Specifically, at high signal powers, the propagation of wave-packets that have wave-number located inside the K-gap becomes accessible since the nonlinear phase shift experienced by the signal can balance the linear effects (group-delay and coupling). Under these conditions, the two signal components can travel without changing as a localized unit, a so-called *resonance soliton* solution of Eqs. (1-2) (9,10), which can be found in closed form in the limit of negligible GVD, and numerically otherwise. Such solitons are intimately associated with the presence of the grating and can have any wave-number inside the K-gap, and any intermediate velocity (between those of $E_{1,2}$ modal envelopes) controllable by changing the input power imbalance $|E_1/E_2|^2$. Their characteristic behavior is illustrated in Fig. 2 with reference to the exactly resonant case (center of K-gap and still soliton in the grating frame which requires balanced input $|E_1/E_2|^2 = 1$). As shown in Fig. 2(a), in the absence of the grating, the dynamics of the signal is dominated by the group-delay, and the pulses E_1 and E_2 take off in time to yield well separated pulses at the output. However, when the grating is raised to the level required to balance the signal nonlinear phase-shifts, the two pulses remain trapped, as shown in Fig. 2(b). A leakage of signal power from input (a) to output (b) originates mainly from grating wave distortions which are accounted for in the simulation reported in Fig. 2.

3. Experiment

In order to observe experimentally the trapping phenomenon we have developed a special source (see Ref. (10) for details) that releases two signal pulses with about 4 ps duration and about 4 W peak power at wavelengths tunable around 1.3 μm, as well as grating lines around 1.5 μm made by 540 ps square pulses that ensures quasi-cw operation. The resonance condition in our fiber (Teralight by Alcatel, with zero dispersion at 1420 nm) is ensured by operating the system with wavelengths $\lambda_{g1,g2}$ = 1538, 1551.1 nm (grating), and $\lambda_{s1,s2}$ = 1293.4, 1302.6 nm (signal), which correspond to a detuning $\Omega = 1.64\pi$THz. The dynamical nature of the grating allows us to employ a long fiber ($L = 1$ km) that overcomes the weak coupling (at maximum grating power $P_g = 17.5$ Ω, Γ is of the order 10^{-3} cm^{-1}) due to the fable nonlinearity, yielding a high figure of merit (about $\Gamma L = 100$ comparable with a permanent fiber Bragg grating).

The results of the experiment are summarized in Fig. 3. The left frame shows the measured output spectrum obtained when only the high-frequency signal component is injected into the fiber, in the absence (dashed line) and in the presence (solid line) of the two grating waves, respectively. The dynamic grating scheme is proven to be effective by the measured coupling to the low-frequency signal mode (about 40 dB above the baseline relative to the absence of grating, see inset in log scale). Spontaneous blue-shifted broadband fluorescence is also observed which, however, vanishes when the trapping experiment is performed with both signal modes injected at the input. In this case, we measure the temporal signal waveform at the output when the grating power is raised. As shown in the right frames (a-d) the two pulses emerge well separated in time when the grating is still inefficient (P_g=5 W), whereas higher grating powers P_g induce the group-delay to be progressively compensated, until eventually the two pulses merge to form a bound state when the coupling strength (at P_g = 17.5 W) and the nonlinear signal phase-shift mutually balance. The measured envelope is in good agreement with our numerical expectation (reported as dashed line in Fig. 3(d)) when the description includes all the fiber effects (losses, Raman scattering, etc.) that have been neglected in the simple model (1-2). Note that the fast oscillation due to the beating between the two modes and shown in Fig. 2(b) is beyond resolution of our streak camera. Nevertheless, our data clearly support the proposed picture, where a dynamic grating photo-induced through the nonlinear response of a standard telecom fiber allows for trapping a resonant soliton, leading to cancel the modal group-velocity.
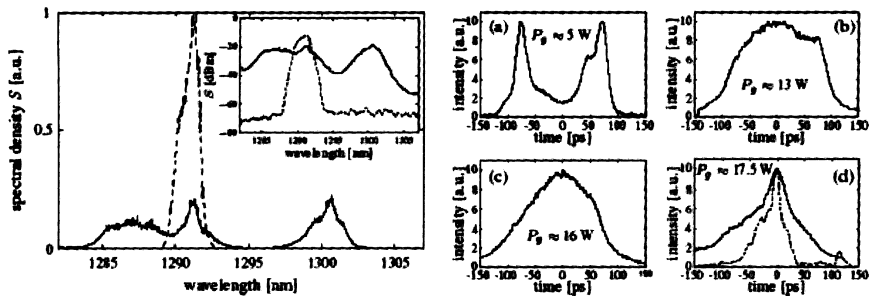
FIG. 3

Left: Output spectral density measured in the presence (solid line, P_g=16 W) and in the absence (dotted line) of the grating waves, when only one signal component is injected at the input. Right: (a-d) Output signal temporal profile obtained when both the signal components are injected and the grating power P_g is raised progressively. The dashed line in (d) is the theoretical expectation.

REFERENCE

(1) R.E. SLUSHER, B.J. EGGLETON, Eds., *Nonlinear Photonics Crystals* (Springer-Verlag, Berlin, 2003).

(2) J.W. FLEISCHER, M. SEGEV, N.K. EFREMIDIS, D.N. CHRISTODOULIDES, Nature, **422**, 147 (2003).

(3) B.J. EGGLETON, R.E. SLUSHER, C.M. DE STERKE, P.A. KRUG, J.E. SIPE, Phys. Rev. Lett., **76**, 1627 (1996).

(4) N.G.R. BRODERICK, D. TAVERNER, D.J. RICHARDSON, M. IBSEN, R.I. LAMING, Phys. Rev. Lett., **79**, 4566 (1997).

(5) S. PITOIS, M. HAELTERMAN, G. MILLOT, J. Opt. Soc. Am., **B19**, 782 (2002).

(6) S. TRILLO, S. WABNITZ, G. I. STEGEMAN, IEEE J. Lightwave Technol., **6**, 971 (1988).

(7) S. Trillo, S. Wabnitz, W.C. Banyai, N. Finlayson, C.T. Seaton, G.I. Stegeman, R.H. Stolen, IEEE J. Quantum Electron., **QE-25**, 104 (1989).

(8) J.N. KUTZ, B.J. EGGLETON, J.B. STARK, R.E. SLUSHER, IEEE J. Selected Topics in Quantum Electron., **3**, 1232 (1997).

(9) S. WABNITZ, Opt. Lett., **14**, 1071 (1989).

(10) G. VAN SIMAEYS, S. COEN, M. HAELTERMAN, S. TRILLO, Phys. Rev. Lett. (in press)

A new microwave sensor based on space-filling Hilbert curves

MATTEO CERRETELLI (*), MARIANO LINARI (*),
VASCO TESI (*), GUIDO BIFFI GENTILI (*)

SUMMARY. – In this paper the use of a metamaterial as microwave sensing device is suggested and briefly analysed. The proposed sensor device, called Hilbert MetaSensor (HMS), is based on a surface slot resonator made of a Hilbert space-filling curve of the third iteration order. The electromagnetic (EM) interaction between HMS and Material Under Test (MUT) is analysed with the Method of the Moment (MoM) and with the time domain Finite Integration Technique (FIT). A HMS prototype has been realised and tested as thickness sensor device for high permittivity liquid layers, for instance water. Simulations results have been compared with measurements evidencing similar behaviour but an unexpected frequency shift that could be attributed to the unsuitability of the EM simulators of correctly modelling all the EM coupling phenomena that arise among the very near slots inclusions composing the Hilbert labyrinth.

1. Introduction

We have studied a metamaterial surface made of Hilbert shaped slot curve etched on a thin metallic layer supported by a dielectric slab. One of the most interesting property of such a kind of curves is that a long line can be compacted into a small surface area so that a resonant structure at a wavelength much longer than its footprint can be designed. The advantage of using a Hilbert slot structure (1) for microwave sensing of material physical properties is investigated. Microwave sensors are employed in the industry for measuring material properties like thickness, density, moisture content and presence of dielectric/metallic inclusions. Thickness of plastic slabs, ceramic tiles, layers of water and other fluids can be measured in real time with a resonant microwave sensor.

(*) Dept. of Electr. and Telec., University of Florence, Via S. Marta 3 I 50134 Firenze, Italy.

2. Problem background

Most of the microwave sensors used in the industrial environment are of the resonant type because high measuring sensitivity can be obtained with a simple and cheap microwave circuit. If the thickness of a layered material is concerned, a calibration curve must be preliminarily determined for each processed material to accurately retrieve the thickness from the actual measured resonant frequency. A monotonic behaviour of the inversion function can be generally guaranteed only if the material thickness is smaller than $\lambda/4$, where λ is the bulk material wavelength at the sensor resonant frequency.

If the maximum material thickness is *a priori* known the sensor can be designed choosing the resonant frequency so that the material thickness is below $\lambda/4$. When the permittivity of the material is high (more than 50 for most aqueous mixtures) and the material layer is several mm thick, the appropriate resonant frequency could be much less than 1 GHz. At that relatively low frequency a resonant element of conventional shape could be too big for practical uses. For this reason we investigated a space-filling Hilbert curve as sensing element, which allows to reduce the resonant frequency down to the required value, while keeping the sensor very compact. In order to simplify experimental tests, we have chosen water as MUT, fixing at 25 mm its maximum thickness, which forces the pertinent resonant frequency near 350 MHz.

3. HMS description

The Hilbert MetaSensor (HMS) consists essentially of a resonant planar slot interacting with the MUT (Material Under Test) through a protective radome substrate 0,8 mm thick ($<<\lambda$ at 350 MHz). A thin dielectric substrate supports the resonant slot fed by a microstrip line printed on the opposite side of the substrate. This sensor structure is interesting for practical applications because its simplicity and robustness.

A metal sheet is placed as a reflector below the microstrip at a distance very small as compared to the wavelength in air to emphasize the EM coupling between the MUT and the resonant slot and eliminate back-radiation. The slot shape is based on a horizontal repetition of an Hilbert curve of third order, as shown in Fig. 1.

Essentially the new HMS device appears as a two-port, high Q, very compact ($53 \times 16 mm^2$) sensing element resonating near 350 MHz in air, that is without MUT loading.
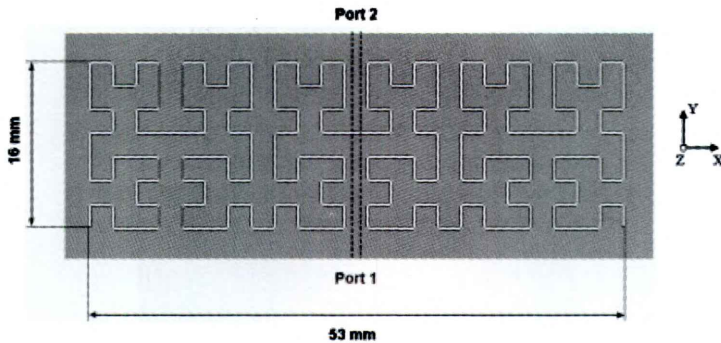
HMS sensing element: the feeding line (*dot line*) is printed on the opposite side of the slot surface.

4. Numerical analysis and Measurement Set-up

The complex nature of the EM interaction between the Hilbert surface and the MUT has been analysed with two commercial codes: Ensemble (2) and CST Microwave Studio (3). The first one, based on the Method of Moments (MoM), is a 2.5D simulator particularly suitable for analysing multilayer structures with some limitation concerning layer thickness and permittivity. Using this code only infinite layers can be analysed, thus a MUT layer of limited longitudinal dimensions can not simulated.

CST MWS is a full-wave, 3D simulator based on a time domain Finite Integration Technique (FIT), useful for analysing the interaction of the Hilbert sensor with a arbitrarily thick MUT having limited longitudinal dimensions. In this case the EM analysis has been performed in the 200-600 MHz frequency range employing 450.000 meshcells to discretize the entire 3D spatial domain with PML (Perfect Matched Layers) boundary conditions. The qualitative results more strictly related to the measured data encourage the use of the FIT approach.

The sensor was built by cutting the Hilbert slot surface on a single layer FR4 board 0,8 mm thick, with copper on both sides. The feeding strip was realized on the opposite side using the same milling machine. The board has about 115 mm×145 mm surface area and the reflector, made of the same metallized board is put at a 8 mm distance from the strip plane. The upper board is the "active" part of the sensor containing the planar Hilbert shaped slot, clearly visible in Fig. 2. The microstrip line is terminated on both sides by SMA connectors, used to connect the sensor assembly to an HP8713B scalar network analyzer, operating in the transmission measuring mode.

The sensor interacts with the MUT through a thin radome made by a 0,8 mm unmetallized FR4 sheet. The material used for experiments is

distilled water, phisically confined by a 9 cm diameter cylindrical plastic container.
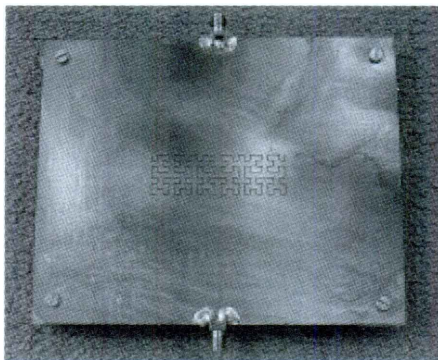
FIG. 2

The HMS prototype.

5. Results and Discussion

We started to consider a infinite water layer interacting with the sensor. In this case the numerical analysis can be performed by using the Ensemble simulator, which predicts a 370 MHz resonance frequency in air, corresponding to the unloaded sensor condition. The scattering parameter S_{21} as a function of frequency has been calculated varying layer thicknes in the range from 0 to 120 mm (from 0 to λ). Results are plotted in Fig. 3(a) in the range from 0 to 30 mm (from 0 to $\lambda/4$). A monotonic behaviour of the resonant frequency versus water thickness is observed for layer thickness ranging from 0 to 30 mm (from 0 to about $\lambda/4$), as shown in Fig. 3(b).

Considering a "water disk" with a 9 cm diameter, CST Microwave Studio has been used for the EM simulation. In this case we obtain a 340 MHz resonant frequency for the unloaded sensor but, surprisingly, a monotonic behaviour for the water loaded sensor in a thickness range largely exceeding the $\lambda/4$ limit as shown in Fig. 4(a).

Finally, using the realised HMS prototype, we have measured the S_{21} scattering parameter for different water layers, obtaining the same behaviour of Fig. 4(a), but shifted toward higher frequencies. Unambiguous responses are obtained for water layer thickness exceeding the $\lambda/4$ limit confirming the numerical results obtained with the CST simulator.
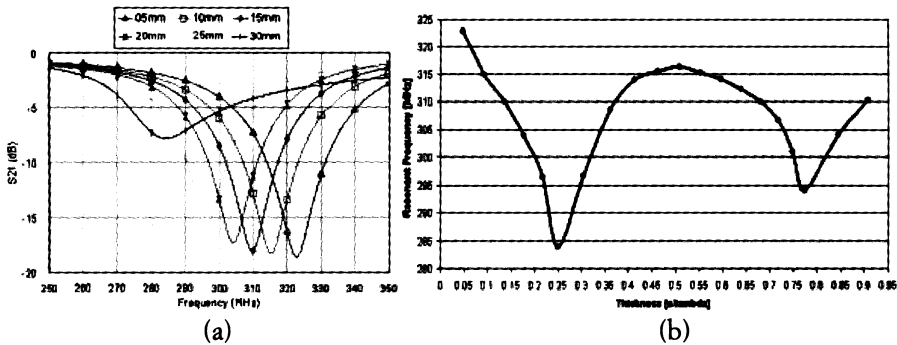
FIG. 3

HMS interacting with an infinite water slab: (a) calculated S_{21} vs. frequency for different water layer thicknesses; (b) calculated sensor resonant frequency vs. water thickness, normalized to the resonant λ.
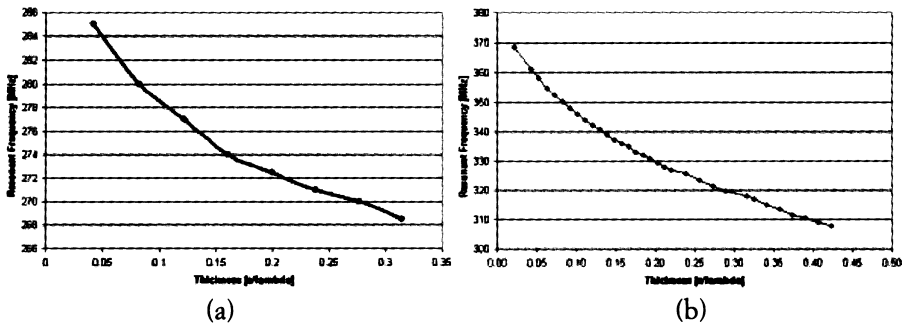
FIG. 4

HMS interacting with an finite water slab (9 cm diameter): (a) calculated and (b) measured resonant frequency vs. water thickness normalized to resonant λ

6. Conclusion

A metamaterial surface made of Hilbert shape slot curve has been numerically and experimentally investigated for the use as microwave sensor. The observed frequency shift between measurements and numerical results can be attributed to the very involved geometry of the Hilbert curve that is not perfectly analysed by both simulators. This could be due to the inability of the simulators to accurately model the strong EM couplings arising among the unitary elements that compose the Hilbert surface. The hypothesis should be confirmed with further investigations.

REFERENCES

(1) J. McVay, A. Hoorfar, N. Engheta, *Radiation characeristics of microstrip dipole antennas over a high-impedance metamaterial surface made of Hilbert inclusions*, IEEE MTT-S Int. Microwave Symp. Dig., **1**, 587-590, 2003.

(2) *Ensemble Design v.5.1*, Ansoft Corporation-Boulder Microwave Division.

(3) *CST Microwave Studio v.4.3*, Computer Simulation Technology Gmbh, Darmstatd Germany.

A high Q mono-modal accelerating cavity based on a photonic band-gap crystal.

ANTONELLO ANDREONE (*), FERDINANDO FRANCOMACARO (*),
EMILIANO DI GENNARO (*), GIANRICO LAMURA (*),
MARIA ROSARIA MASULLO (**), VITTORIO GIORGIO VACCARO (***)

SUMMARY. – *The use of high quality factor (Q) resonant cavities has become an integral part of the accelerator technology applicable to present and future experiments in high energy physics. An important requirement, in connection with high intensity beams, is that the resonators must exhibit very low Q values for all high order modes (HOMs). We propose here a new type of a high gradient accelerator cavity based on Photonic Band Gap (PBG) concepts and operating in the microwave region. The cavity consists of a two-dimensional lattice, composed of either metallic or dielectric or superconducting posts, sandwiched by two conducting or superconducting plates. The study and optimisation of the PBG structure will be presented focusing on understanding how the band structure depends on the detailed choice of lattice distance between cylinders, height and diameter of each cylinder. Then, the related RF measurements (scattering parameters) carried out at room temperature and at 77K in the frequency range 0.5-20 GHz on a metallic (Copper) prototype.*

1. Introduction

In the last years the electromagnetic properties of artificial complex materials have been largely investigated in the frequency spectrum from the microwaves to the optical waves. Meta-materials can be classified depending on the ratio between the size of their spatial inhomogeneity and the e.m. field wavelength. The photonic-band gap (PBG) structures (1), object of

(*) Dip. Scienze Fisiche and INFM Coherentia, Università di Napoli "Federico II", Piazzale Tecchio 20, 80125 Napoli, Italy.
(**) Istituto Nazionale di Fisica Nucleare, Via Cinthia, 80126 Napoli, Italy.
(***) Dip. Scienze Fisiche, Università di Napoli "Federico II" and Istituto Nazionale di Fisica Nucleare, Via Cinthia, 80126 Napoli, Italy.

our research, have characteristic dimensions which are comparable or smaller than the wavelength. These devices are characterized by a strong periodicity (from 1D-3D case). They have recently emerged as powerful devices to be used for a wide range of applications from filters to resonators from the microwave (2,3) to the optical frequency region (4).

A PBG system is formed by a periodic alignment of macroscopic objects, like rods, which can be metallic or dielectric. The structure presents frequency band-gaps which prevent the propagation of e.m. radiation along some directions in the structure itself. In such a system one can create a cavity by removing rods. In fact when the lattice contains such "defects", new modes (known as defect modes) can exist in the frequency stop-bands; they will be localized in the "cavity" decaying exponentially in all directions away from the defect site. In this way, one can get cavities with a very high quality factor, Q, excited at defect-modes. By optimising the lattice geometry one can also make Higher Order Modes (HOMs) falling into the frequency pass bands. These modes present very low Q.

Due to their intrinsic mono-modal behaviour, PBG structures can be used as accelerating cavities for particle accelerators: the fundamental mode is localized around the defect and HOMs filling all the cavity can be easily removed.

Here we present the study and the design of an all-metallic accelerating cavity at 14 GHz. Comparison between simulations and experimental data, taken at room temperature and at 77 K are reported.

2. The design of the structure and the simulation of the electromagnetic behaviour

The cavity consists of a two-dimensional hexagonal lattice, composed of thirty-six metallic cylinders (height 4.6 mm, diameter 3 mm, lattice constant 8.58 mm), sandwiched between two metallic plates. One cylinder in the centre of the structure is missing (symmetry break). In this position a hole was created on both conducting plates allowing for the entrance of the particles; the hole is also used for the coupling to the pick-ups for the experimental characterization. The lack of the central rod behaves like a defect, allowing for a new electromagnetic mode spatially confined in the defect zone itself. In order to use our structure as a cavity for accelerating particles we need to study its resonant modes, their spectrum and their spatial distribution.

The study and the optimization of our PBG based cavity have been performed by means of a 3D electromagnetic CAD simulator (CST Microwave Studio). Starting from our previous experience on a squared PBG lattice at 3 GHz[5], we analyzed various geometrical configurations; the final cavity is shown in Fig. 1 and Fig. 2.
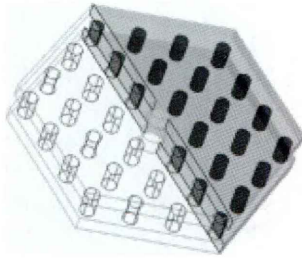
FIG. 1

e.m. design of the simulated
PBG cavity
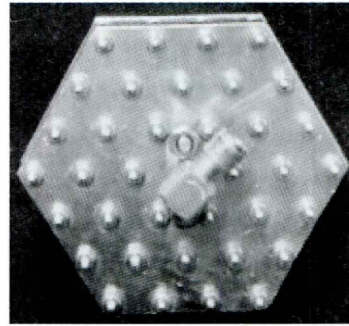
FIG. 2

Picture of the real PBG cavity
(metallic)

The electromagnetic behaviour has been investigated in the range 0.5-20 GHz looking at the Scattering matrix, in order to compare it with the measurements. The simulation behaviour is presented in Fig. 3.

The fundamental resonant mode (TM_{01}) appears at a frequency of roughly 14.42 GHz. It is clearly confined in the centre of the structure only slightly penetrating in the second "row" as shown in Fig. 4 (E and H transverse field distribution). Simulations done by adding another "row" of cylinders gave a fine prove of it. The HOMs are propagating in all the volume going outside the structure, as it can be seen looking at the transverse field distributions.

Simulations taking into account mechanical tolerances have been performed before the final design showing the sensitivity of the central zone to the cylinder dimensions and to their relative distance.
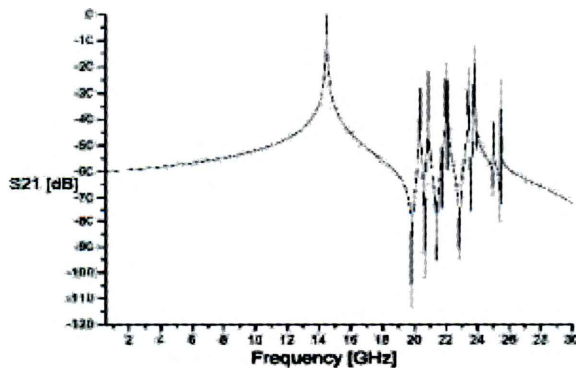
FIG. 3

Simulation: transmitted power (S_{21} parameter)
in the full frequency range of interest
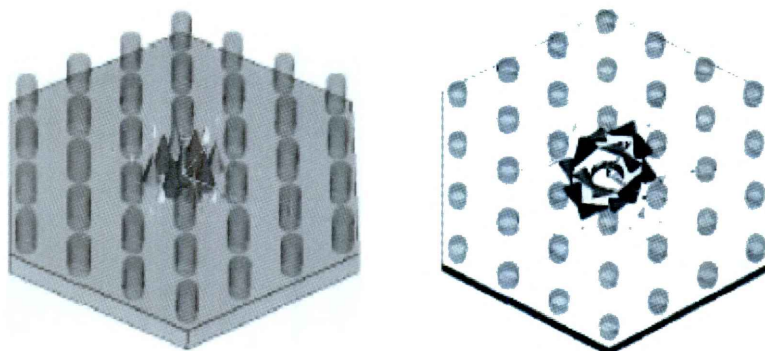
FIG. 4

The fundamental mode: the electric field E (on the left) and the magnetic field
H (on the right) confined in the centre of the PBG structure (MWS images).

3. Measurements and discussion

For the experimental e.m. characterization the Scattering matrix was
measured using two pick-ups inserted through the plate holes. These two
antennas were connected to a Network Analyzer that excites all the modes
in the range from 0.5 to 20 GHz. In this way we could measure the
reflected signal (parameter S_{11}) and the transmitted one (parameter S_{21})
from the structure. The comparison between the experimental and the
simulation data are shown in Fig. 5. In the last simulation the real final
dimensions of the cavity have been taken into account. It is worthwhile to
emphasize the very good agreement between theory and experiment on the
fundamental mode ($\Delta f/f = 0.13\%$), which is strongly localized and not
influenced by the external environment. This is not the case for the higher
mode, where the differences between simulations and experimental data are
due to the influence of the boundaries as it was expected. The Q-factor of
the fundamental mode was found to be 1200 at room temperature.

In order to study, for the fundamental mode, the Q-factor behaviour
with temperature we measured the structure at low temperatures (in liquid
nitrogen) till 77 K. A LabView code has recorded the values of Q for each
temperature step. A Q-value increase with the inverse of temperature was
measured. The best value of Q was 1700 at 77 K, lower then the expected
one from simulations (4100), due to construction imperfections.
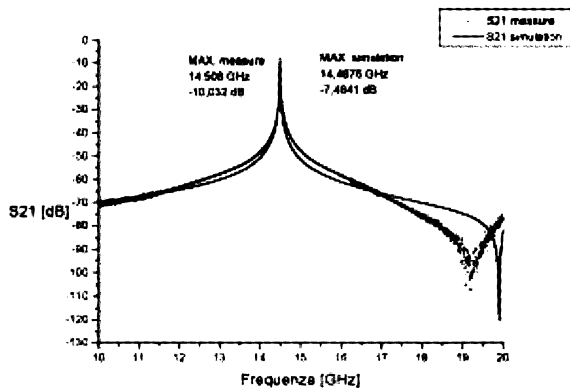
FIG. 5

The transmission parameter S_{21}: a comparison between simulation
and measurement

4. Conclusions and future work

A copper PBG cavity at 14 GHz was examined. Simulations and
measurements at room temperature and at 77 K are in a very good
agreement. The structure proves to be a promising candidate for an
accelerating cavity due to its intrinsic mono-modal behaviour. In the
fundamental mode the e.m. fields are strictly confined all the way through
the passage of particle beam with the electric field parallel to the axis of
the cylinders. Furthermore, the structure can be easily scaled with frequency
avoiding constructive problems linked to the required damping of HOMs
(ad hoc waveguide can be really cumbersome at high frequencies).

On the basis of this experience we have also studied and designed a
hybrid (dielectric/metallic) PBG cavity that will be tested at low temperatures.

REFERENCES

(1) J. YABLONOVITCH, *Photonic band-gap structures*, J. Opt. Soc. Am., **B10** (2), 1993.
(2) J.D. JOANNOUPOLOUS, R.D. MEADE, J.N.WINN, *Photonic crystals: Molding the flow of light*, (Princeton Univ. Press, Princeton, NJ, 1995).
(3) D.R. SMITH, R. DALICHAOUCH, N. CROLL, S. SCHULTZ, S. L. MCCALL, P. M. PLATZMAN, *Photonic band structure and defects in one and two dimension*, J. Opt. Soc. Am., **B10** (2), Febraury 1993.
(4) M.A. SHAPIRO, W.J. BROWN, I. MASTOVSKY, J.R. SIRIGIRI, R.J. TEMKIN, Phys. Rev., ST Accel. Beams, 4, 042001 (2001)
(5) A. BALZANO, *Studio, progetto e test di un prototipo di cavità acceleratrice a banda fotonica*, Tesi di Laurea (Univers. di Napoli), 2001

Mathematical models of smart obstacles

PAOLO CORNA (*), LORELLA FATONE (**),
MARIA CRISTINA RECCHIONI (°), FRANCESCO ZIRILLI (°°)

SUMMARY. – *Some mathematical models of smart obstacles are proposed. In particular smart obstacles that when illuminated by an incoming electromagnetic field react trying to be undetectable in a definite band of the frequency space are modelled through an optimal control problem.*

1. Introduction

In this paper a mathematical model for an electromagnetic time dependent scattering problem involving smart obstacles is formulated. Smart obstacles are obstacles that when hit by an incoming electromagnetic field react in order to pursue an assigned goal. The goal pursued by the smart obstacles considered in this paper is to be undetectable in a definite band in the frequency space, we call this goal: definite band furtivity. This smart obstacle pursues its goal circulating a surface electric current density on its boundary. We show that the surface electric current density necessary to pursue the goal can be determined as the solution of a suitable optimal control problem for the Maxwell equations. This way of modelling smart obstacles is due to the authors and their coworkers. Note that in recent years the design and realization of smart obstacles through the use of sensors, electronic chips and actuators have been greatly developed. A practical application of the smart obstacles studied here is in the design and implementation of smart radar absorbers. The most common approaches to

(*) Via Silvio Pellico 4, 20030 Seveso (Milano), Italy.
(**) Dip. Matematica Pura e Applicata, Università di Modena e Reggio Emilia, 41100 Modena, Italy.
(°) Dip. Scienze Sociali "D. Serrani", Università Politecnica delle Marche, 60121 Ancona, Italy.
(°°) Dip. di Matematica "G. Castelnuovo", Università di Roma "La Sapienza", 00185 Roma, Italy.

get the absorbing effect in radar absorber are destructive interference (for example in the Salisbury screen and in the Jaumann stack) and the conversion into heat of the incident energy (for example in the Dallenbach layer). Recently phase-switched screens have been used in the design and implementation of smart radar absorbers (see (1)) and these screens can be seen as smart obstacles that pursue the definite band furtivity goal.

The authors and their coworkers have studied similar models for several classes of smart obstacles in acoustic and electromagnetic scattering (see for example (2)-(5)). The obstacle considered pursue one of the following goals:

1. to be undetectable (i.e.: furtivity problem);
2. to appear with a shape and a boundary impedance different from its actual shape and impedance (i.e.: masking problem);
3. to appear in a location in space different from its actual location eventually with a shape and boundary impedance different from its actual one (i.e.: ghost obstacle problem).

The scattering problems corresponding to 1-3 have been formulated as optimal control problems for the wave equation (acoustic case) or for the Maxwell equations (electromagnetic case) and the first order optimality conditions for these control problems have been derived applying the Pontryagin maximum principle. Thank to these conditions highly parallelizable numerical methods have been developed to solve the optimal control problems considered. We want to treat similarly the case when the goal is pursued in a definite band in the frequency space and we begin, in this paper, formulating the definite band furtivity problem in electromagnetic scattering, as an optimal control problem for the Maxwell equations.

In Sect. 2 we formulate the mathematical model for the electromagnetic definite band furtivity problem. In the websites: http://www.econ.univpm.it/recchioni/w6 and http://www.econ.univpm.it/recchioni/w10 the visitor can see some animations and virtual reality applications about furtivity problems in acoustic and electromagnetic scattering.

2. The mathematical model for the electromagnetic definite band furtivity problem

Let us begin introducing some notations: let R be the set of real numbers, R^3 be the three dimensional real Euclidean space and $x=(x_1,x_2,x_3)^T \in R^3$ be a generic vector, where the superscript T means transposed. We denote with $(\cdot,\cdot)$ the Euclidean scalar product in R^3, with $\|\cdot\|$ the corresponding Euclidean vector norm and with $[\cdot,\cdot]$ the usual vector product.

Let R^3 be filled with a homogeneous isotropic medium of constant electric permittivity $\varepsilon > 0$, constant magnetic permeability $\upsilon > 0$ and zero

electric conductivity. Let us suppose that R^3 contains an obstacle given by a bounded simply connected open set Ω with locally Lipschitz boundary $\partial\Omega$. Let clΩ be the closure of Ω. Note that in the previous hypotheses the outward unit normal vector to $\partial\Omega$, i.e. $n(x) = (n_1(x), n_2(x), n_3(x))^T \in R^3$, $x \in \partial\Omega$ exists almost everywhere. We assume that Ω has a known constant real boundary electromagnetic impedance $\chi \geq 0$ and we denote the smart obstacle with the couple (Ω,χ). Moreover we assume that the medium that surrounds the obstacle does not contain free electric charges and currents.

We consider an incoming electromagnetic field $(E^i(x,t), B^i(x,t))$, $(x,t) \in R^3 \times R$. The electric vector field $E^i(x,t) \in R^3$, $(x,t) \in R^3 \times R$ and the magnetic induction vector field $B^i(x,t) \in R^3$, $(x,t) \in R^3 \times R$ associated to the incoming electromagnetic field satisfy the Maxwell equations, that is equations [1], [2], for $(x,t) \in R^3 \times R$. When the incoming electromagnetic field $(E^i(x,t), B^i(x,t))$, $(x,t) \in R^3 \times R$, hits the surface of the obstacle (Ω,χ), generates a scattered electromagnetic field $(E^s(x,t), B^s(x,t))$, $(x,t) \in (R^3 \backslash \text{cl}\Omega) \times R$, which is the solution of an exterior problem for the Maxwell equations. A passive obstacle, when illuminated by an incoming electromagnetic field $(E^i(x,t), B^i(x,t))$, generates a scattered electric vector field $E^s(x,t) \in R^3$, $(x,t) \in (R^3 \backslash \text{cl}\Omega) \times R$ and a scattered magnetic induction vector field $B^s(x,t) \in R^3$, $(x,t) \in (R^3 \backslash \text{cl}\Omega) \times R$ solutions of the following equations (see (5)):

[1]
$$\left(\text{curl } E^s + \partial B^s / \partial t\right)(x,t) = 0, \ \left(\text{curl } B^s - \left(1/c^2\right)\partial E^s / \partial t\right)(x,t) = 0,$$
$$(x,t) \in \left(R^3 \backslash \text{cl}\Omega\right) \times R,$$

[2] $\quad \text{div } E^s(x,t) = 0, \ \text{div } B^s(x,t) = 0, \ (x,t) \in \left(R^3 \backslash \text{cl}\Omega\right) \times R,$

with the boundary condition:

[3]
$$\left[n(x), \ E^s(x,t)\right] - c\chi\left[n(x), \ \left[n(x), \ B^s(x,t)\right]\right] = \left[n(x), \ b(x,t)\right],$$
$$(x,t) \in \partial\Omega \times R,$$

where:

[4] $\qquad b(x,t) = -E^i(x,t) + c\chi\left[n(x), \ B^i(x,t)\right], \ (x,t) \in \partial\Omega \times R,$

the condition at infinity:

[5] $\qquad\qquad E^s(x,t) = O(1/r), \ r \to +\infty, \ t \in R,$

and the radiation condition

[6] $\quad \left[B^s(x,t), \ x/\|x\|\right] - (1/c)E^s(x,t) = O(1/r), \ r \to +\infty, \ t \in R,$

where $\mathbf{0} = (0,0,0)^T$, $c = 1/\sqrt{\varepsilon\upsilon}$, $\mathbf{x} \neq \mathbf{0}$, $r = \|\mathbf{x}\|$, curl $\cdot$ and div $\cdot$ denote respectively the curl and the divergence of $\cdot$ with respect to the $\mathbf{x}$ variable, $\partial \cdot/\partial t$ denotes the time derivative of $\cdot$, and $o(\cdot)$, $O(\cdot)$ are the Landau symbols.

The limit case of perfectly insulating obstacles (i.e.: $\chi = +\infty$) can be treated with a minor modification of condition [3]. Furthermore we assume that the incoming electromagnetic field vanishes when $t \to -\infty$, that is $\mathbf{E}^i(\mathbf{x},t)$, $\mathbf{B}^i(\mathbf{x},t) \to \mathbf{0}$, $\mathbf{x} \in R^3$, $t \to -\infty$ so that the scattered electromagnetic field vanishes when $t \to -\infty$ as well, that is $\mathbf{E}^s(\mathbf{x},t)$, $\mathbf{B}^s(\mathbf{x},t) \to \mathbf{0}$, $\mathbf{x} \in (R^3 \backslash \mathrm{cl}\Omega)$, $t \to -\infty$.

The smart obstacle studied in this paper when illuminated by an incoming electromagnetic field reacts circulating on its boundary an electric current density so that the electromagnetic field scattered by the smart obstacle satisfies equations [1], [2], [5], [6] and the following boundary equation:

$$[7] \quad \begin{aligned} & \left[\mathbf{n}(\mathbf{x}), \ \mathbf{E}^s\!\left(\mathbf{x},t\right)\right] - c\chi\!\left[\mathbf{n}(\mathbf{x}), \ \left[\mathbf{n}(\mathbf{x}), \ \mathbf{B}^s\!\left(\mathbf{x},t\right)\right]\right] = \left[\mathbf{n}(\mathbf{x}), \ \mathbf{b}\!\left(\mathbf{x},t\right)\right] \\ & + \left(1+\chi\right)\Psi\!\left(\mathbf{x},t\right), \ \left(\mathbf{x},t\right) \in \partial\Omega \times R, \end{aligned}$$

where $\Psi(\mathbf{x},t)$, $(\mathbf{x},t) \in \partial\Omega \times R$ is a vector field tangential to $\partial\Omega$, that is $(\Psi(\mathbf{x},t)$, $\mathbf{n}(\mathbf{x})) = 0$, $\mathbf{x} \in \partial\Omega$, $t \in R$. Let $K \subseteq R$ be an open set symmetric with respect to the origin. Later we refer to K as the assigned frequency band. The vector field $\partial\Psi/\partial t$ is the electric current density that must circulate on $\partial\Omega$ and that we choose in order to solve the following problem:

Definite Band Furtivity Problem. Given the incident electromagnetic field $(\mathbf{E}^i(\mathbf{x},t)$, $\mathbf{B}^i(\mathbf{x},t))$, $(\mathbf{x},t) \in R^3 \times R$, the obstacle (Ω,χ) and the frequency band K choose a surface electric current density defined on $\partial\Omega \times R$ in a suitable class of admissible controls, in such a way that the Fourier transform with respect to time of the electromagnetic field scattered by (Ω,χ) when hit by the incoming electromagnetic field is "as small as possible" in the frequency band K and in such a way that the current density employed on $\partial\Omega$ is as small as possible.

The obstacle (Ω,χ), thanks to the action of the control vector field Ψ reacts to the incoming incident electromagnetic field trying to be undetectable in the frequency band K. This fact makes the obstacle (Ω,χ) a smart obstacle.

We determine the electric current density that realizes the goal pursued by the smart obstacle proposed solving the following optimal control problem. Let C be the space of the admissible controls, that is a function space, made of vector functions defined on $\partial\Omega \times R$, tangential to $\partial\Omega$ that we leave undetermined in this paper. We must solve:

$$[8] \qquad\qquad \min_{\Psi \in C} F_{\lambda,\mu}\!\left(\Psi\right)$$

subject to conditions [1], [2], [5]–[7] where $F_{\lambda,\mu}(\Psi)$ is the following cost functional:

$$F_{\lambda,\mu}(\Psi) = (1+\chi)\int_R dt \int_{\partial\Omega} ds_{\partial\Omega} \left\{ \mu\varsigma\left(\Psi(x,t), \Psi(x,t)\right) \right.$$

[9] $$+\lambda\left(\left[n(x), \int_R d\tau\, I_K(t-\tau)E^s(x,\tau)\right]\left[n(x), \int_R d\tau\, I_K(t-\tau)E^s(x,\tau)\right]\right)$$

$$\left. +\lambda c^2\left(\left[n(x), \int_R d\tau\, I_K(t-\tau)B^s(x,\tau)\right]\left[n(x), \int_R d\tau\, I_K(t-\tau)B^s(x,\tau)\right]\right)\right\}$$

$ds_{\partial\Omega}$ is the surface measure on $\partial\Omega$, ς is a positive dimensional constant and $\lambda \geq 0$, $\mu \geq 0$ are adimensional constants such that $\lambda + \mu = 1$ and $I_K(t)$, $t \in R$ is the inverse Fourier transform of the characteristic function of the set K.

Note that the mathematical model proposed to describe the behaviour of the smart obstacle is an optimal control problem for the Maxwell equations and that the cost functional $F_{\lambda,\mu}(\Psi)$ depends only on the values of Ψ, E^s, B^s on $\partial\Omega \times R$, that is the values more easily accessible in many practical situations.

The choice of the control vector field Ψ that minimizes the cost functional [9] is the one that makes the obstacle furtive in the band K. In (4), (5) and in the website http://www.econ.univpm.it/recchioni/w10 the case $K = R$ has been studied using the Pontryagin maximum principle. Very interesting results that validate the model proposed have been obtained on test problems. Further investigation is needed to derive the first order optimality condition corresponding to problem [8], [1], [2], [5]-[7] and to develop a suitable numerical method of the type proposed in (2), (5). We believe that the modelling of smart obstacles with optimal control problems is an interesting research topic that deserves further attention.

REFERENCES

(1) B. CHAMBERS, *A smart radar absorber*, J. Smart Materials and Structures, **8**, 64-72, 1999.

(2) F. MARIANI, M.C. RECCHIONI, F. ZIRILLI, *The Use of the Pontryagin Maximum Principle in a Furtivity Problem in Time-Dependent Acoustic Obstacle Scattering*, Waves in Random Media, **11**, 549-575, 2001.

(3) L. FATONE, M.C. RECCHIONI, F. ZIRILLI, *A masking problem in time dependent acoustic obstacle scattering*, ARLO (Acoustics Res. Lett. Online), **5** (2), 25-30, 2004.

(4) L. FATONE, M.C. RECCHIONI, F. ZIRILLI, *Some control problems for the Maxwell equations related to furtivity and masking problems in electromagnetic obstacle scattering*, in G.C. Cohen, E. Heikkola, P. Joly and P. Neittaanmaki eds, *Mathematical and Numerical Aspects of Wave Propagation. Waves 2003*, (Springer Verlag, Berlin, 2003), 189-194.

(5) L. FATONE, M.C. RECCHIONI, F. ZIRILLI, *Furtivity and masking problems in time dependent electromagnetic obstacle scattering*, to appear in J. of Optimization Theory and Applications, 2004.

Study of carbon nanotubes process for their application in the aerospace engineering

MARCO REGI (*), FRANCO MANCIA (**),
MARIO MARCHETTI (*), LUCA AMANTINI (*)

SUMMARY. – *The unique carbon nanotubes properties (mechanical, electrical, thermal, etc.) are considered as a key factor for future improvement of technical characteristics of many engineering macro and nano systems. The synthesis, the purification and the characterizations of carbon nanotubes are the primary requirements for a realistic use of it in many engineering sectors (structures, electronics devices, biomedical systems, advanced composites). A possible field of application of carbon nanotubes, for example, is represented by electromagnetic applications and telecommunication for Aerospace Technologies. Using the theoretical electrical and electromagnetically carbon nanotubes properties, is possible to improve the characteristics of many apparatus installed on space systems. This new generation of material find concrete and interesting application in the modern aerospace engineering. This paper reports the authors' studies on the synthesis (arc discharge with inert gas, in water immersion and laser ablation methods), purification (oxidation and chemical etching) and morphological analysis (Optical, SEM, TEM, X-Ray and Chemical) of carbon nanotubes. In particularly the morphological analysis is discussed as the fundamental instrument necessary to evaluate the carbon nanotubes characteristics and therefore their concrete integration for space applications. Besides, is shown a simple numerical examples about the reduction of weight of a space structure employing carbon nanotubes.*

1. Introduction

Using the properties (mechanical, electrical, magnetic) of the carbon nanotubes (CN) (discovered by S. Ijima in the 1991) it is possible to improve the characteristics of many advanced Engineering System (aero-

(*) Dip. Aerospace and Astronautics Engineering, University of Rome "La Sapienza", Via Eudossiana 18, 00184 Roma, Italy.
(**) C.S.M. Centro Sviluppo Materiali of Rome, Via di Castel Romano 100, 00128 Roma, Italy.

space structures, nano-electronics devices, biomedical apparatus, etc.) (2). The primary goal for a realistic use of this new futuristic material, is the ability to synthesize and purify high quantity of CN, with high quality and low cost. The microscopy analysis (optical, SEM, TEM, chemical EDS) is the principal tool for understand the CN morphological configuration (single o multi wall, arm chair, zig zag, chiral). For the space applications the study of the CN dispersion in a polymeric matrix (composite materials) is requested. With the CN mechanical properties (theoretical Young's modulus = 1 TPa) is possible to obtain a significant gain in the mass structure reduction.

2. Synthesis of carbon nanotubes

Three CN synthesis facilities are developed (arc discharge in inert environment (7), arc discharge water immersed (9), laser ablation CO_2 (6)). Figure 1 shown the arc discharge facilities (dc current, 20-23 V, 50-60 A, argon pressure: 0.2 bar) and the SEM analysis of the deposit on the cathode electrode surface.
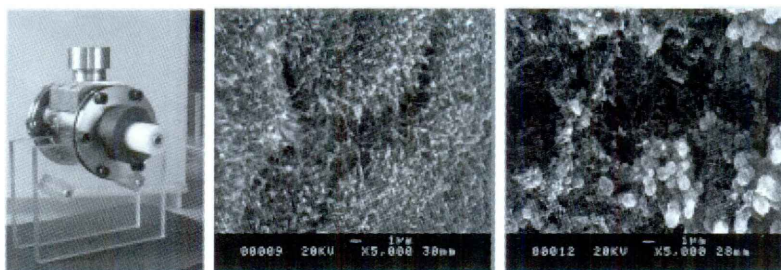
FIG. 1

Arc discharge facilities and the SEM analysis of the cathode electrode deposit

Figure 2 shown the arc between two graphite electrodes in the water immersed conditions (dc current, 20-25 V, 60-90 A) and the relative SEM analysis. Finally, figure 3 reported the laser ablation CO_2 (900 W, wave length: 10.6 mm, Argon flux: 60 l/min) and the SEM analysis. All test are performed using graphite rod (diameter: 6.15 mm, purity: 2 ppm).

FIG. 2

Water immersed arc discharge and the SEM analysis
of the cathode electrode deposit
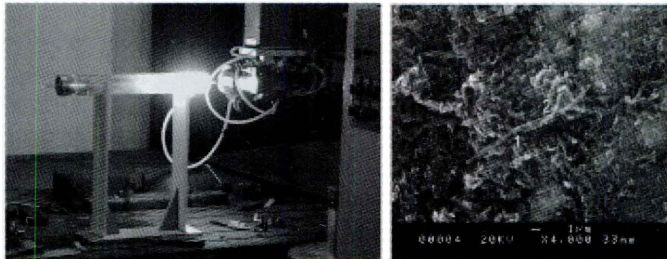
FIG. 3

Laser ablation test and the SEM analysis of the collector deposit

3. Purification of carbon nanotubes

To maximize the CN properties integrated in a advanced system, after the synthesis, a purification phase is required to eliminate all impurities (catalysts, amorphous elements, etc.). A chemical etching (DT-TGA analysis, oxidation flux: N_2 90%, O_2 10%, $T_{max} = 530$ °C for 5 hours) was applied on raw CN produced with the arc discharge method. Figure 4 shows the deposit before and after the purification test.

Besides, a purification experiment with ultrasounds treatment (time test: 25 minutes in ethylic alcohol) was tested (4). Figure 5 shows that by this method there is not significant improvement of the deposit morphology.
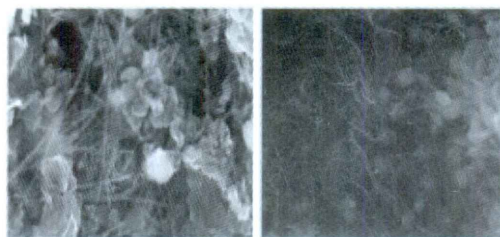
FIG. 4

The arc discharge deposit before and after the chemical etching purification test
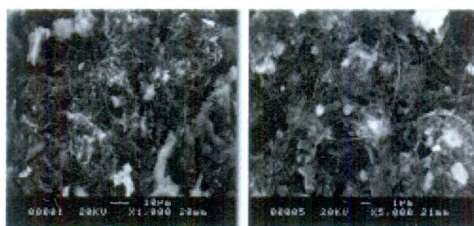
FIG. 5

The deposit morphology before and after the ultrasound purification test

4. Morphological analysis

Since the CN are characterized by nanometric dimensions, it is necessary to use optical, SEM and TEM microscopy and EDS analysis. The electronic microscopy is the principal tool to investigate the characteristics of the CN synthesized and purified. The preparation methodologies of the samples (1) are important. In order to reduce time and costs, the target is to acquire the ability to determine the CN presence with only a reduced number of analysis. With the studies performed, for example, has been determined that in the cathode electrode (arc discharge method) the CN are contained in a grey zone of the deposit in full agreement with the bibliography (5). Figure 6 show the optical, EDS, SEM and TEM analysis.
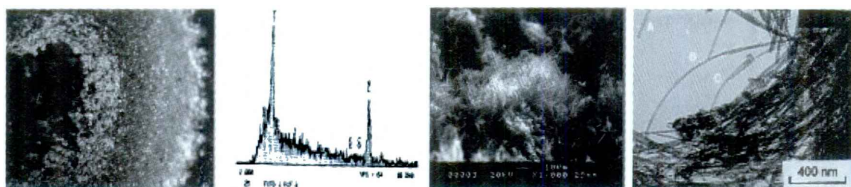
FIG. 6

Optical, EDS, SEM and TEM analysis

5. Application of carbon nanotubes in space structures

The anisogrid lattice structures are realised in the form of thin walled cylindrical or conical shell and consist of a system of helical and circumferential ribs (respect to the element axis) with an angle ±φ (Fig. 7). By means of the Vasiliev model (3) the mass *M* of these structures was calculated, using a typical aeronautics alloy (Al2024), a composite (Hs/Ep: epoxy resins + unidirectional carbon fibers (8)) and the Hs/Ep composite with a 5% in wt of carbon nanotubes dispersed (Table 1).
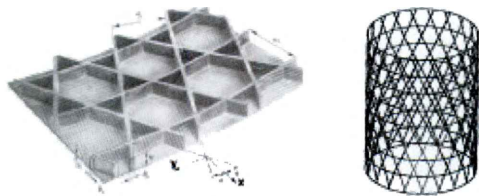
FIG. 7

The anisogrid lattice structures cylindrical configuration

Table I
The anisogrid lattice structure mass (*M*) in function of the employed material

MATERIAL	Al 2024	Hs/Ep	Hs/Ep +5% CN
YOUNG'S MODULUS [Pa]	70E9	12E10	16E10
MASS [Kg]	206.3	84.1	69.7

The dispersion of the nanometric powder in a polymeric matrix (epoxy resin) are studied. In Fig. 9 are showed the SEM fracture analysis of a specimen (epoxy resin + powder with carbon nanotubes) mechanically tested. The use of CN improved the mechanical behaviour (the Young's modulus increases).
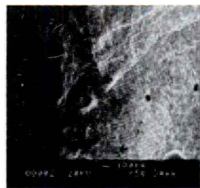
FIG. 8

The SEM fracture analysis of the composite specimen

6. Conclusions

This paper shows how the synthesis and the purification of CN requires a significant improvement (parameters control, reliability) for a real application in advanced Engineering Systems. The microscopy analysis allows to define the morphological characteristics of the synthesized material. Beside, using the Vasiliev model, the reduction of the anisogrid lattice mass was shown, when replacing the traditional aerospace materials (aluminum alloy) with a composite (epoxy resin + unidirectional carbon fibers) carbon nanotubes reinforced.

Acknowledgments

REFERENCES

(1) M. Regi, M. Marchetti, F. Mancia, G. Allegri, *Analisi Sem di Carbon Nanotubes*, Aerotecnica Missili e Spazio, **82** (4), anno 2003.

(2) K. Lau, D. Hui, *The Revolutionary Creation of New Advanced Materials - Carbon Nanotubes Composites*, Composite: Part B, **33**, 263-277, 2002.

(3) V. Vasiliev, V. Barynin, A. Rasin, *Anisogrid Lattice Structures – Survey of Development and Application*, Composite Structures, **54**, 361-370, 2001.

(4) S. Arepalli, P. Nikolaev, O. Gorelik, *Working Toward Nanotube Composite*, Sixth Applied Diamonds Conference/Second Frontier Carbon Technology (Auburn University, July 2001), NASA/CP-2001-210948.

(5) H. Takikama, O. Kusano, T. Sakakibara, *Graphite Spot Produces Carbon Nanotubes in Arc Discharge*, Appl. Phys., **32**, 2433-2437, 1999.

(6) H. Zhang, Y. Ding, C. Wu, Y. Chen, Y. Zhu, Y. He, S. Zhong, *The Effect of Laser Power on the Formation of Carbon Nanotubes Prepared in CO_2 Continuous Wave Laser Ablation at Room Temperature*, Physica, **B325**, 224-229, 2003.

(7) H. Zeng, L. Zhu, G. Hao, R. Sheng, *Synthesis of Various Forms of Carbon Nanotubes by AC Arc Discharge*, Carbon, **36**, 259-261, 1998.

(8) M. Marchetti, D. Cutolo, *Tecnologie Dei Materiali Compositi*, 2a ed., Editoriale ESA 1991.

(9) H. Lange, M. Sioda, A. Huczko, Y.Q. Zhu, H.W. Kroto, D.R.M. Walton, *Nanocarbon Production by Arc Discharge in Water*, Carbon, **41**, 1617-1623, 2003.

GaN HEMT MMIC's:
prospects for space applications and technology issues.

MARCO PERONI (*), ANTONIO CETRONIO (*),
CLAUDIO COSTRINI (*), SIMONE LAVANGA (*),
CLAUDIO LANZIERI (*), PIER FILIPPO MAGRINI (*),
PAOLO ROMANINI (*) LORETTA VENTURELLI (*)

SUMMARY. – *Gallium nitride (GaN) technology is becoming an increasingly interesting candidate for microwave solid-state power amplifiers in the near future, including satellite applications. In addition, since GaN is a wide band gap material, with inherent high breakdown voltage capability, reduced thermal sensitivity and high radiation hardness, making GaN HEMT ideal devices for space environment. However, many issues still need to be overcame to fully exploit the potentials of this technology: Drain current collapse effects are limiting power output and efficiency, and the huge power density dissipation requires adequate thermal management. AMS R&D activity in this field, in cooperation with several Italian academic and research institutes, is concentrating on how to overcome these critical aspects, as will be illustrated in this work.*

1. Device fabrication and physics.

GaN HEMT devices are Field Effect Transistor, with n type channel, obtained by the formation of a two dimensional electron gas (2DEG) at the interface of Gallium Nitride (GaN)/Aluminium Gallium Nitride (AlGaN) layers. This kind of semiconductor material is obtained by epitaxial growth of GaN and AlGaN thin layers (down to few tents of nm), on Sapphire or SiC wafer substrates by using metalorganic chemical vapor deposition (MOCVD) technique.

(*) Alenia Marconi Systems S.p.A., Via Tiburtina Km 12.400 ROMA.

The fabrication procedure involves all the technological steps typically used for GaAs MMIC production (Fig. 1) (1): ohmic contacts formation, for Source and Drain electrodes, active device fabrication via: device isolation by ion implantation or "mesa" etching, and Schottky barrier metallization (Ni/Au) for Gate electrode deposition. Finally, integrated circuit fabrication is completed with the deposition of Silicon Nitride (SiN) film on the device surface for its passivation, as well as metal layers deposition for interconnection, passive lines and elements (i.e. MIM capacitors, inductors etc.).
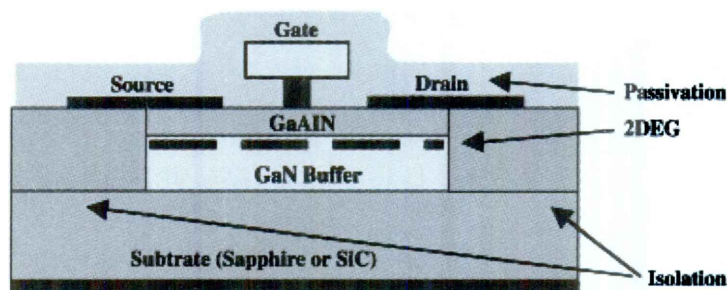
FIG. 1

Schematic cross section of the GaN HEMT active device

With respect to other heterostructures used for epitaxial growth for HEMT wafers fabrication (like GaAs/AlGaAs/InGaAs for GaAs based PHEMTs, or InGaAs/InAlAs for InP based HEMTs), the peculiarity of GaN/AlGaN heterostructures is the presence of a strong lattice polarization at the GaN/AlGaN interface, due to spontaneous and piezoelectric polarization (2). These effects can create a positive interface charge, forming a high concentration 2 DEG ($>1 \times 10^{13}$ cm^{-2}) for the FET device channel, in a much more effective way than doping, thus the semiconductor material used for GaN HEMT fabrication is often completely undoped. Another fundamental aspect of said devices is that they are based on wide bandgap semiconductor materials: GaN forbidden band gap is 3.49 eV, much higher than Silicon (1.1 eV) or GaAs (1.4 eV).

2. Advantages of GaN HEMT for space applications

A direct consequence of the higher bandgap is the superior breakdown voltages. In facts the critical breakdown electric field is for GaN is 3.3 MV/cm, making feasible devices with maximum Drain to Source Voltage exceeding 50 V, while for Si or for GaAs that critical Electric Field is respectively 0.3 MV/cm and 0.4 MV/cm. This aspect, in conjunction with

the higher carrier concentration, contributes to a dramatic increase of the maximum output power density of over one order of magnitude. A comparison between the maximum Drain Voltage, as well as the maximum Drain current, of static characteristics of state of the art GaAs and GaN Power HEMT, shown in Fig. 2, clearly indicates the difference.
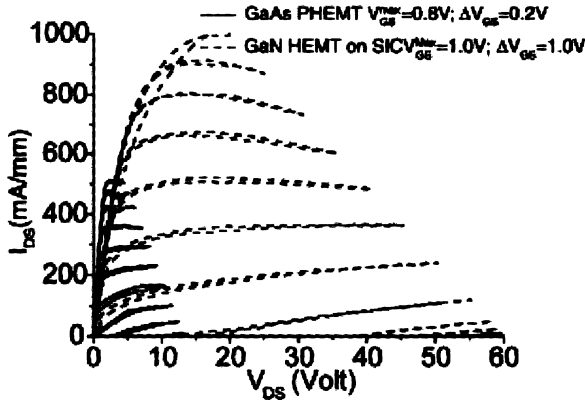
FIG. 2

Example of static charachteristics of GaAs (continuos line) and GaN (slashed line) of state of the art devices (AMS fabrication).

The higher power density, as well as the possibility of GaN HEMT to operate at very high Drain voltage (with respect to GaAs devices), contributes to volume and weight saving of T/R modules, because it allows to reduce MMIC size (for given device output power), and increases the optimal load impedance for maximum output power, avoiding the use of transformers for impedance matching with the outer lines. In addition, GaN HEMT's higher operating voltage elimicates or reduces the need of using DC-DC power conversion.

All these aspects has major impact on the total system cost, because they simplify the modules fabrication, and the lower weight and size on board of the satellites have an important positive influence on the launcher cost.

Another consequence of the high bandgap, is the higher isolation of the substrate even at high environment temperatures: the low intrinsic carrier density is directly related to the bandgap energy E_G via the equation

$$n_i = \sqrt{N_C \times N_V} \times \exp\left(-\frac{E_G}{kT}\right)$$

where N_C and N_V are respectively the conduction and valence density of states. This is a very important aspect for satellite applications, because of the on-board large thermal excursion. However this does not eliminate the

devices temperature sensitivity, because of the lower electron mobility at higher temperatures, and consequent Drain current reduction, that must be taken in account, and eventually compensated, during circuit design phase. In any case, this technology allows to fabricate devices operating at temperatures higher than 250°C.

Another critical requirement of microwave devices in the space environment is the radiation hardness, because of the higher exposition to cosmic rays. Also in this aspect GaN HEMT reveals its advantages with respect to GaAs or Si devices (3).

GaN HEMT devices are also attractive for small signal high frequency amplification and low noise utilization. In facts, in spite of the lower 2 DEG low field mobility (less than 2000 cm²/Vs vs. 8000 cm²/Vs), these devices offer good performances up to the higher microwave range (4), with good noise figure performance in comparable to GaAs devices (5). In addition, thanks to the high breakdown voltage and the higher barrier, GaN HEMTs guarantee height input signal robustness, avoiding the requirement of input protection circuitry, which normally limits the low noise performances of GaAs or InP HEMT MMICs.

Regarding reliability of GaN HEMT devices, in spite of the inherent robustness of the material GaN, long-term failure test still has to demonstrate the expected higher operating lifetime of these devices (6).

3. Critical issues on fabrication aspects and thermal management.

In the recent years the progresses of GaN HEMT has been rapid and significant, both in material fabrication or in thin film processing. However, in order to fully exploit the potential of this technology, need to several issues be solved.

One of the major problems concerns the so called "Drain current collapse" phenomena: it basically consist on the reduction of the Drain output current and knee voltage increase under RF and/or pulsed input signal, from what is expected from static measurements. This problem consequently reduces the output power of the device, as well as its power added efficiency (7). The characteristics in Fig. 3 shows a consequence of this effect: the drain current I_{DSS} at $V_{GS}=0$ Volt is reduced to 25% of the static conditions, if measured with a 80μs pulse from the quiescent bias point $V_{GS}=-20V$. After a Silicon Nitride (SiN) dielectric deposition on the device surface, it is observed that the pulsed I_{DSS} is the 50% of the static I_{DSS}, showing that the SiN presence on top the device surface can be beneficial for the problem, even though the phenomenom is not completely eliminated.
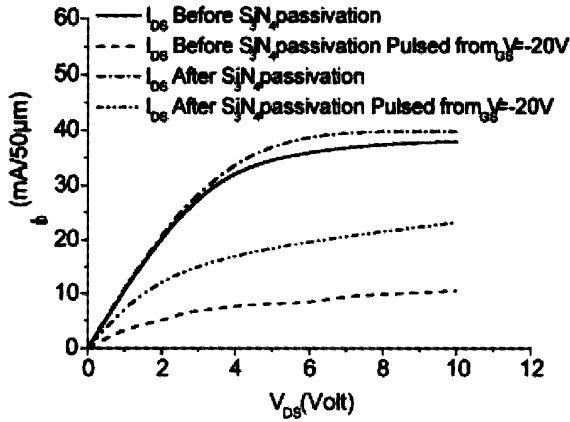
FIG. 3

Comparison of I_{DSS} at $V_{GS}=0V$, in static conditions and after 80μs Gate pulse from $V_{GS}=-20V$ quiescent bias, before and after SiN deposition on the device surface.

The origin of this effect is related to the presence of carrier traps on the semiconductor surface, above the extrinsic device channel, that are charged by Gate and Drain bias. This contributes to carrier depletion between the Gate and the Source/Drain electrodes, increasing the parasitic access Source and Drain resistances, if compared to the static conditions (8,9), since during the fast RF or pulsed Gate modulation, because of the much slower carrier emission/capture times, the trapping surface states remains charged without following the modulation.

With the increase of power density, thermal management become a much more important issue: the potential power density increase of more than one order of magnitude cannot be transformed in equivalent device absolute power boost without adequate heat sink generated by the active device, since the reduction of mobility can decrease significantly devices performances.

Thanks to the higher thermal conductivity of SiC (3.3 Watt/cm °C) with respect to sapphire substrates (0.35 Watt/cm °C), it provides a much better thermal dissipation via the chip backside. However, SiC substrates are much more expensive with respect to Sapphire, and are often highly defective. Thus, if sapphire or other more economic (but with less thermal conductivity) substrates should be used, other approaches should be considered to provide better thermal dissipation. One of the most attractive solutions could be flip-chip approach (10), it consists in contacting the device by bonding the Au or AuSn bumps present onto the device chip and external substrate (i.e: AlN for example, an excellent material for heat dissipation), as schematically shown in the pictures in Fig. 4.
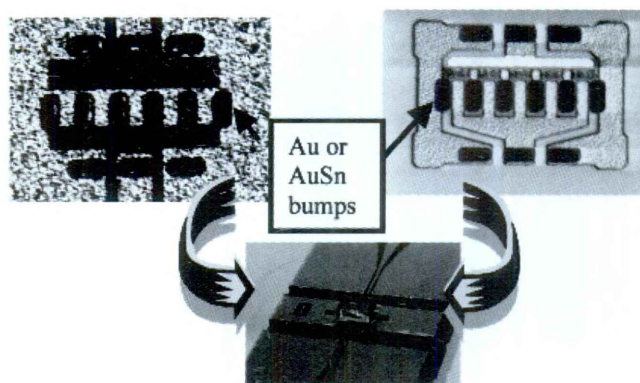
FIG. 4

Schematic picture of GaN HEMT device flip chip bonding: A) AIN sustrate;
B) GaN HEMT chip; C) Flip-chip assembly

Since the bumps are close to the heat source represented by the device channel, they can effectively work as heat sink: thermal simulations, confirmed by photocurrent monitor of channel temperature associated to bandgap variation measurements (11), shows that a reduction of a factor four in thermal resistance can be achieved from substrate to flip-chip bonding (134 °C/Watt vs. 34 °C/Watt).

It's worth to mention that flip-chip mounting also has advantages on the microwave and mm-wave circuit design by lowering the parasitic inductances of the module, while the transparency of SiC or Sapphire substrates allows the visual inspection of the flip-chip mounted device (a mandatory requirement for space applications).

4. Conclusions

GaN HEMT devices represent a new disruptive technology for most future microwave systems requirements. To date, physical and electrical properties of GaN HEMTs, can better respond to the features required by space applications than any other semiconductor device. Consequently, the advantages in terms of space systems performances as well as system cost impact largely compensate the higher cost of technology development and device fabrication. Before fully exploiting the potentials of these devices, thus reaching the maturity for the applications, progress must be reached in fabrication processing and thermal management.

Acknowledgments

REFERENCES

(1) U.K. MISHRA, P. PARIKH, YI-FENG WU, *AlGaN/GaN HEMTs-an overview of device operation and applications*, Proc. IEEE, **90** (6), 1022–1031, June 2002.

(2) O. AMBACHER, B. FOUTZ, J. SMART, J.R. SHEALY, N.G. WEIMANN, K. CHU, M. MURPHY, A.J. SIERAKOWSKI, W.J. SCHAFF, L.F. EASTMAN, *Two dimensional electron gases induced by spontaneous and piezoelectric polarization in undoped and doped AlGaN/GaN heterostructures*, J. Appl. Phys., **87** (1), .334-344, Jan. 1ˢᵗ, 2000.

(3) B.D. WHITE, M. BATAIEV, L.J. BRILLSON, B.K. CHOI, D.M. FLEETWOOD, R.D. SCHRIMPF, S.T. PANTELIDES, R.W. DETTMER, W.J. SCHAFF, J.G. CHAMPLAIN, U.K. MISHRA, *Characterization of 1.8 MeV Proton Irradiated AlGaN/GaN Field-Effect Transistor Structures by Nanoscale Depth-Resolved Luminescence Spectroscopy*, IEEE Trans. Nucl. Sci., **49**, 2695-2701, 2002.

(4) C. LEE, P. SAUNIER, J. YANG, M. ASIF KHAN, IEEE El. Dev. Lett., Vol. 24, NO. 10, pp.616-618, Oct. 2003.

(5) J.S. MOON, M. MICOVIC, A. KURDOGHLIAN, P. JANKE, P. HASHIMOTO, W.-S. WONG, L. McCRAY, Electronics Letters, **38** (22), Oct. 24ᵗʰ, 2002.

(6) S. YOSHIDA, J. SUZUKI, *High-Temperature Reliability of GaN Electronic Devices*, MRS Internet J. Nitride Semiconductor Res., **5S1**, http://nsr.mij.mrs.org/5S1/W4.8/, 2000.

(7) B.M. GREEN, V. TILAK, V.S. KAPER, J.A. SMART, J.R. SHEALY, L.F. EASTMAN, *Microwave Power Limits of AlGaN/GaN HEMTs Under Pulsed-Bias Conditions*, IEEE Trans. on MTT, **51** (2), Feb. 2003.

(8) S.C. BINARI, P.B. KLEIN, T.E. KAZIOR, *Trapping effects in GaN and SiC microwave FETs*, Proc. IEEE , **90** (6), 1048–1058, June 2002.

(9) T. MIZUTANI, Y. OHNO, M. AKITA, S. KISHIMOTO, K. MAEZAWA, *A study on current collapse in AlGaN/GaN HEMTs induced by bias stress*, IEEE Trans. on Electron Devices, **50** (10), 2015- 2020, Oct. 2003.

(10) J. SUN, H. FATIMA, A. KOUDYMOV, A. CHITNIS, X. HU, H.-M. WANG, J. ZHANG, G. SIMIN, J. YANG, AND M. ASIF KHAN, *Thermal Management of AlGaN–GaN HFETs on Sapphire Using Flip-Chip Bonding With Epoxy Underfill*, IEEE ELECTRON DEVICE LETTERS, **24** (6), 375-377, June 2003.

(11) D. SAVIAN, A. DI CARLO, R. LUGLI, M. PERONI, C. CETRONIO, C. LANZIERI, G. MENEGHESSO, E. ZANONI, *Channel temperature measurement of PHEMT by means of optical probes*; Electronics Letters, **39** (2), 247–248, Jan. 2003.

Nanodiamond-based and other nanostructured carbon materials for spatial technology

SILVIA ORLANDUCCI (*), MARIA LETIZIA TERRANOVA (*),
VITO SESSA (*), MARCO ROSSI (**), FABRIZIO FREZZA (***),
ALESSANDRO CIORBA (***)

SUMMARY – *The fascinating mechanical, chemical, electromagnetic and opto-electronic properties of carbon-based nanomaterials suggest wide potential applications in many technological areas. We are currently exploiting the possibilities offered by the fairly advanced nanotechnology developed in our labs and capable of building diamondoid nanomaterials for components and devices used in spatial technology. In particular we are testing some nano-diamond-based composite layers, as protective coatings for Mo electrode grids of ion-beam extraction systems used in ionic propellers which can control the orbital parameters in small satellites. It is known that in working conditions, the gas propeller ions (mostly Xe) generated inside the extraction apparatus collide with the acceleration grids, producing a process of ion-sputtering which reduces the life-time of the device. A suitable protective coating, combining the properties of diamond should reduce the ion-induced erosion and prolong the working-life of the propellers.*

1. Introduction

Carbon-based nanostructures represent today the most innovative and promising materials to be used in advanced technologies and their development is expected to produce large scientific and economic benefits. The various advanced form of inorganic carbon (nanostructured diamond and diamond-like films, nanocomposites, nanotubes and nanofibres, onions, modified forms of nanographite) present an high interest in many advanced technical realizations, because of the combination of peculiar characteristics.

(*) Dip. Scienze e Tecnologie Chimiche, Università di Roma "Tor Vergata", Via della Ricerca Scientifica, 00133 Roma, Italy.
(**) Dip di Energetica, Università di Roma "La Sapienza", Via A. Scarpa 14, 00161 Roma, Italy.
(***) Dip. di Ingegneria Elettronica, Università di Roma "La Sapienza", Via Eudossiana 18, 00184 Roma, Italy.

In the aerospace technology, nanostructured C-based materials are extremely attractive for their strength and toughness and, at present, are mainly and widely investigated for developing high performance composite nanomaterials. Various electromagnetic applications are also envisaged and additional aerospace applications include flat panel displays, allowing smaller displays to be manufactured that require less power and weigh less than current displays.

In particular, we are working to assess a process for the coating by hard carbon-based films of some components of ion propulsion systems used in spatial technology (1). The working capabilities of such thrusters depend mainly on the functional characteristics of the ion extraction grids. Several studies indicated that one of the most remarkable phenomena which reduce the working-time of the device is the erosion of the acceleration grid caused by ion sputtering (2). The resulting sputtering processes are found to change the overall geometry of the grids by eroding the precisely shaped profile of the hole edges and modifying, as a consequence, the ion extraction capability.

On the other hand, the feasibility to shield the grids by means of suitable coatings is dependent on other properties of the layers, such as thermal and electrical conductivity and thermal expansion. Protective coatings able to meet at the same time also these specific functional requirements (3,4) could be, in principle, realized by incorporating aggregates, clusters or dispersions of metallic nanoparticles into a diamond matrix or by Carbon nanotube-based composite materials.

In this context we tested the possibility to use W-containing nanodiamond films as protective coatings of Mo grids against erosion by accelerated ions. Further investigations regarding the use of single-wall carbon nanotubes in nanostructures meeting this particular functional requirement are in progress.

2. Experiment and Results

The materials that we are currently depositing and investigating can be grouped in three different classes: i) polycrystalline diamond; ii) doped diamond; iii) carbon nanotubes. The deposition experiments are carried out in a hot filament CVD reactor (Fig. 1) connected to a purpose-designed and patented (5) powder-flowing system. The different nanostructured materials are generated by the action of hydrocarbon/hydrogen mixtures activated by a hot-filament and introducing reactant species at controlled delivery rates by a system of gas fluxes.

In order to achieve a suitable protection of Mo grids against ion erosion, we investigated the properties of W-containing diamond films. The deposits were performed on Mo samples obtained from the electrode grids

realized by PROEL-Laben Technologies; the grids are plain Mo plates (diameter: 100 mm; thickness: 1 mm) characterized by a uniform distribution of regularly shaped circular holes (diameter: 1.3 mm; distance between two adjacent holes: 1.4 mm).

The morphological features of the deposits have been investigated by scanning electron microscopy (SEM) and by TEM (Transmission Electron Microscopy); the structural analysis was carried out by high energy electron diffraction (RHEED), using an AEI-EM6G apparatus equipped with a high-resolution diffraction stage and operating at an acceleration voltage of 60 kV.
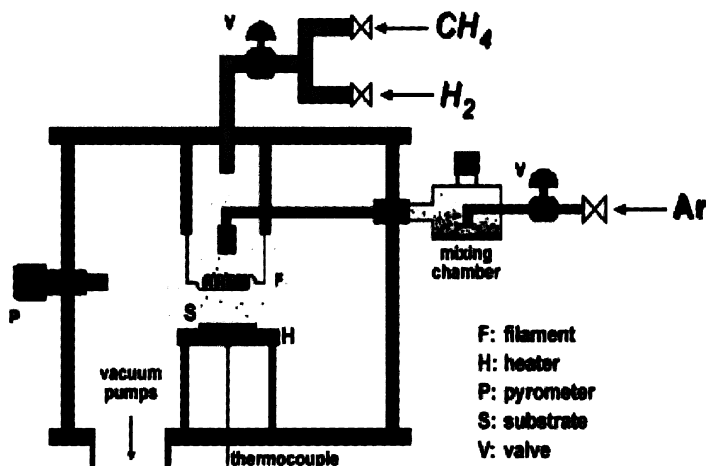
FIG. 1

Schematic drawing of the HF-CVD reactor set up

Ion sputtering experiments have been performed by using a 1 keV Ar+ beam bombarding the target surfaces at an incidence angle of 45°. Sputtering runs lasting up to 10 hours have been performed. The diamond-based layers were not weared out, and consequently the underlying Mo substrates did not result exposed, by sputtering processes lasting up to 10 hours and corresponding to a delivered dose of about 6×10^{19} ions/cm². Secondary electrons energy distributions were recorded on the as-prepared surfaces and on the sputter-eroded surfaces, by a single-pass CMA operating in the first derivative mode, using the coaxial electron gun ($E_p = 3$ keV) as exciting source.

The sample analysis indicated that the better deposits were those produced at 750 °C, with 1% of CH_4, introducing W fine-grained powders carried by N_2 gas flowing at a rate of 30 cm^{-3} min^{-1}. Under these conditions, the SEM analysis revealed that Mo substrates are covered by a continuous and homogeneous polycrystalline layer. The experimental results obtained with the previously described techniques are reported in Figs. 2-6.

Measurements of the conduction properties demonstrated resistivity values at room temperature of the order of $10^{-2}\Omega$ cm (6).

The sputtering yield was evaluated by measuring with a micro stylus profilometer the depth of the erosion craters, and assuming that such valley depth represents an average volume removed per unit area (7). Following this procedure, values of sputtering yields ranging between 0.6 and 0.9 atoms/ion were evaluated for the various coatings.
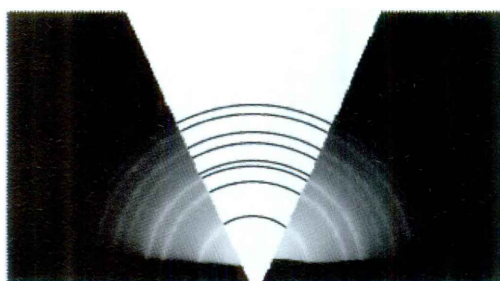
d-spacings		hkl
experimental	ref. data	
2.06	2.0592	1 1 1
1.26	1.2610	2 2 0
1.07	1.0754	3 1 1
1.03		double diffr
0.89	0.8916	4 0 0
0.82	0.8182	3 3 1
0.73	0.7280	4 2 2
0.68	0.6864	5 1 1
0.63	0.6305	4 4 0
0.60	0.6029	5 3 1

FIG. 2

RHEED pattern taken from a typical composite diamond-based film and matching with diamond diffraction pattern calculated on the basis of reference data (8). Measured *d*-spacings (A) and reference interplanar distances are reported for comparison

3. Conclusions

Proper procedures have been selected for the coating of Mo plates and grids by protective diamond films able to improve operational stability of the devices. The main results obtained can be summarized as it follows: *I)* a uniform coverage by W-containing diamond films of both the plain Mo surfaces and the hole edges of the grids has been obtained using an innovative CVD technique; *II)* the inclusion of the metallic species allowed to reduce the resistivity of the coatings up to the required value of about $10^{-2}\Omega$ cm; *III)* the composite coatings were found to withstand at least 10 h of bombardment by an intense 1 keV Ar$^+$ beam; *IV)* the analysis of the secondary electron emission indicated that the emission from the coatings is comparable with that from Mo samples up to incident ion energy of 2 keV, and that at larger energies is mainly due to the direct ion-target collisions.

The unique combination of hardness, adherence and conductivity exhibited by these composite diamond-based materials should find considerable application as sputtering-resistant coatings able to limit premature failure of the propulsion systems. The secondary electron emission meets the current density which can be tolerated for successful operation of the discharge chamber.
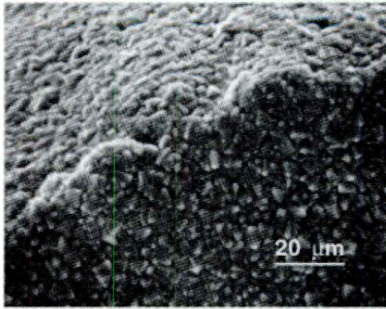
FIG. 3

Tilted-view SEM image showing the edge and the internal wall of a diamond-coated hole of a Mo grid.
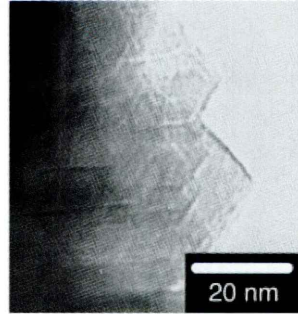
FIG. 4

TEM view of nanosized grains in a diamond film deposited in the same conditions of the sample of Fig. 3.
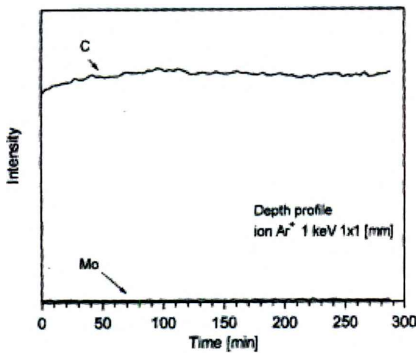
FIG. 5

Auger C(KVV) and Mo (MVV) signals detected during the 300 min lasting sputtering experiments on a composite diamond-based coatings.
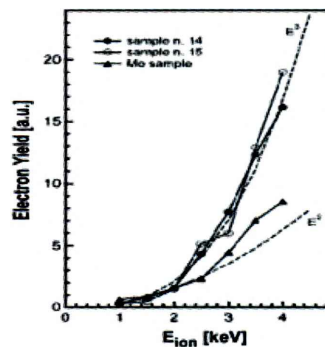
FIG. 6

Secondary electrons yield as a function of the ion energy for two composite films and for a Mo reference sample.

Further investigations are now in progress in order to assess the possibility to achieve a proper functionalization of carbon nanotubes-based composite materials, able to meet the working requirements for accelerating grids resistant to ion-erosion.

REFERENCES

(1) M. ROSSI, G. GABRIELLI, T. PAPA, S. PICCIRILLO, V. SESSA, M.L. TERRANOVA, S. VALERI, M. MATERASSI, Surf. Coat. Techn., **87**, 139, 2001.

(2) C.M. MARRESE, J.E. POLK, J. MUELLER, Mater. Res. Soc. Symp. Proc., **621**, R4.7.1, 2000.

(3) S. LEE, S. LEE, D. JEN, K.R. LEE, J. Vac. Sci. Technol., **B15**, 457, 1997.

(4) J.H. JUNG, B.K. JU, Y.H. JANG, M.H. OH, J. Vac. Sci. Technol., **B17**, 486, 1999.

(5) M.L. TERRANOVA, M. ROSSI, V. SESSA, S. PICCIRILLO, Italian Patent n. 1.301.365, 1999.

(6) M.L. TERRANOVA, V. SESSA, S. PICCIRILLO, M. ROSSI, A. SERRA, Appl. Phys. Lett., **79**, 2007, 2001.

(7) J.J. BLANDINO, D.G. GOODWIN, C.E. GARDNER, Diam. Rel. Mat., **9**, 1992, 2000.

(8) ICDD Diffraction Database.

Giornata di Studio
su

La figura di Giorgio Barzilai
nella ricerca italiana
in elettromagnetismo e in elettronica

15-16 Aprile 2004

Sala del Chiostro, Facoltà di Ingegneria,
Università "La Sapienza" di Roma
Via Eudossiana 18, Roma

Università "La Sapienza" di Roma

Giornata di studio

LA FIGURA DI GIORGIO BARZILAI NELLA RICERCA ITALIANA IN ELETTROMAGNETISMO E IN ELETTRONICA

Sala del Chiostro
Facoltà di Ingegneria, Università "La Sapienza"
Via Eudossiana, 18 - Roma

Ricordo del Professor Giorgio Barzilai,
in occasione della "ultima lezione"
dei Professori
Giovanni d'Auria e Giorgio Gerosa,
che furono
suoi assistenti

Comitato organizzatore
Paolo Bernardi
Paolo Lampariello
Dipartimento di Ingegneria Elettronica

Con il patrocinio di

SIEm ◆IEEE ◆URSI ITeS AEIT

15-16 aprile 2004

INDICE

Presentazione

Il convegno "La figura di Giorgio Barzilai nella ricerca italiana in elettromagnetismo e in elettronica" si è tenuto presso la Facoltà di Ingegneria dell'Università "La Sapienza" di Roma i giorni 15 e 16 aprile 2004 allo scopo di ricordare la figura e l'opera del prof. Giorgio Barzilai, il fondatore dell'allora Istituto di Elettronica della nostra Università, uomo di straordinarie qualità scientifiche e umane, che non pochi di voi hanno avuto la fortuna e l'onore di conoscere personalmente. Egli è stato pioniere delle attività di ricerca in Italia in settori scientifici e tecnologici cruciali per lo sviluppo della società moderna, l'elettromagnetismo e l'elettronica.

Tale convegno è stato organizzato nel quarantesimo anniversario dacché Giorgio Barzilai assunse la carica di Direttore dell'Istituto di Elettronica e inoltre vicini a commemorare i vent'anni dalla sua scomparsa. Se si tratta di un vuoto personale impossibile da colmare, tuttavia la tristezza è attenuata dalla constatazione che, dopo circa vent'anni, a partire da lui e attraverso i suoi discepoli, i germogli delle sue idee e attività sono cresciuti ramificandosi e dipanandosi ormai in molte Università italiane. È una felice coincidenza inoltre che in questi mesi i suoi due primi discepoli, Giorgio Gerosa e Giovanni d'Auria, abbiano completato il loro ciclo di insegnamento presso il nostro Ateneo e, per l'occasione, hanno svolto la loro "lectio magistralis".

L'impostazione del convegno ha seguito proprio il fluire delle varie generazioni di studiosi e ha consentito di riflettere su come siano cambiate nel tempo le modalità del lavoro di ricerca e di didattica.

Riteniamo che conoscere e meditare sulla vita e l'opera del prof. Barzilai possa essere anche un'importante "lezione" per le giovani generazioni di ricercatori che si affacciano ora, in tempi meno pionieristici ma non meno difficili, alle sfide che tali affascinanti discipline presentano intatte. La tempra dell'uomo inoltre era tale da non trovarsi così facilmente al giorno d'oggi, come sicuramente è emerso dalle vive testimonianze di coloro che più da vicino l'hanno frequentato.

Il Convegno, organizzato dal Dipartimento di Ingegneria Elettronica dell'Università "La Sapienza" di Roma ha avuto il patrocinio dell'*IEEE Central and South Italy Section*, della Società Italiana di Elettromagnetismo, del Centro Interuniversitario MECSA, dell'*URSI (Union Radio Scientifique*

Internazionale) – Commissione italiana, dell'AEIT-ASTRI, Gruppo Specialistico di Elettromagnetismo.

Sono riportati di seguito il curriculum vitae, scritto di suo pugno, e le pubblicazioni del prof. Barzilai. Seguono tre brevi testimonianze del prof. Giorgio Franceschetti, del prof. Franco Giannini e del prof Roberto Sorrentino. Concludono una galleria fotografica del Convegno, e alcune poesie scritte da Giorgio Barzilai.

Paolo Bernardi, Paolo Lampariello
Università "La Sapienza" di Roma

Curriculum vitae e pubblicazioni di Giorgio Barzilai

GIORGIO BARZILAI

Il curriculum vitae del professor Giorgio Barzilai è stato diviso in quattro periodi: 1935-1941, attività dopo la laurea fino alla seconda guerra mondiale; 1941-1946, attività durante la guerra; 1946-1954, attività in Gran Bretagna e negli Stati Uniti; 1954-1986, attività in Italia presso l'Università di Roma.

1935-1941. Il professor Giorgio Barzilai nacque il 23 giugno 1911 e si laureò nel 1935 in Ingegneria Industriale presso l'Università di Roma. Dopo la laurea lavorò per un anno presso l'industria elettromeccanica romana MATER. Successivamente fu presso il laboratorio radio del Ministero delle Poste. Presso questo laboratorio progettò e realizzò diversi strumenti elettronici per uso di laboratorio. Egli si occupò anche di trasmettitori di potenza e relativi sistemi di antenne. Su incarico dell'allora direttore generale Amm. Pession, trasformò la stazione sperimentale costruita dalla Marconi a Fiumicino per le comunicazioni con la Sardegna, in stazione ad onde corte per le comunicazioni commerciali con la Libia e l'Africa orientale. Durante tale periodo fu nominato vice-direttore del centro sperimentale Guglielmo Marconi a Torrechiaruccia (Civitavecchia), dove lavorava lo stesso Marconi. Presso questo centro eseguì ricerche sulle antenne e sulla propagazione delle onde radio. Collaborò alla costruzione di un'apparecchiatura per la misura delle costanti del suolo.

1941-1946. Allo scoppio della guerra egli fu richiamato come soldato semplice, nominato tenente delle armi navali per meriti scientifici, e successivamente tenente del GARI (Genio Aeronautico Ruolo Ingegneri) avendo vinto il relativo concorso per esami. Fu quindi chiamato a Guidonia presso la Divisione Radio della DSSE (Direzione Superiore Studi Esperienze).

Presso tale Divisione egli fu principalmente interessato nella costruzione di radar sia di avvistamento (lunga portata) sia di bordo per autosiluranti e caccia. Si occupò anche del disturbo dei radar nemici e contribuì all'installazione di diverse apparecchiature in Sicilia.

Dopo l'armistizio (8 settembre 1943) lasciò Roma e raggiunse l'Aeronautica Italiana a Bari. Nel gennaio 1944 fu invitato per due mesi a Londra

dall'Air Force inglese, come esperto italiano in radar.

Al suo ritorno dall'Inghilterra fu alla Divisione Comunicazioni dell'Aeronautica italiana e fu inviato in diversi aeroporti dove si occupò dell'installazione, sia a terra che a bordo di caccia e bombardieri americani che gli alleati avevano dato all'Italia, di apparecchiature radio. Durante questo periodo egli portò a termine alcune ricerche teoriche sulle antenne e sulla propagazione.

1946-1954. Durante questo periodo il Prof. Giorgio Barzilai è stato quasi sempre all'estero in Inghilterra e negli USA. Nel 1946 vinse una borsa di studio per ricerche sulle microonde e si recò, per un anno solare, presso l'Università di Birmingham, Inghilterra. Presso questa Università egli eseguì ricerche teoriche sulle antenne e sulla ricezione "diversity" a microonde a quei tempi particolarmente importanti.

Un lavoro sperimentale sulla misura della distribuzione di corrente a carico sulle antenne cilindriche fu uno dei primi del genere e fu accolto con molto favore dagli specialisti del campo.

A conclusione di tali ricerche ottenne dall'Università di Birmingham il diploma di "Master of Science in Electrical Engineering".

Nel 1948, ritornato in Italia, ottenne la libera docenza in Radiotecnica. Nel giugno dello stesso anno si recò, prima a Schenectedy e poi a Syracuse, N.Y., USA per conto della Magneti Marelli come ingegnere di collegamento tra la General Electric e la suddetta società, che era licenziataria dei brevetti G.E. per apparecchiature elettroniche.

Terminata l'associazione con la Marelli, fu assunto dal Polytechnic Institute of Brooklin, N.Y. con la posizione di Assistant Professor e successivamente di Associate Professor. Presso il Polytechnic insegnò corsi in Elettronica, transistori nei circuiti lineari, Antenne e Teoria Elettromagnetica. Presso il "Microwave Research Institute" del Polytechnic eseguì ricerche per conto della Navy e della Air Force.

1954-1986. Ritornato in Italia fu assunto dalla Fondazione Ugo Bordoni dove si occupò di ricerche in elettronica ed elettromagnetismo insegnando un corso di microonde.

Istituito presso la Facoltà di Ingegneria dell'Università di Roma il corso di Elettronica, ne ottenne l'incarico come professore esterno.

Nel 1957 vinse il concorso di Elettronica applicata bandito dall'Università di Padova e fu chiamato a Roma per coprire la cattedra di elettronica. In seguito essendo stato istituito il corso di Campi elettromagnetici e circuiti ne ottenne l'incarico come professore interno.

Durante questo periodo egli ottenne un contratto con la Air Force americana per lo studio teorico della propagazione delle onde elettromagnetiche nelle guide d'onda con ferrite magnetizzata. Tale contratto ebbe la durata complessiva di dieci anni e finì nel 1967 perché gli americani ridussero in modo drastico i contratti di ricerca che avevano con i laboratori scientifici europei.

Nel 1964 fu nominato direttore dell'Istituto di Elettronica, posizione che mantenne fino al 1970 quando dette le dimissioni per dedicare più tempo alla didattica e alla ricerca. Tuttavia nel 1972 riprese la direzione dell'Istituto fino al 1978, quando rassegnò ancora le dimissioni per le stesse ragioni di cui sopra.

Nel 1974 chiese e ottenne il trasferimento alla cattedra di Campi elettromagnetici e circuiti della Facoltà di Ingegneria dell'Università di Roma.

Durante i semestri invernali del 1976, 1977 e 1978 fu inviato dall'Università di Roma, tramite il Ministero degli Esteri, per insegnare Fisica ed Elettrotecnica presso l'Università Nazionale Somala a Mogadiscio.

Per nove anni e fino al 1985 egli è stato Presidente della Commissione italiana URSI (Union Radio Scientifique Internazionale) e ne fu membro fino alla sua morte.

Il primo gennaio 1978 fu nominato Fellow dell'IEEE (Institute of Electrical and Electronic Engineers) e nel 1985 ricevette una medaglia del centenario dell'IEEE in Italia, presso l'Accademia Nazionale dei Lincei dal Presidente dell'Istituto in riconoscimento dei servizi prestati nel nostro Paese in relazione alla fondazione della Sezione Centro-Sud Italia.

Il professor Barzilai è autore di 40 pubblicazioni scientifiche, 3 brevetti e 2 libri didattici.

Dopo aver brevemente riassunto il curriculum vitae, sembra più opportuno entrare in qualche dettaglio relativo a quelle ricerche che sembrano essere le più significative della sua produzione scientifica.

Tali ricerche riguardano essenzialmente le antenne e la propagazione delle onde elettromagnetiche. Un primo gruppo di lavori riguarda infatti le antenne [1-6]. Nel lavoro [2], che a suo tempo destò un certo interesse, si è cercato di dare una sistemazione, con qualche soluzione originale, a tutto quel materiale, allora alquanto impreciso, che riguardava la progettazione delle antenne a "dipoli" e dei loro sistemi di alimentazione. Sui metodi indicati in tale lavoro si è basata la costruzione di sistemi irradianti per le comunicazioni con la Libia e l'Etiopia.

Un argomento che si ricollega a quanto sopra riguarda il calcolo teorico dell'influenza mutua dei vari dipoli fra loro e ciò è riportato nel lavoro [5], insieme a calcoli relativi a casi pratici.

Allo studio teorico della propagazione delle onde ultracorte, strettamente legato alla progettazione dei sistemi trasmittenti e riceventi, si riferiscono i lavori [4] e [6] che hanno dato origine al brevetto n. 1.

Un argomento molto importante dal punto di vista scientifico era la determinazione sperimentale della distribuzione di correnti su un'antenna irradiante, che fu oggetto di studi teorici importanti da parte di Hallen (Svezia), Bawcourf (Olanda) e Icing (USA).

La pubblicazione [8] tratta appunto di questo argomento. Tale lavoro

è il primo del genere ma purtroppo, terminato nel 1947, fu pubblicato solo nel 1949. Tutte le apparecchiature per questa ricerca furono costruite personalmente dall'autore presso l'Università di Birmingham (Inghilterra).

Negli USA, con l'eccezione del lavoro [9], che tratta un argomento circuitale, tutte le altre ricerche riguardano le antenne e la propagazione delle onde elettromagnetiche.

Le ricerche teoriche riguardano l'indagine di questioni delicate come il "paradosso" che deriva dal fatto che, assumendo una distribuzione sinusoidale di corrente (in contrasto con le condizioni al contorno sulla superficie di un'antenna) si ottengono valori molto vicini a quelli misurati.

I lavori successivi riguardano principalmente la propagazione delle onde elettromagnetiche in guide d'onda riempite con ferrite magnetizzata. Tali strutture sono importanti per i componenti a microonde.

In questo campo il lavoro forse più significativo è quello relativo al cosiddetto "paradosso termodinamico". Esitono strutture costituite da guide d'onda parzialmente riempite con una lastra di ferrite magnetizzata appoggiata ad una parete che consentono la propagazione dell'energia in un solo senso. Se tali strutture vengono chiuse ad un'estremità, non potendo l'energia tornare indietro, sembra verificarsi una violazione del principio di conservazione dell'energia.

Si è realizzato un esperimento utilizzando vernici termoreversibili, e si è mostrato come l'energia ritorna sempre nel sottile strato, che in pratica non può essere annullato, che esiste tra la superficie della ferrite e quella della guida metallica [35].

Un altro gruppo di ricerche è relativo ai cristalli liquidi. Lo scopo della ricerca era di realizzare visualizzatori molto rapidi, così da poter essere usati in televisione. I brevetti n. 2 e n. 3 si riferiscono a questo argomento.

Le ultime ricerche riguardano la propagazione delle onde elettromagnetiche nell'atmosfera. A tale scopo fu realizzato un collegamento tra il terrazzo della Facoltà e Trevignano, nelle vicinanze del lago di Bracciano, della lunghezza di circa 20 km.

L'esperienza durò parecchi anni e fu iniziata con frequenze di 10 GHz.

Uno degli scopi era di studiare la struttura del fronte d'onda e la coerenza di esso mettendolo in relazione con l'ora del giorno e altri parametri. Tali esperimenti furono successivamente estesi a frequenze di 30 GHz.

ELENCO DELLE PUBBLICAZIONI

L. Sacco, G. Barzilai, *Sulla misura delle costanti elettriche del suolo alle altissime frequenze*, Rassegna delle Poste e delle Telecomunicazioni, fasc. 9, settembre 1940.

G. Barzilai, *Aerei direttivi a dipoli e loro sistemi di alimentazione*, Rassegna delle Poste e Telecomunicazioni, fasc. 1/3/5, gennaio-marzo-maggio 1941.

G. Barzilai, B. Peroni, *Considerazioni sulla irradiazione delle antenne*, Ricerca scientifica e ricostruzione, n. 5/6, giugno 1946.

G. LATMIRAL, G. BARZILAI, *Osservazioni sulla propagazione delle onde ultracorte*, Alta Frequenza, XVI, 3/4, 147, giugno-agosto 1947.

G. BARZILAI, *Mutual impedance of parallel aerials*, Wireless Engineer, nov. 1948.

G. Barzilai, G. Latmiral, *Diversity Reception in U.S.W. Radio Links*, Wireless Engineer, dic. 1948.

G. BARZILAI, B. PERONI, *Antenna*, Enciclopedia Treccani, App. I, 1947.

G. BARZILAI, *Experimental determination of the distribution of current and charge along cylindrical antennas*, Proc. of the IRE, **37**, luglio 1949.

G. BARZILAI, *Network Response to frequency pulse modulated wave*, Research Report R-299-52, PIB-238 27/3/53, Office of Naval Research, Pol. Inst. of Brooklyn.

G. BARZILAI, *Radiation from antennas with sinusoidal current distribution*, Research Report R-335-53, 11/9/53, Pol. Inst. of Brooklyn.

G. BARZILAI, *Field strength computations for an antenna situated over a homogeneous spherical earth*, Final Report R-341-53, PIB-276, Contract AF-30 (062-387), Task B2 30/9/53, Pol. Inst. of Brooklyn.

G. BARZILAI, *On the input conductance of thin antennas*, Proc. of the IRE, **AP-3**, 1, Genn. 1955.

G. BARZILAI, *Su una definizione intrinseca dell'operatore Nabla*, Piccole note, Recensioni e Notizie Ist. Sup. PP.TT., luglio-agosto 1955.

G. BARZILAI, *Radiation from aerials*, Wireless Engineer, agosto 1955.

G. BARZILAI, *Metodo di calcolo per la conduttanza di antenne cilindriche*, Alta Frequenza, XXIV, 4-5, agosto-ottobre 1955.

G. BARZILAI, *Admittance of thin antennas*, IRE Trans. On Antennas and Propagation, **AP-4**, aprile 1956.

G. BARZILAI, *Definizione della forza cimomotrice*, Piccole note, Recensioni e Notizie, n. 6, 1956.

G. BARZILAI, *Sulla registrazione automatica dei diagrammi di direttività delle antenne*, Atti del Congresso Scientifico-Sez. Elettronica, vol. II, III Rass. Internazionale Elettronica Nucleare, 1956.

G. BARZILAI, *Sulla misura delle caratteristiche dinamiche dei termistori*, Note, Recensioni e Notizie, n. 3, maggio-giugno 1957.

G. Barzilai, C. Montebello, F. Serracchioli, *Sul diagramma di radiazione del paraboloide in varie condizioni di illuminazione*, IV Rassegna Internazionale Elettronica Nucleare-luglio 1957.

G. BARZILAI, G. GEROSA, *Modes in rectangular guides filled with magnetized ferrite*, Rapporto Interno, Istituto Elettrotecnico dell'Università di Roma, ottobre 1957.

G. BARZILAI, G. GEROSA, *Modes in rectangular guides filled with magnetized ferrite*, Il Nuovo Cimento, Serie X, 7, 685-697, marzo 1958. Pubblicato anche su: l'Onde Electrique, Suppl. Spec. 38e année, 376 ter, 612-617, agosto 1958.

G. BARZILAI, G. GEROSA, *Properties of ion-filled waveguides*, Proc. of the IRE, **47**, 1, 83, gennaio 1959.

G. BARZILAI, G. GEROSA, *Modes in rectangular guides partially filled with transversely magnetized ferrite*, Istituto Elettrotecnico dell'Università di Roma-Contract AF 61 (052), 101 Techn. Note n. 1, 3 giugno 1959.

G. BARZILAI, G. GEROSA, *Modes in rectangular guides partially filled with transversely magnetized ferrite*, IRE Trans. on AP, **AP-7**, Special Supplement, S471-S474, dicembre 1959.

G. BARZILAI, G. GEROSA, *Modes in rectangular guides loaded with a transversely magnetized slab of ferrite away from the side walls*, Istituto di Elettronica dell'Università di Roma-Contract AF 61 (052), 101 Techn. Note n. 2, 30 luglio 1960.

G. BARZILAI, G. GEROSA, *An exact modal solution for a rectangular guide loaded with longitudinally magnetized ferrite*, Istituto di Elettronica dell'Università di Roma-Contract AF 61 (052), 101 Techn. Note n. 3, 2 gennaio 1961.

G. BARZILAI, G. GEROSA, *Research on propagation of electromagnetic waves in guides loaded with magnetized ferrite*, Contract AF 61 (052), 101, Techn. Summary Report n. 2, 19 maggio 1961.

G. BARZILAI, G. GEROSA, *Modes in rectangular guides loaded with a transversely magnetized slab of ferrite away from the side walls*, IRE Trans. on MTT, **MTT-9**, 5, 403-408, settembre 1961.

G. BARZILAI, G. GEROSA, *Modes with complex propagation constant in rectangular guides loaded with transversely magnetized lossless ferrite*, Istituto di Elettronica dell'Uni-

versità di Roma-Contract AF 61 (052), 101 Techn. Note n. 5, 20 giugno 1962.

G. BARZILAI, G. GEROSA, *A modal solution for a rectangular guide loaded with longitudinally magnetized ferrite*, in: E.C. Jordan, *Proc. of the Symposium on Electromagnetic theory and antennas*, Copenaghen, June 25-30, 1962, Pergamon Press, 1963, 573-590.

G. BARZILAI, "Antenna", Enciclopedia Treccani, App. II, 1963.

G. BARZILAI, G. GEROSA, *Propagation of electromagnetic waves in rectangular guides loaded with magnetized ferrite*, Istituto di Elettronica dell'Università di Roma, 1964.

G. BARZILAI, G. GEROSA, *Propagation of electromagnetic waves in rectangular guides loaded with magnetized ferrite*, Istituto di Elettronica dell'Università di Roma-Contract AF 61 (052), 101 Final Techn. Report, 11 marzo 1964.

G. BARZILAI, G. GEROSA, *Rectangular waveguides loaded with magnetised ferrite and the so-called thermodynamic paradox*, Proc. of the IEE, vol. n. 2, febbraio 1966.

F. BARDATI, G. BARZILAI, G. GEROSA, *Elastic waves excitation in piezoelectric slabs*, IEEE Trans. on Sonics and Ultrasonics, **SU-4**, ottobre 1968.

G. BARZILAI, P. MALTESE, C.M. OTTAVI, P. REALI, *Microsecond pulse activated liquid crystal cells*, Rapporto interno, Istituto di Elettronica, giugno 1972.

G. BARZILAI, P. MALTESE, C. M. OTTAVI, P. REALI, *Fast liquid crystal cells suitable for television display*, 1972 IEEE Conference on Display Devices, New York, N. Y., 11-12 ottobre 1972.

G. BARZILAI, *Research on statistical aspects of tropospheric propagation*, Radio Science, **10**, 7, luglio 1975.

G. BARZILAI, *Antenna*, Enciclopedia Treccani, App. III, 1980.

Libri

(1) G. BARZILAI, *Lezioni di Elettronica Applicata*, Siderea, Roma.
(2) G. BARZILAI, *Fondamenti di Elettromagnetismo*, Siderea, Roma.

Brevetti

(3) G. LATMIRAL, G. BARZILAI, *Dispositivi per ridurre le evanescenze e le distorsioni nei collegamenti con onde cortissime tra punti elevati sul suolo*, Ministero dell'Industria e del Commercio, Roma, Italia, 420.709.

(4) G. BARZILAI, C.M. OTTAVI, P. MALTESE, P. REALI, *Perfezionamento negli schermi, per la presentazione di immagini, del tipo a cristalli liquidi adatti in particolare per immagini televisive e/o dati alfanumerici*, Brevetto italiano n. 965.475, data di accettazione 31/1/1974. Questo brevetto è stato esteso ai seguenti paesi: Argentina, Belgio, Canada, Francia, U.K., Israele, Spagna, Svizzera, U.S.A.

(5) G. BARZILAI, C.M. OTTAVI, P. MALTESE, *Cella ad intercapedine e procedimento per ottenerla*, Brevetto Italiano n. 1.015.905, data di accettazione 20/5/1977. Questo brevetto è stato esteso ai seguenti paesi: Belgio, Canada, Francia, U.K., Israele, U.S.A.

Un ricordo lontano, ma non svanito

GIORGIO FRANCESCHETTI (*)

Quanto sto per ricordare è accaduto negli anni '60: a livello accademico i "Campi elettromagnetici" sarebbero nati come "Campi elettromagnetici e circuiti", dove "Campi elettromagnetici" erano intesi come una appendice di "Circuiti", questi ultimi rigorosamente a costanti concentrate. E questo dovunque, tranne che in pochissime sedi universitarie, da contare sulle dita di una mano sola: in particolare a Roma, all'Università, e a Napoli, presso l'Istituto Universitario Navale. E presso quest'ultima sede, di fronte al porticciolo da cui si dipartono i vaporetti per Capri, si riunivano, ogni due o tre mesi, due gruppi di studiosi, aggregati intorno a due figure leggendarie: i professori Giorgio Barzilai e Gaetano Latmiral. Tra questi e il gruppo dei più giovani (tra i quali inizialmente Giorgio Franceschetti e successivamente Paolo Lampariello, Roberto Sorrentino e qualche altro) c'era poi il professor Giorgio Gerosa, in una veste di sacerdote intermedio tra le due divinità e il gruppo dei fedeli. E noi, i fedeli, ascoltavamo, con qualche timido intervento, i discorsi dei due mitici professori, che vertevano su argomenti esaltanti. In particolare, ricordo Barzilai che presentava il paradosso di modi che si propagavano attenuandosi in un verso in guide con ferrite magnetizzata senza perdite; e Latmiral che cercava di darne spiegazione, invocando le condizioni di fisica realizzabilità connesse al modello della ferrite, e la non consistenza con le relazioni di Kramers-Koenig. E Gerosa, il grande sacerdote, ogni tanto dispiegava tabelle immense di calcoli, ottenute facendo girare primordiali calcolatori a schede perforate... Ricordi meravigliosi, di un tempo vivo, ma irrimediabilmente lontano. E sarei certamente disposto ad azzerare quel pochissimo che ho costruito, per poter tornare a quel tempo magico, e sentire le voci di Latmiral e Barzilai, e occhieggiare i tabelloni di Gerosa, ed essere mentalmente sollecitato, e discutere timide ipotesi con Lampariello e Sorrentino, e pensare, pensare, pensare... Non v'è dubbio che questi ricordi fan parte integrante della mia vita, e ho voluto dividerli con tutti voi.

(*) Professore di Campi elettromagnetici, Università di Napoli "Federico II"

Giorgio Barzilai

FRANCO GIANNINI (*)

Mi sono laureato con Giorgio Barzilai che, già allora, era *Il Professore*, senza altri aggettivi.

Era circondato infatti da tale deferenza da parte di tutte le altre persone dell'Istituto, che sembrava nato per incutere soggezione in chi lo contattasse.

La sua storia personale, il fatto di essere stato uno dei primi professori ordinari di Elettronica, ed uno dei pochi allora in Italia, lo rendeva naturalmente *diverso* dagli altri, sicché, per molti mesi i miei contatti con lui furono assolutamente inesistenti e comunque solo tramite Cesare Ottavi, che seguiva giornalmente i lavori della mia tesi sperimentale. Persino durante la discussione della tesi, ricordo, era il mio relatore e non gli altri membri della commissione che mi mettevano soggezione.

Il primo vero contatto con Giorgio Barzilai fu, perciò, subito dopo la laurea quando (su impulso di Cesare Ottavi, come seppi più tardi) mi chiese di restare nell'Istituto di Elettronica.

Passarono così i miei primi mesi da giovane laureato, per la verità non molto diversi da quelli che avevo passato da laureando, ed i contatti si limitarono, al di là di alcuni casuali incontri nei corridoi, a quelli relativi alle prime sedute d'esame cui partecipai come "esperto della materia", a poche battute cioè, che non cambiarono assolutamente il mio atteggiamento nei suoi confronti.

La svolta nei nostri rapporti personali avvenne solamente un anno dopo, nel 1969.

Da sempre Settembre è il mese delle conferenze scientifiche ed in quell'anno se ne svolgevano due in Inghilterra: una ,la European Microwave Conference a Londra, l'altra la Solid State Device Conference ad Exeter.

Ebbene, il solito Cesare aveva ottenuto per me l'autorizzazione a partecipare ad entrambe, visto che si svolgevano in due settimane successive e

(*) Professore di Elettronica, Università di Roma "Tor Vergata"

gli argomenti erano vicini ai nostri interessi scientifici, ma il supporto economico per una sola delle due, la seconda, più affine alle mie attività di ricerca. Restava inteso che avrei partecipato alla prima a mie spese.

Così sarebbe avvenuto se, durante il weekend tra le due conferenze, il Professore non avesse chiesto ad Adelio Salsano, Cesare Ottavi ed al sottoscritto di accompagnarlo in macchina in un viaggio a Lemington Spa, al centro dell'Inghilterra.

Alla domanda "chi di voi sa guidare?" rispose affermativamente e con sicurezza Cesare Ottavi. Non sto a raccontare cosa combinò. Ricordo solo un tamponamento e la successiva discussione in una lingua sconosciuta con un camionista gallese alquanto sovraeccitato.

Ebbene, sarà stato lo scampato pericolo, non l'incidente ma l'incontro ravvicinato con il camionista, ovvero la forzata permanenza per alcune ore nell'automobile, ma qualcosa cambiò nei miei rapporti con Giorgio Barzilai.

Il resto del viaggio infatti fu particolarmente piacevole e, rotto il ghiaccio, ebbi il mio primo colloquio vero con lui.

In verità, avrei voluto parlare delle mie "scoperte" con l'entusiasmo tipico del giovane ricercatore, visto che avevo la fortuna di avere a disposizione tempo ed attenzione di tanto interlocutore, ma il discorso prese subito altra piega. Furono due ore di chiacchiere sugli Inglesi, sulle loro abitudini, specie sul loro pessimo modo di mangiare e, soprattutto, sulla sua passione per il Golf che, a quanto capii, ero l'unico nell'Istituto di Elettronica a non conoscere.

Arrivati a destinazione il Professore continuava a sapere molto poco della mia attività scientifica. Io, in compenso, avevo imparato a capire qualcosa di più sul suo modo disincantato di vedere la vita e, lo scoprii più tardi, avevo superato il mio primo vero esame accademico, guadagnando la simpatia del mio Capo.

A proposito, la sera a cena, Cesare mi comunicò che il Professore aveva deciso di non farmi pagare più le spese sostenute a Londra.

Ricordo di Giorgio Barzilai

ROBERTO SORRENTINO (*)

Premessa

Vorrei ringraziare Paolo Bernardi e Paolo Lampariello per questa iniziativa di commemorazione di Giorgio Barzilai.

Nell'ansia e nella concitazione della vita quotidiana, particolarmente nel periodo oscuro e drammatico che stiamo vivendo, siamo troppo spesso indotti a guardare al presente e all'immediato futuro, dimenticando di considerare il passato, di valutarlo quale esperienza che ha determinato la condizione presente e condiziona i giorni avvenire.

È l'occasione per un esercizio di memoria teso a far riemergere la figura umana e scientifica di Giorgio Barzilai: è un'esperienza utile per tutti noi, non una mera ricerca documentaria, ma una ricerca dentro noi stessi, è l'esperienza di ritrovare in ciascuno di noi il pezzo di eredità che Giorgio Barzilai ha lasciato, con la sua attività, le sue opere, e soprattutto con la sua umanità.

Siamo qui a commemorare e ricordare la figura di Giorgio Barzilai, a ricostruirla attraverso la pluralità delle singole esperienze che ciascuno di noi ha vissuto, in un collettivo e personale esercizio di memoria che ha valore per ciascuno di noi. La mia personale esperienza di lui è quella di un uomo che ha amato la vita profondamente a dispetto delle traversie patite, con spirito di umanità, di comprensione e di tolleranza. Valori questi che tanto più necessari sentiamo in questi giorni drammatici per il mondo.

Sono pertanto convinto che questo incontro tra coloro che Giorgio Barzilai hanno conosciuto e amato, nel far rivivere la sua figura, varrà proprio come insegnamento per noi tutti, per prendere coscienza dei semi che il suo insegnamento ha gettato e dei valori che ci ha lasciato in eredità, affinché la nostra vita non sia travolta dall'incalzare degli avvenimenti, ma sia più consapevole della forza dei valori fondamentali che soli possono darle senso.

(*) Professore di Campi Elettromagnetici, Università di Perugia

Ricordo di Giorgio Barzilai

Un signore, amante del vivere e del mangiare, si trovava a cena, ospite di un amico in una lussuosa casa di campagna in Inghilterra. Terminato il lauto pasto, mentre conversavano piacevolmente sorseggiando del Cognac e assaporando un buon sigaro, scoppia una tempesta violentissima tale da rendere rischioso il rientro in città. L'ospite accetta quindi di passare la notte a casa dell'amico, sistemandosi per dormire sul divano dello studio. Verso le due del mattino, il tale si sveglia per una necessità e, nel buio completo, comincia a cercare con le mani gli occhiali e un lume. Le sue dita incontrano, appoggiato sulla scrivania, un bicchiere di acqua, che rovesciandosi gli bagna la mano. Comincia allora a tastare le pareti della stanza alla ricerca dell'interruttore della luce, che finalmente trova. Quando la luce si accende, l'amico realizza che il bicchiere era in realtà un calamaio: la parete rivestita di parati era tutta imbrattata di manate di inchiostro. Di fronte a tanto disastroso spettacolo, disperato, le mani nei capelli, si lascia cadere a peso morto sulla poltrona. Si ode un lieve squittio smorzato. Sulla poltrona dormiva, ormai per sempre, il cane pechinese dell'amico inglese. Senza più speranza di riscatto, il tale si rivestì in fretta, e fuggì per la finestra nella notte tempestosa.

Questa è un storia, raccontatomi come autentica, da Barzilai. Ho voluto cominciare così il mio contributo, perché credo che essa caratterizzi bene un aspetto della sua personalità. Sono diverse le storielle e barzellette che amava raccontare, e lo faceva con un tale gusto e una vivacità cordiale che, pur ora, conservo nettissimo il ricordo del suo sorriso divertito e gioviale.

Io ho avuto meno di altri colleghi intrinsecità con Barzilai. Credo tuttavia di poter cogliere nella mia esperienza una faccia di lui, una porzione di una personalità certo complessa, piena e interessante.

Il mio ricordo di lui è soprattutto questo: la sua personalità giocosa, il suo humour, la sua bonomia, la sua curiosità, il suo sano senso della vita. Nel rammentare questa gustosa storiella, che lui raccontava come autentica, ma se lo fosse o meno non importa, a distanza di tanti anni, rivedo con nitida lucidità il suo sorriso divertito, mi par quasi risentire la sua voce. Questo ricordare le persone con tanta vivezza è un fenomeno non comune, che attiene evidentemente alla sua spiccata "presenza" nell'interlocutore, alla sua simpatia.

Conobbi Barzilai da studente, nel 1969. Seguii, oltre a quello di Elettronica I, il suo corso di Campi em e circuiti (così si chiamava allora), che mi affascinò, benché lo trovassi il più difficile del mio curriculum di studi (o forse proprio per questo). Non fummo in molti, in verità, ad arrivare in fondo al corso. Si determinò, così, una speciale confidenza tra Barzilai e i

pochi allievi che continuarono a seguire, quasi un circolo ove si stabilì un legame di simpatia quasi cameratesca e goliardica. Partecipava a quel gruppo Patrizia Basili, e la non comune presenza femminile dava forse un brio particolare a un ambiente di norma quasi esclusivamente maschile.

Le lezioni avevano un carattere tutt'altro che accademico, scorrevano con un tono quasi confidenziale, ravvivate di molti connotati aneddotici, con il tono di un amico che ti mette a parte dei problemi ma non ti impone una soluzione. In quel fare semplice e diretto, senza enfasi e senza retorica stava il fascino della sua personalità.

All'esame mi volle porre una domanda a piacere. Gli presentai uno degli argomenti più complicati sul quale mi ero scervellato, il calcolo dell'effetto ai bordi nel condensatore piano tramite la trasformazione di Schwarz-Christoffel. Dopo la mia esposizione, Barzilai si volle divertire ponendomi un quesito che era una sorta di quiz-paradosso, sul quale egli stesso si era dilettato fino a un attimo prima con i suoi assistenti. Si trattava del mancato bilancio energetico di un condensatore che viene caricato istantaneamente da una batteria ideale tramite chiusura di un tasto. Mi persi completamente. A differenza di molti professori universitari, egli era ben alieno dal godere delle difficoltà dello studente, e mi elargì ugualmente un 30 e lode.

Certamente a lui devo il mio interesse per l'elettromagnetismo. Come spesso avviene, sono i primi incontri quelli che determinano le scelte della nostra vita.

Mi piace ancora ricordare un episodio agli inizi della mia carriera. Nel 1979 mi recai per la prima volta a un congresso internazionale (MTT-S) negli USA, a Orlando, Florida. Lì incontrai, inaspettatamente, il prof. Barzilai e Pietro De Santis, che allora lavorava in Selenia, e che era stato, per quel che so, il primo laureato in Microonde del prof. Gerosa, con il quale allora lavoravo. A quel tempo, come ogni giovane ricercatore, coltivavo l'ambizione di sperimentare un'attività di ricerca in America. In quell'occasione Barzilai mi procurò diversi contatti, mi fece conoscere il prof. Oliner, visitammo insieme i laboratori della Comsat. Ma non poté mancare una visita a Disney World! Il buon De Santis, che disponeva di una vettura a nolo pagata da Selenia, fu ingaggiato per accompagnarci. Barzilai montò sulla macchina con una sua borsa da golf, provvista di mazze e tutti gli accessori, che doveva spedire non so dove, per la quale operazione girammo diversi Post Office alla ricerca di uno che accettasse di spedire la borsa a destinazione, con il povero De Santis che non sapeva dove andare a sbattere. Dopo di che andammo a DisneyWorld. Giugno in Florida non è la migliore stagione. Visitammo non so più quanti padiglioni, giostre e amenità varie, con Barzilai che ci incalzava dall'uno all'altro, finché De Santis, stremato, non ce la fece più e supplicò un ritiro, mentre Barzilai, tranquillo e sereno avrebbe continuato non so ancora per quanto!

Non posso terminare questa breve serie di ricordi senza rammentare il periodo delle "sedute spiritiche", perché esso rappresenta un'altra faccia

della complessa e per certi versi contraddittoria personalità di Barzilai.
Verso la fine della sua carriera, convinto dell'esistenza di fenomeni che
sfuggono alla normale comprensione scientifica, egli fu preso di interesse
per lo studio dei fenomeni paranormali e volle tentare di applicare una
metodologia scientifica sperimentale per verificarne l'effettiva esistenza. Or-
ganizzò pertanto, con una cerchia di collaboratori in rapporto di più stretta
confidenza, una serie di incontri nella presidenza dell'istituto. Io mi trovai a
partecipare ad alcune di queste riunioni, armato di una curiosità venata
ahimè di alquanto scetticismo. Si tentarono diversi esperimenti, essenzial-
mente sulla trasmissione del pensiero, con risultati purtroppo deludenti.
Barzilai era anche questo: una gioia, talora quasi infantile, del ricercare e
del conoscere, senza pregiudizi, aperta all'incanto della natura e delle sue
infinite complessità.

Galleria fotografica (*)

PARTE I
Foto di GIORGIO BARZILAI

FIG. 1

Ritratto di Giorgio Barziali

(*) Le prime foto (FIG. 1-3) qui pubblicate sono state gentilmente concesse dalla famiglia Barzilai, le altre foto (FIG. 4-10) si riferiscono alla Giornata di Studio su "La figura di Giorgio Barzilai nella ricerca italiana in elettromagnetismo e in elettronica" e sono state fornite da Fabrizio Frezza.
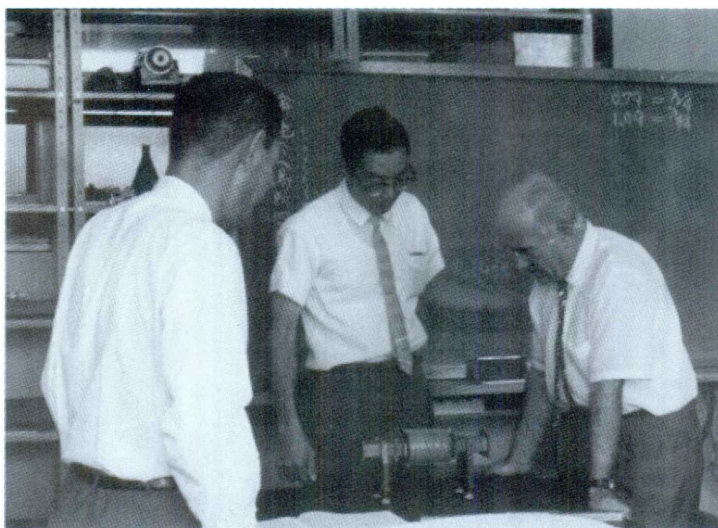
FIG. 2

Il professor Barzilai durante una visita ad un laboratorio giapponese
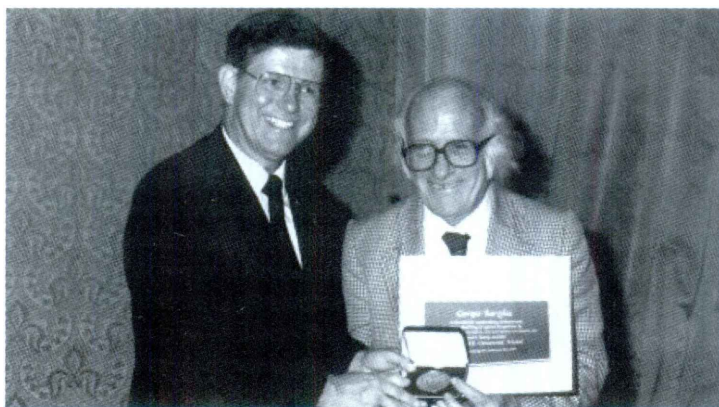
FIG. 3

Cerimonia della consegna della IEEE Centennial Medal da parte
del Presidente dell'IEEE al professre Barziali (1985)

PARTE II
Foto della Giornata di Studio su "La figura di Giorgio Barzilai
nella ricerca italiana in elettromagnetismo e in elettronica".

FIG. 4

Paolo Lampariello e Paolo Bernardi organizzatori
della Giornata di Studio su "La figura di Giorgio Barzilai
nella ricerca italiana in elettromagnetismo e in elettronica"

FIG. 5

Dalla prima generazione di allievi del Prof. Barziali.
Da sinistra: Cesare M. Ottavi, Paolo Bernardi, Giovanni d'Auria
e Giorgio Gerosa (Università di Roma "La Sapienza")

FIG. 6

Dalla seconda generazione di allievi del Prof. Barzilai. Da sinistra: Franco Giannini (Università di Roma "Tor Vergata" e Presidente del Gruppo "Elettronica"), Paolo Lampariello (Università di Roma "La Sapienza"), Roberto Sorrentino (Università di Perugia e Presidente della Società Italiana di Elettro magnetismo) e Patrizia Basili (Università di Perugia)

FIG. 7

Il Prof. Giovanni d'Auria durante la sua *lectio magistralis*

FIG. 8

Il Prof. Giorgio Gerosa durante la sua *lectio magistralis*

FIG. 9

Piero Marietti (Università "La Sapienza" di Roma), responsabile del Centro Studi "Giorgio Barzilai", che ha anche recitato alcune poesie di Barzilai.

FIG. 10

Foto di gruppo di alcuni partecipanti alla Giornata di Studio su "La figura di Giorgio Barzilai nella ricerca italiana in elettromagnetismo e in elettronica"

Poesie

Il professor Barzilai si è dedicato anche alla poesia. Sono qui riportate alcune sue composizioni, tratte dal volume "... a tempo perso" (Siderea, Roma, 1982), pubblicato con lo pseudonimo di "Zirba". Le prime tre poesie sono state recitate dal professor Piero Marietti durante la Giornata di studio. Seguono altri tre componimenti, di argomento "scientifico".

Punti de vista (luglio 1971)

Lo so che se comporta male Nina,
m'hai da pensa' che quella cià trent'anni
e Checco è tutto pieno de malanni
e ha superato già la settantina.

Certo capisco che sarebbe mejo
che nun cambiasse tanto de frequente,
farebbe chiacchiera' meno la gente
e l'interesse resterebbe svejo.

Ma invece tu lo sai quer che m'ha detto:
"S'io restassi fedele a mi' marito
farei contento solamente Checco,

Se invece accetto un po' de spasimanti,
lui nun lo vie' a sape', chè 'n po' svanito,
e restano contenti tutti quanti."

La Bellezza (giugno 1972)

I

'Na vorta 'n omo disse a 'n pipistrello:
"Ammazzete però quanto sei brutto,
me pari 'n sorcio invece d'un ucello,
co' quer pelaccio che te copre tutto.

Fai proprio schifo, co' quer corpo mollo,
pe' nun fatte vede' voli de notte
e dormi appennolone come 'n pollo
de giorno rintanato ne 'le grotte.

Ma chi lo sa perché madre natura
assieme a 'na bestiaccia come te
ha fatto la farfalla, 'na cratura
che co' l'ali dorate in faccia ar sole
pare proprio che dica: guarda me,
pe' la bellezza mia 'n ce so' parole!"

II

"Amico", j'arispose er pipistrello,
"a parte che me pari 'n po' villano,
ma dimme 'n po' indove ciài er cervello
che ce dovrebbe ave' 'n essere umano?

Tu dichi quant'è bella la farfalla?
ma hai mai provato tu a pija' 'na lente
e mettete co' quella a riguardalla?
vedrai che de bellezza 'n c'è più gnente,

c'è solo 'n verme brutto più de me.
Ma 'n'hai capito amico mio frescone
ar monno la bellezza si che d'è?

somija molto a la felicità
solo a distanza te dà l'iilusione
ma appena t'avvicini se ne va".

Er Serpentello Velenoso (luglio 1981)

Mentre che 'n serpentello velenoso
se stava a fa 'na pennica in un prato,
poco mancò che nun restò acciaccato
da n'omo che passava frettoloso.

"Ma li mortacci tua" disse er serpente,
"ma guarda 'ndo cammini, disgraziato!",
e già pe' mozzicallo era sartato
che se fermò; "ma nun m'ha fatto gnente,

e poi a rifa' er veleno me ce vò".
Ma l'omo s'era accorto der serpente
je dette 'na serciata e lo schiacciò.

"Mi madre me diceva: fijo mio"
mentre moriva j'arivenne in mente,
"nun sparagnà er veleno der bon Dio".

L'Università (novembre 1971)

Ar tempo mio, quann'ero 'no studente
e frequentavo l'Università,
te rimbambivi tanto pe' studia'
che questo era er pensiero della gente:

Diceva che quer sito era 'n palazzo
dove, contrariamente a quanto avvie' in amore
entrava 'n omo pieno de vigore
pe' usci' 'na testa...co' la rima in azzo.

Ma mo, co' 'sta conquista democratica
che fa entra' tutti all'Università,
le cose so' diverse ne' la pratica

ch'è facile pija 'na cantonata
che puro co' la bbona volontà
poi confonne l'uscita co' l'entrata.

L'Elettronica (aprile 1982)

La chiamano elettronica pe' via
ch'a falla funziona' so' l'elettroni;
e in un qualunque ordigno che se pija
te la ritrovi sempre fra i cojoni.

Ma tu pensa: se 'n giorno 'st'elettroni,
scocciati d'esse sempre controllati,
se svortassero contro li padroni
doppo d'ave' ricorso ai sindacati.

Li telefoni, i treni, l'ospedali,
l'aeroprani, le banche, li partiti,
se fermerebbe tutto, e molti mali
po' esse che sarebbero finiti.

Infatti, nonna mia sai che m'ha detto,
quanno che je spiegai 'sti ritrovati:
"È questo 'n caso" dice "te l'ammetto
che darebbe ragione ai sindacati".

La Scenza (maggio 1982)

Tu voi sape' da me che d'è la scenza?
È n'intrujo de cose inciafrujate
che l'omo faticanno s'è create
pe' dà a 'sto monno 'na logica parvenza.

Perché, capischi, l'omo pe' natura,
ha da spiegasse quello che cià 'ntorno
e questo lo capisco, ma oggi giorno
co' li progressi de la scenza pura

S'è montato la testa e mo' se crede
puro capace de 'nventa' la vita,
ma spesso la conquista che nun vede

è che scoprenno un po' de verità
mejo capisce quanto sia infinita
'sta meraviglia e quanto poco sa.

Seconda Giornata di studio
su

Il metodo degli elementi finiti nelle applicazioni dell'ingegneria elettrica e dell'informazione

Genova, 3-4 Giugno 2004

Salone del piano nobile di Villa Giustiniani-Cambiaso,
Facoltà di Ingegneria, Università degli Studi di Genova,
Via Montallegro 1, 16145 Genova

INDICE

Preface

In the last decade the research activity in the field of computational electromagnetics was impressive. In the same period the finite element method has become one of the numerical techniques most widely used in different engineering areas. Among these, particular interest has been devoted to the area of Electrical and Information Engineering, which includes Computer Engineering, Biomedical Engineering, Electronics, Electromagnetic Engineering, Automation Engineering and Telecommunications. Even though several commercial simulators based on the finite element method are now available, the interest on the theory and applications of this method has even grown and several research groups have devoted their efforts to these topics.

In this context, this workshop, which follows the first initiative dedicated to the "Application of the finite element method to Electrical and Information Engineering" held in Cassino on April 19-20, 2001, was meant to expand the scenario by involving researchers working on both theory and applications of the finite element method. The aim was not only to provide and overall review on the state-of-the-art on the research developments and applications of the finite element method, but also an opportunity to discuss and compare different experiences.

The workshop lasted two days, which were dedicated to the presentation and discussion on the results of the research activities currently involving the finite element method in Italy. The aim was to point out the interests and the experiences which are common to the different research areas. Besides, our purpose was also to support the possible establishment and strengthening of useful collaborations among the involved research groups.

Our attention has been devoted to both theoretical and practical aspects. In particular, three tutorials and three scientific sessions were devoted, respectively, to the theoretical aspects of interest in Electrical/Electromagnetic Engineering, to the Electrical Engineering applications and to the Electromagnetic Engineering applications.

Beside the aforementioned initiatives, the workshop allowed the academic researchers to discuss how to integrate the most significant aspects of the research on computational electromagnetics and, in particular, on the finite element method as applied to Electrical and Information Engineering, in the university curricula.

Salvatore Caorsi
University of Pavia

Some considerations on the finite element approximation of time-harmonic electromagnetic boundary value problems

ANA MARIA ALONSO RODRIGUEZ (*), SALVATORE CAORSI (**),
PAOLO FERNANDES (°), MIRCO RAFFETTO (°°)

SUMMARY. – *Some recent developments make it possible to state some general results on the convergence of the finite element approximation to the solution of time-harmonic electromagnetic boundary value problems. In particular, the main target of this paper is to provide some considerations on such results when metamaterials and when different types of boundary conditions are involved.*

1. Introduction

A lot of electromagnetic problems of practical interest, such as those considered in the study of the behaviour of microwave components or in the analysis of radiation devices or even in electromagnetic scattering, are formulated as time-harmonic boundary value problems, especially when all materials involved in the problem can be considered as linear.

The finite element method (FEM) is one of the most widely used approaches to approximately solve problems as those indicated above. For this reason, in the last decade several research groups have devoted their efforts to the study of the properties of this method and, in particular, on its reliability.

In this paper we provide an overview of the recent developments which make it possible to state some results on the convergence of the

(*) Università di Trento, Dipartimento di Matematica, Via Sommarive 14, 38050 Povo, Trento, Italy
(**) Università Studi di Pavia, Dipartimento di Elettronica, Via Ferrata 1, 27100 Pavia, Italy
(°) Istituto di Matematica Applicata e Tecnologie Informatiche, C.N.R., Via De Marini 6, 16149 Genova, Italy
(°°) Università di Genova, Dip. Ingegneria Biofisica ed Elettronica, Via all'Opera Pia 11a, 16145 Genova, Italy

finite element approximations even when metamaterials and/or different types of boundary conditions are involved.

2. The electromagnetic boundary value problem of interest

Since we are interested in providing results on the convergence of the FEM solution for general electromagnetic boundary value problems our starting point is

$$
[1] \quad
\begin{cases}
\operatorname{curl} H(r) - j\omega\underline{\underline{\varepsilon}}(r)E(r) = J_e(r) & \text{in } \Omega \\
\operatorname{curl} E(r) + j\omega\underline{\underline{\mu}}(r)H(r) = -J_m(r) & \text{in } \Omega \\
H(r) \times n(r) = \overline{F}_n(r) & \text{on } \Gamma_v \\
E(r) \times n(r) = F_d(r) & \text{on } \Gamma_\tau \\
H(r) \times n(r) - \underline{\underline{Y}}(r)\big(n(r) \times E(r) \times n(r)\big) = F_r(r) & \text{on } \Gamma_b
\end{cases}
$$

where Ω is the open, bounded and connected domain of the problem, $\Gamma = \Gamma_v \cup \Gamma_\tau \cup \Gamma_b$ is its Lipschitz continuous boundary, $n(r)$ is the outward unit vector normal to Γ, $\underline{\underline{Y}}(r)$ is the complex matrix-valued admittance involved in impedance boundary conditions, $\underline{\underline{\varepsilon}}(r)$ and $\underline{\underline{\mu}}(r)$ are the effective (1) permittivity and permeability tensor, respectively, $\overline{J}_e(r)$ and $J_m(r)$ are the electric and the magnetic current densities, respectively, and $F_n(r)$, $F_d(r)$ and $F_r(r)$ are the known terms involved in the boundary conditions on the electric field, on the magnetic field and of impedance type, respectively.

3. The finite element approximation

The finite element approximation of the above continuous problems is deduced from the variational formulation of the problem itself. To skip some technical details necessary to write it (2) we denote by V the appropriate Hilbert space and by V_b the corresponding finite dimensional subspace of V obtained by using a finite element together with a particular triangulation of Ω identified by the usual parameter h. We denote by $L_t^2(\Gamma_b)$ the space of "tangential vector fields" on Γ_b (2) and by BC_n and BC_d the spaces to which $F_n(r)$ and $F_d(r)$ belong, respectively (2).

With these hypotheses, the finite element formulation of problem [1] is: Given $\omega > 0$, $J_e(r)$, $J_m(r) \in (L^2(\Omega))^3$, $F_r(r) \in L_t^2(\Gamma_b)$, $F_n(r) \in BC_n$, $F_d(r) \in BC_d$ find $E_b(r) \in V_b$ such that

$$
[2] \quad
\begin{aligned}
&\left(\mu^{-1}\operatorname{curl} E_b, \operatorname{curl} v_b\right)_{0,\Omega} - \omega^2\left(\varepsilon E_b, v_b\right)_{0,\Omega} + j\omega\left(Y\left(n \times E_b \times n\right), n \times v_b \times n\right)_{0,\Gamma} \\
&= -j\omega\left(J_e, v_b\right)_{0,\Omega} - \left(\mu^{-1}J_m, \operatorname{curl} v_b\right)_{0,\Omega} - j\omega\left(F_r, n \times v_b \times n\right)_{0,\Gamma} \quad \forall v_b \in V_b
\end{aligned}
$$

It is important to point out that the above continuous formulation [1] and the corresponding finite element approximation [2] are representative of a huge class of electromagnetic boundary value problems. In Fig. 1 such class of problems is represented by using a Venn diagram.
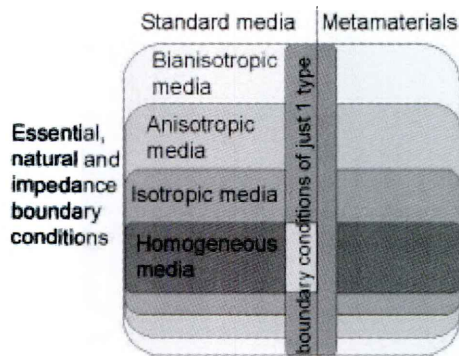

FIG. 1

Venn diagram for the set of all time-harmonic electromagnetic boundary value problems involving linear media. In a problem belonging to the biggest set all linear media and all type of boundary conditions can be involved. Horizontal stripes identify subsets where just particular media can be involved. Vertical stripes identify subsets with restrictions on the possible boundary conditions. A further subdivision is exploited to distinguish between standard materials and metamaterial.

At the end of the last century the only class of problems which was known to be reliably solvable by the finite element method was the one where just homogeneous media and one type of boundary conditions could be involved. Thus just the problems belonging to the small white rectangle in Fig. 1 were reliably solved by the finite element method (actually another small white rectangle should be indicated in Fig. 1 representing the class of problems involving a homogeneous "truly" anisotropic medium)

Thus, five years ago, even for the trivial problem indicated in Fig. 2 there was no indication on the fact that the finite element method was able to find a "converging" approximation.

However, quite recently, the limitation due to the inability to deal with inhomogeneous media was overcome (3). Such a result can even be extended to cover cases where inhomogeneous metamaterials are involved. Moreover, in (4) all limitations connected to the presence of "mixed" boundary conditions were overcome, when the finite element space is generated by using meshes of tetrahedral and edge elements of any order of the first Nedelec family.

Thus, nowadays, the white box of Figure 1 has recently been significantly extended to cover "many" cases of practical interest. Just bianisotropic

medium cannot be dealt with. From a practical point of view, all other classes are almost completely covered. Figure 3 represents schematically the present situation.

FIG. 2

A perfect electric conductor box with an aperture where the tangential components of the magnetic field is enforced. In the box the medium is not homogeneous.
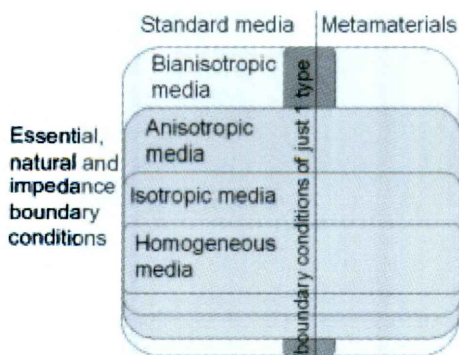

FIG. 3

Venn diagram for the set of all time-harmonic electromagnetic boundary value problems involving linear media. The small white rectangle of Fig. 1 has been significantly extended.

REFERENCES

(1) R.W. ZIOLKOWSKI, N. ENGHETA, *Metamaterial special issue introduction*, **51** (10), 2546-2549, Ottobre 2003.

(2) P. MONK, *Finite Element Methods for Maxwell's Equations*, Oxford Univ. Press, May 2003.

(3) S. CAORSI, P. FERNANDES, M. RAFFETTO, *On the convergence of Galerkin finite element approximations of electromagnetic eigenproblems*, SIAM J. on Numerical Analysis, **38** (2), 580-607, 2000.

(4) M. RAFFETTO, *Discrete compactness for edge elements in the presence of mixed boundary conditions*, SIAM J. on Numerical Analysis, in press.

Elementi finiti di tipo edge per cristalli fotonici

LUCIA GASTALDI (*), DANIELE BOFFI (**)

I cristalli fotonici sono strutture periodiche composte da materieli dielettrici. L'interesse crescente in questo campo è dovuto al fatto che lo spettro dell'operatore di Maxwell per questi materiali presenta dei "gap". La presenza di questi gap significa che ci sono delle frequenze proibite di propagazione delle onde elettromagnetiche attraverso i cristalli. Questo fatto ha molte possibili applicazioni, per esempio, in comunicazioni ottiche, filtri, laser e microonde. Si vedano (3, 4), per un'introduzione ai cristalli fotonici, alla struttura delle bande proibite e ad alcune loro applicazioni.

Usando la teoria di Bloch, il modello matematico può essere scritto nella forma di un problema agli autovalori per le equazioni di Maxwell con condizioni al bordo periodiche, come segue:

$$\nabla_\alpha \times \varepsilon^{-1} \nabla_\alpha \times u = \omega^2 u \quad \text{in } \Omega$$
$$\nabla_\alpha \cdot u = 0 \qquad\qquad \text{in } \Omega$$

dove $\nabla_\alpha = \nabla + i\alpha \, Id$.

Si noti che affinché si presentino delle bande proibite, la costante di permittività ε deve essere costante a tratti e Id è l'operatore identità.

Seguendo (2), abbiamo considerato una modifica degli elementi edge di Nédélec per l'approssimazione dello spettro. Presentiamo un'analisi rigorosa della convergenza, basata su ipotesi minimali sulla regolarità delle autosoluzioni e sulle reticolazioni.

(*) Dipartimento di Matematica, Università di Brescia, Via Valotti 9, 25133 Brescia
(**) Dipartimento di Matematica "F. Casorati", Università di Pavia, via Ferrata 1, 27100 Pavia

Infine, mostriamo alcuni risultati numerici preliminari ottenuti in 2D che confermano la robustezza del metodo.

I risultati qui descritti brevemente sono riportati in (1).

BIBLIOGRAFIA

(1) D. BOFFI, M. CONFORTI, L. GASTALDI, *Modified edge finite elements for photonic crystals* (preprint).

(2) D.C. DOBSON, J.E. PASCIAK, *Analysis of an algorithm for computing electromagnetic Bloch modes using Nédélec spaces*, Comput. Methods Appl. Math., 1(2):138—153, 2001.

(3) J.D. JOANNOPOULOS, R.D. MEADE, J.N. WINN, Photonic crystals: molding the flow of light, Princeton University Press, 1995.

(4) C.M. SOUKOULIS, ed., *Photonic band gap materials*, Kluwer, Dordrecht, 1996.

Metodi Discontinuous Galerkin per le equazioni di Maxwell time-harmonic

ILARIA PERUGIA (*)

Negli ultimi anni si è sviluppato un considerevole interesse, soprattutto nel contesto della fluidodinamica computazionale, nei confronti di metodi agli elementi finiti di tipo "Discontinuous Galerkin" (DG), basati su spazi di approssimazione costituiti da funzioni polinomiali a tratti discontinue alle interfacce degli elementi. Tra i vantaggi che tali metodi presentano, si sottolinea la grande flessibilità nel mesh design, in quanto tali metodi consentono di utilizzare in modo naturale reticolazioni contenenti i cosiddetti "hanging nodes" e gradi di approssimazione non uniformi o non isotropi.

Questa comunicazione riguarda l'uso di metodi DG per l'approssimazione numerica di equazioni di Maxwell time-harmonic. Nel caso di regime di bassa frequenza, si considera un metodo basato su una formulazione di tipo misto del problema, in cui il vincolo di divergenza nulla per il campo elettrico all'interno di mezzi isolanti è imposto mediante l'introduzione di un moltiplicatore di Lagrange. Nel caso di regime di alta frequenza, vengono presentate sia una formulazione nella sola incognita campo elettrico, che una formulazione mista, basata sulla decomposizione di Helmholtz del campo elettrico. Tutti i metodi considerati presentano proprietà ottimali di convergenza, sia in norma dell'energia che in norma L^2.

(*) Dipartiemento di Matematica, Universita' di Pavia, via Ferrata 1, 27100 Pavia, Italy

Singular vector expansion functions for Finite Methods

GUIDO LOMBARDI (*), ROBERTO D. GRAGLIA (*)

ABSTRACT. – *This paper describes the fundamental properties of new singular vector bases that incorporate the edge conditions in curved triangular elements. The bases are fully compatible with the interpolatory or hierarchical high-order regular vector bases used in adjacent elements. Several numerical results confirm the faster convergence of these bases on wedge problems and the capability to model regular fields when the singularity is not excited.*

1. Introduction

Several electromagnetic structures for microwave applications contain wedges or vertices of either penetrable or impenetrable materials. In the vicinity of these geometrical discontinuities the electromagnetic fields and currents could have singular behavior (1-2). These physical quantities reach great values, at worst infinite, although the energy is finite in the region of the singularity. In the scientific literature, several papers deal with singular bases for finite methods, but most of these papers are unsatisfactory. This paper presents some of the results obtained during a pluriennal research activity that concerned the analytical and numerical study of the electromagnetic interactions with structures including wedges. We have defined new singular vector bases for numerical codes based on the finite element method or on the moment method. The new singular bases are of either polynomial or hierarchical kind and incorporate the edge singularity on curvilinear elements (3-4). These functions are compatible with high-order regular vector functions of either polynomial or hierarchical kind (5-6) and they correctly model the physical behavior as described by Van Bladel and Meixner (1-2).

(*) Dipartimento di Elettronica, Politecnico di Torino- Corso Duca degli Abruzzi 24, 10129 Torino, Italy

Several numerical results confirm the faster convergence of these new singular vector bases (3).
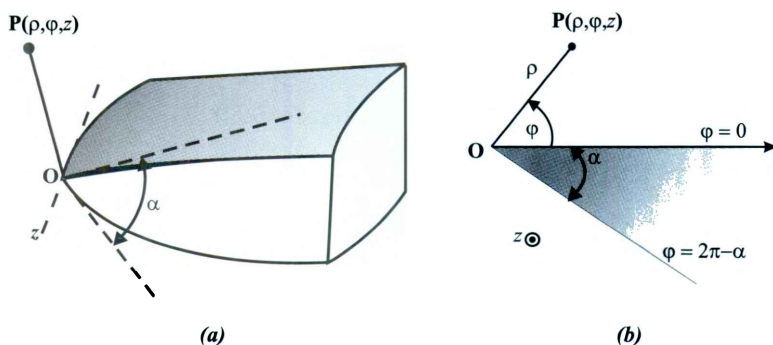
FIG. 1

(a) Cross-sectional view of the region around a sharp but curved wedge of aperture angle α and local longitudinal axis z; (b) Local straight infinite wedge model with aperture angle α and local longitudinal axis z.

[1]
$$J_s = \frac{\nu A}{\rho^{1-\nu}}\hat{z} + j\omega\varepsilon_0 B\rho^\nu\hat{\rho} \pm \mathrm{cons\tan t}\ \hat{\rho}$$

[2]
$$\begin{cases} E_z = j\omega\mu_0 A\rho^\nu\sin\nu\phi \\ H_t = \dfrac{\nu A}{\rho^{1-\nu}}\left(\sin\nu\phi\hat{\phi} - \cos\nu\phi\hat{\rho}\right) \end{cases}$$

[3]
$$\begin{cases} H_z = j\omega\varepsilon_0 B\rho^\nu\cos\nu\phi + \mathrm{cons\tan t} \\ E_t = -\dfrac{\nu B}{\rho^{1-\nu}}\left(\cos\nu\phi\hat{\phi} + \sin\nu\phi\hat{\rho}\right) \end{cases}$$

2. Fundamental properties of the singular bases

We investigated several ways to derive singular and complete lowest-order vector bases. We define singular bases to be lowest-order complete when the following properties are fulfilled:
1. the basis set is complete just to the regular zeroth order, and for curl (or divergence) conforming bases the curl (divergence) of the bases is also complete to regular zeroth order;
2. the singular element is fully compatible to adjacent zeroth-order regular elements attached to its nonsingular edges, and to adjacent singular

elements of the same order attached to the other edges;

3. the basis functions can model the static, $\rho^{\nu-1}$ singular behavior of the transverse electromagnetic fields (curl-conforming case), or of the surface current and charge density (divergence-conforming case), in the neighborhood of the wedge (first term of Meixner's series (2)), ρ being the radial distance from the wedge sharp-edge profile;

4. the curl-conforming bases are able to model a nonsingular transverse field with curl that vanishes at the edge of the wedge as ρ^ν, whereas the divergence conforming bases can model the radial component of the current density that vanishes as ρ^ν at the wedge sharp edge ($\nu \neq 1$ and not integer).

The singular bases reported in (3) contain as a subset the regular p-th order bases given in (5). Only for the elements attached to the edge of a wedge we introduce an irrational algebraic vector subset (Meixner subset) in addiction to the regular basis subset. By using complete interpolatory polynomials of order s, in (5) we make the Meixner subset complete to arbitrary high-order s. Since these new bases are formed by the union of p-th order regular plus an s-th order singular part, there is no need to limit the size of the mesh in the neighborhood of the edge of the wedge. Above all, these new bases permit one to deal with all the cases where the singularity of the fields is not excited.

3. Numerical results and modeling capabilities
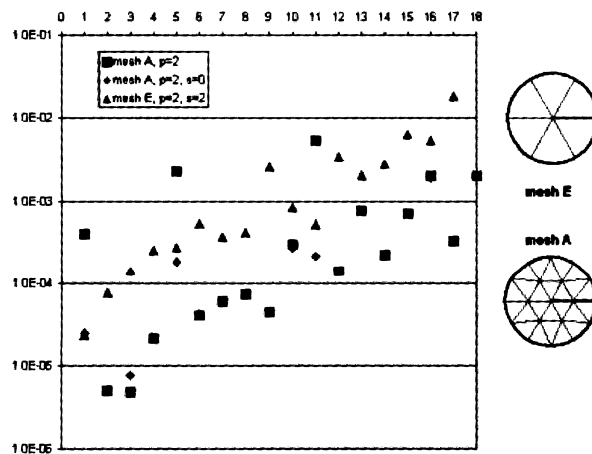
FIG. 2

Fig. 2 reports the relative errors of the computed square value of the longitudinal wavenumber (kz^2) for each of the first eighteen modes of the circular vaned waveguide at $ko^*a = 11$, where a is the WG radius. Errors are reported in logarithmic scale for two different kind of meshes (Mesh A has 24 triangles and mesh E has 6 triangles) and for different kind of bases (regular bases with $p=2$, singular bases with $p=2$ and $s=0$ and finally singular bases with $p=2$ and $s=2$).

Table 1 reports the mean values of the relative errors for the three simulations reported in Fig. 2.

Table 1

	mesh A $p=2$	mesh A $p=2$, $s=0$	mesh E $p=2$, $s=2$
Mean value 1	7.738E-04	8.700E-05	5.542E-04
Mean value 2	1.991E-03	1.088E-04	2.087E-04

"Mean value 1" is the relative error among the first 11 eigenmodes and "mean value 2" is among the first 3 singular eigenmodes.

4. Acknowledgements

REFERENCES

(1) J. VAN BLADEL, *Singular Electromagnetic Fields and Sources*, Clarendon Press, Oxford, 1991

(2) J. MEIXNER, *The behavior of electromagnetic fields at edges*, IEEE Trans. Antennas Propagat., **20**, (4), 442-446, July 1972

(3) R.D. GRAGLIA, G. LOMBARDI, *Singular higher-order complete vector bases for Finite Methods*, IEEE Trans. Antennas Propagat., **52**, (7), 1672-1685, July 2004

(4) R.D. GRAGLIA, G. LOMBARDI, *Hierarchical singular vector bases for the FEM solution of wedge problems*, Proceedings of 2004 URSI International Symposium on Electromagnetic Theory (EMT-S), Pisa, Italy, 834-836, 23-27 May 2004

(5) R.D. GRAGLIA, D.R. WILTON, AND A.F. PETERSON, *Higher order interpolatory vector bases for computational electromagnetics*, IEEE Trans. Antennas Propagat., **45**, (3), 329-342, Mar. 1997

(6) J.P. WEBB, *Hierarchal vector basis functions of arbitrary order for triangular and tetrahedral finite elements*, IEEE Trans. Antennas Propagat., **47**, (8), 1244-1253, Aug. 1999

Alcune proprietà sugli elementi finiti edge, con particolare riferimento alla compattezza discreta

DANIELE BOFFI (*)

Gli elementi finiti più naturali per l'approssimazione di problemi di elettromagnetismo, che fanno riferimento allo spazio funzionale $H(\text{curl})$, sono i cosiddetti elementi finiti di tipo edge. L'analisi teorica di tali elementi ha raggiunto un buon livello di completezza, soprattutto per quanto riguarda le proprietà di approssimazione e la cosiddetta proprietà di compattezza discreta. Quest'ultima proprietà, che è legata all'assenza di modi spuri nell'approssimazione degli autovalori interni di Maxwell, è stata in particolare oggetto di un ampio studio ingegneristico e solo in questi ultimi anni è stato dimostrato rigorosamente, dal punto di vista matematico, che gli elementi edge la verificano con un grado di generalità che copre una vasta gamma di problemi ingegneristici.

Quasi tutte queste dimostrazioni si riferiscono alla versione "h" degli elementi finiti; al caso, cioè, in cui l'unico parametro di raffinamento è collegato al massimo diametro degli elementi. Accanto a questa versione, esiste il metodo "p" (il tradizionale metodo degli elementi spettrali, dove p è legato al grado dei polinomi usati per l'approssimazione) e il più flessibile metodo "hp", capace di coniugare raffinamenti locali in h (più adatti laddove il dominio presenta forti singolarità, come in presenza di angoli o spigoli rientranti) a raffinamenti locali in p (più efficienti in presenza di soluzioni regolari). L'analisi della compattezza discreta per gli elementi edge di tipo "hp" è stato oggetto di studio solo recentemente, utilizza tecniche dimostrative diverse e costituisce un problema ancora aperto nel caso di mesh simplettiche.

Si desidera inoltre portare all'attenzione della comunità ingegneristica il degrado (in certi casi drammatico) delle proprietà di approssimazione degli elementi finiti di tipo edge nel caso di mesh di quadrilateri generici. Diverse soluzioni sono disponibili per risolvere questo problema.

(*) Dipartimento di Matematica "F. Casorati", Universita' di Pavia

Divergent bases for Finite Elements analysis of guiding structures

JURI MASONI (*), GIUSEPPE PELOSI (*), STEFANO SELLERI (*)

SUMMARY. – *This paper presents some preliminary results obtained by defining special bases for the Finite Element solution of the electromagnetic field within a guiding structure section. Said bases exhibits a singularity able to correctly model the physical divergence of the electromagnetic fields in correspondence of a perfectly sharp edge. Numerical results prove the superior behavior of proposed bases.*

1. Introduction

The electromagnetic field in the proximity of a perfectly sharp edge of a wedge assume a singular behaviour (1). Numerical methods, on the other hand, usually model the electromagnetic field by expanding it onto a set of basis functions that are continuous and non-singular, hence yielding to inaccurate modelling for singular fields.

Among the different numerical methods the finite elements method (FEM) is largely used tanks to his versatility and accuracy (2). Since, as stated above, it cannot take into account singularities – in its usual formulation – in a waveguide cross-section, where an edge is present, FEM analyses are usually accomplished by introducing a significant mesh refining in the neighbourhood of the edge, hence greatly increasing the number of degree of freedom used.

New bases – exhibiting singular behavior – can hence be introduced to correctly model the singular field without the need to refine an hence introduce additional degrees of freedom. Some different solutions have been presented in literature, either additive (2, 3), where new singular bases are added on top of existing, regular, elements so as to be able to model the singularity or substitutive (4), where part of the bases of an element are substituted with different, singular, bases.

(*) Department of Electronics and Telecommunications, University of Florence, Via C. Lombroso 6/17, 50134 Florence, Italy

In this paper a new type of singular substitutive bases is introduced, differing from those in (4) in the way they model the curl space, which is the same as in (2).

2. Formulation

The FEM approach used here to compute the modes in a waveguide is the 2.5D one (2), where both the longitudinal and transverse components of the electric (magnetic) field are taken into account. The longitudinal electric field is expanded with conventional scalar bases of order one:

[1] $$\Omega_\beta = \xi_\beta, \qquad \beta = 1, 2, 3$$

being (ξ_1, ξ_2, ξ_3) the simplex coordinates of the triangle (2). The transverse electric field is better expanded with vector curl-conforming bases, to avoid spurious modes. In each triangular element not adjacent to a wedge, and hence far from the singularity, ordinary first order Whitney functions can be used (2):

[2] $$\Omega_\beta = \xi_\beta \nabla \xi_{\beta+1} - \xi_{\beta+1} \nabla \xi_\beta, \quad \beta \text{ cycling on } \underline{1 \to 2 \to 3}$$

Meixner's theory (1) states that the field near a perfectly conducting wedge in free space is singular and the singularity is of the kind $\rho^{\nu-1}$, being ρ the distance from the edge of the wedge. The real number ν depends only on the wedge's geometry; for a perfectly conducting wedge of internal angle α it is $\nu = \pi/2\pi - \alpha$.

To correctly model such singularity the transverse electric field in elements adjacent to the wedge, that is elements having one of their vertices on the edge of the wedge, is expanded with bases exhibiting the same singular behaviour predicted by Meixner theory:

$$\Omega_1^s = \left[\left(1 - \xi_1 \right)^\nu + \nu \xi_1 \right] \Omega_1$$

[3]
$$\Omega_2^s = \Omega_1^s - \left(1 - \xi_1 \right)^{\nu-1} \left[\nabla \xi_3 + \left(1 - \nu \right) \frac{\xi_3}{\left(1 - \xi_1 \right)} \nabla \xi_1 \right]$$

$$\Omega_3^s = \Omega_1^s - \left(1 - \xi_1 \right)^{\nu-1} \left[\nabla \xi_2 + \left(1 - \nu \right) \frac{\xi_2}{\left(1 - \xi_1 \right)} \nabla \xi_1 \right]$$

These three functions replace Whitney functions. The curl of [3] is

[4] $$\nabla \times \Omega_i^s = \frac{2 + \nu}{J} \left(1 - \xi_1 \right)^\nu \hat{n} - \frac{\nu}{J} \left(1 - 3\xi_1 \right) \hat{n} \quad \text{with} \quad i = 1, 2, 3$$

being J the Jacobian of the triangular element mapping. Hence the longitudinal magnetic field is correctly modeled, as in (2).

3. Numerical results

As a first test case a single ridge waveguide is analysed. The geometry is depicted in Fig. 1. If even (odd) modes are sought, a perfectly magnetic (electric) conductor can be inserted in the symmetry plane and only half domain can be analysed. Fig. 1 also reports a very coarse mesh in this half region, used as a starting point for refinement.
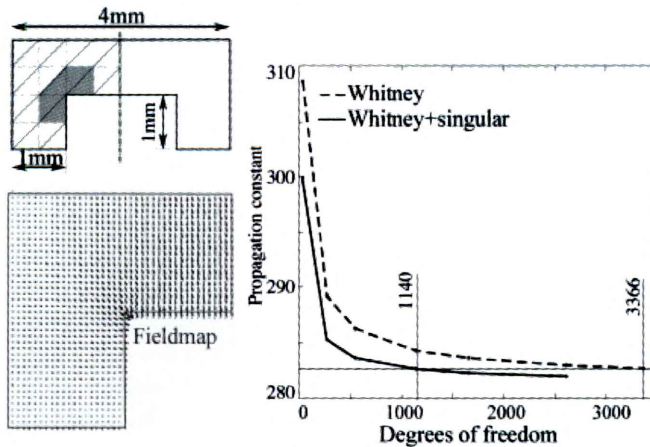

Fig 1

Ridged waveguide cross-section (top left); resulting field, with singular elements, for the first mode at 30GHz (bottom left) and pertinent convergence, as a function of degrees of freedom, for singular and non-singular elements (right).

The convergence of propagation's constant (β) of the first mode at 30 GHz as a function of the increasing number of degrees of freedom is studied and presented in Fig. 1. Graphs are relative to a reference solution, obtained exploiting only Whitney's (non-singular) elements, and the proposed a solution, where the five elements surrounding the wedge are the one defined by [3]; the other elements remaining of Whitney's kind. For the convergence study the regular mesh is recursively refined. For the present case singular field is in presence of rectangular wedge hence, from [2], it is $\nu = 2/3$. It is clear that with singular functions the solution's convergence is faster than with Whitney elements only. The transverse electric field's behaviour is showed in Fig. 2 in the inset.

As a second example a vaned rectangular waveguide is considered (Fig. 2). This guide too has a symmetry plane so, by introducing a perfect magnetic wall, only half section can be considered and only even solution

are found. The field singular behaviour is defined by $\nu = 0.5$ this time. Fig. 2 reports both the field obtained with and without singular elements. It is evident the smoother behaviour of the field when singular elements are used. Like in previous example Fig. 2, also shows the convergence of β for the fundamental mode, this time at 20 GHz, with and without singular elements. In this example the better performances of singular elements is even more evident.

4. Conclusions

A novel set of divergent bases are presented for the Finite Elements solution of divergent fields next to a wedge in a waveguide problem. Comparing numerical results with a conventional FEM solution has showed the better performances of the proposed elements.
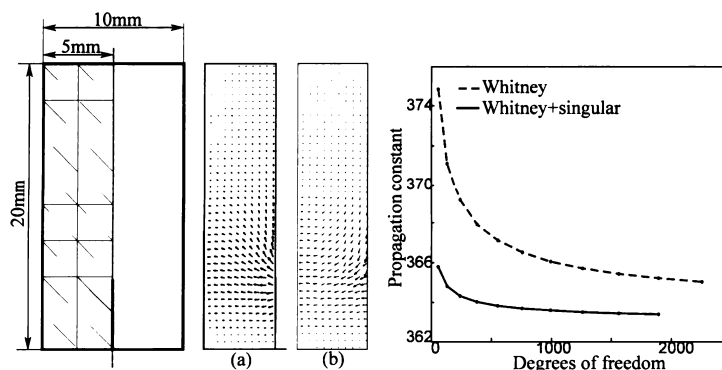
FIG. 2

Vaned waveguide cross-section (far left); resulting field, with singular elements (middle - a) and with regular elements (middle - b), for the first mode at 20 GHz and pertinent convergence, as a function of degrees of freedom, for singular and non-singular elements (far right).

REFERENCES

(1) J. MEIXNER, The Behavior of Electromagnetic Fields at Edges, IEEE Trans. Antennas and Propagat., 20 (4), 442-446, 1972.

(2) J.M. GIL, J.P. WEBB, A New Edge Element for the Modeling of Field Singularities in Trasmission Lines and Waveguides, IEEE Trans. Microwave Theory Thech., 45(12), 2125-2130, 1997.

(3) R.D. GRAGLIA, G. LOMBARDI, Hierarchical singular vector bases for the FEM solution of wedge problems, in Proc. URSI Symposium, 23-27 May, 2004, 834-836.

(4) R.D. GRAGLIA, G. LOMBARDI, Vector Functions for Singular Field on Curved Triangular Elements Truly Defined in the Parent Space, In Proc. IEEE APS Symposium, 16-21 Jun., 2002, 62-65.

(5) G. PELOSI, R. COCCIOLI, S. SELLERI, Quick Finite Elements for Electromagnetic Waves, Artech House, Boston (MA) 1998, 61-67.

An analysis of MHD interaction
in hypersonic flows

ANDREA CRISTOFOLINI (*)

SUMMARY. – *A model for the analysis of the magneto-plasmadynamic regime in hypersonic flows is presented. In the assumption of a low magnetic Reynolds number regime, the model couples a time dependent formulation of fluid dynamics with a steady state electrodynamics. The Navier-Stokes equations are discretized by means of a finite volume formulation. The electrodynamics is discretized by means of a finite element method. The model has been utilized for the analysis of the MHD interaction in the shock layer of a test body in a wind tunnel. The activity is aimed to the design of the experimental activity in the frame of an ASI research project on the MHD interaction in hypersonic flows.*

1. Introduction

The concept of hypersonic flight has recently received an increasing interest. Hypersonic flight has been usually linked to the re-entering of space vehicles in the atmosphere. A new wide range of applications of hypersonic flight is related to the development of a single stage to orbit (SSTO) vehicle, that is now one of the main prerequisite for the commercial exploitation of space flight. Many applications of the MHD interaction in hypersonic vehicle has been proposed and discussed (1). An MHD system has been proposed to control the fluid dynamics at the inlet of the scramjet; the Russian AJAX project, MHD techniques are utilized to bypass kinetic energy of the working fluid from the supersonic diffuser to the nozzle, reducing the flow velocity in the combustion chamber to acceptable value, even for high vehicle Mach numbers. Another interesting opportunity is to control boundary layer phenomena, shock waves and heat fluxes by means of MHD interaction.

(*) Dipartimento di Ingegneria Elettrica, Università di Bologna, Viale Risorgimento 2, 40136 Bologna, Italy

A magneto fluid dynamic model is generally based on the assumption that the plasma can be regarded as a continuum, and thus may be characterized by relatively few macroscopic quantities. The requirement for the applicability of this approach is that the plasma be collision dominated. Under this assumption, an MHD model is constituted by the continuity equation for mass, momentum and energy, and by the Maxwell equations.

In the models presented in this paper, a convenient approximation will be utilized, assuming that the characteristic time for the macroscopic variations is much greater than the inverse of the plasma frequency. Under this assumption, the displacement current density, given by the time derivative of the displacement field D may be neglected compared to the conduction current density. Under the assumption of $Re_m \ll 1$, some other approximations can be applied (2). Most notably, when an externally generated magnetic flux density B_0 is applied to the plasma flow, the magnetic flux density B_j due to the current density in the plasma can be neglected. Thus, the total magnetic flux density B may be considered equal to the externally applied field B_0.

2. Numerical method

The fluid dynamic equations are:

$$[1] \quad \frac{\partial U}{\partial t} + \nabla \cdot F = Q, \ U = \begin{vmatrix} \rho \\ \rho u \\ e_i \end{vmatrix}, \ F = \begin{vmatrix} \rho u \\ \rho u u + pI - \tau \\ e_i u - \tau \cdot u - k\nabla T \end{vmatrix}, \ Q = \begin{vmatrix} 0 \\ J \times B \\ E \cdot J \end{vmatrix}$$

Assuming that the applied magnetic flux density does not vary in time, or varies slowly, electrodynamics is described by the equation (2):

$$[2] \qquad\qquad \nabla \cdot \left[\sigma \left(-\nabla \varphi + u \times B \right) \right] = 0$$

It is worth noting that the assumptions made above lead to a steady state electrodynamics, described by means of an elliptical partial differential equation.

This does not mean that the electrodynamic quantities do not vary in time. Electrodynamics may rather be considered to vary as a sequence of steady state solutions driven by the evolution in time of the fluid dynamics. This is because, in the frame of the assumptions described earlier, the electrodynamics has a negligible characteristic time compared to the fluid dynamics. Electrodynamic quantities are accordingly assumed to adapt themselves instantaneously to the time variation of the flow field.

At each time step the space discretization is performed. A cell-centered finite volume formulation, based on a Galerkin approach, has been adopted

for the spatial discretization of the fluid dynamics. Fluxes are evaluated by means of a centered scheme, corrected by a Roe scheme. A second order accuracy is obtained, utilizing a MUSCL approach, by a combination of upwind and centered discretization of the gradient. Electrodynamics is discretized by means of a finite element approach (3).

Time integration is performed utilizing an explicit scheme, based on a fourth-order Runge-Kutta method. The coupling between the fluid and the electrodynamics is accomplished quite straightforwardly. As previously stated, the time dependent behavior of the model is governed by the fluid dynamics. At the generic n^{th} time step, the fluid dynamic solver evaluates the source terms in the continuity equation for momentum and energy utilizing the values of E and J calculated at the previous time step. The steady state electrodynamic model then utilizes the value of u at the nth step to compute E and J. These quantities will be utilized as input for the $(n+1)^{th}$ time step of the fluid dynamic solver.

3. Application and discussion
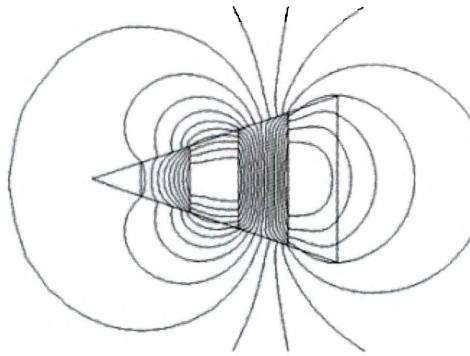
FIG. 1

Magnetic flux density around the wedge

The model described has been utilized to analyze the magnetohydrodynamic field over a wedge in hypersonic regime. The distribution of the magnetic flux density produced by the described arrangement is shown in Fig. 1. The magnetic flux density is about 1 T on the surface of the wedge. The calculation of the flow condition around the wedge has been performed on a 26,000 node unstructured triangular mesh. The simulation aim is to reproduce the conditions in the a wind tunnel facility located at the Centrospazio laboratories, Pisa, Italy, capable to produce a hypersonic flow up to 7 Mach. Thus, the MHD regime around the wedge subject to a

Mach 7 argon flow is analyzed. A free stream flow with a 76 Pa pressure and a 9.8 10^{-4} Kg m^{-3} density are is considered. Under these conditions, the upstream flow velocity is 2310 m s^{-1}. Some calculation results are shown in the following figures. In fig. 2, the mach lines are shown with the B field off (2.a) and on (2.b). Fig. 3 show a comparison of pressure and friction coefficient with and without the applied magnetic flux density.

a)   b)
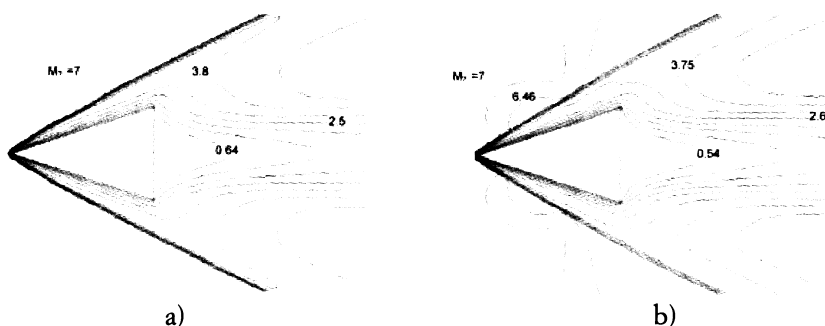
FIG. 2

Mach lines without (2.a) and with (2.b) MHD interaction.

a)   b)
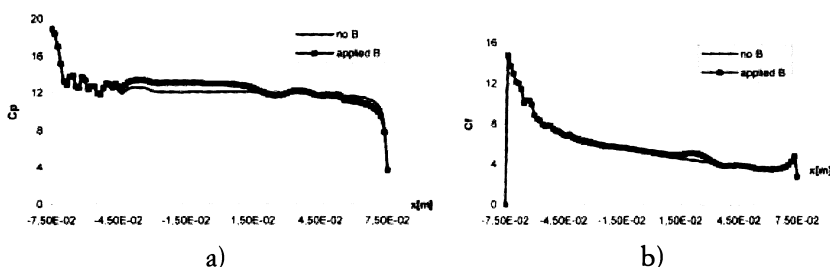
FIG. 3

Pressure coefficient (3.a) and friction coefficient (3.b) are compared with
and without the applied magnetic flux density.

REFERENCES

(1) V.A. BITYURIN, A.N. BOTCHAROV, V.G. POTEBNYA, J.T. LINEBERRY, *MHD Effects in Hypersonic flows around Blunt Body*, 2nd Workshop on Magneto Plasma Aerodynamics In Aerospace Appications, Moscow, April 2000.

(2) M. MITCHNER, C.H. KRUGER, *Partially Ionized Gases*, Wiley-Interscience, New York, 1973.

(3) C.A. BORGHI , M.R. CARRARO, A. CRISTOFOLINI, *Numerical Modelling of MHD Interaction in the Boundary Layer of Hypersonic Flows*, IEEE Transactions on Magnetic, **39** (3), 1507-1510, May 2003

Numerical solution of micromagnetic problems

CINZIA GIUFFRIDA (*), CARLO RAGUSA (*), MAURIZIO REPETTO (*)

SUMMARY. – *The study of micromagnetic problems requires the solution of electromagnetic field coupled with the Landau-Lifshitz or Gilbert equation governing magnetization dynamics. In this paper Finite Formulation of Electromagnetic fields is used to compute maxwellian field effects on a structured hexahedral grid while magnetization dynamics is evaluated by an implicit formulation. Results on one benchmark configuration is presented.*

1. Introduction

The analysis of magnetization dynamic on a nano-metric scale requires an approach which is substantially different from the usual macro-scale one. On this spatial scale, in fact, magnetization vector M must be considered as variable in direction but fixed in magnitude at the saturation magnetization level M_S; on the other hand M can be still considered as a continuous function of space and time neglecting the discrete effect of atomic magnetic moments. The time variation of magnetization is dictated by the Gilbert or Landau-Lifshitz which relates the time derivative of M to an effective magnetic field acting on the medium. This effective magnetic field is the sum of four terms: two are defined by Maxwell equations and take into account magneto-static effects and the interaction with the externally applied magnetic field; the other two contributes come from the interaction of magnetization with material structure: one is the anisotropy field due to the interaction of the magnetization with the crystalline lattice and the last one is the exchange field which forces magnetization moments to be aligned.

The analysis of the time evolution of M requires the evaluation of several contributes which must be recomputed during the time marching procedure so that their evaluation must be fast and accurate.

In the following sections the main points of the procedure used to solve micromagnetic problems will be highlighted.

(*) Politecnico di Torino, Dipartimento di Ingegneria Elettrica Industriale, Corso Duca degli Abruzzi 24, 10129 Torino, Italy

2. Gilbert equation

Magnetization vector is written as a unit vector m multiplied by the saturation magnetization M_S value which is function of material characteristics and of temperature and will be considered here as a constant:

[1] $$M = M_S m$$

The time evolution of magnetization can be written by the Landau-Lifshitz equation or by the equivalent form known as Gilbert Equation (GE), which, expressed in normalized quantities (1), becomes:

[2] $$\frac{\partial m}{\partial t} = -m \times \left(h_{eff} - \alpha \frac{\partial m}{\partial t} \right)$$

where α is the damping constant. Vector h_{eff} is the effective magnetic field acting on the magnetization which is expressed by:

[3] $$h_{eff} = h_M + h_a + h_{anis} + h_{exch}$$

where h_M is the maxwellian term taking into account magnetostatic and possible eddy current effects, h_a is the applied field, h_{anis} is the anisotropy field and h_{exch} is the field due to the exchange interaction between magnetic dipoles. All terms of the effective field but the applied one are function of the spatial distribution of magnetization and this makes [2] nonlinear.

Since m is a unit vector it is particularly convenient to express it in spherical coordinates assuming a unit radial component, in this case [2] becomes:

[4] $$\begin{cases} \dot{\vartheta} + \alpha\sin\vartheta\dot{\phi} = -h_{effx}\sin\phi + h_{effy}\cos\phi \\ \alpha\dot{\vartheta} + \sin\vartheta\dot{\phi} = h_{effz}\sin\vartheta - \left(h_{effx}\cos\phi + h_{effy}\sin\phi \right)\cos\vartheta \end{cases}$$

Equation [4] can be efficiently integrated in time by a Crank-Nicholson procedure while nonlinearity can be handled by a simple iteration scheme (2).

3. Maxwell equations

A medium aimed by spontaneous magnetization creates a magnetic field which is ruled by Maxwell equation. A part form very simple configurations, magnetostatic field must be evaluated numerically and thus a discrete formulation of Maxwell equations has to be defined.

Finite Formulation of Electromagnetic Field (FFEF) has been recently introduced (3) and can be efficiently used in the numerical solution of magnetic field (4).

In this case the source of the magnetostatic problem is the magnetization vector which, together with magnetic permeability, is considered as a material property. Magnetization sources can be introduced in the problem as material dependent magneto-motive forces added to the constitutive equation:

[5] $$F = \mathcal{R}\varphi - F_M(M)$$

where F is the magneto-motive force along a dual edge, φ is the magnetic flux on the related primal edge, $\mathcal{R}$ is the reluctance depending on geometry and material constant and F_M is the line integral of known magnetization vector along the dual edge. Neglecting the presence of free currents in the domain, and making reference to the matrix notation used in (3), Ampère theorem can be written in matrix form as:

[6] $$\left[\tilde{C}\right]\{F\} = 0 \Rightarrow \left[\tilde{C}\right]\left[\mathcal{R}\right]\{\varphi\} = \left[\tilde{C}\right]\{F_M(M)\}$$

by introducing the line integral of magnetic vector potential along primal edges p, the problem can be written as:

[7] $$\left[\tilde{C}\right]\left[\mathcal{R}\right]\left[C\right]\{p\} = \left[\tilde{C}\right]\{F_M(M)\}$$

Uniqueness of p is ensured by a tree gauging (4). Equation [7] requires the discretization of the whole space to get proper boundary conditions. A reduction in terms of number of unknowns can be achieved by setting proper integral conditions on the boundaries of the domain containing M. In fact, the Ampere law of the primal edges lying on the boundary of the mesh can be written as function of M. In this case, in fact, the path around the primal edge is not closed because part of this line lies in air which is not modelled. The contributes to the circulation for the part outside the mesh can be obtained by expressing the external magneto-motive force as function of the known magnetization inside the domain by means of the well known integral expression of magnetic scalar potential. As a result [7] will have another known term depending on integral effect of magnetization:

[8] $$\left[\tilde{C}\right]\left[\mathcal{R}\right]\left[C\right]\{p\} = \left[\tilde{C}\right]\{F_M(M)\} + \{T_{int}(M)\}$$

The solution of [8], once M is known, gives the magnetic vector potential and then the magnetostatic field h_M can be computed in all points of the domain.

4. Solution of the micromagnetic problem

Given a volume discretization of the geometrical domain, the solution of micromagnetic problem requires to follow the time evolution of magnetization unit vector in all the elements of the mesh. At each time instant the forcing

terms of [4] must be recomputed. Particular attention must be devoted to the exchange term which comes from a second order derivative term:

$$[9] \qquad h_{exch} = l^2_{exch} \nabla^2 m \qquad l_{exch} = \sqrt{\frac{2A_{exch}}{\mu_0 M_S^2}}$$

where l_{exch} is a material dependent parameter (1). The order of the derivation on m can be lowered by considering the volume average of the forcing term of (1) and applying the second Green formula:

$$[10] \qquad \frac{1}{V}\int_V m \times h_{exch} dV = \frac{l^2_{exch}}{V} \int_V m \times \nabla^2 m dV = \frac{l^2_{exch}}{V} \oint_{\partial V} m \times \frac{\partial m}{\partial n} dS$$

Using a structured hexahedral discretization the normal derivatives of m can be approximated as incremental ratios and thus the forcing term due to the exchange interaction can be evaluated.

The time integration of [4] is performed by considering that exchange interaction is a short scale phenomenon with respect to other effective field terms and that this fact calls for a strict coupling between spatial evolution of m and exchange terms. Consequently exchange effects are computed implicitly by using [10] and its contributes are brought on the unknown side of the equation. As a result the matrix form of [4] becomes:

$$[11] \qquad \left[A(x)\right]\left\{\frac{dx}{dt}\right\} + \left[B(x)\right]\left\{x\right\} = \left\{Q(x)\right\}$$

where $\{x\}$ is the unknown vector containing the θ and ϕ polar coordinates of m in each volume cell, $[A]$ is the time derivative coefficient matrix coming directly from equation [4], $[B]$ is the exchange term coefficient matrix obtained by equation [10] and $\{Q\}$ is the known term vector containing magnetostatic, anisotropy and external field contributes. Equation [11] is integrated using the Crank-Nicholson scheme while all matrices and vectors are updated iteratively in a simple iteration scheme.

5. An application: magnetization reversal in one nanometric cube

The proposed 3D numeric approach for the study of micromagnetic dynamics, has been applied to the solution of the magnetization reversal in one cube with edge length equal to 5 times the exchange length. Data of the material are: saturation magnetization $M_S = 1.4$MA/m, exchange energy $A_{exch} = 1.4*10^{-11}$ J/m, $\gamma = 2.211*10^5$ m/As, $a = 1$, no anisotropy is considered and the edge of the cube is 12.5 nm. The initial magnetization is directed 1 degree off the positive x direction while the applied field is along the negative direction $H_a = 160$ kA/m. In Fig. 1 the time variation of the average magnetization of the cube is shown. These results are in good agreement with other found in the literature.
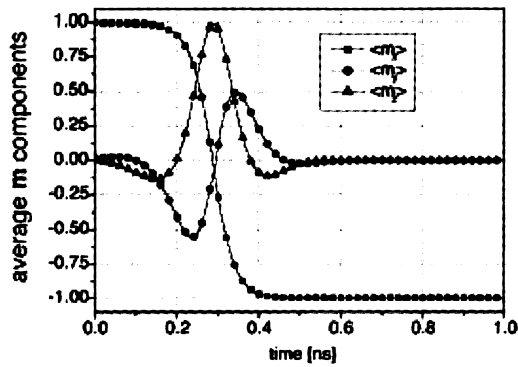
FIG. 1

Pattern of cube average magnetization dynamics

REFERENCES

(1) G. BERTOTTI, *Hysteresis in magnetism*, Academic Press (San Diego), 1998
(2) C. SERPICO, I.D. MAYERGOYZ, G. BERTOTTI, *Numerical technique for integration of the Landau-Lifshitz equation*, J. Appl. Phys., **89** (11), 6991-6993, 2001.
(3) E. TONTI, *Finite Formulation of Electromagnetic Field*, IEEE Trans. on Magnetics, **38** (2), 333-336, 2002.
(4) M. REPETTO, F. TREVISAN, *Global formulation of 3D magnetostatics using flux and gauged potentials*, Int. J. on Numerical Methods in Engineering, **60**, ???, 2004.

The inexact Newton method applied for the solution of a magnetostatic problem

ANDREA CRISTOFOLINI (*)

SUMMARY. – *Inexact Newton solvers can offer many attractive features for the solution of non linear problem in the field of electromagnetics. A critical point for the optimal set up of the solver is the choice of the best algorithm for the evaluation of the approximate solutions of the linear systems at each Newton step, and the most effective preconditioning strategy. In this paper, the NITSOL method is proposed for the solution of a non linear linear magnetostatic problem. The problem has been discretized by means of a finite element approach. The GMRES method has been adopted as linear solver, and three preconditioners have been tested. The performance of the procedure are evaluated for different meshes with increasing number of discretization points.*

1. Introduction

Newton solvers are well established methods for the calculation of a zero of a non linear function F, and have successfully been applied to large scale problems in several scientific fields. An inexact solver can improve the performance of the Newton-Raphson method, by means of the inexact Newton condition (1):

[1]
$$\left\| F\left(f_k\right) + F'\left(f_k\right)s_k \right\| \le \eta_k \left\| F\left(f_k\right) \right\|$$

where F' is the Jacobian of the function F, s_k is the solution increment at the kth step and $\eta_k \in (0.1)$ is a forcing term enhancing the convergence efficiency. In the initial non linear iterations, a large forcing term avoids the risk of imposing a too high accuracy on the solution, leading to a possible substantial disagreement between $F(f_k+s_k)$ and its linear approximation $F(f_k)+F'(f_k)s_k$. As the solution gets close to convergence, η_k decreases, so that [1] tends towards the exact Newton condition.

(*) Dipartimento di Ingegneria Elettrica, Università di Bologna, Viale Risorgimento 2, 40136 Bologna, Italy

Condition [1] yields a linear system at each non linear iteration, which is solved by means of a GMRES algorithm (3). As a general rule, the robustness and the convergence rate of GMRES are strictly dependent on the preconditioner quality rather than on other factors. For the purpose of this paper, three preconditioners has been utilized ILUK, ILUT, and ILUTP. A more extensive description of these preconditioners can be found in (2) and (3).

2. Application and discussion: a magnetostatic problem

A magnetostatic problem with a ferromagnetic material has been considered. The physical formulation, constituted by the Maxwell equations and the material laws, yields the following equation:

[2] $$B = \nabla \times A, \ \nabla \times \left(\frac{1}{\mu} \nabla \times A \right) = J.$$

The non linear function F is found discretizing [2] in a two-dimensional symmetry frame by means of a weighted residual FEM approach (4):

[3] $$F = K(a)a - j = 0,$$

where a is the array constituted by the nodal values of the unknown vector potential.

Two test cases have been chosen for the analysis of magnetostatic problems with the techniques described above. The non-linear ferromagnetic materials considered are pure iron and mumetal, hereafter labelled as material 1 and material 2 respectively.

In the case A, a ferromagnetic structure is used to strenghten the magnetic field generated by two solenoids as shown in Fig. 1. The windings cross section is 0.126 m². In the test case B material 1 and material 2 have been used to form the structure shown in Fig. 2, excited by a solenoid with a 12 10⁻⁴ m² cross section.

The non-linear problem has been studied analysing both test cases with two different meshes. The coarse mesh in case A contains 6751 nodes (3390 nodes in the non-linear region), whereas the fine mesh contains 14312 nodes (6646 nodes in the non-linear region). The coarse and fine mesh in case B are made of 4777 (680 in the non-linear regions) and 9825 nodes (1700 in the non-linear regions) respectively. All the calculations have been carried out on a PC with 256 MB RAM, and 1200 MHz processor.
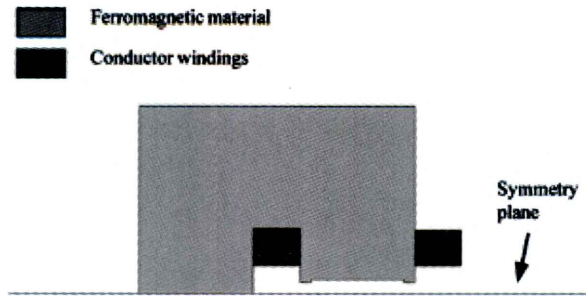
FIG. 1

Test case A
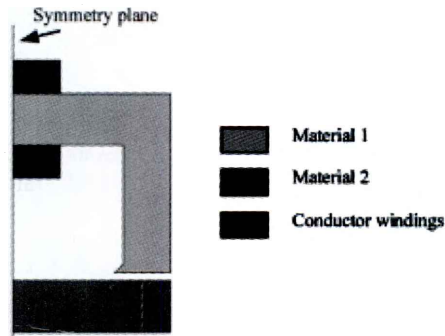
FIG. 2

Test case B

A first set of simulations has been dedicated to the comparison between the proposed inexact Newton solver and the well established exact Newton procedure. The results obtained utilising the ILUTP preconditioner are shown in Table 1 for all the different test cases considered. In all cases a remarkable reduction of the solution time has been achieved by means of the inexact Newton solver with respect to the exact one. This result is due to a very significant decrease of the total number of linear iterations, as the non linear iterations number is generally higher with the inexact Newton procedure. A typical convergence process obtained for the last two runs reported in Table I (case B, fine mesh) is described in Fig. 3.

The higher number of non linear iterations required to reach convergence by the inexact Newton solver shown in Fig. 3.a is compensated by a much lower computation time required by each iteration as shown in Fig. 3.b. This can be explained considering that the inexact Newton solver utilizes a less strict convergence condition, given by [1], in the first non-linear iterations, when the solution is far away from the exact solution. As a result, the linear solver, in the first non-linear iterations, converges more

quickly, reducing the norm with a low computational time. As the non-linear solver gets closer to convergence, both the forcing term and the residual norm in the right end side of [1] decrease. Thus, the convergence condition for the linear solver becomes more severe, increasing the computational burden of the final non linear steps.

(a)   (b)
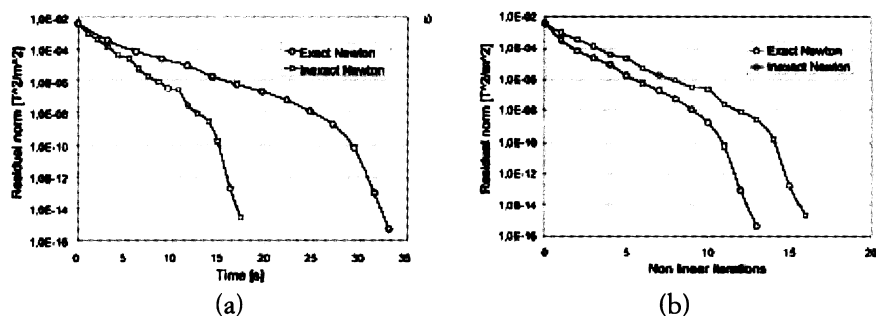
FIG. 3

Convergence processes of exact and inexact Newton solvers with respect to calculation times (a) and non linear iterations (b).

A second set of simulations has been devoted to a comparison between the different preconditioners implemented, and is shown in Table 2 for case A, coarse mesh, high current.

Table 1
Comparison Between Inexact and Exact Newton Solvers

	Non lin. Iterations	Linear iterations	Solution time (s)
Case A Coarse Mesh			
Exact Newton	11	235	17.5
Inexact Newton	13	62	8.9
Case A Fine Mesh			
Exact Newton	12	653	62.0
Inexact Newton	15	94	22.9
Case B Coarse Mesh			
Exact Newton	12	199	12.8
Inexact Newton	13	48	6.2
Case B Fine Mesh			
Exact Newton	13	367	33.7
Inexact Newton	16	68	17.4

Table 2
Comparison between different Preconditioners

	Non linear iterations	Linear iterations	Solution time (s)
ILUK	22	153	16.0
ILUT	19	88	12.2
ILUTP	19	88	12.7

REFERENCES

(1) R.S. DEMBO, S.C. EISENSTAT, T. STEIHAUG, *Inexact Newton methods*, SIAM Jour. Numer. Anal., **19**, 400-408, 1982.

(2) C.A. BORGHI, M. BRESCHI, M.R. CARRARO, A. CRISTOFOLINI, *Solution of the Magnetostatic Problem Using an Inexact Newton Method*, IEEE Trans. on Magnetics, **40** (2), 1076-1079, March 2004

(3) Y. SAAD, *Iterative methods for sparse linear systems*, PWS Publishing Co., Boston, 1996.

(4) C. ZIENKIEWICZ, *The Finite Element Method in Engineering Science*, Mc Graw Hill, London, 1977.

An electric and magnetic fields virtual laboratory based on the Matlab FEM toolbox

MASSIMILIANO DE MAGISTRIS (*)

SUMMARY. – *This paper reports the realization of a Matlab™-based Virtual Laboratory for introducing FEM techniques in EM-Fields at both undergraduate and graduate university courses. The choice of the developing environment is discussed in the light of authoring issues and user advantages. The virtual laboratory is described in terms of its functionalities, the pedagogical ideas behind it, the kind of resources and with a sample showing its actual potential and possible extensions.*

1. Introduction

The fast increase of the diffusion of Computer Aided Education, as well as the web related concept of e-learning, seem to dominate the nowadays discussion on the creation and delivery of modern learning resources, at least in the field of Engineering Education (1). Many important educational institutions have ongoing programs for converting large part of their learning material in electronic format, and let it available on the web (see for example the MIT Open CourseWare program (2)).

In the area of Electrical Engineering Education the use of simulation as supplementary didactic tool is largely diffused. Several specialized tools have been developed and tested in classroom and standard simulators are routinely used also in introductory courses. For the teaching of Electromagnetic fields, especially at the introductory level, the situation is less developed than for other areas; nevertheless a large discussion and some practical experiences have been reported (3-6).

(*) Dipartimento di Ingegneria Elettrica, Via Claudio, 21, 80125 Napoli, Italy

We have realized, and presently experimenting, a web learning environment based on a catalogue of FEM-MATLAB simulations, which allows the integrate delivery of simulations, text and hypertext, audio and video resources. It follows the idea of a Virtual Laboratory to be associated to the traditional lessons (7). In this paper we discuss the choice of the simulation environment, describe the realized environment and show a sample of the learning resources realized.

2. Authoring a Matlab-based virtual laboratory

Building self-consistent "courseware" to integrate traditional teaching with simulations and multimedia is extremely time consuming, as experienced by many. Therefore before embarking in the resources creation one is advised try to answer some basic, practical questions. In particular they concern the diffusion and availability of the hardware and software required to the user (student), the relative difficulty and time expenditure for the creation of the resources, the possibility of reusing and easy maintenance of the resources in the future, and the relative effort for enlarging the base of examples and cases. Finally, it is recommended to consider the problem of web integration and delivery of the resources.

Several solutions and strategies are available; each one responds, for better or worse, to the points mentioned. For those who are familiar with the major features of the Matlab environment it is easy to understand how its capabilities can be positively exploited to developing examples in vector field analysis, answering at the same time most of the mentioned points. In particular somewhat sophisticated possibilities are offered by the use of the Matlab Partial Differential Equation (PDE) Toolbox, which provides a powerful and flexible environment for the study and solution of partial differential equations in two space dimensions and time. The package, described in (8), is intended: 1) to define the PDE problem, in terms of geometry, boundary conditions, and coefficients; 2) to define a triangular mesh over the considered geometry; 3) to discretize the equations by the Finite Element Method (FEM) and numerically solve them by producing an approximation to the solution, and 4) finally, to visualize results by means of specialized graphic tools. Clearly, this tool significantly enlarges the possibilities in designing examples and case studies. Moreover, the PDE toolbox results are fully visible and available to the Matlab environment, allowing the variables and the source files to be accessed directly, and to further manipulate the solution. Lastly, from version 5.2 Matlab provides a well integrated Common Gateway Interface (CGI) for a web server, which allows easily deployment of any Matlab-based application via the World Wide Web, eventually interfacing multimedia and other resources. This improved version provides the opportunity for the user to run simulations remotely, without the need for licensed software or appropriate hardware.

3. A virtual laboratory for EM fields analysis

The Electric and Magnetic fields Virtual Laboratory, as designed and realized, could actually be considered a general learning environment with on-line, interactive, FEM EM-field simulations. In the present version a general web interface has been developed, as shown in figure 1. The web server provides for the execution of the simulation and creation of the output page in html style. A full demonstration of the interface and the virtual laboratory itself can be viewed at the web site address www.elettrotecnica.unina.it/multimedia.

With reference to present utilization for an introductory course, the virtual laboratory is structured in three sections, Electrostatics, Magnetostatics, and Stationary Current Field, with some examples of different difficulty levels.

Currently, a tenth of the examples of interactive simulations are fully available, each with several associated didactic resources as Power Point presentations, text, etc. Some examples have the main goal of illustrating the field configuration and some significant properties of the analyzed structures. Others are designed with the double purpose of analyzing and gaining insight into a specific problem, as well as familiarizing students with simulation problems and eventual numerical techniques. In a third category of examples, the goal is to illustrate the relationships of geometry and material properties versus some global parameters such as resistance, capacitance, or inductivity. A fourth category shows fields animations.
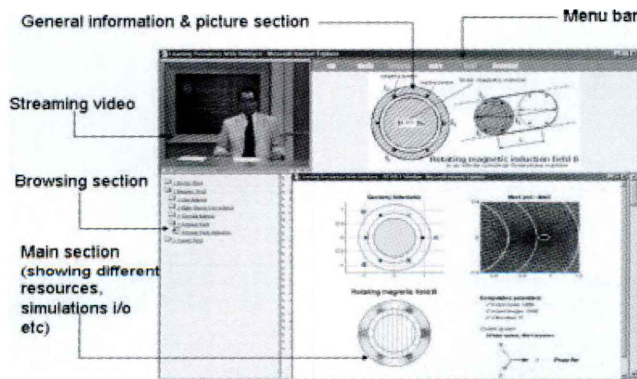
Fig. 1

A screenshot of the first page web interface of the virtual laboratory.

To describe the major ideas behind we take an example from the Current Field folder, namely the grounding conductor analysis. With reference to a structure of two cylindrical grounding conductors in the ground, the earth resistance is evaluated for a set of parameters chosen by the student, such as electrode's length, distance, and conductivity, and the ground conductivity. After the simulation, the potential and field distribution is also shown with other associated information.

The proposed example is fully realized with the PDE toolbox and immediately integrated to the structure of the Virtual Laboratory. A set of examples specifically built to introduce FEM technique and numerical problems in electromagnetic can easily be implemented following the same line.
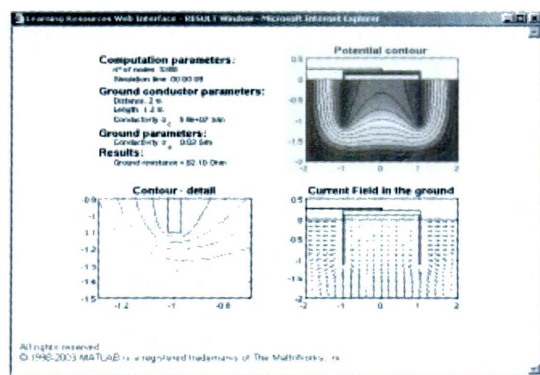
FIG. 2

Output window for the grounding conductors example

REFERENCES

(1) R. UBELL, *Engineers turn to e-learning*, IEEE Spectrum, **37** (10), October 2000.
(2) http://ocw.mit.edu/index.html
(3) J.F. HOBURG, *Can computers really help students understanding Electromagnetics*, IEEE Trans. on Education, **36** (1), February 1993.
(4) D.A. LOWTHER, E.M. FREEMAN, *A new approach to using simulation software in the Electromagnetics Curriculum*, IEEE Trans. on Education, **36** (2), May 1993.
(5) R.R. DELYSER, *Using Mathcad in Electromagnetics Education*, IEEE Trans. on Education, **39** (2), May 1996.
(6) B. BEKER, D.W. BAILEY, G.J. COKKINIDES, *An Application Enhanced Approach to Introductory Electromagnetics*, IEEE Trans. on Education, **41** (1), February 1998.
(7) M. DE MAGISTRIS, *A Matlab-Based Virtual Laboratory for Teaching Introductory Quasi-Stationary Electromagnetics*, IEEE Trans. on Education, (in press).
(8) AA.VV. *Partial Differential Equations Toolbox User' Guide*, the MathWorks Inc., 1997.

Electromagnetic CAD for the analysis and design of waveguide and FSS devices based on a hybrid MM-FEM

PAOLO GRASSI (*), AGOSTINO MONORCHIO (*),
DOMENICO ARENA (**), GIULIANO MANARA (*)

SUMMARY – *A new Hybrid Mode Matching (MM)/Finite Element (FE) tool for the rigorous analysis of discontinuities between inhomogeneous filled waveguides or inductive FSS is presented. The problem of the spurious solutions is avoided by the use of both Whitney's Edge elements to interpolate transverse field components and Lagrange polynomials to reconstruct the longitudinal ones. The Generalized Eigenvalue Problem (GEP) involved in the FEM analysis has been efficiently solved with a modified Implicitly Restarted Arnoldi Method (IRAM). Some examples are presented to demonstrate the effectiveness of this approach.*

1. Introduction

This paper presents a new hybrid MM/FE technique for the rigorous analysis of inhomogeneously filled structures. This approach combines the above two methods in order to retain the advantages of both, i.e., the numerical efficiency of the MM and the capability of the FEM to analyze irregular structures. More specifically, MM is used to ensure the continuity of transverse electric and magnetic fields at the discontinuities, while inhomogeneously filled waveguides (apertures) are analyzed by means of FE. The two methods are therefore combined to obtain the Generalized Scattering Matrix (GSM) of each discontinuity. In the last years, other examples of such hybrid methods have been proposed for the analysis of homogeneously filled devices (1, 2). None of the above mentioned methods deals with

(*) Department of Information Engineering, University of Pisa, Via G. Caruso, I-56122 Pisa, Italy
(**) Telecom Italia Lab (formerly CSELT), Via G. Reiss Romoli, 274, I-10148 Torino, Italy

inhomogeneous structures; for this kind of problems a MM technique has been conventionally utilized for regularly shaped devices (3, 4). The hybrid technique proposed in this paper allows us to analyze such complex structures, where hybrid modes must be accounted for, even in presence of arbitrary waveguide cross-sections or non-canonical filling. The formulation makes use of the GSM of the single discontinuity; the GSM of the entire device is then reconstructed as a cascade connection of the GSM of each single discontinuity and reference plane shifts (5).

2. Formulation

Let us consider a *boundary enlargement* discontinuity consisting of the junction between an arbitrarily shaped inhomogeneously filled waveguide (wg#1) and a regular cross-section one (wg#2). In addition to the specific example here discussed, it is important to note that the proposed approach is rather general and it can be easily extended either to every kind of arbitrary cross-section to arbitrary cross-section inhomogeneous waveguide junctions or to the analysis of thick inductive Frequency Selective Surfaces (FSSs). The GSM approach (6) has been adopted in the context of a MM procedure so that, starting from the modal expansion of the fields at both sides of the discontinuity, the following coupling and power integrals need to be evaluated:

$$[1] \quad \underline{C}(i,j) = \iint_{\Omega_1} \left(\vec{e}_j^{(1)} \times \vec{h}_i^{(2)*} \right) \cdot \hat{i}_z \; d\Omega, \quad \underline{P}_u(i,j) = \iint_{\Omega_u} \left(\vec{e}_j^{u} \times \vec{h}_i^{u*} \right) \cdot \hat{i}_z \; d\Omega, \quad u = 1,2.$$

In Eq. [1], $\hat{i}_z$ represents the unit vector in the propagation direction in a standard Cartesian reference system, $\vec{e}_j^{u}$ is the electric vector eigenfunction of the jth mode in the uth waveguide, while $\vec{h}_i^{u}$ denotes the magnetic vector eigenfunction of the ith mode in the uth waveguide. In the working example here presented, an analytical expression of $\vec{e}_j^2(\vec{h}_i^2)$ is available due to the canonical shape of the waveguide; on the other hand, the eigenfunctions of the inhomogeneous filled waveguide must be evaluated numerically by means of a FE procedure. In order to evaluate the electric field distribution for an inhomogeneously filled waveguide, the following boundary value problem has to be solved (7):

$$[2] \quad \vec{\nabla} \times \frac{1}{\mu_r} \vec{\nabla} \times \vec{E} - k_0^2 \varepsilon_r \vec{E} = 0 \quad \text{in } \Omega,$$

$$\vec{E} \times \hat{n} = 0 \quad \text{on } p.e.c. \text{ wall}, \quad \nabla \times \vec{E} \times \hat{n} = 0 \quad \text{on } p.m.c. \text{ wall},$$

where Ω is the waveguide cross-section which can be arbitrarily shaped, $\hat{n}$ denotes the normal vector to the walls, ε_r and μ_r are the isotropic electric permittivity and magnetic permeability, respectively, and $k_0 = \omega \sqrt{\mu_0 \varepsilon_0}$ represents

the free-space wavenumber. The dielectric medium inside the waveguide is isotropic, but can be lossy, while the boundaries are perfectly conducting. The electric field and the curl operator can be therefore decomposed into the transverse and longitudinal components; after some manipulations, the so called weak form of [2] has been obtained. The transverse electric field components are expressed as a linear combination of Whitney functions, while Lagrange polynomials are used to expand the longitudinal component of the electric field. By using a Galerkin procedure, the following matrix problem has to be solved:

[3]
$$\begin{bmatrix} \underline{\underline{A}} & \underline{\underline{0}} \\ \underline{\underline{0}} & \underline{\underline{0}} \end{bmatrix} \begin{bmatrix} e_\tau \\ e_z \end{bmatrix} = -\gamma \begin{bmatrix} \underline{\underline{B}} & \underline{\underline{C}}^T \\ \underline{\underline{C}} & \underline{\underline{D}} \end{bmatrix} \begin{bmatrix} e_\tau \\ e_z \end{bmatrix},$$

where

$$\vec{e}_\tau = \sum_{m=1}^{3} E_{\tau m} \vec{W}_m \quad \text{and} \quad e_z = \sum_{i=1}^{3} E_{zi} L$$

are the transverse and longitudinal electric field expansions over each element, respectively; $\gamma = k_z^2$, being k_z the complex propagation constant, and the elements of the matrices are:

[4]
$$\underline{\underline{B}}_{m,n} = \frac{1}{\mu_r} \iint_T \vec{W}_n \vec{W}_m dT, \quad \underline{\underline{A}}_{m,n} = \frac{1}{\mu_r} \iint_T \left(\vec{\nabla}_t \times \vec{W}_n \right) \left(\vec{\nabla}_t \times \vec{W}_m \right) dT - k_0^2 \varepsilon_r \mu_r \underline{\underline{B}}_{m,n}$$

$$\underline{\underline{C}}_{i,n} = \frac{1}{\mu_r} \iint_T \vec{\nabla}_\tau L_i \vec{W}_n dT, \quad \underline{\underline{D}}_{i,j} = \frac{1}{\mu_r} \iint_T \vec{\nabla}_\tau L_j \vec{\nabla}_\tau L_i dT + k_0^2 \varepsilon_r \iint_T L_j L_i dT.$$

The FEM employed provides only the electric field distribution for each mode; therefore, by using the first Maxwell equation in the frequency domain and some algebraic properties (8), the power integrals in the wg$_{\#1}$ become:

[5]
$$P_1(i,j) = \frac{1}{\omega \mu k_{zi}} \left[\oiint_S \vec{e}_{\tau i} \cdot \vec{\nabla}_t \vec{e}_{zj} dS - \oiint_S \vec{e}_{\tau i} \cdot \vec{e}_{\tau j} dS \right].$$

The proposed field expansion provides a simple and straightforward procedure for computing the coupling integrals that can be written as:

[6]
$$C_{ijTE}^{FEM} = \frac{-jk_{zi}^*}{k_{zj}\omega\mu} \int_\Omega \left(e_{xj}^1 H_{yi}^2 - e_{yj}^1 H_{xi}^2 \right) d\Omega, \quad C_{ijTM}^{FEM} = \frac{-j}{k_{zj}} \int_\Omega \left(e_{xj}^1 H_{yi}^2 - e_{yj}^1 H_{xi}^2 \right) d\Omega,$$

where H_{xi}^2 and H_{yi}^2 denote the Cartesian components of the normalized eigenfunctions in the rectangular waveguide. The sparse non-symmetric generalized eigenvalue problem [3] has been solved by resorting to the IRAM modified with a very efficient shift-invert preconditioner (9) (avoiding the problems that arise when system matrices are not positive definite). Moreover, the highly sparse linear system of equations is solved by using the multifrontal approach available in form of public domain library

UMFPacK. The whole sparse matrices have been directly filled in compressed Row-Wise format storage in order to decrease the memory requirement and speed-up matrices operations.

3. Numerical Results
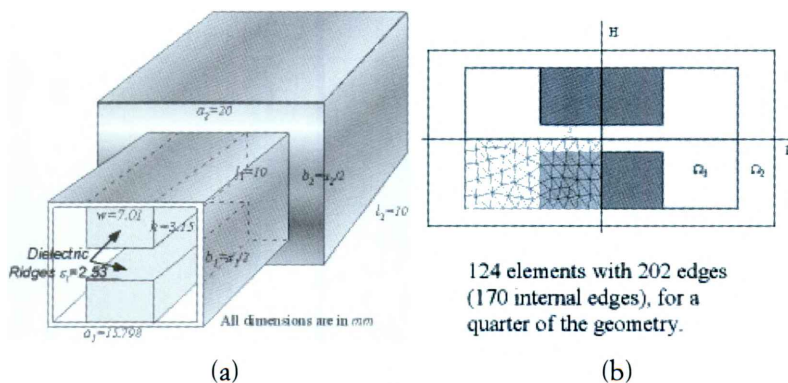
The junction under analysis is shown in Fig. 1-a.

124 elements with 202 edges (170 internal edges), for a quarter of the geometry.

(a)   (b)

FIG. 1

a) Geometry of the junction under investigation ($l_1=l_2=10$ mm, $a_1=15.798$ mm, $b_1=7.899$ mm, $a_2=20$ mm, $b_2=10$ mm, $w=7.01$ mm, $h=3.15$ mm, $\varepsilon_r=2.53$); b) The discretized domain is a quarter of the double ridged waveguide due to the E and H symmetry planes.

A comparison of the results found by means of this approach with those obtained by *Ansoft HFSS* is provided to show the effectiveness of the hybrid technique. Some junctions between rectangular waveguides with different dimensions and different fillings have been analyzed with both of the methods and the results compared quite well. The selection of modes has been performed according to the spectral criterion introduced in (2): after performing a convergence test, the first 19 TE and 13 TM modes have been taken into account into standard waveguide, while 20 modes have been considered into the double ridged waveguide. In particular, the S_{11} and S_{21} scattering parameters as a function of frequency are plotted in Fig. 2. Each frequency point analysis has required about 6.3 sec for HFSS simulation and 3.3 sec for the MM/FEM procedure on a Pentium IV 1.4 GHz workstation. The accordance between the computed parameters confirms the accuracy of the hybrid technique.
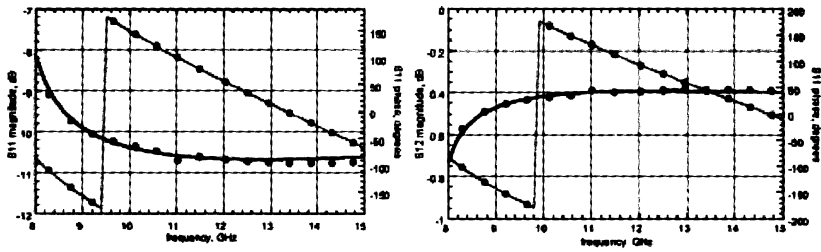
FIG. 2

Amplitude and phase of the S_{11} and S_{12} parameter in the single mode frequency range (8-15 GHz) of the junction of Fig. 1. Dots: HFSS simulation; continuous line: Hybrid MM/FEM method.

REFERENCES

(1) F. ARNDT, R. BEYER, J.M. REITER, T. SIEVERDING, T. WOLF, *Automated design of waveguide components using Hybrid Mode-Matching / Numerical EM building blocks in Optimization Oriented CAD frame-works. State-of-the-art and recent advances"*. IEEE Trans. on MTT, 45 (5), 747-759, May 1997.

(2) D. ARENA, M. LUDOVICO, G. MANARA, A. MONORCHIO, *Analysis of waveguide discontinuities using edge elements in a hybrid mode matching/finite elements approach*, IEEE M. & W. Components Lett., 11 (9), 379 -381, Sept. 2001.

(3) K.A. ZAKI, S.W. CHEN, C. CHEN, *Modeling Discontinuities in Dielectric-Loaded Waveguide*, IEEE Trans. on MTT, 36 (12), 1804-1810, December 1988.

(4) J. STRUBE, F. ARNDT, *Rigorous Hybrid-Mode Analysis of the Transition from Rectangular Waveguide to Shielded Dielectric Image Guide*, IEEE Trans. on MTT, 33 (5),.391-400, May 1985.

(5) G. CONCIAURO, M. GUGLIELMI, R. SORRENTINO, *Advanced Modal Analysis*, John Wiley & Sons, Ltd, 1999.

(6) A.S. OMAR, K. SCHÜNEMAN,*Transmission Matrix Representation of Finline Discontinuities*, IEEE Trans. on MTT, 33 (9), 765-770, Sept. 1985.

(7) F. LEE, D.K. SUN, Z.J. CENDES, *Full-Wave Analysis of Dielectric Waveguides Using Tangential Vector Finite Elements*, IEEE Trans. on MTT, 39 (8), 1262-1271, August 1991.

(8) J.L. VOLAKIS, A. CHATTERJEE, L. KEMPEL, *Finite element Method for Electromagnetics*, IEEE Press, 1998.

(9) V.V.S. PRAKASH, M. KUZUOGLU, R. MITTRA, *An efficient solution of the generalized eigenvalue problems for planar transmission lines*, Wiley, Microwave and Optical Technology Letters, 31 (3), 194-197, November 2001.

Studio di guide a microonde su substrati semiconduttori

FRANCESCO BERTAZZI (*), MICHELE GOANO (*),
GIOVANNI GHIONE (*)

Le linee di trasmissione su substrati semiconduttori sono ampiamente utilizzate nei dispositivi optoelettronici e nei circuti integrati. La presenza di strati con elevata conducibilità modifica in modo significativo le caratteristiche di propagazione delle guide a microonde. Le cariche libere nel semiconduttore schermano il campo elettrico dalle regioni piu drogate, mentre il campo magnetico penetra in profondità nel substrato; questo effetto determina un aumento della capacità per unità di lunghezza e di conseguenza un aumento dell'indice di rifrazione efficace della linea. Questa propagazione ad *onda lenta* costituisce una seria limitazione per i dispositivi distribuiti per applicazioni optoelettroniche, in cui è richiesta una condizione di sincronismo tra il segnale modulante a microonde e il segnale ottico modulato. In questo lavoro, viene presentato un solutore elettromagnetico ad elementi finiti basato sull'ipotesi di propagazione quasi-statica, ben giustificata dalle dimensioni micrometriche delle guide. Per descrivere l'interazione tra il campo elettromagnetico e le cariche libere nel semiconduttore, il modello elettromagnetico è stato accoppiato in modo autoconsistente con un modello di trasporto di deriva e diffusione.

Il simulatore numerico così sviluppato è stato applicato allo studio di modulatori ad elettroassorbimento ad onda progressiva, in cui esiste una complessa interazione tra il campo a microonde e il campo ottico. La fotogenerazione di portatori è stata inclusa nel simulatore introducendo un termine di generazione radiativa nel modello di trasporto.

(*) Dipartimento di Elettronica, Politecnico di Torino, Corso Duca degli Abruzzi 24, 10129 Torino

Study of photonic-crystal based photonic components employing the Finite Element Method

LORENZO ROSA (*), ANNAMARIA CUCINOTTA (*),
DAVIDE FERRARINI (**), MORENO MAINI (**),
FEDERICA POLI (*), STEFANO SELLERI (*), LUCA VINCETTI (**),
MAURIZIO ZOBOLI (**), ALTAF HUSSAIN BOUK (*)

SUMMARY. – *Photonic crystals are a remarkable platform for the construction of novel components, both in integrated optics and fiber technology, with interesting spectral performance, compactness and low loss. Analytical study of these devices is difficult due to a typically complex geometry and the nanometric scale necessary to obtain a photonic band gap at optical frequencies. The Finite Element Method (FEM), due to its inherent flexibility in describing complex geometries and index profiles, allows accurate analysis with efficient use of computational resources. This work presents some results obtained through the FEM study of the spectral properties of photonic crystal components in integrated optics, using time-domain and frequency-domain solvers for spectral analysis, and the non-linear, dispersion and amplification properties of photonic crystal fibers, using eigenvalue solvers for modal analysis.*

1. Introduction

Photonic crystals (PCs) are currently the subject of intense worldwide investigation by many research groups, because of their unconventional optical properties. PCs consist of a periodic structure built of dielectric materials with the purpose of obtaining a periodic crystal-lattice-like refraction index variation, resulting in a Photonic Band Gap (PBG), i.e. a wavelength range in which light propagation through the crystal is inhibited. Structures using a homogeneous dielectric medium with a lattice of air holes have been investigated. When a defect is introduced in the lattice, such as by removing a row of air holes, the resulting perturbation in the index perio-

(*) Dipartimento di Ingegneria dell'Informazione, Università di Parma, Parco Area delle Scienze 181/A, 43100 Parma, Italy
(**) Dipartimento di Ingegneria dell'Informazione, Università di Modena e Reggio Emilia, via Vignolese 905/b, 41100 Modena, Italy

dicity causes a localization of the electromagnetic field around the defect, enabling light guidance. PCs are used in a wide range of optical components such as optical waveguides, resonant cavities, directional couplers, beam splitters. In this way, it is possible to build compact devices with highly interesting spectral properties and low power loss.

Obtaining a PBG at optical frequencies involves the design of nanometric-scale devices which also typically employ complex geometries for the lattice definition, thus making analytical study very difficult. Many numerical methods have been devised over the years to overcome this handicap, and the relatively recent availability of low-cost and high-performance desktop computers has permitted the development of efficient solver codes. FEM is a very powerful general-purpose tool for the study of PCs, owing to its unique ability to describe complex lattice geometries, hole shapes and sharp refracting index variations. In fact it allows a discretization technique employing unstructured meshes which can be custom-tailored to the device structure. This usually requires a more complex formulation and implementation of the method, but permits an extremely efficient use of memory and computational resources, increasing the dimension of solvable problems while reducing solution time.

In this work, FEM is applied in different formulations to investigate the optical behaviour of PCs, both for spectral analysis in time-domain and frequency-domain and for modal analysis using eigenvalue solvers. The spectral solvers were employed for the study of optimal coupling characteristics in tapered junctions between conventional and PC waveguides, while the eigenvalue solvers were used in the study of the properties of PC fibers, especially regarding the minimization of losses.

2. Time-domain formulation

This approach (1, 2, 3) is based on the wave equation for a bidimensional domain in the yz-plane as follows

$$\frac{q_x}{c^2}\frac{\partial^2 \phi_x}{\partial t^2} + 2j\omega \frac{q_x}{c^2}\frac{\partial \phi_x}{\partial t} - \omega^2 \frac{q_x}{c^2}\phi_x - \frac{\partial}{\partial y}\left(p_z \frac{\partial \phi_x}{\partial y}\right) - \frac{\partial}{\partial z}\left(p_y \frac{\partial \phi_x}{\partial z}\right) = 0$$

where ϕ_x is the x-component of the complex wave amplitude of the electric or magnetic field, and p_i and q_i are the elements of the tensors

$$\begin{cases} \overline{\overline{p}} = \overline{\overline{\mu}}_r^{-1}, & \overline{\overline{q}} = \overline{\overline{\varepsilon}}_r & \text{when} \quad \phi_x = E_x \quad \text{for TE modes,} \\ \overline{\overline{p}} = \overline{\overline{\varepsilon}}_r^{-1}, & \overline{\overline{q}} = \overline{\overline{\mu}}_r & \text{when} \quad \phi_x = H_x \quad \text{for TM modes.} \end{cases}$$

The relative permittivity and relative permeability tensors are defined for an anisotropic medium as

$$\overline{\overline{\varepsilon}}_r = \begin{pmatrix} \varepsilon_x & 0 & 0 \\ 0 & \varepsilon_y & 0 \\ 0 & 0 & \varepsilon_z \end{pmatrix}, \quad \overline{\overline{\mu}}_r = \begin{pmatrix} \mu_x & 0 & 0 \\ 0 & \mu_y & 0 \\ 0 & 0 & \mu_z \end{pmatrix}.$$

Choosing the complex amplitude approach instead of the full-wave one, which varies very quickly in time, allows a much larger time step for the simulations, greatly reducing the computational time required for a given time interval analysis. The spatial domain is discretized using second-order triangular elements and, through a standard Galerkin procedure, the differential equation is reduced to a second-order equation in the time variable, which is then solved in time by applying again FEM to obtain a two-step time-marching scheme.

The field values obtained through the simulation are then Fourier-transformed and integrated on the input and output boundaries of the device to obtain reflection and transmission coefficients as a function of frequency. In this way the spectral properties are investigated on a large wavelength range with a single simulation, by employing a broadband impulse as the initial condition for the problem.

Reflections from the domain boundaries are avoided through the use of perfectly matched anisotropic (PMA) layers that completely enclose the domain.

3. Frequency-domain formulation

This approach (2, 3) is based on the curl-curl equation in the frequency domain, considering the full-wave field component Φ_x and the anisotropic medium described in the previous section:

$$\frac{\partial}{\partial y}\left(p_z \frac{\partial \Phi_x}{\partial y}\right) + \frac{\partial}{\partial z}\left(p_y \frac{\partial \Phi_x}{\partial z}\right) - \frac{\omega^2}{c^2} q_x \Phi_x = 0.$$

By once again applying spatial domain discretization using second-order triangular elements, solution through the Galerkin method yields the field distribution over the whole domain at a fixed frequency, as a function of a known input field defined on a portion of the domain boundary. Also in this case PMA boundary conditions have been implemented. The simulation is then repeated over a number of frequencies to obtain the field distribution from which the spectral properties are then calculated. While this approach is most resource-effective in analysing device properties over a narrow frequency bandwidth, a large number of simulations is required to obtain accurate wideband data, giving this formulation complementary characteristics with respect to the time-domain one.

Both approaches were employed in a recent study regarding the coupling between traditional dielectric and PC waveguides characterized by a

triangular lattice of air holes (4). The structure was investigated to provide guidelines for the design of efficient tapers in a wavelength range around 1550 nm, aiming for transmission spectra no lower than 80% and as flat as possible, in order to obtain a device suitable for WDM applications. Several structures have been simulated and checked by means of two-dimensional FEM solvers. For the time-domain simulation, a gaussian pulse with the magnetic field perpendicular to the domain plane, a TM mode, is launched along the waveguide and sampled after the photonic crystal taper in the output waveguide. If the guides are directly butt coupled, there is substantial loss due to scattering and reflection in the transition region, because of the different spatial mode profiles and the impedance mismatch at the guide interface, especially because traditional dielectric slabs are usually much larger than a single-defect PC waveguide. The problem is overcome by employing a larger PC waveguide, three-defect or five-defect, which gradually tapers to a single-defect one, by varying the diameter of the air holes and shifting their position with respect to the interface. Several simulations have been carried on by changing the taper properties to achieve a flat transmission spectrum, removing oscillations and dips or moving them out of the third telecommunications window. Coupling values over 85% were achieved over a range larger than 100 nm around the 1550 nm wavelength with a traditional slab as large as a five-defect PC waveguide (Fig. 1).

(a)   FIG. 1   (b)
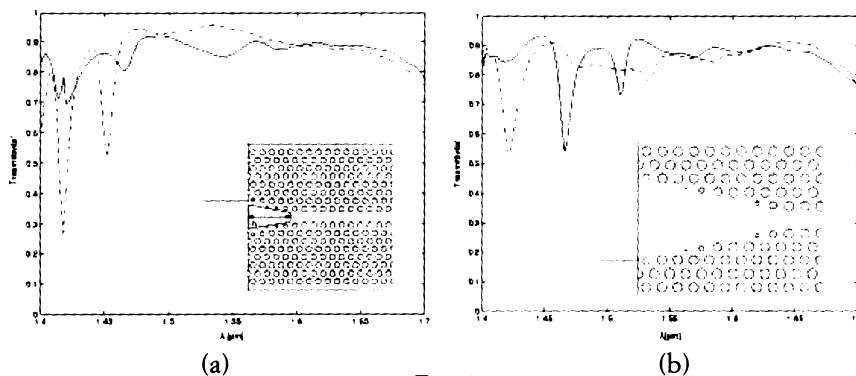
Transmittivity spectra for two taper structures between a single-defect PC waveguide and (a) a three-defect wide slab, and (b) a five-defect wide slab

4. Eigenvalue formulation

This formulation (5) is based on the full-vector curl-curl equation

$$\overline{\nabla} \times \left(\overline{\overline{\varepsilon}}_r^{-1} \overline{\nabla} \times \overline{H} \right) - k_0^2 \overline{\overline{\mu}}_r \overline{H} = 0$$

where H is the magnetic field, ε_r and μ_r are the relative dielectric permittivity and magnetic permeability tensors and k_0 is the wave number in the vacuum. By applying the variational FEM, the curl-curl equation yields the algebraic problem

$$\left(\left[A\right]-\gamma^{2}\left[B\right]\right)\left\{h\right\} = 0$$

where the eigenvector $\{h\}$ and the eigenvalue γ^2 provide, respectively, the full vectorial magnetic field distribution and the propagation constant of the mode. The solution spectrum is polluted by non-physical solutions called spurious modes, which are overcome by using high-order edge elements resulting also in better propagation constant accuracy. In order to save computational resources, structure symmetries are exploited for the numerical simulations. From the propagation constant, various parameters such as the group delay parameter and the dispersion parameter can be derived using higher-order finite difference formulas, and the complex index itself yields the phase constant and the attenuation constant, from which the loss properties of the guide can be determined. This formulation is able to deal with anisotropic material both in terms of dielectric permittivity and magnetic permeability, allowing anisotropic PMLs to be directly implemented.

This approach was recently used to study the losses arising in photonic crystal fibers (PCFs) in the third telecommunications window (6, 7). From the theoretical point of view, lossless propagation is possible only with a lattice of infinite extent, in this case made of longitudinal air holes in the fiber glass, but in practice the number of holes is finite and this causes the modes of the fiber to become leaky. A FEM solver based on a complex formulation was applied to the analysis of the leakage properties of modes in holey fibers, with both circular and non-circular holes, either with or without a photonic band gap. Three types of fibers were compared, that is PCFs based on a triangular lattice of air holes, honeycomb fibers and cobweb fibers.

In triangular PCFs the losses quickly decrease by increasing the number of hole rings and the hole diameter, yielding a loss ranging from 5×10^7 dB/km to a lower value of 10^{-2} dB/km which is negligible with respect to all the other causes of losses, like absorption and Rayleigh scattering (Fig. 2).

In honeycomb fibers, where the defect consists of an extra hole with the same diameter as that of the lattice holes, guidance of light is due to a photonic band gap. Due to the resulting lower air filling factor, the mode is less confined, which yields losses always higher than 10^4 dB/km at a wavelength of 1550 nm, even considering eight hole rings. A weaker dependence on the number of rings is also observed, which can be ascribed to the fiber guidance mechanism, as the fiber lattice determines a truly photonic band gap only if the number of rings is very high.
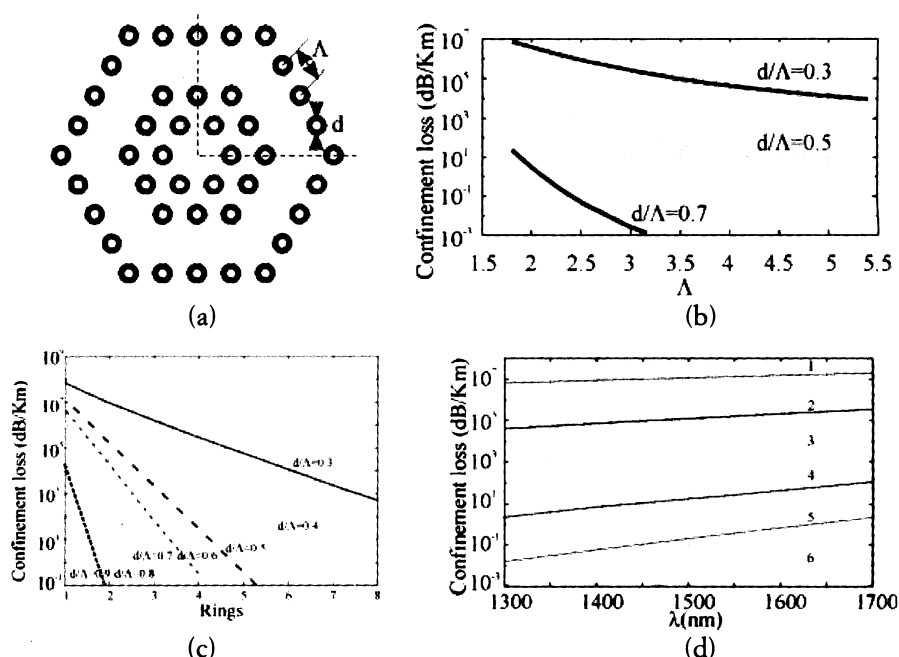
FIG. 2

(a) Triangular PCF cross-section, confinement loss of triangular PCF as a function of (b) Λ for a three-ring structure and different d/Λ values, (c) the number of rings for $\Lambda = 2.3$ μm and different d/Λ values, and (d) the wavelength for $\Lambda = 2.3$ μm and $d/\Lambda = 0.5$ and different number of rings.

Cobweb fibers consist of a non-periodic arrangement of large non-circular air holes, separated by very thin silica bridges with a thickness of about 120 nm, resulting in very low losses. Small effective area and very high negative dispersion are other features which make this type of fiber very interesting. Analysis shows that the wavelength dependence of confinement loss is stronger than the previous fibers and increases by increasing the number of rings, resulting in changes of six order of magnitudes between 1300 and 1700 *nm*. However, in the whole wavelength range the losses remain lower than 10^3 dB/km with one ring and lower than 10^{-2} dB/km with three rings, mainly due to the field which passes through the silica bridges.

These results prove that very-low-loss PCFs can be designed. In particular, fibers with negligible confinement losses can be obtained for both triangular and cobweb fibers. On the contrary, it has been observed that honeycomb fibers exhibit higher losses also with cross sections having many air holes. These results confirm that proper design of PCFs opens the possibility to achieve very low losses, comparable to those of standard telecommunication fibers.

REFERENCES

(1) A. BERTOLANI, A. CUCINOTTA, S. SELLERI, L. VINCETTI, M. ZOBOLI, Opt. Quantum Electron., **35**, 1005-1023 (2003).

(2) A. CUCINOTTA, S. SELLERI, L. VINCETTI, M. ZOBOLI, Appl. Phys, **B 73**, 595-600 (2001).

(3) A. CUCINOTTA, S. SELLERI, L. VINCETTI, M.ZOBOLI, Proceedings ECIO 2001, April 4-6 (2001), pp. 437-440.

(4) G. CHIETERA, A. BOUK, F. POLETTI, F. POLI, S. SELLERI, A. CUCINOTTA, Micr. Opt. Tech. Letters, **42**, 1096-1099 (2004).

(5) A. CUCINOTTA, S. SELLERI, L. VINCETTI, M. ZOBOLI, J. Lightw. Technol., **20**, 1433-1442 (2002).

(6) D. FERRARINI, L. VINCETTI, M. ZOBOLI, A. CUCINOTTA, L. SELLERI, Optics Express, **10**, 1314-1319 (2002).

(7) D. FERRARINI, L. VINCETTI, M. ZOBOLI, A. CUCINOTTA, F. POLI, S. SELLERI, Proc. OFC 2003, Vol. 2, pp. 699-700 (2003).

Finite-element method in antenna feed systems design: an application to corrugated waveguide E-Plane low-pass filter

ANTONINO INCORVAIA (*), TINDARO CADILI (*),
ENRICO FRANCESCHI (**)

SUMMARY. – *The increasing complexity of passive microwave components for antenna feed systems requires analysis and design tools based on more powerful and flexible numerical methods than in the past. The extension of Finite-Element Method from engineering and physics to electromagnetics for the solution of Maxwell's equations has allowed to solve EM relationships for arbitrary geometries and materials. The Finite-Element Method has been applied in conjunction with Mode-Matching Method, a classical technique in electromagnetics, for the analysis and design of corrugated waveguide E-plane low-pass filters with high performance requirements in terms of rejection band and insertion loss. A well-known commercial software, Ansoft HFSS v9.0, has been used for numerical simulation of insertion losses due to finite conductivity of filter material. A good agreement with measured results shows the accuracy of the analyses performed by Finite-Element Method applied in electromagnetics.*

1. Introduction

Satellite communications ground segment requires high isolation level between TX and RX bands. In order to achieve the system architecture specifications, low-pass filters with low insertion loss and high stop-band rejection levels are requested. In particular a corrugated waveguide E-plane low-pass filter has been designed and manufactured for an antenna feed system application for satellite antennas test.

(*) Marconi Selenia Communications, Via S. Sonnino 6, 95045 Misterbianco (CT), Italy
(**) Marconi Selenia Communications, Via A. Negrone 1/A, 16153 Cornigliano (GE), Italy

In Tab. 1 the main relevant requirements are summarized:

Tab. 1
Low-pass Filter requirements

Pass-band	10.70÷12.45 GHz
Reject-band	12.75÷14.5 GHz
In-band Insertion Loss	≤ 0.5 dB
In-band Return Loss	≤ -24 dB
Min Stop-band Rejection	≥ 100 dB@12.75÷13.50 GHz
	≥ 50 dB@14.00 GHz
	≥ 25 dB@14.25 GHz

In order to achieve the requested stop-band rejection a fast slope of insertion loss needs between RX and TX bands that are separated by a frequency gap of 300 MHz only. Therefore a low-pass filter with a remarkable number of cavities, i.e. nine cavities, has been to be designed in order to achieve the requested stop-band rejection level.

2. Filter Analysis and Synthesis

The analysis and synthesis of corrugated waveguide E-plane filters has been performed by means of Mode-Matching Method, a well-known and confirmed technique for analysis and design of millimetric-wave waveguide components. The fields on both sides of the discontinuity are expanded in terms of normal modes of the respective waveguides, so the boundary conditions are transformed into a matrix equation in the expansion coefficients. Unfortunately a strong increase of complexity in theoretical formulation of normal modes expansions occurs when rounded geometries or finite conductivity losses are involved.

The corrugated waveguide E-plane low-pass filters type is affected by strong interactions between effects of material finite conductivity and resonant cavities. Therefore the insertion loss increases dramatically near the end of RX passband up to levels not compliant to system requirements. This problem can be solved taking into account a frequency margin on upper limit of RX band so the increase of insertion loss occurs outside RX passband. A trade-off between frequency margin and rejection value at lower stop-band limit allows to optimize filter performance in order to be compliant to system requirements.

Filter design has been performed in two phases. The low-pass perfect conductor filter design has been obtained by means of *FORTRAN* code including optimization routines to carry out the exact analysis and synthesis of lossless waveguide component based on Mode-Matching Method.

In order to perform the actual filter analysis a reliable design tool needs to take into account material finite conductivity as a part of resonant cavity problem, a demanding task for Finite-Element Method applied in electromagnetics. A well-known commercial software, *Ansoft HFSS v9.0*, has been used for this application. Silver finite conductivity has been considered for solving material losses problem. The conjunction of Mode-Matching optimization and FEM analyses has allowed to achieve the filter specifications meeting system requirements.

3. Simulations vs. measured results comparison

In order to obtain more accurate results *HFSS* simulations have been performed splitting the extended frequency range (10.70÷14.50 GHz) into three intervals.

A suitable adaptive frequency has been chosen inside each interval, at more critical frequency points, i.e. near upper RX passband limit and lower stop-band frequency. Adaptive passes have been performed at passband center frequency also. Following adaptive analyses, Fast Frequency Sweep has been performed in each interval. The width of frequency intervals has been defined reducing critical ranges near the gap between RX and TX bands.

Scalar Network Analyzer and Spectrum Analyzer measurements have been performed on production articles in order to test return loss and insertion loss, and stop-band rejection respectively.

HFSS simulations vs. measured results are reported in Figs. 1, 2 and 3. Passband return loss does not exceed -24 dB and a good agreement of

····· Insertion Loss (measured)
—— Return Loss (measured)
---- Insertion Loss (HFSS v9)
---- Return Loss (HFSS v9)
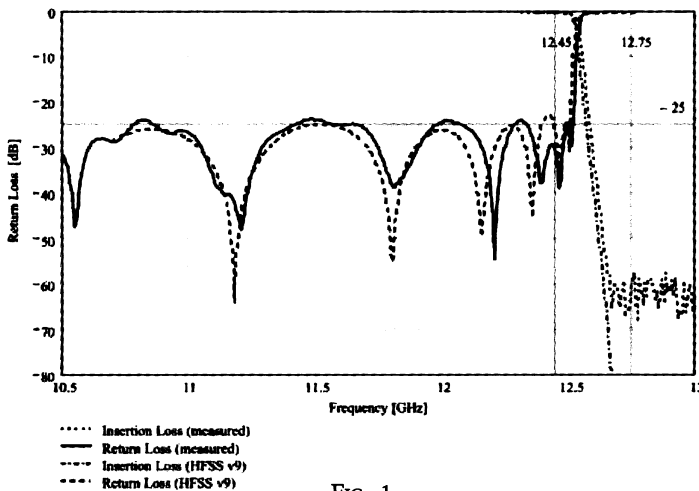
FIG. 1

Theoretical and experimental return loss and insertion loss

zeros frequencies has been obtained, taking into account the dimensional differences due to production tolerances. Excellent agreements on passband insertion loss and stop-band rejection level have been obtained also.
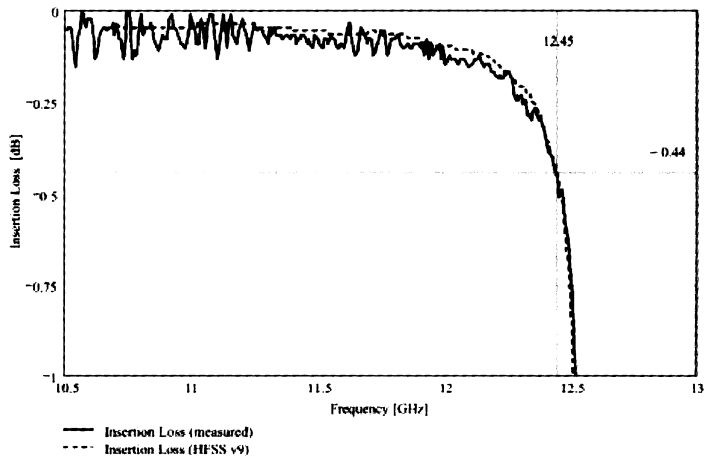
FIG. 2

Theoretical and experimental insertion loss at upper limit of RX band
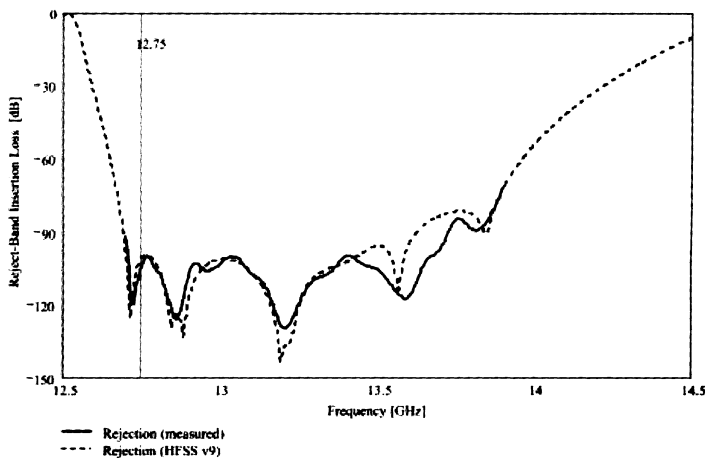
FIG. 3

Theoretical and experimental rejection level

4. Conclusion

A well-known commercial software implementing Finite-Element method, *Ansoft HFSS v9.0*, has been used for numerical simulation of corrugated waveguide E-plane filter. A good agreement of FEM simulations to Mode-Matching results for perfect conductor case and Scalar Network and Spectrum Analyzers measurements for finite conductivity material shows the accuracy of the analyses performed by Finite-Element Method applied in electromagnetics.

REFERENCES

G.L. MATTHAEI, L. YOUNG, E.M.T. JONES, *Microwave Filters, Impedance Matching Networks and Coupling Structures*, McGraw-Hill, New York, 1965

Analysis of signal integrity and electromagnetic interference of high-speed digital systems

ANDREA ALÙ (*), FILIBERTO BILOTTI (*),
ALESSANDRO TOSCANO (*), LUCIO VEGNI (*)

SUMMARY. – *Il principale obiettivo di questo contributo è quello di fornire una nuova formulazione variazionale che permetta di generalizzare il metodo agli elementi finiti per permettere lo studio dell'integrità di segnale e delle emissioni elettromagnetiche proprie di sistemi digitali ad alta velocità realizzati su substrati non convenzionali. Successivamente questo risultato verrà applicato al caso di strutture elettromagnetiche aperte in presenza di piani di massa di dimensione finita.*

1. Introduction

In the realm of high-speed digital design, signal integrity has become a critical issue, and is posing increasing challenges to the design engineers. In this contribution, we will discuss what the typical signal integrity problems are, where they come from, why it is important to understand them and how we can analyze and solve these issues.

Signal integrity (SI) is not a new phenomenon and it did not always matter in the early days of the digital era. But with the explosion of the information technology and the arrival of Internet age, people need to be connected all the time through various high-speed digital communication/computing systems. In this enormous market, signal integrity analysis will play a more and more critical role to guarantee the reliable system operation of these electronics products. Without pre-layout SI guidelines, prototypes may never leave the bench; without post-layout SI verifications, products may fail in the field.

(*) Università Roma Tre, Dip. Elettronica Applicata, Via della Vasca Navale 84, 00146 Rome, Italy

Many SI and EMC computer simulation tools are based upon the finite element method (FEM). The FEM solves for voltages and currents in the space surrounding the conductor and dielectric structures and requires a calculation grid to be extended well beyond the structures if reasonable accuracy is to be achieved. The FEM is preferred for high-power equipment applications (such as magnetics analysis for power transformers and rotating machinery) and in conjunction with the boundary integral (BI) for detailed power and ground plane modelling in PCBs. Some SI tools forsake field analysis altogether and depend entirely on approximate mathematical equations to estimate parasitics. This approach yields very poor accuracy and usually unacceptable results. The boundary element methodologies favoured are generally considered to be the most accurate available. These methods not only result in excellent accuracy, but also stable matrices and computational efficiency.

In this paper we present a new variational formulation for microstrip lines loaded by general bi-anisotropic materials and/or metamaterials. Such a formulation is very general and allows to study as particular cases structures with isotropic, anisotropic and also bi-isotropic (e.g. chiral), homogeneous and inhomogeneous substrates. The electromagnetic problem is then numerically solved by using a hybrid finite element-boundary integral method.

2. Solution of the electromagnetic field

The substrate material is described by means of the following constitutive relations:

[1]
$$\begin{cases} D = \underline{\varepsilon}(r) \bullet E + \underline{\xi}(r) \bullet H \\ B = \underline{\zeta}(r) \bullet E + \underline{\mu}(r) \bullet H \end{cases}$$

being E and H being the electric and magnetic field, respectively; D and B the electric displacement and the magnetic flux density, respectively; $\underline{\varepsilon}(r)$, $\underline{\mu}(r)$ the permittivity and permeability tensor, respectively; $\underline{\xi}(r)$, $\underline{\zeta}(r)$ the tensors describing the magneto-electric effect. It is to be remarked that the material here considered is a general inhomogeneous bi-anisotropic material with a spatial variation of the electromagnetic parameters and that even metamaterials are described by this formulation.

Starting from the curl Maxwell equations written for a time dependence $\exp[j\omega\tau]$ we found that the functional $F(f, f^a)$ that is stationary for arbitrary variations of f and f^a around a stationary point is given by:

$$F\left(E, E^a\right) = <\mu^{a-1} \bullet \left(\nabla \times E^a + j\omega \underline{\xi} \bullet E^a\right),$$

$$\nabla \times E + j\omega\underline{\zeta} \bullet E > + \omega^2 < E^a, \ \underline{\varepsilon} \bullet E > +$$

[2]
$$- < E^a, \ j\omega J > - < j\omega J^a, \ E > +$$

$$+2\omega\frac{k_0}{\eta_0}\int_{S_{ap}}\left(\hat{n} \times E^a\right)^* \bullet \left[\int_{S_{ap}}\underline{G}(r,r') \bullet \left[\hat{z} \times E(r')\right]dS'\right]dS$$

with

$$\underline{G}(r,r') = \left[\underline{I} + \frac{1}{k_0^2}\nabla\nabla\right]\frac{e^{-jk_0|r-r'|}}{4\pi|r-r'|}.$$

The functional $F(f, f^a)$ is completely equivalent to the boundary value problem under consideration.

In order to evaluate the electromagnetic quantities, the finite volume is discretized in N elements of proper shape (brick, tetrahedral, etc.) and the unknown field E, E^a are expanded in terms of a proper set of vector basis functions W_i.

Applying a properly modified Rayleigh-Ritz procedure the following equation holds:

[3]
$$\underline{A} \bullet X = B$$

where

$$A_{ij} = A_{ij}^{(B.I.)} + \sum_{k=1}^{5} A_{ij}^{(k)}, \quad B_i = \int_V W_i \bullet J \, dV \quad \text{and} \quad X_i = E_i$$

and:

$$A_{ij}^{(1)} = -\int_V \left(\nabla \times W_i\right) \bullet \underline{\mu}^{-1} \bullet \left(\nabla \times W_j\right)dV$$

$$A_{ij}^{(2)} = -j\omega\int_V \left(\nabla \times W_i\right) \bullet \underline{\mu}^{-1} \bullet \left(\underline{\zeta} \bullet W_j\right)dV$$

$$A_{ij}^{(3)} = j\omega\int_V W_i \bullet \underline{\xi} \bullet \underline{\mu}^{-1} \bullet \left(\nabla \times W_j\right)dV$$

$$A_{ij}^{(4)} = -\omega^2\int_V W_i \bullet \underline{\xi} \bullet \underline{\mu}^{-1} \bullet \left(\underline{\zeta} \bullet W_j\right)dV$$

$$A_{ij}^{(5)} = \omega^2\int_V W_i \bullet \left(\underline{\varepsilon} \bullet W_j\right)dV$$

$$A_{ij}^{(B.I.)} = 2\omega\varepsilon_0\lambda_i\lambda_j\int_{S_{ap}}\left(\hat{z} \times W_i\right) \bullet \left[\int_{S_{ap}}G_0(r,r')\left[\hat{z} \times W_j\right]dS'\right]dS +$$

$$-2\omega\mu_0^{-1}\lambda_i\lambda_j\int_{S_{ap}}\nabla \bullet \left(\hat{z} \times W_i\right) \bullet \left[\int_{S_{ap}}G_0(r,r')\left[\nabla' \bullet \left(\hat{z} \times W_i\right)\right]dS'\right]dS$$

3. Numerical results

As a numerical example, we consider a PCB board which is 10 cm long, 6 cm wide and 50 mils (1.3 mm) thick (Fig. 1). The relative permittivity of the FR4 material is approximate 4.5. A gap is cut in the middle of the ground plane. The gap is 4 cm long and 5 mm wide. An 8.2-cm long trace crosses the gapped ground plane. The trace is terminated at one end by a 47 Ω SMT resistor. A hybrid FEM/BI code (Ray[3]) developed at "Roma Tre" (1) is used to model this problem.

BI is used to model the fields on the surface of the board while FEM is used to model the fields within the dielectric. Triangular elements are used to approximate the surface fields, and tetrahedral elements approximate the fields within the dielectric.
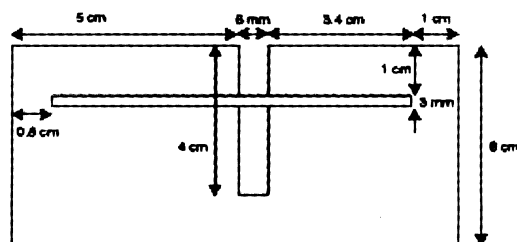
FIG. 1

Geometry of a trace crossing a gapped ground plane

The measured results are compared with the numerical results obtained with a commercial code in Fig. 2. In Ray[3], a minimal mesh (requiring 75 Mbytes of memory) is used since a normal-size mesh requires 400 Mbytes of memory. The problem is more efficiently modeled using the hybrid approach because the dielectric is modeled using FEM, which requires less computer memory. Figure 3 shows that below 200 MHz, the trace can be treated as a 50-Ω transmission line. When the frequency is higher than 200 MHz, the trace is no longer a 50-Ω transmission line.
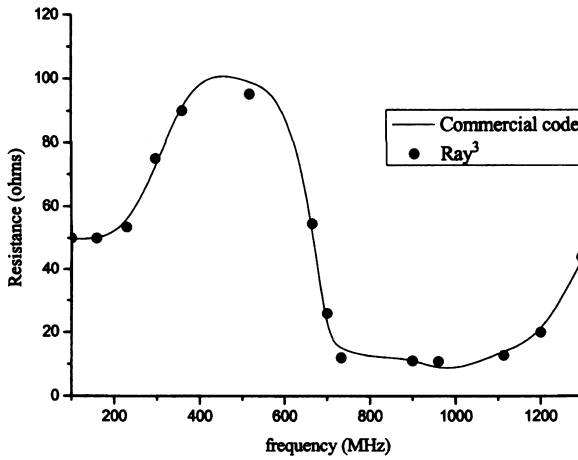
FIG. 2

Input resistance vs. frequency.

REFERENCES

(1) F. BILOTTI, L. VEGNI, A. TOSCANO, *Radiation and Scattering Features of Patch Antennas with Bianisotropic Substrates*, IEEE Trans. on Antennas and Propagation, **51** (3), 449–456, 2003.

The Finite Element Method for the assessment of the shielding effectiveness

SALVATORE CAORSI (*), GAIA CEVINI (*)

SUMMARY. – *This paper is focused on the application of the finite element method for the evaluation of the scattering properties and the shielding performance of simple geometries in a 2D configuration. Both a frequency-domain FEM formulation and a time-domain one are used to evaluate the shielding effectiveness of a circular enclosure as a function of the spatial coordinates and of the geometric characteristics of the shield. The computational performances of both algorithms will be compared.*

1. Introduction

The problem of determining the scattering properties and the shielding performances of enclosures has a relevant importance for the electromagnetic compatibility analysis of systems and circuits. In particular, the design of protection structures needs a suitable electromagnetic simulation of the effects that the structures produce in the existing electromagnetic field distribution in the investigated environment. Moreover, it is well known that the shielding efficiency of the enclosures in mitigating the transmitted electromagnetic field is strongly influenced by the dielectric parameters of the enclosure's material, by the dimensions of the structure and by other factors such as the roughness of the surface and the presence of holes and apertures. Besides the aforementioned features, it is worthy to note that the shielding effectiveness (SE) evaluation is also dependent on the spatial coordinates of the observation point and on the relative position between the electromagnetic source and the observation point. In this sense, the shielding effectiveness is a local quantity. Only recently, a new definition for the shielding performances of enclosures has been proposed (4), on the basis of

(*) Department of Electronics, University of Pavia, via Ferrata 1, 27100 Pavia, Italy

a "global" figure of merit (GSE) related to the integral of the electromagnetic field.

For the purpose of numerical modelling the electromagnetic problem described, the finite element method provides flexible codes capable to handle complex geometries and inhomogeneous materials, thanks to the possibility of exploiting unstructured and non-uniform spatial grids. In the present paper, a finite element formulation is used for the computation of the electric field in the presence of simple shielding structures. Besides, both the frequency-domain formulation of the finite element algorithm and the time-domain formulation are considered with the purpose of wide-band modelling the electromagnetic scattering from the structures and to compute the transient fields (1)-(2).

The present investigation considers 2D geometries involving lossy cylindrical structures. We have used a total field finite element formulation based upon the second-order vector wave equation. The numerical domain is truncated by means of an absorbing boundary condition (3). The electromagnetic source is an infinite current line radiating a TM wave while the scatterer and the observation points are placed in its near field region.

The scattering from the shielding structures is computed to evaluate the shielding effectiveness of the enclosure as a function of the spatial position, the geometric features and the frequency. Finally, some computations are made to evaluate the "global" shielding effectiveness proposed in (4). Both the frequency-domain algorithm and the time-domain one are used and their accuracy and computational cost, in performing a wide-band simulation, compared.

2. FEM formulation

Both the frequency-domain and the time-domain algorithms exploited a non-uniform mesh of triangular elements, truncated by a rectangular boundary, on which the first-order ABC is applied. Since the problem is two-dimensional and the electric field has only one component, we have chosen to approximate the unknown field by nodal linear interpolation functions.

The time-domain formulation leads to a matrix equation in an implicit scheme (3), solved by a conjugate gradient method. The time step Δt has been always set to 20 ps and the transient fields have been observed for 2^{10} time steps.

3. Numerical results

The simple geometry considered here is a cylindrical enclosure of circular cross section, embedded in air. The electromagnetic source is lo-

cated 0.04 m far away from the structure and it radiates a bipolar pulse obtained by a gaussian modulation of a 250 MHz sine carrier. This way, the duration of the pulse is nearly equal to 4 ns while its frequency content extends slightly above 1000 MHz.

As a first step of analysis, we have exploited the time-domain FE algorithm, combined with the discrete Fourier transform (DFT), to calculate the transmitted electric field at the center of the shell and to perform a wide-band calculation of the shielding effectiveness achieved at that point. The shell is characterized by $\varepsilon_r = 8.0$, $\mu_r = 1.0$ and $\sigma = 1.0$ S/m, while the thickness is equal to 0.005 m. The results of the numerical simulations are reported in Fig. 1, where we have plotted the SE achieved by varying the external radius of the structure. As can be observed, the value of the SE are very small due to the small conductivity of the structure but the resonance frequencies can be identified with a satisfactory accuracy even if the resonance peaks are very broad. Besides, as can be expected, the resonance frequency increases by decreasing the radius of the structure.
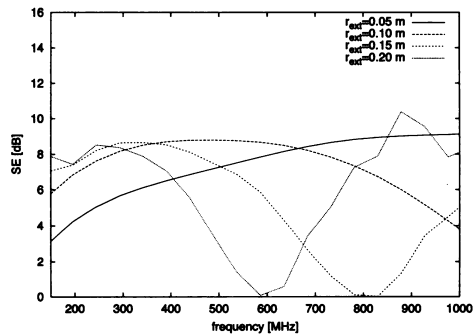
FIG. 1

Circular enclosure: varying radius.
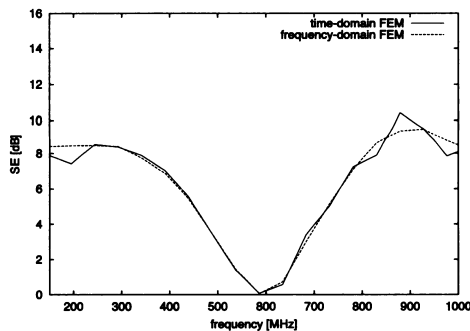
FIG. 2

Time-domain versus frequency-domain.

Also the frequency-domain FE algorithm has been used to perform the same kind of computation and the result is plotted in Fig. 2, as compared to the curve obtained by using the time-domain code. To perform the wide-band computation, we considered 40 frequency steps, separated by $1/(2^{10}\Delta t)$. The SE is computed for the shell characterized by an external radius equal to 0.20 m. Both the algorithms have been made to run on the same mesh with 26041 unknowns. As can be seen, the results are characterized by the same accuracy. As far as CPU time is concerned, while the time-domain algorithm performs its computation in 176.26 seconds, the frequency-domain code took about 1225.45 seconds.

The second step of analysis considered an enclosure of different shape. The evaluation of the shielding effectiveness of a cylindrical enclosure of square cross-section is now addressed. For comparison purposes, let's consider a shell with the same dielectric characteristics of the circular enclosure. In Fig. 3 we reported the result of the wide-band computation achieved by means of the TDFEM/DFT algorithm for a square shell of external dimension equal to 0.40 m and thickness 0.005 m, as compared to the one achieved by the circular enclosure with external radius equal to 0.20 m.
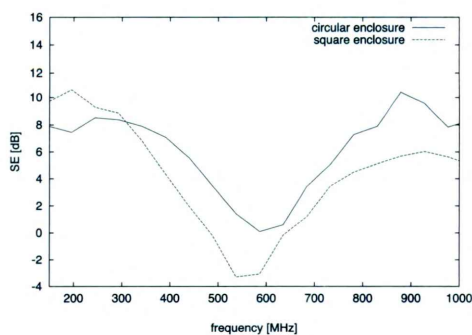
Fig. 3

Enclosure: varying shape.
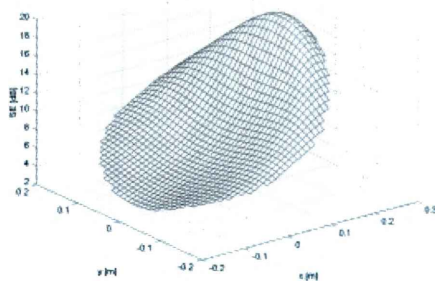
Fig. 4

SE distribution at 250 MHz.

Finally, we considered the evaluation of the spatial distribution of the SE and the computation of the GSE (4) as

$$GSE\left[dB\right] = 20\log\frac{\int_{encl} E_i dS}{\int_{encl} E_t dS}$$

where E_i is the amplitude of the incident field and E_t is the amplitude of the transmitted one into the shell and the integral is computed over the area enclosed by the shield. To perform this kind of analysis we exploited the frequency-domain FE algorithm. In Figs. 4-6, we plotted the SE computed inside the circular enclosure of radius 0.20 m by varying the frequency of a monochromatic current line source (250 MHz, 500 MHz and 1000 MHz). As can be seen from the graphs, while at low frequency the highest SE is achieved at those points which are more distant form the source, when the frequency increases the distribution changes due to the appearing of resonance phenomena. The values of the GSE calculated for the same geometric configuration are reported in table 1.
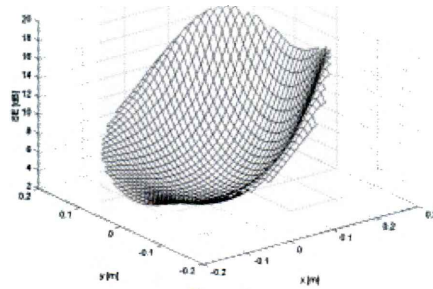
FIG. 5

SE distribution at 500 MHz.
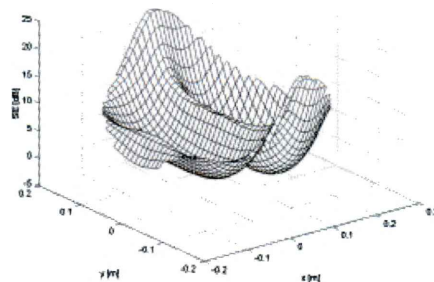
FIG. 6

SE distribution at 1000 MHz.

Table 1
Values of the global SE.

Frequency	GSE [dB]
250 MHz	8.374 dB
500 MHz	6.592 dB
1000 MHz	5.822 dB

4. Conclusions

The finite element method has been applied to evaluate over a wide-band the shielding effectiveness of simple geometric structures like circular enclosures as a function of the geometric parameters and the spatial position. Both the frequency-domain and the time-domain algorithms have been considered and their performances compared. The computation of a recently introduced new figure of merit has been also taken into account.

REFERENCES

(1) J.-M. JIN, *The finite element method in electromagnetics,* John Wiley & Sons, 1993.

(2) J.-F. LEE, R. LEE, A.C. CANGELLARIS, *Time-domain finite-element methods,* IEEE Trans. on Antennas and Propagation, **45** (3), 430-445, 1997.

(3) S. CAORSI, G. CEVINI, *Assessment of the performances of first- and second-order time-domain ABCs for the truncation of finite element grids,* Microwave and Optical Technology Letters, **38** (1), 11-16, 2003.

(4) S. CELOZZI, *New figures of merit for the characterization of the performance of shielding enclosures,* IEEE Trans. on Electromagnetic Compatibility, **46** (1), 142, 2004.

"L'avventura della radio"
Un viaggio nella storia, scienza e arte
delle Telecomunicazioni - "Collezione Patanè"

Firenze, 4-28 giugno 2004

Salone Brunelleschi, Istituto degli Innocenti
P.zza SS. Annunziata 12

INDICE

Presentazione

La radio ha svolto un ruolo fondamentale a partire dai primi esperimenti della fine del XIX secolo: ha contribuito al cambiamento della società, ha promosso lo sviluppo tecnico e scientifico, ha permesso la nascita di nuove espressioni artistiche.

Questa mostra di radio di epoca, organizzata nell'ambito delle manifestazioni degli 80 anni dell'Università degli Studi di Firenze, propone un percorso storico dell'evoluzione tecnologica di apparecchiature e strumentazione radio di circa 40 anni a partire dall'inizio del Novecento. I 71 esemplari in mostra, messi gentilmente a disposizione dal CNIT, provengono dalla più ampia "Collezione Patanè" (385 pezzi), oggetto di un lascito testamentario del collezionista Don Giovanni Patanè, che include una ricca e pregevole raccolta di radio e di fonografi d'epoca ed è una delle più importanti del settore in Italia, ben nota negli ambienti degli appassionati.

La mostra è articolata in quattro sezioni tematiche: la prima illustra i primi ricevitori nelle varianti tecniche dei modelli storici dell'epoca (a cristallo, a 'galena', a carborundum e a polveri), la seconda le successive radio a valvole, la terza mostra una selezione "Marconiphone" e la quarta alcuni esempi di strumentazione speciale per trasmissione e apparati di crittografia.

I primi apparecchi ricevitori consentivano la riproduzione del segnale con limitata amplificazione e qualità che richiedevano l'impiego di cuffie per l'ascolto. L'importanza strategica della comunicazione via onde radio diede un impulso formidabile alla ricerca e un passo decisivo fu fatto con l'impiego delle valvole che, aumentando qualità e amplificazione dei ricevitori e migliorando le prestazioni dei dispositivi di trasmissione, rese possibile la radiodiffusione. Nel primo dopoguerra ebbe così inizio la produzione industriale di radio a valvole anche per un mercato commerciale di più largo consumo fino all'introduzione delle radio a transistor della fine degli anni '50.

Parallelamente il design esterno assumeva a sua volta una grande importanza: doveva nascondere la tecnologia e proporre mobili eleganti e raffinati per i salotti dove i nuovi apparecchi generalmente venivano collocati anche con funzione di arredamento e di socializzazione.

La dimensione popolare della radio ha agito sulle espressioni artistiche, di cui un esempio è la utilizzazione scenografica degli apparecchi radio nel cinema muto dell'epoca. L'immagine della radio era capace di 'sonorizzare'

una storia senza parole perché, come ad esempio il grammofono, suggeriva immediatamente con la sua stessa fisicità il suono corrispondente. La sua presenza nell'arredo era il segno anche di una società più evoluta, solitamente cittadina: uno *status symbol* gemellare rispetto al cinema stesso. Radio e cinema insieme evocavano e raddoppiavano il richiamo al progresso. Il cinema faceva eco alla radio e viceversa la radio amplificava i contorni di uno spettacolo che si annunciava sempre più multimediale.

Enrico Del Re
Università di Firenze

PARTE I

La "Collezione Patanè"

In occasione dell'ottantesimo anniversario della fondazione dell'Università degli Studi di Firenze, il Consorzio Nazionale Interuniversitario per le Telecomunicazioni (CNIT), di cui l'Ateneo fiorentino è stato socio fondatore nel 1995, ha voluto offrire il materiale per una mostra di "Radio d'epoca" al godimento della comunità scientifica fiorentina e della cittadinanza, come testimonianza di un impegno a collaborare in modo sempre più stretto con le sue istituzioni pubbliche, scientifiche e di alta formazione.

La collezione è stata donata al CNIT con atto testamentario nel 2000 dal compianto don Giovanni Patanè, luminosa figura di sacerdote e collezionista, che l'ha raccolta lungo tutto l'arco della sua vita con passione e competenza inusuali.

Nato e cresciuto nella sua bella e mai dimenticata Catania, Giovanni Patanè si trasferì a Parma dalla Sicilia per essere vicino allo zio, anch'egli sacerdote, nella cui parrocchia, a Campora, fu ordinato prete nel 1946 dal vescovo, monsignor Colli. Subito dopo l'ordinazione, iniziò la sua missione nella provincia di Parma, che l'avrebbe visto operare in vari luoghi lungo tutto l'arco della sua vita, con personalità spiccata, affrontando conschiettezza e decisione le questioni, arrivando ai risultati. Inviato, quale coadiutore, per un anno a Mezzano Rondani, gli fu successivamente affidato il ministero parrocchiale di Ballone di Corniglio, sito sulle pendici del monte Caio, nel profondo Appennino Parmense. Qui nel 1954 creò dal nulla il primo asilo per i bambini del paese, prima di essere trasferito a Corniglio, capoluogo di comune, dove ebbe modo di ampliare il suo raggio d'azione, interessarsi anche delle altre frazioni del comune, spesso prive di strade, acquedotti e telefono ed offrire il suo aiuto e il suo incoraggiamento ai confratelli della zona. Qui promosse e realizzò nel 1956, ripetendola nel 1957, una mostra di arte sacra della valle, veramente antesignano nell'intento di salvaguardare e valorizzare i tesori d'arte delle chiese della vallata.

Lasciati i nitidi monti di Corniglio nel 1958, don Giovanni approdò a Mezzano Superiore, nella nebbiosa Bassa Parmense, portando comunque con sé la sua grande voglia di fare. Per dodici anni, Mezzano Superiore vide Don Patanè operare nel sociale organizzando corsi di specializzazione per giovani della zona, e immergersi contemporaneamente nello studio tenace dei documenti dell'archivio parrocchiale, con i quali arrivò a ritrovare i resti dell'abside della primitiva chiesa.

La missione pastorale lo portò nel 1970 a Gaione, sede di una delle più antiche pievi di Parma (sec. VII-VIII), tra Parma e Fornovo, dove rimase per ben diciannove anni e dove la sua passione per la ricerca si manifestò in tutta la sua incontenibile forza. Nel campo dell'arte, innanzitutto,

riuscendo a localizzare l'antica vasca battesimale della pieve e progettando di riportare la pieve alla primitiva bellezza offuscata da sovrastrutture accumulatesi nel tempo, e, nuovo interesse,nel campo della tecnica. Fu proprio a Gaione infatti che all'amore per l'arte si affiancò il vivo interesse di don Giovanniper la storia della radiofonia e del telefono, così da divenire nel tempo uno dei migliori esperti in campo nazionale, e arrivare con notevolissima perizia a costruirsi personalmente apparati radio di elevata complessità. La ricca collezione da lui pazientemente, e con sacrifici economici non piccoli per i suoi mezzi, messa insieme e premurosamente ordinata una volta ritornato nella parrocchia di Mezzano Rondani (1989), può considerarsi un tesoro con pezzi unici,una delle più importanti in Italia.

La collezione conta 385 pezzi che vanno dai primi esemplari di radio a galena fino agli apparecchi radio domestici ed ai fonoriproduttori dei primi anni del dopoguerra. Alcuni di questi pezzi, insieme a quelli di altri collezionisti, erano stati già stati esposti a Gaione dallo stesso don Patanè, durante la sua permanenza alla pieve, dal 7 al 23 dicembre 1984 per celebrare il centenario della scoperta delle onde hertziane, avvenuta nel 1885.

Come alle opere di apostolato da lui compiute con incessante zelo, a questa splendida collezione resterà legato il ricordo di questo prete siciliano, che ha fatto dono alla diocesi di Parma della sua intensa e generosa attività pastorale, sociale e culturale.

Giunto infatti il momento di ritirarsi, don Giovanni girò lo sguardo per individuare chi potesse prendersi cura della sua amatissima collezione. Dopo qualche tentativo deludente, don Patanè fu messo in contatto con il CNIT dall'allora Presidente della Provincia di Parma, Corrado Truffelli. Ricordo con qualchecommozione le visite fatte alla collezione, e a don Patanè stesso, di cui una con l'intera Giunta del CNIT, e l'emozione con cui i colleghi si aggiravano per le stanze piene di scaffali semplici e ordinati, si chinavano sin dentro gli apparati, quasiintimiditida quei tesori del nostro passato professionale. Seppi poi che don Patanè, richiesto del perché avesse scelto il CNIT per il lascito, proprio a valle di quella visita, abbia risposto: "quei signori non mi hanno chiesto quanto vale".

Da quando ha ricevuto la "Collezione Patanè", il CNIT reca l'impegno a valorizzare il patrimonio storico, tecnico, culturale, di costume, insito in essa. Per questo mette a frutto la rete delle Università che lo costituiscono, ben 34 ad oggi, per portare quasi a domicilio, ogniqualvolta possibile, ciò che ciascuno di noi può ritrovare, sia esso appunto di storia, tecnica, cultura, costume, nella paziente raccolta di Don Giovanni. Dapprima a Pisa nel 2001, successivamente a Perugia nel 2002, ora a Firenze e poi a Genova e a Napoli, una parte della collezione è stata, viene e sarà esposta, selezionando i pezzi più significativi sotto il profilo dell'evoluzione sia della tecnica che del *design*, tutti perfettamente restaurati e funzionanti.

Desideriamo pertanto esprimere la nostra gratitudine all'amico Enrico Del Re per avere concepito e portato a compimento l'iniziativa fiorentina e al Rettore dell'Università di Firenze Augusto Marinelli, per il determinante supporto e collaborazione, senza i quali la mostra non avrebbe visto la luce in una cornice di così alto prestigio.

<div align="right">

Giancarlo Prati
Direttore del CNIT

</div>

Guglielmo Marconi e la nascita
di un nuovo mezzo di comunicazione: la radio

La storia della radio è inscindibilmente connessa all'opera scientifica e tecnica di Guglielmo Marconi (Fig. 1). In particolare le sue prime trasmissioni radiotelegrafiche a grande distanza provarono che la trasmissione e la ricezione delle onde elettromagnetiche non erano semplici curiosità da laboratorio. Il risultato positivo delle esperienze di Marconi, come egli stesso ebbe a dire, «fece intravedere agli studiosi intelligenti quali fossero le vere possibilità e potenzialità di questo nuovo mezzo di comunicazione».

FIG. 1

Guglielmo Marconi (Bologna, 1874; Roma, 1937).

Marconi iniziò a ottenere risultati interessanti già nel 1893, quando, stabilitosi definitivamente a Bologna, intensificò i suoi rapporti con Augusto Righi, docente di fisica nel locale ateneo, che a quel tempo studiava la propagazione delle onde elettromagnetiche sulla base delle esperienze effettuate alcuni anni prima da Heinrich Hertz. Nel 1895, a villa Griffone (Pontecchio, Bologna), Marconi, perfezionando i suoi apparati, compì l'espe-

rimento decisivo con un trasmettitore e un ricevitore, separati da circa 1500 metri e da un ostacolo naturale, la celebre collina dei Celestini. Marconi otteneva la radiofrequenza del trasmettitore mediante scintille, mentre per il ricevitore impiegava limatura di ferro, che, sottoposta a campi oscillanti, veniva a disporsi secondo le linee di forza permettendo il passaggio di una corrente elettrica (*coherer*).

Nel 1896 Marconi andò in Inghilterra e presentò la prima sua richiesta di brevetto per un sistema di telegrafia senza fili. In seguito effettuò una serie di esperienze: particolare menzione meritano quelle condotte nel golfo della Spezia e sulla Manica, nelle quali la portata delle trasmissioni superava l'orizzonte ottico. L'anno seguente, per sviluppare e commercializzare il suo nuovo metodo di comunicazioni senza fili, costituì la *Wireless Telegraph and Signal Company Ltd.*, che qualche anno dopo, nel 1900, divenne la *Marconi's Wireless Telegraph Co.* Sempre nel 1900 ottenne il famoso brevetto 7777 per il suo sistema di «telegrafia accordata o sintonizzata e multipla su una sola antenna di nuovo tipo». In questi brevetti compaiono componenti reattivi – induttori e capacitori – formanti circuiti volutamente selettivi in frequenza.

Nel 1901 Marconi tentò la prima trasmissione attraverso l'Atlantico. La stazione trasmittente dalla parte europea venne posta a Poldhu, all'estremità occidentale della penisola di Cornovaglia (Inghilterra), già teatro di precedenti esperienze di Marconi. Purtroppo l'antenna originale di Poldhu venne distrutta da una bufera prima che l'esperimento avvenisse; in sostituzione ne fu costruita una più semplice (Fig. 2). Anche la stazione ricevente americana, pensata in origine a Cape Cod (Massachusetts, USA), venne interamente distrutta da un ciclone prima di poter essere impiegata. La stazione ricevente di fortuna sorse allora su una collina presso San Giovanni, nell'isola di Terranova (Terranova, Canada) (Fig. 3).
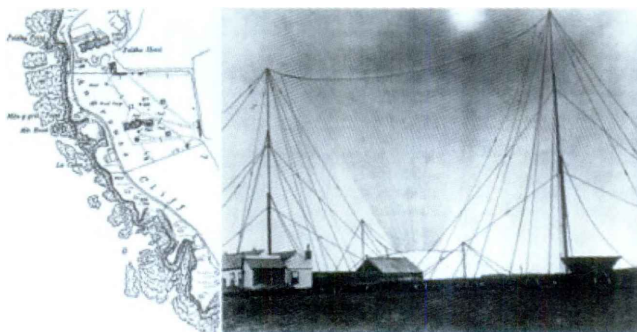
FIG. 2

La stazione trasmittente di Poldhu (Cornovaglia, Inghilterra)
per la prima trasmissione transatlantica del 1901.

Fig. 3

La stazione ricevente per la prima trasmissione transatlantica di S. Giovanni di Terranova sulla collina di Signal-Hill (12 Dicembre 1901).

L'antenna di questa stazione ricevente era costituita da un aquilone (allora chiamato alla francese "cervo volante") che portava un filo conduttore a circa 120 metri di altezza. La mattina del 12 dicembre 1901, verso le ore 12:30 locali, Marconi ricevette al telefono del ricevitore una successione ritmica dei 3 punti, che corrispondevano alla lettera S dell'alfabeto Morse. Tali segnali venivano trasmessi dalla stazione di Poldhu, sull'altra sponda dell'oceano, che si trovava a circa 3.000 chilometri di distanza. La lunghezza d'onda del segnale era approssimativamente 1800 m, la potenza era di circa 15 kV.

Il 1902 fu l'anno degli esperimenti effettuati in navigazione da Marconi per capire l'effetto che sulle radiocomunicazioni hanno la luce solaree le grandi estensioni di terreno montagnoso. Inoltre lo scienziato migliorò la strumentazione di cui disponeva (brevetto del *detector magnetico* che fu utilizzato al posto del *coherer*).

Le prime esperienze furono compiute a bordo del transatlantico *Philadelphia*, in navigazione da Cherbourg,porto francese sulla Manica, a New York, e dimostrarono «un effetto deciso e dannoso della luce del giorno sulla trasmissione per telegrafia senza fili e della maggiore facilità con cui i messaggi potevano essere inviati a lunghe distanze durante la notte» (Fig. 4). Le esperienze successive vennero effettuate a bordo dell'incrociatore *Carlo Alberto*, messo a disposizione dello scienziato dalla Marina Militare Italiana (Fig. 5). Il viaggio di Marconi sulla *Carlo Alberto* si snodò dal Baltico al Mediterraneo e consentì di compiere numerosi esperimenti, importanti sia dal punto di vista divulgativo – come la dimostrazione effettuata a San Pietroburgo in presenza del re d'Italia Vittorio Emanuele III e dello zar Nicola II – sia dal punto di vista tecnico, con le trasmissioni Poldhu-Cadice (Spagna) e Poldhu-Cagliari (Fig. 6). Queste ultime dimostrarono che «in un mare chiuso dalle più montuose distese di terra, come il

Mediterraneo, i radiotelegrammi trasmessi da Poldhu pervenivano sempre regolarmente sulla *Carlo Alberto*». Sempre a bordo della *Carlo Alberto* Marconi condusse attraverso l'Atlantico una successiva campagna di misura, che diede sostanziale conferma ai risultati ottenuti a bordo del transatlantico *Philadelphia*.
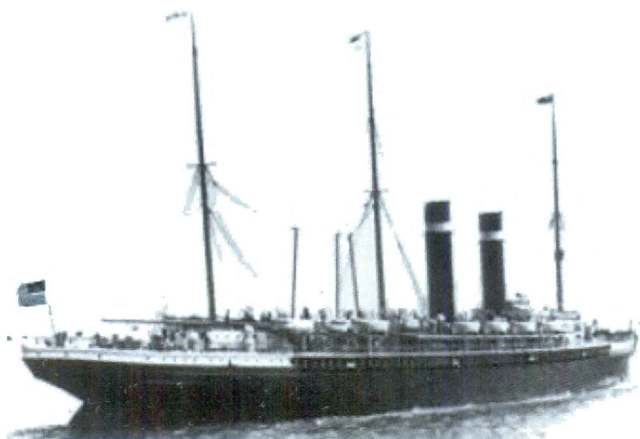
(a)

(b)

FIG 4

La nave Philadelphia con i relativi sistemi di ricezione
(22 Febbraio1902-1 Marzo 1902).
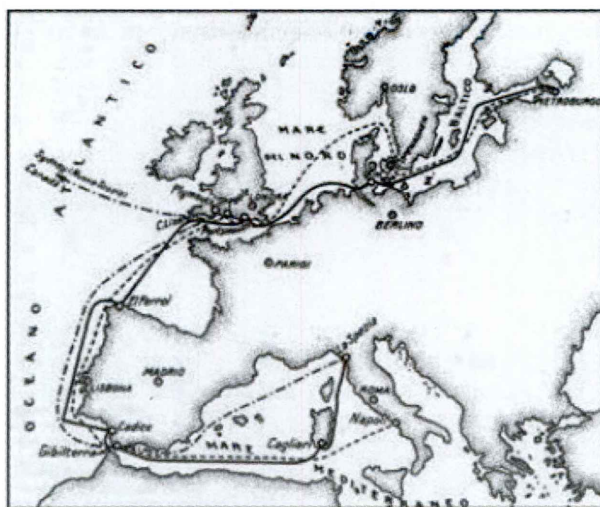
FIG. 5

Le rotte dell'incrociatore Carlo Alberto durante le due campagne di misura del 1902. Durante la primacampagna la nave partì daNapoli (Marconi salì abordo in Inghilterra), raggiunse Kronstad (vicino San Pietroburgo) e fece ritorno a La Spezia. Durante la seconda campagna la nave partì da La Spezia, fece sosta a Plymouth per imbarcare Marconi, e si diresse a Sydney (Nuova Scozia, Canada).

FIG. 6

Messaggio inviato da Poldhu (Inghilterra) a Vittorio Emanuele III e ricevuto dalla Carlo Alberto in acque sarde.

Sempre nel 1902-1903 il collegamento tra l'Europa e l'altra sponda dell'Atlantico divenne permanente e bidirezionale: furono costruite infatti le stazioni di Glace Bay (Nuova Scozia, Canada) e di Cape Cod (Massachusetts,

USA). Nelle sue memorie lo stesso Marconi riconobbe la rilevanza economica e politica di questa seconda stazione, largamente osteggiata dalla compagnia telegrafica via cavo e dai giornali dell'epoca. Nel 1906 Marconi costruì inoltre a Clifden (Irlanda) la prima stazione radiotelegrafica commerciale.

Nel 1903 venne intrapresa anche la costruzione della stazione di Coltano, presso Pisa. Lo sviluppo del sito di Coltano fu lentissimo, tanto che i lavori si protrassero fino al 1911; la stazione fu poi potenziata tra il 1919 e il 1924 (Fig. 7).
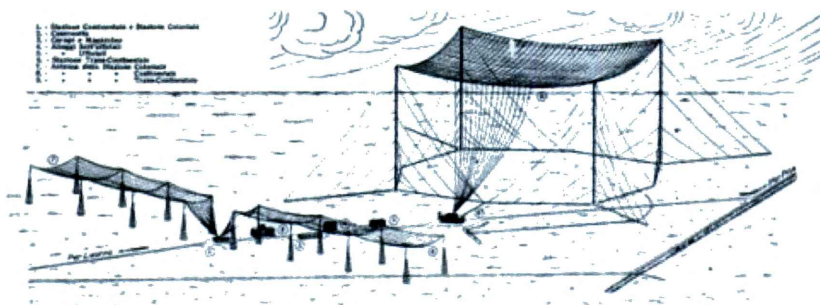
FIG. 7

Il centro radiotelegrafico di Coltano.

Il sito permetteva di comunicare con l'Argentina, con le colonie italiane in Africa e con la concessione di Tien-tsin (Cina). La stazione di Coltano restò la più grande e potente del mondo anche perché la sua tipologia – antenne poco direttive e a onde lunghe – era ormai prossima all'obsolescenza. Già nel primo decennio del secolo Marconi aveva cominciato a interessarsi delle onde corte (1 MHz, lunghezza d'onda 300 m): questo studio lo condurrà, sia pur lentamente, a sperimentare con successo le comunicazioni alla frequenza delle microonde (oltre 300 MHz). Con le onde corte divenne possibile usare antenne veramente direttive e, di conseguenza, raggiungere distanze maggiori con potenze minori; si otteneva inoltre una maggiore disponibilità di banda, incrementando quindi il numero di canali.

Le esperienze di Marconi di cui abbiamo parlato finora si muovono nell'ambito della radiotelegrafia, in altri termini sono fondate sullo scambio di segnali Morse. Costati anni di preparazione e un notevole impegno economico, questi esperimenti aprirono allora la strada della radiodiffusione, resa possibile da un crescendo di risultati tecnici che permisero di passare dal semplice segnale "binario" Morse – assenza di segnale / presenza di segnale (per tempi brevi, punto; per tempi lunghi, linea) – al segnale vocale vero e proprio, con la sua dinamica e il suo contenuto in frequenza. Il segnale vocale deve infatti essere modulato e demodulato fedelmente, e a tale scopo necessita di appositi componenti. Al loro sviluppo contribuirono

molti studiosi. All'inizio del Novecento Henry C. Dunwoody brevettò l'uso del cristallo di carborundum come rivelatore per demodulare il segnale, mentre Greenleaf W. Pickard usò allo stesso scopo i cristalli di silicio. In seguito altri minerali – tra i quali il più famoso è il solfuro di piombo, o galena – permisero una diffusione significativa dei primi apparecchi riceventi. Quasi contemporaneamente (1904) John A. Fleming, che contribuì tra l'altro alla progettazione della stazione di Poldhu, inventò il diodo a vuoto; nel 1906 Lee De Forest ottenne il triodo, aggiungendo un terzo elettrodo a forma di griglia tra il catodo e l'anodo della valvola a due elettrodi di Fleming. Il triodo consentì lo sviluppo di oscillatori in grado di generare radiofrequenza: vennero così abbandonati gli scomodi e inefficienti generatori a scintille, mentre i diodi – a galena o a vuoto – permisero di demodulare non solo il segnale Morse, ma anche il segnale vocale.

FIG. 8

Reginald A. Fessenden (East Bolton, Quebec, 1866 - Bermuda 1932).

Per la nascita delle trasmissioni radiofoniche merita infine particolare menzione il contributo del canadese Reginald A. Fessenden (Fig. 8). Quasi in contemporanea alle esperienze transatlantiche di Marconi, Fessenden compì su breve distanza esperimenti di trasmissione vocale i cui esiti non furono brillanti solo a causa del trasmettitore a scintilla di cui dovette servirsi. Nel dicembre 1906, comunque, lo studioso canadese effettuò la prima vera trasmissione radiofonica della storia: parole e musica vennero udite nel tratto di oceano antistante l'antenna trasmittente situata a Brant Rock, sulla costa del Massachusetts.

Giuseppe Pelosi
Università di Firenze
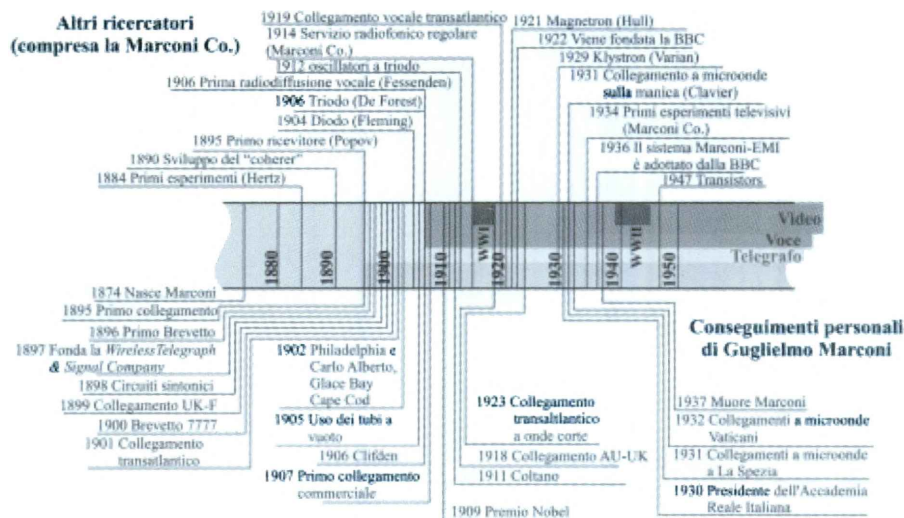
FIG. 9

Cronologia schematica della vita e delle opere di Guglielmo Marconi
e di altri importanti risultati tecnici relativi alla radio.

PARTE II

Dal catalogo della mostra (*)
"L'avventura della radio"

Sezione 1. Ricevitori
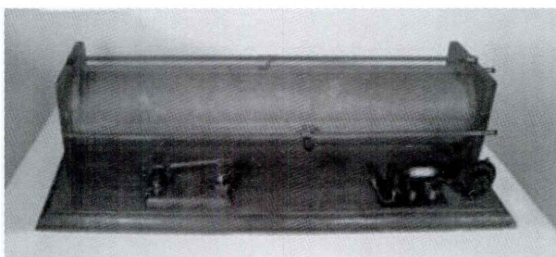
FIG. 1

Galena a induttanza variabile cristallo in aria non protetto

FIG. 2

Ricevitore GEcoPHONE, General Electric Co., Ltd. Sigillo BBC – GPO n. 102

(*) Autorizzazione alla pubblicazione delle foto a firma del prof. G. Prati, prot. n. 106 del 20 luglio 2004.

FIG. 3
Ricevitore a cristallo radiola BTH tipo "C", British
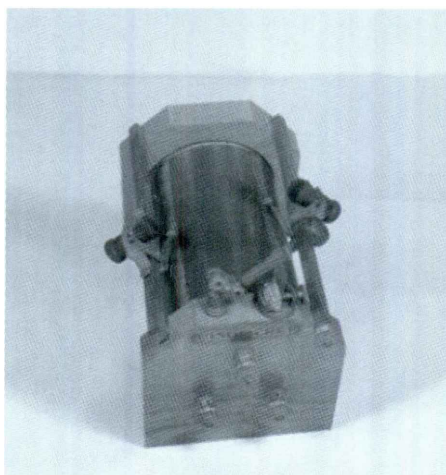
FIG. 4
Radio Galena "L'INDISCRET" con bobina a cursori, Francia

Sezione 2. Radio a valvola
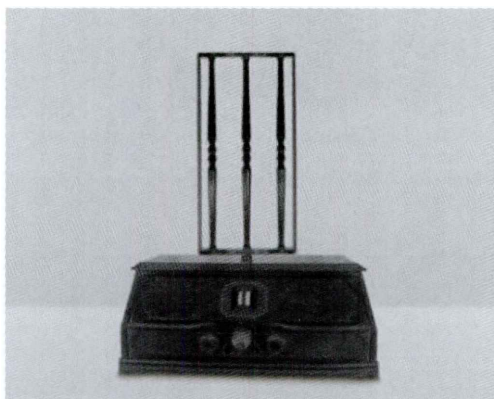
FIG. 1

RCA – Radiola 25 "Supereterodina" mod. AR-919

FIG. 2

Radio Philips 930A a reazione
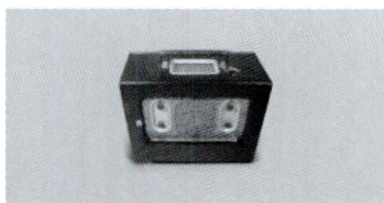
FIG. 3

Radio Saba – tipo 310 WL

FIG. 4

Radio Marelli mod. "CORIBANTE", Italia
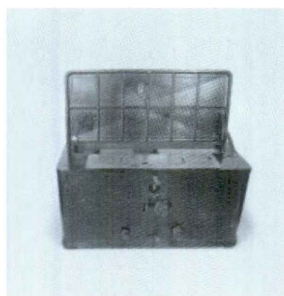
FIG. 5

Radio Telefunken 40 W – a reazione, Germania

Sezione 3. Marconiphone

FIG. 1

Marconiphone mod. T18 da Gran Bretagna
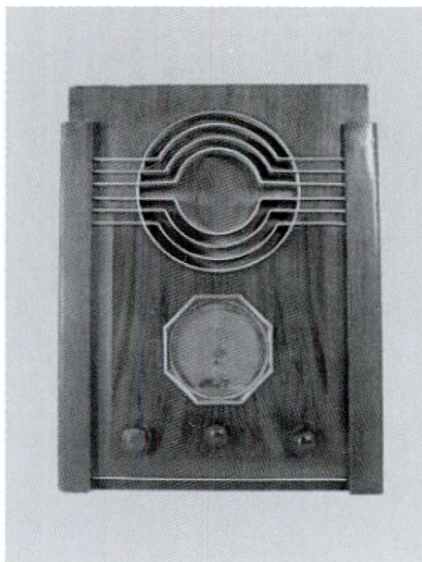
FIG. 2
Marconiphone mod. 435 – tipo n. 30 telaio francese con 5 valvole 1935
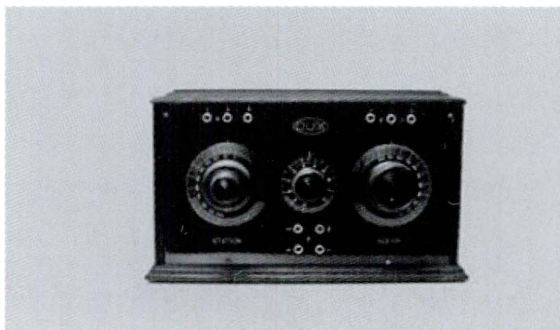
FIG. 3
Telefunken Marconi mod. "DUX" – 2 valvole, Svezia

Sezione 4. Strumenti
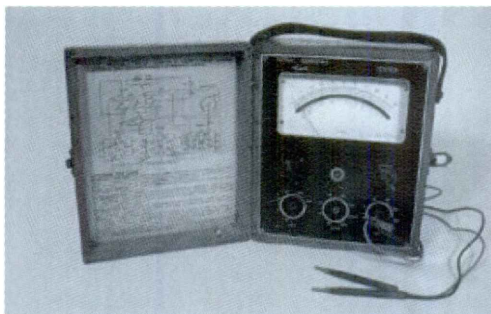
FIG. 1

Tester Universale, Istituto Radiotecnico – Milano – n. 2052

FIG. 2

Ponte di Wheatstone, Officine Galileo - Firenze
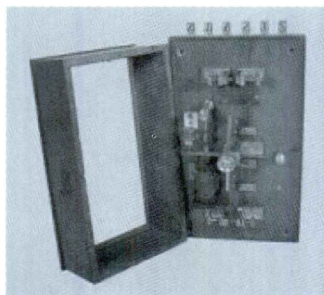
FIG. 3

Soccorritore telegrafico, Telegrapher Werkstätte von G. Hasler – Bern